——— Master Thesis in Physical Chemistry ———

András György Szanthoffer

Chemical Kinetic Modeling of the Combustion of NH_3/H_2 and NH_3/syngas Fuel Mixtures Using a Large Amount of Experimental Data

Supervisor: **Tamás Turányi**

Department of Physical Chemistry, Eötvös Loránd University, Hungary

Examiner: **Per Uvdal**

Division of Chemical Physics, Lund University, Sweden

LUND
UNIVERSITY

——— Faculty of Science, Lund University ———
——— Department of Chemistry ———
— Lund, Sweden, May 2022. —

Abstract

Nowadays, due to the global climate change, it is extremely important to find alternative fuels to reduce the utilization of fossil fuels and the emission of air pollutants such as carbon dioxide (CO_2), hydrocarbon pollutants, and soot. Ammonia (NH_3) is a promising carbon-free fuel candidate that can store and transport renewable hydrogen (H_2) energy.

Ammonia has several advantages over hydrogen in practical applications, but the combustion characteristics of NH_3 are different from traditional hydrocarbon fuels. A possible solution to improve the disadvantageous combustion properties of ammonia is to blend it with other fuels. For this purpose, two of the most usually used co-fuels are hydrogen and syngas (H_2/CO).

This study reports a collection of currently available chemical kinetic mechanisms from the literature that can be applied for modeling the combustion of NH_3/H_2 and NH_3/syngas fuel mixtures. An indirect experimental data collection is also presented which can be used for testing the performance of these combustion mechanisms.

In this work, 19 detailed reaction mechanisms were investigated that had been published in the last 13 years. Their performance was quantitatively assessed based on how well they can reproduce the results of indirect experiments. Almost 5000 experimental data points were utilized in the mechanism comparison including ignition delay times measured in shock tubes, concentration measurements in jet stirred and flow reactors, and laminar burning velocity measurements. Based on the results, it can be concluded that there are significant differences between the performances of the different models, and the performance of a mechanism may also vary significantly with the type of experiments.

Local sensitivity analysis was carried out on the best-performing mechanisms to identify the kinetic and thermodynamic parameters to which model outputs are most sensitive. Even though the investigated models are different, sensitivity analysis identified largely the same set of important reactions and thermodynamic data in these mechanisms.

Results presented in this work may serve as a good basis for further mechanism development for the combustion of NH_3/H_2 and NH_3/syngas fuel mixtures.

Popular science summary

In recent years, one of the most frequently heard terms in media has been *global climate change* because it raises concerns about the future of humanity. One cause of this phenomenon is the so-called *greenhouse effect*, which is due to the presence of *greenhouse gases* (GHGs) in the atmosphere. There are many GHGs, but based on quantity, the most important anthropogenic GHG is carbon dioxide (CO_2), whose main anthropogenic source is the combustion of biomass and fossil fuels.

Combustion of fossil fuels is the primary way of energy production nowadays. These processes take place in industry, heating of households, transportation, etc. The main fuel used in combustion devices is a hydrocarbon or a mixture of hydrocarbons, such as methane, gasoline, diesel, or kerosene. During the combustion of these fuels, not only CO_2 is released into the atmosphere, but also various carbonaceous air pollutants including carbon monoxide (CO), hydrocarbon pollutants, volatile organic compounds (VOCs), polycyclic aromatic hydrocarbons (PAHs), and soot, which are harmful to human health.

Exhaust gas of fossil fuel combustion in industry. Figure was taken from the internet[1].

Due to these reasons, it is crucial to find alternative carbon-free fuels that can be used efficiently for energy production. A promising candidate for this purpose is ammonia (NH_3). Some of the advantageous characteristics of ammonia are that it can be produced using renewable energy sources in an entirely carbon-free process, and there exists an already established and reliable infrastructure for its storage and transportation. However, NH_3 also has disadvantageous combustion properties as compared to conventional fossil fuels such as its low heat of combustion and high ignition energy, which must be improved to utilize ammonia as a fuel in practical combustion processes.

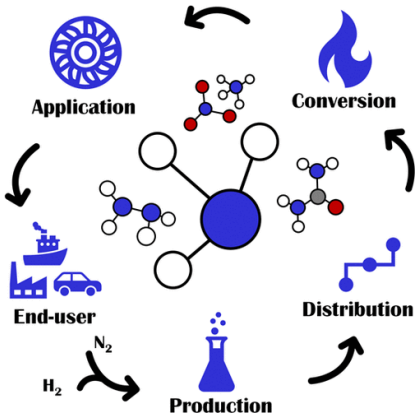

Scheme of the utilization of ammonia as fuel from production to the end-users. The figure was adapted from the work of Elishav et al. [1].

[1] http://esdatcodyhighschool.blogspot.com/2011/05/descriptiondefinition-of-fossil-fuel.html [accessed 20 May 2022].

To design new NH_3-based engines or power plants, detailed knowledge is necessary about the processes that take place during ammonia combustion. The rates of the occurring chemical reactions have to be described quantitatively, that is, accurate chemical kinetic mechanisms are needed for the combustion of ammonia under conditions relevant to industrial applications.

Several readily useable models exist in the literature that may be utilized for this purpose. This study aims to compare the performances of several such reaction mechanisms based on how accurately they can reproduce the results of experimental measurements. From the results, it can be concluded that none of the mechanisms can describe the investigated systems satisfactorily under all circumstances. From this, it follows that further mechanism development is needed to improve the predictive capabilities of the models. The study also reveals more detailed information about some selected models, which gives more insight into the chemistry of ammonia combustion, and most importantly, it can be used in future research to construct a reaction mechanism that can describe these systems better than any existing model.

Contents

1. Introduction

Nowadays, due to the intensive global climate change, it is extremely important to find ways to reduce the carbon dioxide (CO_2) emission stemming from human activities. This can be achieved by applying renewable energy sources and/or carbon-free fuels for energy generation. A straightforward chemical reaction that produces energy without CO_2 production is the oxidation of hydrogen (H_2). However, utilization of elementary hydrogen as a carbon-free fuel is not optimal because of its relatively low volumetric energy density, and difficult and relatively expensive storage, handling, and transportation. A good alternative hydrogen source is ammonia (NH_3) because it has the following advantages [2-6]:

– It has high hydrogen density, so it can be used directly in combustion systems as a fuel.
– It has higher volumetric energy density and boiling point than H_2 and can be liquified easily by compression (9.90 atm is needed at ambient temperature or −33.4 °C at atmospheric pressure [7]), so its storage and transportation are easier and more efficient than that of H_2.
– Its mass-based energy density is comparable to that of traditional fossil fuels (e.g., CH_4).

A scheme of the potential green use of ammonia is shown in Figure 1.

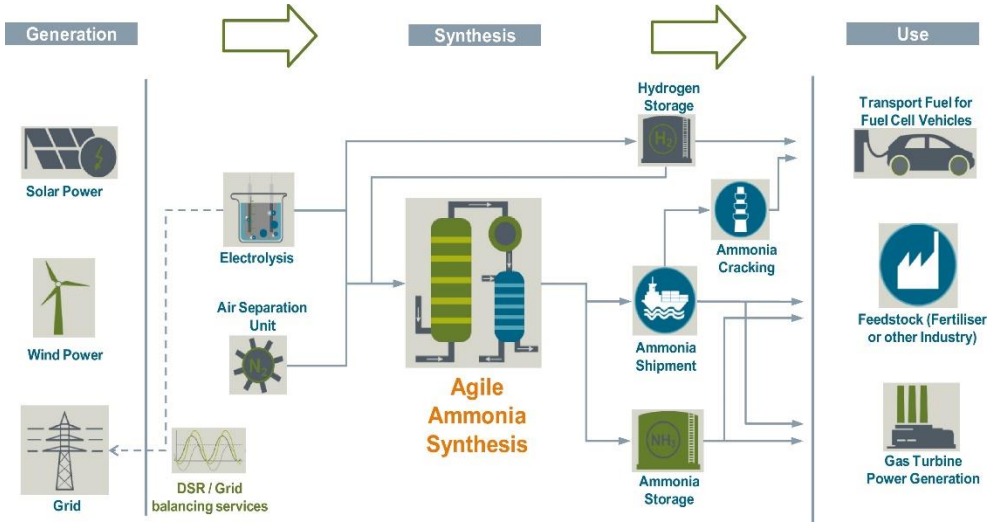

Figure 1. Potential green use of ammonia in transportation and industry. The figure was adapted from the work of Valera-Medina et al.[2].

However, ammonia has also several drawbacks as a pure fuel, [2,8,9], e. g., its

– high ignition energy, long ignition delay time, and small burning velocity relative to traditional hydrocarbon fuels and hydrogen,

– lower heat of combustion and radiation heat transfer from the flame than in the case of traditional hydrocarbon fuels due to the lack of CO_2 among combustion products,
– large amounts of NO_x compounds ($NO + NO_2 + N_2O$) produced during combustion.

To improve these disadvantageous combustion properties of ammonia, it is usually blended with another fuel, most often with hydrogen [10-15], CO or synthesis gas (H_2/CO) [14-17], or methane [13,14]. Hence, NH_3 is often present as a *co-fuel* in the fuel mixture. Note that although the aforementioned three gases are the most popular for blending ammonia in fuel mixtures, other fuels can also be used such as gasoline [18], diesel [19,20], dimethyl ether (DME) [21], or diethyl ether (DEE) [22].

Synthesis gas, or shortly, *syngas*, is of special interest in this study. The term "syngas" is usually used interchangeably with the term "wet CO" in the field of combustion chemistry. In general, "wet CO" is the mixture of carbon monoxide (CO) and at least one chemical substance containing hydrogen atom(s) such as hydrogen (H_2), water vapor (H_2O), or hydrocarbons. In this thesis, "syngas" is used for gas mixtures containing CO and H_2, and possible additional diluted species (e. g., carbon dioxide (CO_2) or H_2O) excluding hydrocarbons. "Dry CO" is the opposite term of "dry CO"; "dry CO" is pure CO gas in the absence of any hydrogen compound but its combustion is not relevant from a practical aspect. Syngas is usually generated by the gasification of coal or biomass [23-25], which can then be used for electricity production in gas turbines, reciprocating engines, and boilers [26]. Energy can be produced in an efficient and well-controllable way using syngas with low emission of hazardous gases; therefore, this process is important for environmental protection [26]. Syngas oxidation is important also from a more fundamental point of view. Nowadays, most internal combustion engines are fueled by a hydrocarbon or a mixture of hydrocarbons, and the chemistry of syngas oxidation is the basis of all hydrocarbon combustion mechanisms [27].

To facilitate the development and design of new ammonia-based reciprocating engines and gas turbines, accurate chemical kinetic models are needed that can describe the combustion of fuel mixtures containing NH_3 under typical conditions of industrial applications [19,20,28]. There are several reaction mechanisms available in the literature that aim to describe the combustion of ammonia–hydrogen [29-37], and ammonia–syngas fuel mixtures [16,17,38-42]. However, while the predictions of these models often agree with experimental results under certain conditions, they deviate from those under other conditions. Therefore, comprehensive validation and further development of these models are needed based on a large set of available experimental data. Consequently, this study aims to test the

performance of several chemical kinetic mechanisms for the combustion of NH_3/H_2 and NH_3/syngas fuel mixtures under a wide range of combustion conditions. Some selected models are also examined by sensitivity analysis to identify the most important model parameters under the investigated experimental conditions.

In addition to its promising application as a fuel, ammonia is also widely used in the power industry as a chemical additive in the *thermal deNO$_x$* process [43-45]. The thermal deNO$_x$ process is a *selective non-catalytic reduction* (SNCR) technique used to reduce the NO$_x$ emission in various combustion processes by adding NH_3 to the exhaust gas. The process can be viewed as the oxidation of NH_3 by NO and reactive H/O radicals (H/O/OH). If the thermal deNO$_x$ process is carried out properly, then the result of NH_3 oxidation is mainly N_2, instead of NO. Therefore, accurate knowledge of NH_3 oxidation chemistry is needed to control the NO$_x$ emission of combustion processes and to find the optimal operating conditions. This can also be facilitated by developing combustion kinetic models for NH_3 oxidation.

2. Objectives of the study

The Chemical Kinetics Laboratory at ELTE Eötvös Loránd University (from now on, "ELTE") [46] mostly investigates the computer modeling of gas-phase combustion processes. The group aims to develop new combustion mechanisms for various combustion systems based on available experimental and theoretically obtained data from the literature. The work presented in this study was carried out within the frame of this research group. The combustion chemistry of ammonia–hydrogen and ammonia–syngas fuel mixtures were investigated.

The aims of this study are as follows:

(i) Collection of experimental data on the combustion of NH_3/H_2 and NH_3/syngas fuel mixtures from the literature and preparation of data files that are suitable for combustion simulation programs for modeling these experiments.

(ii) Collection of recent, detailed reaction mechanisms from the literature that can describe the combustion of NH_3/H_2 and NH_3/syngas fuel mixtures.

(iii) Simulation of the collected experiments with the mechanisms with a widely used combustion simulation program.

(iv) Quantitative evaluation and comparison of the performance of the mechanisms under various conditions based on the agreement of the simulation and the experimental results.

(v) Investigation of the best-performing model(s) by sensitivity analysis to identify the parameters that are most influential on the model outputs.

(vi) Discussion of further research opportunities.

All results and conclusions presented in this study are the results of the individual work of the author of this thesis, except if otherwise stated in the document. The work was facilitated by the guidelines of the supervisor of the author, Prof. Tamás Turányi (head of the Chemical Kinetics Laboratory at ELTE).

3. Literature review, data collection and processing

3.1. Utilization of indirect experimental data from the literature

When researchers develop reaction kinetic models, they may utilize various types of data from the literature: results of theoretical computations, and direct and indirect experimental data. For this study, only the last category is of interest. In the case of *indirect experiments*, a quantity that is characteristic of the whole combustion process (not only one reaction step) is measured. A reaction mechanism must always be validated against experimental data, which means that indirect experiments are simulated with the mechanism, and the model predictions are compared to the results of indirect experiments. The accuracy of model predictions characterizes the performance of the mechanism.

3.1.1. Indirect experimental techniques in combustion chemistry

Since this work involves the simulation of indirect experiments, some indirect experimental techniques relevant to this study are briefly introduced in this section. These methods may be categorized into two groups. One group contains experiments that are simulated using a homogeneous gas mixture model ([47] and p. 339. in [48]). Experimenters can approximate the homogeneity of the gas mixture by premixing the reactants to aim "perfect" mixing of the reactor zone. Computer simulation of these experiments is usually referred to as *zero-dimensional* (0D) as the physical-chemical properties of the reacting systems do not depend on any spatial coordinate during the simulation. Experimental studies of flames belong to the other category of methods, which reveal additional chemical and physical information about the combustion characteristics of the investigated system. One- or more-dimensional models are applicable for the simulation of flames, so these computations are much more complicated and time-consuming than the 0D simulations. In this work, only *one-dimensional* (1D) flames are investigated in which the physical-chemical properties are a function of only one spatial coordinate. Combustion mechanisms are usually validated against flame experiments that can be simulated using a one-dimensional flame model since they can be simulated relatively simply using easily available computer codes.

3.1.1.1. Experiments in reactors with spatially homogeneous modeling

a) Measuring ignition delay times (IDTs) of gas mixtures:

- **Shock tube (ST)**

A *shock tube* (ST) is a typically 5–10-meter-long tube made of steel with an inner diameter of approximately 5–10 cm. A membrane, which is also called a diaphragm, divides the tube into two compartments initially (Figure 2). In one compartment (*driver section*), the inert driver gas (usually Ar) can be found, and this section is at high pressure at the beginning of the experiment. The other compartment (*driven section*) contains the fuel–oxidizer–diluent gas mixture at low pressure.

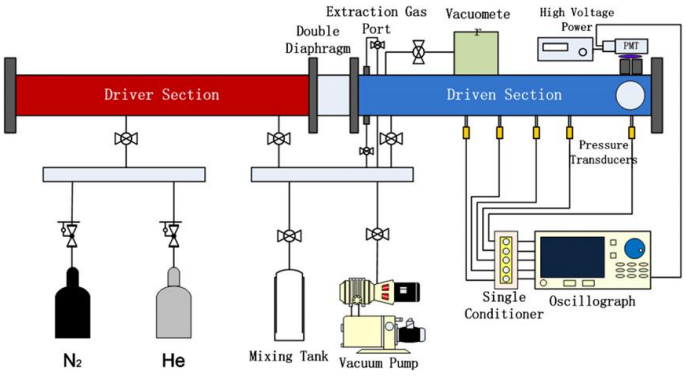

Figure 2. Schematic of a shock tube.
The figure was adapted from the work of Zhang et al. [49].

The measurement begins when the diaphragm is ruptured, and therefore a shock wave starts propagating in the tube compressing the gas mixture. This results in a sudden increase in the temperature and pressure of the gas located in front of the shock wave, which may cause the gas mixture to ignite. However, ignition does not occur immediately when the shock wave arrives, only after a certain amount of time, if the radical concentrations are large enough to induce the ignition. The elapsed time between the compression of the gas mixture (i. e., the arrival of the shock wave) and the ignition (the exact time of ignition can be defined in various ways) is called the *ignition delay time* (usually denoted by τ, τ_{ign}, or IDT, see Figure 3), and the shock tube is very often used for determining this property. Burke et al. [50] overview several modern shock tube devices that are used for IDT determinations.

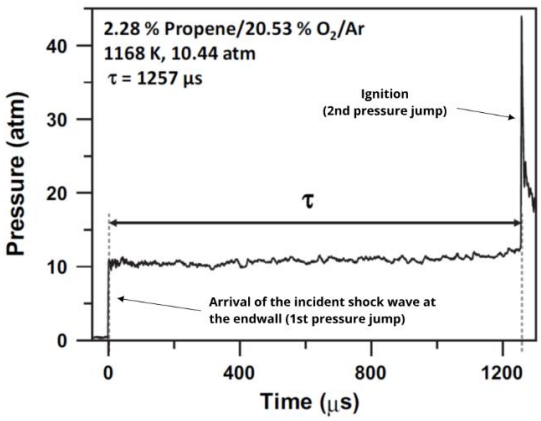

Figure 3. Pressure–time history of a shock tube measurement in which the incident shock wave induces the ignition. The figure was adapted and modified from the work of Burke et al. [50].

- **Rapid compression machine (RCM)**

Rapid compression machine (RCM) is essentially a cylindrical steel tube with a typical inner diameter of 5–10 cm into which the fuel–air–diluent gas mixture is filled. The gas mixture is compressed with one or two pneumatically driven pistons to induce ignition (Figure 4). In the two-piston (twin-piston) setup, the sudden compression is done by two opposing pistons that compress the gas mixture simultaneously.

Figure 5 shows typical pressure–time profiles during an RCM experiment (black line: reactive gas mixture, blue line: non-reactive gas mixture). The first pressure rise occurs due to the sudden (nearly adiabatic) compression; in this case, the maximum compression pressure (P_c) is around 20 bar. This pressure rise occurs for both the reactive and non-reactive mixtures. During compression, the temperature also increases sharply because of the compression heat. After the compression (after the pressure maximum), the volume of the reactor is constant. The pressure starts decreasing slowly due to heat loss to the environment at constant volume. Then, in the case of the reactive mixture, a second steep pressure (and temperature) rise can be observed, which is caused by the ignition of the gas mixture. The elapsed time between the end of compression and the onset of ignition is the ignition delay time. In Figure 5, its exact definition is the time between the pressure maximum and the steepest slope of the pressure trace during the ignition (red curve).

While shock tubes are typically used for measuring IDTs below about 1 ms, RCMs are more accurate if the IDTs are longer than about 10 ms. A more detailed discussion about RCMs can be found in Chapter 7 of the book of Battin-Leclerc et al. [51].

Figure 4. Twin-piston rapid compression machine located in the Combustion Chemistry Centre of NUI Galway. Source of the figure: p. 168. of the book of Battin-Leclerc et al. [51]

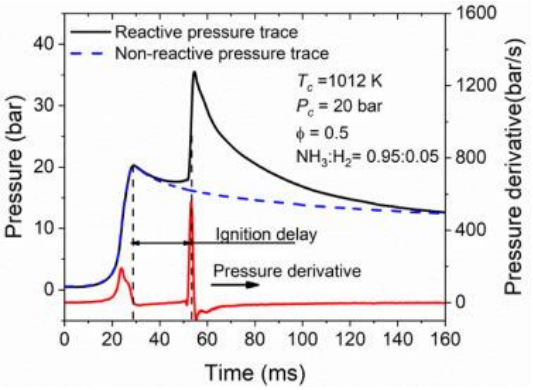

Figure 5. Recorded pressure traces during the investigation of an $NH_3/H_2/O_2$ gas mixture using a single-piston RCM equipment. For the non-reactive experiments, O_2 was replaced by N_2 in the gas mixture. The figure was adapted from the work of He et al. [52].

b) Analyzing the composition (outlet concentrations) of reacting gas mixtures:

- **Jet stirred reactor (JSR)**

The main part of a *jet stirred reactor* (JSR), which is often referred to as *perfectly stirred reactor* (PSR), is a sphere with a glass or quartz wall (Figure 6). During experiments, the reactor is surrounded by a thermostat. On one side of the sphere (the inlet), the reactant and the diluent gases are continuously introduced into the reactor through nozzles that point in different directions, which results in a turbulent flow within the sphere. Therefore, perfect mixing of the reactants can be assumed within the reactor, so homogeneous gas mixture model can be applied in the simulations. A gas sampling tube can also be found on the wall of the reactor. After steady state has been realized in the reaction chamber, the concentrations of the outlet gases are measured by the appropriate analytical technique(s). Battin-Leclerc et al.[51] discuss the JSR in Chapter 8 of their book in more detail.

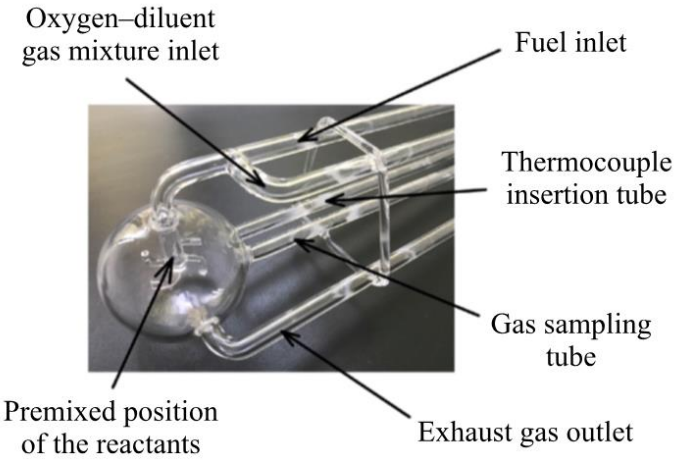

Figure 6. Jest stirred reactor used in the work of Ding et al. [53].
The figure was adapted and modified from the same work.

- **Tubular flow reactor (FR)**

A *tubular flow reactor* or *plug flow reactor* (FR) is a tube made of quartz or glass, heated by electric cartridges externally (Figure 7). The reactant and diluent gases enter at one end of the tube, and they start flowing through it. The chemical reaction occurs within the tube, whose central part is called the reaction zone, and at the opposite end of the tube, the outlet gas mixture is cooled down and analyzed by the appropriate analytical technique(s). Homogeneous combustion is approximated by placing a mixing zone for the reactants before

the high-temperature reaction zone. Battin-Leclerc et al. discuss some theoretical and technical details of flow reactor experiments in Chapter 9 of their book [51].

To ensure a uniform temperature profile in the reaction zone, the inlet gases are preheated by separate thermostats. However, a uniform temperature profile still cannot be created along the whole tube despite this effort; the ends of the tube are always cooler than the reaction zone (the middle part). Sometimes, the authors publish the experimentally measured temperature profiles along the reactor axis (Figure 8). In these cases, the simulations of flow reactor experiments can be performed using these temperature profiles, the length and the diameter of the reactor, and the flow velocity of the inlet gas mixture as inputs. As can be seen in Figure 8, it usually can be achieved that the reaction zone has a constant temperature within a few kelvins. Therefore, in the lack of experimental temperature profiles, it is a good approximation that the reaction takes place at a constant temperature. In these cases, the residence time of the gas mixture in the reaction zone and the isothermal temperature are used as input parameters for the simulations. However, this approximation is less accurate than using the experimental temperature profiles.

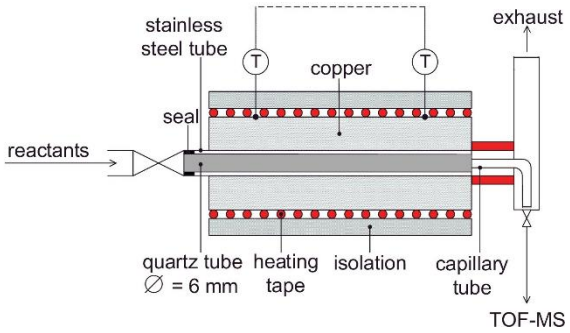

Figure 7. Schematic of a tubular quartz flow reactor. T = thermocouple, TOF-MS = time-of-flight mass spectrometer. The figure was adapted and modified from the work of Sen et al. [54].

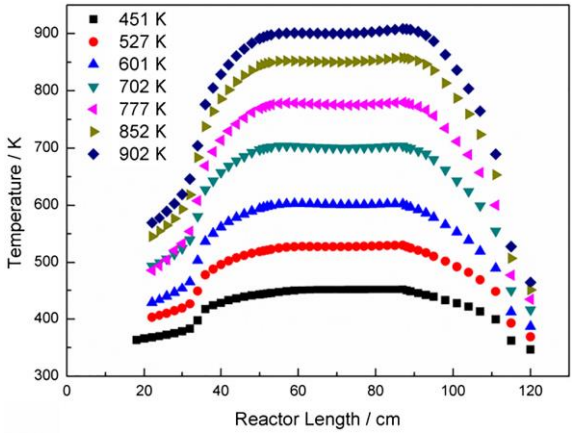

Figure 8. Measured temperature profiles along the axis of a tubular flow reactor at different isothermal zone temperatures during ammonia oxidation [30]. The figure was adapted from the work of Song et al. [30].

3.1.1.2. Experimental investigation of flames

a) Measuring the laminar burning velocity (LBV) of gas mixtures:

Laminar burning velocity (LBV), often denoted by v_L or S_L^0, is a very important physical parameter of flames. By definition, it is the traveling speed of the laminar flame front if it is

(i) infinitely large (no wall effect),

(ii) adiabatic (no net heat loss),

(iii) planar (no curvature),

(iv) without stretch (no cross-flow perpendicular to the direction of flame propagation).

Laminar burning velocity is a physical constant of a given gas mixture at a given pressure and temperature. The (i)–(iv) conditions are stringent, and it is difficult to ensure them experimentally. Therefore, the determination of the true laminar burning velocity of a gas mixture is a challenging task, and usually, mathematical corrections (most usually, extrapolations) need to be performed on the measured flame speed data. However, extrapolation always increases the error of the determined LBVs. Various methods exist to measure the LBV of gas mixtures, of which the most widely applied are summarized in Table 1. All of these methods are discussed in the recent review paper by Konnov et al. [71] in detail. In the review work of Egolfopoulos et al. [72], the OPSF, CTF, and HFB methods are discussed. Chapter 10 of the book of Battin-Leclerc et al. [51] discusses the FC, OPSF, CTF,

Table 1. Experimental techniques for measuring the laminar burning velocities of gas mixtures.

Measurement technique	References
flame cone or *Bunsen flame* (BF) method	Kick et al. [55], Hu et al. [56]
outwardly propagating spherical flame (OPSF) method	Mével et al. [57], Bane et al. [58]
counterflow twin-flame (CTF) method (a realization of the *stagnation flame* method)	Lund University [59], Egolfopoulos et al. [60], Veloo et al. [61]
single jet–plate (SJP) method (a realization of the *stagnation flame* method)	Vagelopoulos and Egolfopoulos [62], Wu and Law [63]
annular stepwise diverging tube (ASDT) method	Kim and Kim [64], Liu et al. [65,66]
heat flux burner (HFB) method	de Goey et al. [67], Bosschaart and de Goey [68]
externally heated diverging channel (EHDC) method	Akram et al. [69], Varghese et al. [70]

and HFB methods. LBV measurements investigated in this study were performed using outwardly propagating spherical flames (Figure 9), heat flux burners (Figure 10), or Bunsen flames.

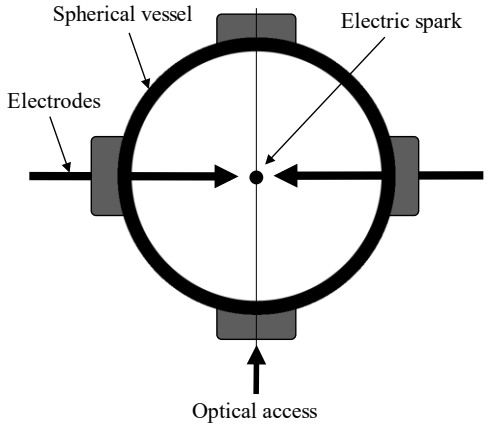

Figure 9. Combustion chamber of the outwardly propagating spherical flame method. The figure was redrawn from the work of Mével et al. [57].

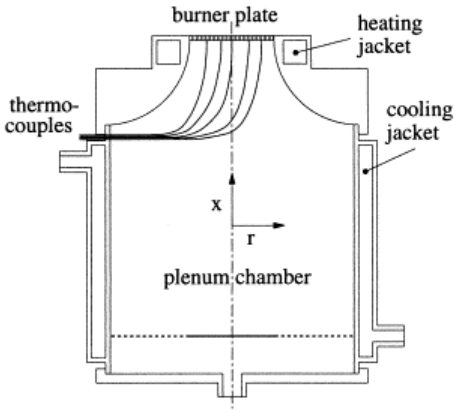

Figure 10. Schematic of an experimental setup used for the heat flux burner method. The figure was adapted from the work of Bosschaart and de Goey [68].

b) Measuring concentrations in burner stabilized flames (BSFs):

It is also possible to experimentally measure concentrations of various species at different spatial locations of flames. This can be done by directly probing the flame with an appropriate optical spectroscopical technique, or by sampling the flame with a quartz nozzle and then analyzing the composition of the sample. The so-called *flat flame burner* is the most often applied experimental apparatus for the analysis of flame structures. In these experiments, a burner head stabilizes the flame; hence, the stationary assumption applies to the system. The physical-chemical properties such as concentrations are a function of the distance from the flat burner plate.

In BSF experiments, the flame front is not adiabatic, because there is heat loss towards the burner plate from the flame front. Consequently, the temperature profile in the flame cannot be accurately estimated using an adiabatic model, and therefore it is essential to know the experimentally measured temperature profiles for the accurate computer simulations of BSF experiments. Note that flat flame burners can also be used for LBV measurements if a series of experiments are performed with different but known heat losses, and the measured flame speeds are then extrapolated to zero heat loss [73]. The heat flux burner method is essentially a further development of simple flat flame burners [67], in which this extrapolation is not needed, and therefore the errors of the determined LBVs are much smaller.

3.1.2. Indirect experimental data collected

In this section, indirect experimental data collected from the literature are presented. A large part of the work was to extract relevant information from collected publications, and then, prepare data files in a specified file format, which contain all necessary information needed to perform simulations of the experiments. The digitization of experimental data is a very time-consuming task because there is no standard way of publishing experimental data in the combustion chemistry community. Experimental results are usually published as symbols in graphs or numbers in tables, and experimental conditions are often reported in separate tables or the main text of the papers. Also, relevant experimental conditions are sometimes missing from the publications or are not reported appropriately, which necessitates extra personal communication with the authors.

Due to the accumulation of a large number of experimental data in the combustion chemistry literature, there has been a demand for a database that facilitates and standardizes data storing, handling, and manipulation. An example of this is the PrIMe database of Michael Frenklach [74] which contains models, model parameters, and experimental data from the field of combustion chemistry.

ReSpecTh [75] is an online database, which is a result of the collaboration of the ELKH-ELTE Complex Chemical Systems Research Group [76], Laboratory of Molecular Structure and Dynamics [77], and Chemical Kinetics Laboratory at ELTE [46]. The database contains a large amount of literature data in the field of reaction kinetics (“Re”), spectroscopy (“Spec”), and thermochemistry (“Th”). The reaction kinetics section includes direct and indirect experimental data, reaction mechanisms, and computer programs that can be utilized for mechanism development.

Indirect experimental data are available in the so-called RKD (ReSpecTh Kinetics Data) [78]. It is essentially an extension of the file format used in the PrIMe database [74]. Each measurement is stored in a separate data file of XML (Extensible Markup Language) format and each file has a unique identifier. The advantage of the use of XML files for data storage is that these files can easily be handled by computer programs and are also well readable by humans.

An RKD-format XML measurement file contains all information about the experiment such as experimental conditions and measurement results, which is necessary to reproduce the experiment by computer simulations and to compare theoretical and experimental results. In addition, it includes bibliographic information about the experiment so that the original data

source can easily be found in the literature. RKD-format XML files were prepared from the indirect experimental data listed below.

The collected experiments are divided into two parts: experiments NH_3/H_2 (Table 2) and NH_3/syngas (Table 3) fuel mixtures. The reason for the separation is that simulations of the former kind of experiments do not require that the mechanism contains a wet CO oxidation submechanism (see Section 3.2.2). However, for NH_3/syngas experiments, a wet CO submechanism has to be included in the model. The number of publications on NH_3/syngas experiments is much smaller than in the case of NH_3/H_2 experiments. This is because a) CO is not a carbon-free fuel contrary to H_2, and b) H_2 addition to ammonia increases the LBV of the gas mixture relative to pure NH_3 more efficiently than CO addition does [14,16,17]. Therefore, the addition of CO to NH_3 is of less practical importance than that of H_2.

Using the *Optima++* program package [79] developed by the Chemical Kinetics Laboratory at ELTE (see Section 4), more details can be extracted from the XML files about the experiments easily, such as the temperature and pressure of the measurement and information about the composition of the investigated gas mixture. These details are summarized in Tables 2 and 3. Altogether, 347 XML-format data files have been constructed so far (258 on NH_3/H_2 experiments and 89 on NH_3/syngas experiments). These experiments cover a wide range of temperature, pressure, and initial gas mixture composition. It is important to highlight that the XML-format data files containing BSF experiments were prepared by Dr. István Gyula Zsély, a member of the research group, and those describing RCM-IDT experiments were created by Dr. László Kawka, another member of the group. Some ST-IDT [38,80] and FR concentration [30,81-83] measurements were investigated in the work of Kawka et al. [84]. XML data files corresponding to these experiments were originally prepared by Dr. László Kawka, and these files were carefully revised by the author of this thesis, and some corrections were made in them wherever it was necessary. All other XML data files were entirely prepared by the author of this thesis. For further investigations, only ST-IDT, JSR, FR, and LBV experiments are used in this study because the simulations of RCM-IDT and BSF experiments are not finished yet.

As shown in Tables 2 and 3, most of the papers were published in the last three years, which shows the enhanced interest in the combustion of ammonia and ammonia fuel mixtures recently.

In Tables 2 and 3, the quantity, Φ, which is often denoted by φ, characterizes the compositions of the investigated initial gas mixtures in terms of the fuel/oxidizer molar ratio. It is called the *equivalence ratio* and is defined as follows:

$$\Phi = \frac{\frac{n_{\text{fuel}}}{n_{\text{oxidizer}}}}{\left(\frac{n_{\text{fuel}}}{n_{\text{oxidizer}}}\right)_{\text{stoichiometric}}} \quad (1)$$

where *n* is the molar amount of the component in subscript. Therefore, if $\Phi < 1$, then the gas mixture is fuel-lean as compared to the stoichiometric mixture, if $\Phi > 1$, it is fuel-rich, and if $\Phi = 1$, the composition of the gas mixture is stoichiometric. The reaction equations that correspond to stoichiometric combustion processes are as follows:

$$H_2 + ½\ O_2 = H_2O, \quad (R1)$$

$$CO + ½\ O_2 = CO_2, \quad (R2)$$

$$4\ NH_3 + 3\ O_2 = 2\ N_2 + 6\ H_2O. \quad (R3)$$

Finally, it must be noted that the literature review of indirect experiments presented herein is exhaustive until the 18th of January, 2022. Experimental results published after this date on this topic are not considered in this study.

Table 2. Indirect experiments with NH_3/H_2 fuel mixtures and the experimental conditions. In the case of the flame experiments, the temperature and the pressure values refer to the states of the unburnt gas mixtures.

Reference	App.[a]	Meas.[b]	XML/Ds./Dp.[c]	Fuel	Ox.[d]	Dopant	Diluent	*T* / K	*p* / atm	Φ
Davidson (1990) [85]	ST	IDT	6/6/29	NH_3	–	–	Ar	2224–3303	0.45–1.02	–
Mathieu (2015) [38]	ST	IDT	12/12/104	NH_3	O_2	–	Ar	1564–2479	1.25–30.40	0.50–2.00
Shu (2019) [80]	ST	IDT	6/6/30	NH_3	O_2	–	N_2	1181–1581	19.05–41.65	0.50–2.00
Chen (2021) [86]	ST	IDT	8/8/66	NH_3(/H_2)	O_2	–	Ar	1022–1956	1.01–12.60	1.00
Subtotal:			**32/32/229**							
He (2019) [52]	RCM	IDT	18/18/107	NH_3(/H_2)	O_2	–	Ar(/N_2)	969–1131	19.59–59.84	0.50–2.00
Pochet (2019) [87]	RCM	IDT	*not processed*	NH_3(/H_2)	O_2	–	N_2(/Ar)	1000–1100	42.83–64.64	0.20–0.50
Dai (2020) [88]	RCM	IDT	8/8/93	NH_3(/H_2)	O_2	–	Ar(/N_2)	952–1210	19.59–69.33	0.50–3.00
Subtotal:			**26/26/200**							
Dagaut (2019) [89]	JSR	c_{out}	4/14/150	NH_3	O_2	–	N_2	1101–1452	1.00	0.06–1.20
Stagni (2020) [34]	JSR	c_{out}	3/7/62	NH_3	–/O_2	–	He	500–1200	1.05	0.01–0.02
Sabia (2020) [90]	JSR	c_{out}	7/21/558	NH_3	O_2	–/H_2O	N_2	965–1293	1.20	0.60–1.40
Manna (2020) [91]	JSR	c_{out}	4/12/144	NH_3	–/O_2	–/H_2O	Ar	953–1313	1.20	1.00
Zhang (2021) [36]	JSR	c_{out}	10/40/376	NH_3(/H_2)	O_2	–	N_2	800–1277	1.00	0.15–0.79
Osipova (2022) [92]	JSR	c_{out}	4/19/361	NH_3(/H_2)	O_2	–	Ar	800–1300	1.00	0.60–1.50
Subtotal:			**32/113/1651**							
Dean (1982) [93]	FR	*c*–*t*	2/4/24	NH_3	O_2	–/H_2O	He	1279	1.18	0.02
Hulgaard (1993) [81]	FR	c_{out}	2/5/50	NH_3	O_2	–/H_2O	N_2	938–1373	1.04	0.02
Caton (1995) [83]	FR	c_{out}	1/3/45	NH_3	O_2	–	N_2	798–1200	1.01	0.01
Wargadalam (2000) [82]	FR	c_{out}	2/4/36	NH_3(/H_2)	O_2	–	N_2	873–1274	1.00	0.00
Song (2016) [30]	FR	c_{out}	6/11/70	NH_3	O_2	–	N_2	451–925	29.61–98.69	0.01–0.62
Stagni (2020) [34]	FR	c_{out}	1/6/114	NH_3	O_2	–	He	1073–1973	1.25	0.38

Reference	App.[a]	Meas.[b]	XML/Ds./Dp.[c]	Fuel	Ox.[d]	Dopant	Diluent	T / K	p / atm	Φ
Abián (2021) [94]	FR	c_{out}	10/56/802	NH_3	–/O_2	–/H_2O	N_2	875–1475	1.00	0.05–2.44
Subtotal:			**24/89/1141**							
Lee (2010a) [95]	OPSF	LBV	3/3/15	NH_3/H_2	O_2	–	N_2	298	1.00	0.60–1.67
Lee (2010b) [96]	OPSF	LBV	5/5/10	NH_3/H_2	O_2	–	N_2	298	1.00	0.60–1.67
Hayakawa (2015) [97]	OPSF	LBV	3/3/13	NH_3	O_2	–	N_2	298	0.99–4.93	0.80–1.20
Ichikawa (2015) [12]	OPSF	LBV	3/3/22	NH_3/H_2	O_2	–	N_2	298	0.99	1.00
Takeishi (2015) [98]	BF	LBV	3/3/28	NH_3	O_2	–	N_2	298	1.00	0.80–1.40
Han (2019) [14]	HFB	LBV	6/6/99	NH_3(/H_2)	O_2	–	N_2	298	1.00	0.70–1.60
Liu (2019) [99]	OPSF	LBV	5/5/26	NH_3	O_2	–	–	298	0.50–1.60	0.40–1.75
Mei (2019) [33]	OPSF	LBV	7/7/51	NH_3	O_2	–	N_2	298	1.00–5.00	0.60–1.50
D. Wang (2020) [100]	OPSF	LBV	9/9/51	NH_3	O_2	–	–/N_2	303–393	0.99	0.60–1.40
S. Wang (2020) [15]	HFB	LBV	5/5/67	NH_3/H_2	O_2	–	N_2	298	0.99–4.93	0.60–1.60
Lhuillier (2020) [101]	OPSF	LBV	40/40/265	NH_3(/H_2)	O_2	–	N_2	298–473	0.99	0.80–1.40
Shrestha (2021) [41]	OPSF	LBV	25/25/112	NH_3(/H_2)	O_2	–	N_2/He	470–476	0.99–9.43	0.80–1.40
Mei (2021) [42]	OPSF	LBV	7/7/40	NH_3/H_2	O_2	–	N_2	298	1.00–10.00	0.70–1.40
N. Wang (2021) [102]	OPSF	LBV	5/5/28	NH_3(/H_2)	O_2	–	N_2	360	0.99–4.93	0.50–1.50
Osipova (2021) [103]	BF	LBV	1/1/9	NH_3/H_2	O_2	–	N_2	368	1.00	0.70–1.50
Gotama (2022) [37]	OPSF	LBV	2/2/14	NH_3/H_2	O_2	–	N_2	298	0.99–4.93	0.80–1.80
Subtotal:			**129/129/850**							
Bian (1991) [104]	BSF	c_{flame}	2/4/60	NH_3/H_2	O_2	–	Ar	400	0.05	0.12–1.00
Vandooren (1992) [105]	BSF	c_{flame}	1/12/215	NH_3/H_2	O_2	–	Ar	576	0.05	1.91
Duynslaegher (2009) [106]	BSF	c_{flame}	8/48/1824	NH_3/H_2	O_2	–	Ar	417–474	0.05–0.12	0.90–1.07
Osipova (2021) [103]	BSF	c_{flame}	4/28/784	NH_3/H_2	O_2	–	Ar	368	1.00	0.80–1.20
Subtotal:			**15/92/2883**							

Reference	App.[a]	Meas.[b]	XML/Ds./Dp.[c]	Fuel	Ox.[d]	Dopant	Diluent	*T* / K	*p* / atm	Φ
Total:			**258/481/6954**							

[a]: Apparatus, [b]: Measured quantity [c]: Number of XML files/datasets/data points, [d]: Oxidizer.

Table 3. Indirect experiments on $NH_3/CO/O_2$, NH_3/syngas/O_2 systems, and the experimental conditions. Note, that in the case of the flame experiments, the temperature and the pressure values refer to the states of the unburnt gas mixtures.

Reference	App.[a]	Meas.[b]	XML/Ds./Dp.[c]	Fuel	Ox.[d]	Dopant	Diluent	*T* / K	*p* / atm	Φ
Ding (2021) [53]	JSR	c_{out}	8/40/229	$NH_3/H_2/CO$	O_2	–	$N_2(/CO_2)$	900–1350	1.00	0.38–1.51
Subtotal:			**8/40/229**							
Wargadalam (2000) [82]	FR	c_{out}	1/2/18	NH_3/CO	O_2	–	N_2	873–1273	1.00	0.01
Subtotal:			**1/2/18**							
Han (2019) [14]	HFB	LBV	5/5/117	NH_3/CO	O_2	–	N_2	298	1.00	0.70–1.70
Han (2020) [16]	HFB	LBV	8/8/172	$NH_3/H_2/CO$	O_2	–	N_2	298	1.00	0.70–1.60
Mei (2020) [17]	OPSF	LBV	15/15/100	$NH_3/H_2/CO$	O_2	–	N_2	298	1.00–10.00	0.70–1.50
S. Wang (2020) [15]	HFB	LBV	18/18/230	$NH_3(/H_2)/CO$	O_2	–	N_2	298	1.00–5.00	0.70–1.60
Zhou (2021) [107]	OPSF	LBV	25/25/180	$NH_3/H_2/CO$	O_2	–	$N_2(/CO_2)$	298–423	1.00	0.70–1.42
Yin (2021) [108]	OPSF	LBV	9/9/82	$NH_3/H_2/CO$	O_2	–	N_2	298–443	1.00–3.00	0.70–1.60
Subtotal:			**80/80/881**							
Total:			**89/122/1128**							

[a]: Apparatus, [b]: Measured quantity, [c]: Number of XML files/datasets/data points, [d]: Oxidizer.

3.1.2.1. Indirect experimental data not utilized in this study

There are other papers in the literature which contain experiments with our target systems, but for some reasons, they are excluded from our investigations.

In the case of ST-IDT experiments, these excluded papers were published in the 1960s–1980s [109-120], and the measured ignition delay times are not reproducible due to the lack of unambiguous experimental details and/or IDT definitions. Moreover, as stated in the work of Chen et al. [86]: "The ignition delay times of ammonia have been reported since the 1960s–80s, however, those early shock tube studies present the undesirable repeatability and low experimental accuracy. Especially, the adsorption of ammonia on the contact surface of the stainless steel equipment was not considered which lead to large experimental uncertainty."

Mathieu et al. [121] investigated NH_3/syngas mixtures in their ST-IDT studies, but in those cases, NH_3 was present only as a trace species in the gas mixtures, and it was not a main component of the fuel. Since this kind of system is not the focus of this study, these results are excluded from the investigations presented here.

In the works of Manna et al. [91] and Sabia et al. [90], flow reactor experiments on NH_3 oxidation and pyrolysis can also be found in addition to the JSR experiments. However, according to the authors, these measurements "cannot be straightforwardly used for modeling activities. For this reason, simulations were performed considering the data from the JSR". Therefore, these measurements are not used in this study either. In the works of Nakamura et al. [31,122], a special kind of flow reactor (micro flow reactor) was used, the modeling of which is more complicated and not possible using our programs.

There are experimental publications whose results are not utilized also in the case of LBV measurements. In the work of Kumar and Meyer [10], the inlet conditions of the experiments are not published unambiguously; therefore, these results cannot be reproduced accurately by simulations. Moreover, they used the Bunsen burner method for the flame speed determination which suffers from stretch effects and heat loss [14], and the authors applied correction only for the heat loss. In the works of Li et al. [11], Takizawa et al. [8], Jabbour et al. [123], Pfahl et al. [124], Ronney [125], and Zakaznov et al. [126], the flames were affected by stretch effects, and no stretch correction was applied to calculate the real LBVs [15,86,96,97]. Davis et al. [127] investigated the oxidation of ammonia in a laboratory-scale version of an industrial combustor. They measured the maximal LBV of the investigated gas mixtures, so these experimental results are not used in this study.

Shmakov et al. [128] performed concentration measurements in $H_2/O_2/N_2$ burner stabilized flames doped with NH_3. However, NH_3 was present only in trace amounts (300–1000 ppm) relative to the main components of these gas mixtures, and therefore these data are not utilized in this work.

Bian et al. [104] carried out measurements in H_2/O_2/Ar burner stabilized flames doped with NH_3. The NH_3-contents of the mixtures were 3.0%–3.4%, and the H_2:NH_3 molar ratios were around 4:1–7:1. Therefore, NH_3 cannot be viewed as a trace component in these cases. A similar conclusion was drawn for the measurements of Vandooren et al. [105]. Hence, these measurements are included in the list of investigated experiments (Table 2).

According to Brackmann et al. [129], the burner stabilized flame measurements of the authors should be simulated by using a "stagnation flame reactor" model, but this kind of reactor is not implemented in the programs that we use for simulations. Therefore, these experiments are excluded from the scope of this work. In the works of Bian et al. [130], the experimental results are not published appropriately: instead of the discrete measurement points, curves are plotted in the graphs. Hence, these results cannot be utilized for quantitative mechanism comparison purposes. Dasch and Blint [131,132] investigated different $NH_3/O_2/N_2$ flames, but these flames are so-called "free flames", as opposed to burner stabilized flames, which cannot be simulated by the utilized computer programs.

3.2. Utilization of kinetic reaction mechanisms from the literature

Computer modeling of combustion systems is carried out by developing detailed reaction mechanisms that can describe the investigated system(s) and can be interpreted by an appropriate combustion simulation code. The aim of developing detailed reaction mechanisms is the accurate chemical kinetic description of combustion systems.

The introduction of a common format in which reaction mechanisms are published and can be interpreted by widely used simulation programs was necessary. This way, published reaction mechanisms could be used by any researcher that had an appropriate simulation package, which facilitated the development of combustion models. The so-called CHEMKIN reaction mechanism format was introduced ca. 35 years ago. It rapidly became widespread, and nowadays, most widely used combustion simulation packages can interpret mechanisms published in this format. In the ReSpecTh database [75], the reaction mechanisms are available in this format, too.

3.2.1. Parameters of a combustion kinetic model

The reaction mechanisms investigated in this study are published in CHEMKIN format, and they contain three fundamental kinds of parameters: thermodynamic and transport properties of the species, and the kinetic parameters that characterize the rates of the reactions. The details of the GAS-PHASE KINETICS part of the CHEMKIN reaction mechanism format can be found in the Theory Manual [133] and Input Manual [134] of the CHEMKIN version 4.0.2, and version 17.0 of the Chemkin Theory Manual of the ANSYS software developer company [135]. The model parameters are briefly discussed here based on these documents.

3.2.1.1. Thermodynamic parameters of species

To describe the temperature dependence of the thermodynamic parameters of the species, the standard isobar molar heat capacity of the species ($c_{p,\,i}^{\ominus}$ for species i) is defined. In principle, a polynomial of arbitrary degree could be used to describe the temperature dependence of the heat capacity. In the CHEMKIN formalism, the so-called NASA

polynomials [136,137] are applied for this purpose. A NASA polynomial defines the heat capacity as a polynomial of degree four in temperature (T):

$$\frac{c_{p,i}^{\ominus}}{R}(T) = a_{1,i} + a_{2,i}T + a_{3,i}T^2 + a_{4,i}T^3 + a_{5,i}T^4, \tag{2}$$

where a_1–a_5 are the polynomial coefficients (parameters of the model) and R is the gas constant (8.314 J mol^{-1} K^{-1}). From this, the standard molar enthalpy of formation ($H_i^{\ominus}$) and standard molar entropy ($S_i^{\ominus}$) can be parameterized as:

$$\frac{H_i^{\ominus}}{RT}(T) = a_{1,i} + \frac{a_{2,i}}{2}T + \frac{a_{3,i}}{3}T^2 + \frac{a_{4,i}}{4}T^3 + \frac{a_{5,i}}{5}T^4 + \frac{a_{6,i}}{T}, \tag{3}$$

$$\frac{S_i^{\ominus}}{R}(T) = a_{1,i}\ln T + a_{2,i}T + \frac{a_{3,i}}{2}T^2 + \frac{a_{4,i}}{3}T^3 + \frac{a_{5,i}}{4}T^4 + a_{7,i}, \tag{4}$$

where a_6 and a_7 are integration constants.

Hence, these three standard thermodynamic functions are parameterized using the seven coefficients, $a_{1,i}$–$a_{7,i}$, for each species i. If these three quantities are known (the coefficients are known), then any other thermodynamic quantity can be computed at any temperature and pressure using fundamental thermodynamic equations [135,138].

3.2.1.2. Temperature and pressure dependence of the rate coefficient

In gas-phase systems at high temperature, the temperature dependence of the rate coefficient is parameterized by the so-called *extended Arrhenius equation*:

$$k(T) = A \cdot T^n \cdot \exp\left(-\frac{E}{RT}\right), \tag{5}$$

where A, n, and E are called Arrhenius parameters. This kind of parameterization is used in CHEMKIN-format mechanism files.

The rate coefficient may also depend on the pressure. In reaction mechanisms, several conventions may be used to describe the pressure dependence of the rate coefficient. These are the Lindemann model [139], Troe parameterization [140,141], SRI parameterization [142], PLOG formalism [143], and Chebyshev polynomials [144,145]. They can be used for different kinds of reactions. A more detailed description of these formulations can be found in Chapter 2 of the book of Turányi and Tomlin [48].

It is sometimes possible that two or more reactions have the same set of reactants and products, but the reactions proceed through completely different pathways (channels). In these cases, it may be appropriate to include the same reaction equation in one mechanism twice but with different rate parameter sets. To comply with the criteria of the CHEMKIN format, a "DUP" or "DUPLICATE" keyword must be provided after each instance of the same reaction equation in the mechanism file. The rate coefficient of this kind of reactions is computed as the sum of the individual rate coefficients of all reaction channels at the given temperature and pressure.

3.2.1.3. Transport parameters of species

From the transport parameters of each species, the viscosity, coefficient of thermal conductivity, and diffusion coefficient of the species can be computed. The parameters for each species are the geometry index (0 for atoms, 1 for linear molecules, and 2 for nonlinear molecules), Lennard-Jones parameters, dipole moment, polarizability, and rotational relaxation collision number. These data are required for one- or more dimensional simulations (e. g., for modeling laminar premixed flames) but not needed for zero-dimensional computations such as ignition delay time simulations.

3.2.2. Detailed reaction mechanisms investigated

In this section, reaction mechanisms collected from the literature and investigated in this study are presented. These mechanisms were published not prior to 2009. Their selected features are summarized in Table 4, and their main target systems are listed in Table 5.

Some of the mechanisms aim to describe more complex combustion systems than NH_3/syngas oxidation (Table 5). For instance, the target system of the original Konnov-2021 model is methane/formic acid flames, and it contains 235 species with 3038 reactions. Therefore, a large part of the model is irrelevant for the modeling of NH_3/syngas combustion. The inclusion of these reactions and species in the mechanism does not influence the model predictions for NH_3/syngas systems, but it increases the computational time substantially, particularly in the case of 1D simulations. Hence, the following reductions of the original mechanisms were applied before the simulations to decrease the computational effort:

- For NH_3/H_2 fuel mixtures: All species (and the corresponding reactions) were removed from the mechanisms that contain an atom other than H, O, N, and noble gases. Noble gases, mostly Ar, are often used as diluents (see Table 2) and may participate in reactions as third body colliders. The numbers of species and reactions that remained in the models after this kind of reduction are listed in the "H/O/N part" column in Table 4.
- For NH_3/syngas fuel mixtures: In addition to the species and reactions included in the H/O/N part, those species (and the corresponding reactions) were also included in the mechanisms that contain a maximum of one carbon atom (such as CO, CO_2, or HCN). The numbers of species and reactions that remained in the models after this reduction are listed in the "H/O/N + C1 part" column in Table 4.

As it was mentioned previously (see Section 3.1.2), mechanisms that do not contain a wet CO submechanism cannot be used for the simulation of those experiments in which the inlet gas mixture contains CO. Table 4 shows that out of the 19 investigated mechanisms, six do not contain wet CO submechanism; therefore, these mechanisms can only be used for the simulation of the experiments with NH_3 and NH_3/H_2 fuels.

In a few measurements, He was used as the diluent gas instead of N_2 or Ar (Table 2). Since He is not applied frequently as a diluent, not all of the mechanisms contain the species He. Four mechanisms cannot be used for the simulations of those experiments in which He is included in the initial gas mixtures.

Table 4. Detailed reaction mechanisms investigated in this study and their selected features. The mechanisms are listed in chronological order (years in the mechanism IDs refer to the publication year of the corresponding mechanism).

Mechanism ID	H/O/N part		H/O/N + C1 part		Wet CO submechanism	He species	OH* submechanism	Ref.
	Species	Reactions	Species	Reactions				
Tian-2009	31	191	60	508	✓	✗	✗	[146]
Mathieu-2015	33	159	52	273	✓	✓	✓	[38]
GDFKin-2016	22	124	45	350	✓	✗	✗	[147]
Nakamura-2017	34	229	–	–	✗	✓	✓	[31]
SanDiego-2018[a]	21	64	33	129	✓	✓	✗	[148]
Otomo-2018	32	213	–	–	✗	✓	✓	[32]
Glarborg-2018	33	211	80	674	✓	✓	✓	[44]
Okafor-2018	25	101	46	262	✓	✗	✗	[149]
ELTE-2020	34	214	–	–	✗	✓	✓	[150]
POLIMI-2020	31	203	–	–	✗	✓	✗	[34,151]
NUIG-2020[b]	37	231	43	253	✓	✓	✓	[152]
Han-2020	32	163	35	177	✓	✓	✓	[16]
Mei-2020	34	237	38	255	✓	✓	✓	[17]
Konnov-2021	36	295	80	858	✓	✓	✓	[153]
KAUST-2021	34	262	–	–	✗	✓	✓	[36]
Shrestha-2021	33	262	63	609	✓	✓	✓	[41]
Mei-2021	35	239	39	257	✓	✓	✓	[42]
Zhou-2021	32	187	34	197	✓	✗	✓	[107]
Gotama-2022	32	165	–	–	✗	✓	✓	[37]

[a]: The mechanism is composed of the 2016/12/14 version of hydrocarbon oxidation and the 2018/07/23 version of the nitrogen chemistry sub-mechanism by the Combustion Research Group at the University of California.
[b]: The updated detailed kinetic mechanism of the authors was used because the indirect experiments investigated in this study were not used for constructing the skeletal mechanism by the authors.

Table 5. Original main target systems of the detailed kinetic mechanisms investigated in this study.

Mechanism ID	Main target system	Reference
Tian-2009	Speciation in premixed $NH_3/CH_4/O_2/Ar$ BSFs at low *p*	[146]
Mathieu-2015	Oxidation of NH_3 at high *T* and related NO_x chemistry (mostly ST-IDT experiments)	[38]
GDFKin-2016	NO formation in premixed alkane BSFs at low *p*	[147]
Nakamura-2017	Speciation in NH_3/air flames at atmospheric *p*	[31]
SanDiego-2018	NO_x emission in hydrocarbon flames	[148]
Otomo-2018	LBVs and IDTs during NH_3 and NH_3/H_2 oxidation	[32]
Glarborg-2018	Comprehensive N-chemistry model during the combustion of light hydrocarbons and fuel-N species (HCN, NH_3, HNCO)	[44]
Okafor-2018	LBV of CH_4/NH_3/air flames	[149]
ELTE-2020	Modeling of the combustion of $H_2/O_2/NO_x$ mixtures	[150]
POLIMI-2020	Comprehensive NH_3 pyrolysis and oxidation model	[34,151]
NUIG-2020	Comprehensive syngas/NO_x combustion model	[152]
Han-2020	LBVs of premixed NH_3/syngas/air flames	[16]
Mei-2020	LBVs of premixed NH_3/syngas/air flames up to 10 atm	[17]
Konnov-2021	LBVs of premixed CH_4/HCOOH/air flames	[153]
KAUST-2021	Comprehensive NH_3 and NH_3/H_2 oxidation model	[36]
Shrestha-2021	LBVs of NH_3/O_2-enriched air flames and NH_3/H_2/air flames up to 10 bar and 473 K	[41]
Mei-2021	LBVs of premixed $NH_3/H_2/N_2$/air flames up to 10 atm	[42]
Zhou-2021	LBVs premixed NH_3/(bio)syngas/air flames up to 423 K	[107]
Gotama-2022	LBVs of premixed NH_3/H_2/air flames	[37]

One more aspect of the mechanisms needs to be considered when they are used for the simulations of ST-IDT measurements. Ignition delay times measured in shock tubes are usually determined based on the concentration profile of a species in the gas mixture. This species is very often a reactive radical in excited state; in the case of NH_3/syngas combustion, the excited OH radical (OH*). This kind of IDT definition was used in the works of Mathieu and Petersen [38], Shu et al. [80], and Chen et al. [86]. In Table 2, however, we can see that six mechanisms do not contain the OH* species and its reactions (OH* submechanism). With these mechanisms, the reproduction of these ST-IDT measurements is not possible. To overcome this issue, the OH* submechanism of the syngas combustion mechanism of Kéromnès et al. [154] was added to the mechanisms that lack this part, and the ST-IDT simulations were carried out using these modified mechanisms. This OH* submechanism was also included in the optimized syngas combustion model of Varga et al. [155]. This submechanism was chosen for this purpose because the Varga et al. model is the best syngas

combustion mechanism published no later than 2016 and it was constructed using an optimization method on a large set of experimental data. Also, this mechanism was developed in the Chemical Kinetics Laboratory at ELTE, so this choice facilitates the hierarchical mechanism development strategy of the group.

Although the Tian-2009 model included the carbon atom species (C) and its reactions, its thermochemical data were not included in the THERMO file of the mechanism. Therefore, for NH_3/syngas simulations with this mechanism, the thermochemical data of C were taken from the Glarborg-2018 model.

Finally, note that the list of mechanisms in Table 4 is not exhaustive; there are many other mechanisms available in the literature, such as [29,30,33,39,40,156-162], that can be used to simulate NH_3/syngas combustion systems. However, they were not selected among the investigated models because a) they have gone through one or more updates since their publication and the latest updated version is investigated in this study, b) their focus is a different system from our target systems, and/or c) they are reduced mechanisms developed for a specific system. Although the selection of the mechanisms for investigation was somewhat arbitrary, the list of investigated mechanisms is suitable to serve as the basis for further model developments.

Like in Section 3.1.2 for the indirect experiments, the literature review of reaction mechanisms that can describe the combustion of NH_3/syngas mixtures finished on the 18th of January, 2022. Mechanisms published after this date on this topic are not investigated in this paper.

4. Applied computational methods

4.1. Simulation of gas-phase combustion systems

To be able to compare the performance of different combustion mechanisms, first, we have to perform simulations with the mechanisms on the target experimental systems. These simulations were carried out with the help of the *Optima++* program package [79] developed in the Chemical Kinetics Laboratory at ELTE. The version of Optima++ available on [79] can be executed from the command line. The current version (v2.3.0) of *Optima++* is compatible with *CHEMKIN-II* (CKII) [163], *FlameMaster* (FM) [164], *OpenSMOKE++* (OS) [165-168], *Cantera* [169], and *ZERO-RK* [170] simulation packages. In this study, *OpenSMOKE++* (version 0.12.0) was used for the simulations.

The necessary input files (CHEMKIN-format mechanism file and RKD-format XML file) have been discussed in Sections 3.1.2 and 3.2.1. In the first step, *Optima++* creates an appropriate binary file from the mechanism file that can be interpreted by the solver. After that, *Optima++* reads the experimental data file(s) provided by the user and prepares the necessary input files for the solver. Then, the solver performs the requested simulation(s), and the results of the simulation(s) are printed in a plain text output file by *Optima++*.

There are various reactor models available in *OpenSMOKE++* that can be used for modeling the investigated experiments. Table 6 lists the reactor models of *OpenSMOKE++* that were used in this study for different experiment types. Application of different simulation settings for the same experiment type was determined based on instructions of the authors of the publications. Since this kind of information was sometimes missing from the publications or it was not complete, personal communication was often necessary with the authors to clarify the details of the simulations.

Most JSR experiments (Section 3.1.1.1) were simulated using the isotherm–isobar Perfectly-Stirred-Reactor model of *OpenSMOKE++*, which is the most common approach for this kind of measurement. In the case of isotherm simulations, the energy balance equation of the system is not considered during the solution of the system of differential equations. However, Manna et al. [91] and Sabia et al. [90] recommended that their JSR experiments should be simulated assuming heat exchange with the external environment. They recommended a global heat exchange coefficient $U = 3.5 \cdot 10^{-3}$ cal cm^{-2} K^{-1} s^{-1}, and therefore this value was used also in our simulations.

Table 6. The reactor models of *OpenSMOKE++* used for the simulations.

Experiment	Solver	Reactor settings	Experiments
ST-IDT	Batch-Reactor	adiabatic–isochor	[38,80,86]
		adiabatic–isobar	[85]
JSR	Perfectly-Stirred-Reactor	isotherm–isobar	[34,36,53,89,92]
		adiabatic–isobar	[90,91]
FR (*c*–*t*)	Batch-Reactor	isotherm–isobar	All such experiments.
FR (c_{out})	Plug-Flow-Reactor	isotherm–isobar	All such experiments.
LBV	PremixedLaminarFlame1D	@Soret true;[a] @Radiation true;[b] @GradientCoefficient 0.01;[c] @CurvatureCoefficient 0.01;[d]	All such experiments.

[a]: Soret effect (thermal diffusion) is considered.
[b]: Radiative heat transfer between the flame and the environment is considered.
[c, d]: Parameters that control the number of grid points inserted in regions of high temperature and species mass fraction gradient and curvature, respectively. Lower parameter values mean more grid points to be used, so the computation is more accurate [171].

As it was mentioned in Section 3.1.1.1, in flow reactor experiments, authors sometimes publish the experimentally measured temperature profiles along the axis of the flow tube. This was the situation in the experiments of Song et al. [30] and Stagni et al. [34]. In these cases, the energy balance equation was turned off during the simulations and the given temperature profiles were considered along the reactor tube. In all other FR (c_{out}) experiments, the temperature of the preheated inlet gas mixture was used as the constant temperature for the simulations.

Numerical solution of spatially 0D experiments is relatively easy, but 1D (premixed flame) simulations require much more computational effort. The reason for this is that the stationary solution of a partial differential equation has to be found as the physical-chemical properties are not only a function of time but also that of one spatial coordinate. To find this stationary solution, a reasonable initial guess of the solution has to be provided in the case of some solvers such as *FlameMaster*. An initial guess is the solution of a previously performed flame simulation that the solvers produce after each successful 1D computation. Instead of looking for a continuous solution as a function of the distance from the burner plate, solvers perform the computations on grid points and look for a stationary solution for each grid point. A solution file contains the stationary values of the physical–chemical quantities (temperature, concentrations, etc.) at each grid point.

In contrast to FM, OS can perform the 1D simulations without the initial estimations ("start from scratch"), though in this case, the simulation time may increase significantly. Hence, in the case of OS, it has to be decided whether initial solutions are used for the flame simulations. To decide, we have to consider that a good initial estimation has the following features:

- It has to be a solution for a system as similar to our target system as possible.
- It is advantageous if the original simulation was carried out with the same mechanism as the one with which we would like to perform the simulation.

If these conditions are not met, simulations may take much longer than starting from an empty database, and/or the number of converged simulations may decrease as compared to the "empty database" case. Therefore, for each mechanism, all flame simulations were started from an empty database. In this run, the majority of simulations converged for all mechanisms. Then, failed simulations were repeated using the previously obtained converged solutions with the same mechanisms. This was repeated a few times for each mechanism until the number of failed simulations did not decrease more. If there were still unsuccessful simulations, they were restarted using a solution file obtained for the same system but with a different mechanism. Applying this procedure, almost all flame calculations converged with all investigated mechanisms.

Flame simulations were carried out by applying approximately 600 grid points, which ensured the required accuracy, and at the same time, simulations did not consume too much time.

4.2. Quantitative performance comparison of reaction mechanisms

The goodness of a mechanism is usually characterized by how accurately it can reproduce the results of indirect measurements. It is advantageous to use a quantitative method for the assessment of mechanism performance, especially if we work with a large set of experimental data points and we want to compare the performance of several models. The method applied in this study for mechanism comparison has been utilized in the Chemical Kinetics Laboratory of ELTE for various combustion systems [47,84,150,155,172-179]. At the moment, a new version of *Optima++* is being developed in the research group which has a graphical user interface and is capable of performing the quantitative comparison of reaction mechanisms. The author of this thesis actively participated in the development of the mechanism comparison part of the program by testing it and suggesting improvements to make it more flexible and user-friendly. All performance comparisons were carried out using this development version of *Optima++*.

4.2.1. The error function

Let us have N indirect experimental datasets utilized in the mechanism comparison. These datasets are stored in N_{XML} experimental data files. $N \geq N_{\mathrm{XML}}$ always, because one data file may contain more than one dataset; for example, the concentrations of several species can be measured during a flow reactor experiment. Let the i-th dataset consist of N_i data points and let $N_{\mathrm{ds},i}$ denote the number of datasets in the data file to which the i-th dataset belongs. The overall error of mechanism predictions relative to experimental results is described by the *averaged error function* as follows:

$$E = \frac{1}{N_{\mathrm{XML}}} \sum_{i=1}^{N} \frac{1}{N_i} \cdot \frac{1}{N_{\mathrm{ds},i}} \sum_{j=1}^{N_i} \left(\frac{Y_{ij}^{\mathrm{sim}} - Y_{ij}^{\mathrm{exp}}}{\sigma\left(Y_{ij}^{\mathrm{exp}}\right)} \right)^2, \tag{6}$$

where

$$Y_{ij} = \begin{cases} y_{ij} & \text{if } \sigma\left(y_{ij}^{\mathrm{exp}}\right) \approx \text{constant} \\ \ln y_{ij} & \text{if } \sigma\left(\ln\left(y_{ij}^{\mathrm{exp}}\right)\right) \approx \text{constant} \end{cases} \tag{7}$$

where y_{ij}^{exp} and $\sigma\left(y_{ij}^{\mathrm{exp}}\right)$ are the j-th data point in the i-th dataset and its standard deviation, respectively. The same applies to the logarithms. The corresponding y_{ij}^{sim} (or $\ln y_{ij}^{\mathrm{sim}}$) value is

the simulation result for that data point. If an absolute error belongs to the measured (experimental) data point, that is, the error is independent of the magnitude of the y_{ij}^{exp} value within the dataset, $Y_{ij} = y_{ij}$ is taken in equation (6) for both the experimental and simulation results. This is the case for some laminar burning velocity measurements. If, however, a relative error describes the data point, that is, the absolute error is linearly proportional to y_{ij}^{exp} within the dataset, $Y_{ij} = \ln y_{ij}$ is taken. This is true for ignition delay time and most concentration measurements, as will be discussed in Section 4.2.3. The error function can also be defined for each experimental data file (E_{XML}), dataset (E_i), and data point (E_{ij}) as follows:

$$E_{\mathrm{XML}} = \sum_{i \in \mathrm{XML}} \frac{1}{N_i} \cdot \frac{1}{N_{\mathrm{ds},i}} \sum_{j=1}^{N_i} \left(\frac{Y_{ij}^{\mathrm{sim}} - Y_{ij}^{\mathrm{exp}}}{\sigma\left(Y_{ij}^{\mathrm{exp}}\right)} \right)^2, \tag{8}$$

$$E_i = \frac{1}{N_i} \sum_{j=1}^{N_i} \left(\frac{Y_{ij}^{\mathrm{sim}} - Y_{ij}^{\mathrm{exp}}}{\sigma\left(Y_{ij}^{\mathrm{exp}}\right)} \right)^2, \tag{9}$$

$$E_{ij} = \frac{Y_{ij}^{\mathrm{sim}} - Y_{ij}^{\mathrm{exp}}}{\sigma\left(Y_{ij}^{\mathrm{exp}}\right)}. \tag{10}$$

We assume that the experimental data follow normal (Gaussian) distribution; therefore, the function E has a chi-square distribution, and because of the normalization by N_{XML} and $N_i \cdot N_{\mathrm{ds},i}$, its expected value is one. Hence, E follows a *reduced chi-square distribution*. $E = 1$ means that the average deviation between the model predictions and experimental data is equal to the scatter (the standard deviation) of the experimental data. In principle, the value of E can be smaller than one, but in practice and in the case of a large number of data points, it rarely happens. A smaller E value means a better mechanism performance. From this, it also follows that if $E \leq 4$ or ≤ 9, then the model can reproduce the measurement results within their 2σ or 3σ uncertainty limits, on average, respectively.

In the above equations, the deviation between Y_{ij}^{sim} and Y_{ij}^{exp} is normalized by the standard deviation of the corresponding data point. It is necessary to include it in the formulae so as not to overweight experimental data determined with large uncertainty. The procedure how $\sigma\left(Y_{ij}^{\mathrm{exp}}\right)$ is determined is discussed in Section 4.2.2.

4.2.2. Estimation of the standard deviation of experimental data

Because equation (6) is used to compare the performance of the investigated mechanisms, the standard deviations of the experimental data are needed to know. To estimate the standard deviation of data point j in the i-th dataset, both the experimental standard deviation ($\sigma_{\mathrm{exp},ij}$) of the data point and the statistical scatter of the i-th dataset ($\sigma_{\mathrm{fit},i}$) are considered as follows:

$$\sigma_{ij} = \sqrt{\sigma_{\mathrm{fit},i}^2 + \sigma_{\mathrm{exp},ij}^2}\,. \tag{11}$$

Aspects of the experimental standard deviations are discussed in Section 4.2.3, while the method to estimate the statistical scatter is summarized in this section. The $\sigma_{\mathrm{fit},i}$ term stems from the statistical scatter of the data points around a trendline fitted to the dataset. To estimate $\sigma_{\mathrm{fit},i}$, the *Minimal Spline Fit* program of Tibor Nagy [180,181] was used. On the webpage of the ReSpecTh database, Version January 5 (2020) of the program is available.

From now on, the indices i and j will not be used for the standard deviations to simplify the notations, so the statistical, experimental, and overall standard deviations of a data point will simply be referred to as σ_{fit}, σ_{exp}, and σ, respectively.

Let us assume that we have a dataset composed of (x_i, y_i) data points (i = 1, …, N). The program performs the least-squares fitting of polynomials with increasing order (n = 0, 1, 2, …) and that of Akima splines [182] with an increasing number of control points (n = 3, 4, 5, …), also called *knots* to the dataset. Akima splines are functions composed of cubic polynomials between the control points, and they are continuously differentiable at the control points. Though the fitting of polynomials is simple and fast, the application of splines has some advantages. In the case of higher-order polynomials, the fitted curve often shows unnatural oscillation, which can be eliminated by using splines. Besides that, more precise fits can be achieved by splines than polynomials.

The program also computes the standard deviation (noise) of the dataset based on the fitted curves. Using goodness-of-fit measures provided by the program and visual inspection of the fitted curves, we can identify the curve that describes the trend of the experimental dataset (the “noise-free” data) best. We can estimate the statistical standard deviation of the dataset by the standard deviation corresponding to this optimal fit.

The fitting is performed by minimizing the root-mean-square deviation ($RMSD_{\mathrm{fit}}$) of the values of the fitting function ($y_{\mathrm{fit}}(x_i)$) from the input data (y_i):

$$RMSD_{\text{fit}} = \sqrt{\frac{1}{N} \cdot \sum_{i=1}^{N} [y_{\text{fit}}(x_i; \mathbf{p}) - y_i(x_i)]^2}, \tag{12}$$

where **p** is the parameter set to be optimized. In the case of a polynomial of degree n, the parameter set is the $n + 1$ coefficients, $\mathbf{p} = \{a_0, \ldots, a_n\}$, while in the case of a spline with n control points, the positions of the control points ($X_1, \ldots, X_n, Y_1, \ldots, Y_n$) are optimized, $\mathbf{p} = \{\mathbf{X}, \mathbf{Y}\} = \{X_1 \equiv x_1, \ldots, X_n \equiv x_N, Y_1, \ldots, Y_n\}$. As can be seen, in the latter case, the first and the last control points are fixed at x_1 and x_N, respectively. Therefore, the number of parameters of the fitting function, p, is $p = n + 1$ in the case of polynomials, while it is $p = 2n - 2$ in the case of splines. The number of degrees of freedom, ν, is

$$\nu = N - p. \tag{13}$$

The quantity $RMSD_{\text{fit}}$ is not the appropriate metric for estimating the standard deviation of the dataset because it does not take into account the number of degrees of freedom of the fit. For this purpose, the standard deviation of the fit (σ_{fit}) can be used:

$$\sigma_{\text{fit}} = \sqrt{\frac{N}{\nu}} \cdot RMSD_{\text{fit}}, \tag{14}$$

The program also helps to decide which model describes the experimental data best by providing the so-called *Akaike information criterion* values (*AIC*) [183]:

$$AIC = 2p + N + N \cdot \ln\left(\frac{2\pi \cdot RMSD_{\text{fit}}^2}{N}\right), \tag{15}$$

which penalizes underfitting as well as overfitting. The lower the *AIC* value, the better the model. However, when the number of data points is small ($N \lesssim 2p^2$), the corrected *AIC* value (*AICc*) gives a better metric for the goodness-of-fit [184-186]:

$$AICc = AIC + \frac{2p(p+1)}{N - p - 1}. \tag{16}$$

When $N >> 2p^2$, the *AICc* value converges to *AIC*.

Equation (12) can be used to estimate the $RMSD_{\text{fit}}$ if we assume that the experimental data follow Gaussian (normal) distribution. In this case, the measured data can be characterized by an absolute error and σ_{fit} gives this absolute estimated standard deviation according to equation (14). However, as it was mentioned in Section 4.2.1, in some cases, the data can be characterized by a relative error. If the relative error is small, that is,

$y_{\mathrm{fit}}(x_i; \mathbf{p}) / y_i(x_i) \approx 1$, this is approximately equivalent to saying that the original data follow lognormal distribution. In this case, the $\{y_i\}$ data are transformed to $\ln\{y_i\}$, and the $RMSD_{\mathrm{fit}}$ is calculated on the transformed data as follows (cf. equation (12)):

$$RMSD_{\mathrm{fit}} = \sqrt{\frac{1}{N} \cdot \sum_{i=1}^{N} \left[\ln\left(y_{\mathrm{fit}}(x_i; \mathbf{p})\right) - \ln\left(y_i(x_i)\right)\right]^2}. \qquad (17)$$

The σ_{fit} value that is calculated according to equation (14) and using the $RMSD_{\mathrm{fit}}$ in equation (17) corresponds to the estimated standard deviation of the transformed data which we assume to follow Gaussian (normal) distribution. It estimates the relative error of the dataset, as long as the relative error is not too large, which we assume in all cases. Note, that if equation (17) is applied for the estimation of $RMSD_{\mathrm{fit}}$, then the zero concentration values must be excluded from the dataset for the fitting.

Note that the program also allows us to transform the $\{x_i\}$ values to estimate the standard deviation of the dataset. This was applied in the case of ignition delay time (τ) measurements, where $\log \tau$ data are usually plotted against the inverse temperature (T^{-1}) [38,121,160,187-190].

It is important to note that even though the *AICc* values and the computed relative probabilities facilitate choosing the optimal model, in some cases, the predicted optimal model seems incorrect based on the visual inspection of the dataset and the fitted curve. Therefore, the *Minimal Spline Fit* program also prepares plots of the experimental data and the fitted curves with the help of *Gnuplot*. For this reason, the visual inspection of the data and the fitted curves is always recommended, but therefore the estimation of the statistical scatter of datasets is a time-consuming task.

An example of the estimation of the standard deviation of a dataset can be seen in Figure 11 and the corresponding statistics are summarized in Table 7. They show the results of an outlet concentration measurement performed by Osipova et al. [92] in a jet stirred reactor. The target species is NH_3, and its outlet concentration is measured as a function of the temperature of the reactor. In this case, we assume that the experimental data have a constant relative error (see Section 4.2.3.2); therefore, the fitting is carried out on the logarithmically transformed data. The mole fraction of NH_3 in the initial gas mixture is $2 \cdot 10^{-3}$ in all experiments. The bath gas is Ar, and the oxidizer is O_2 whose concentration is $1.5 \cdot 10^{-3}$ in mole fraction. There is essentially no ammonia conversion until around 1200 K, and above that temperature, the outlet ammonia concentration decreases rapidly.

Three curves are shown in this figure: two Akima splines, and one polynomial (this is the polynomial with the lowest *AICc* value). The polynomial cannot capture the trend of the experimental data below 1200 K due to the wiggling nature of polynomial functions. The Akima spline with $n = 7$ control points has the lowest *AICc* value (Table 7). It captures the constant ammonia concentration below 1200 K well, but it shows unnatural wiggles in the fall-off regime of the curve. Therefore, it is not the optimal model function (trendline) for this dataset despite its low *AICc* value. The Akima spline with $n = 4$ control points describes both the constant part and the fall-off part of the curve naturally, as we would expect it from a trendline. Hence, it is the ideal model function in this case. The standard deviation of this optimal fit is 0.073, which means a constant relative standard deviation of 7.3% stemming from the statistical scatter of the experimental data around a trendline.

The standard deviations of other datasets were estimated based on similar arguments as described above.

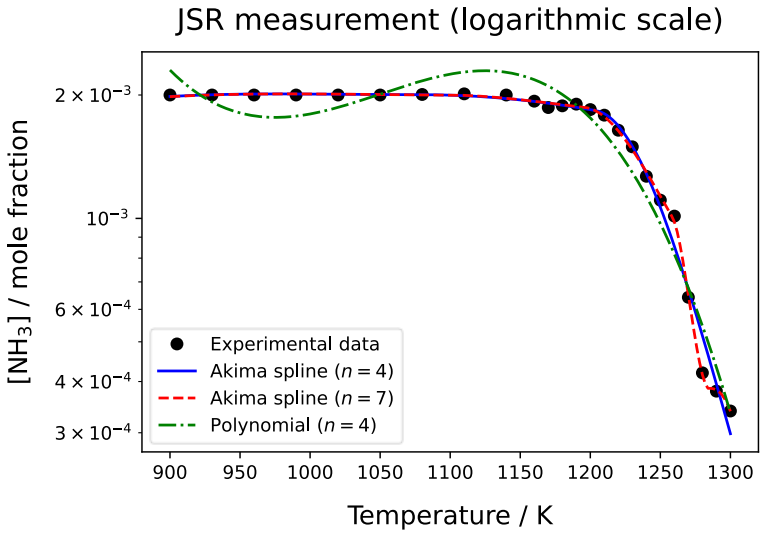

Figure 11. Estimation of the statistical scatter of an outlet concentration measurement in a jet stirred reactor. Experimental data are from the work of Osipova et al. [92].
The Akima spline with $n = 4$ control points was selected as the optimal fitting function.

Table 7. Statistics of the fitted curves from Figure 11. The Akima spline with $n = 4$ control points was selected as the optimal model function.

Fitting function	*n*	*v*	$RMSD_{fit}$	σ_{fit}	*AIC*	*AICc*
Akima spline	4	18	0.063	0.073	−128.5	−123.6
Akima spline	7	12	0.014	0.019	−190.8	−162.5
Polynomial	4	20	0.119	0.130	−102.5	−100.3

4.2.3. Standard deviations of different types of experimental data

In the preceding section, basic principles of the estimation of the statistical scatter of the experimental data were discussed. According to equation (11), the experimental error reported by the experimenters is also considered to calculate the overall σ for a data point. Also, the type of the experimental error (absolute or relative) is important because it determines which model (equation (12) or (17)) is used when the statistical scatter of the dataset is estimated. The aspects of the experimental errors are discussed in this section for each measured quantity. Note, that in most publications where experimental errors are reported, they refer to either the $\pm 2\sigma$ uncertainty limits or the 95% confidence intervals which are approximately equal to $\pm 2\sigma$ in the case of normal distribution. Therefore, unless otherwise stated, the published experimental uncertainties are considered as 2σ.

4.2.3.1. Ignition delay time measurements

In Table 8, the reported experimental errors are collected from the investigated ST-IDT measurement papers. Ignition delay time measurements typically have a constant relative error; therefore, equation (17) was used to estimate the $RMSD_{\text{fit}}$ and σ_{fit}. In the work of Davidson et al.[85], no experimental errors are reported. These measurements were performed at low pressure (< 20 atm), and in this case, the typical experimental uncertainty ($\pm 2\sigma$) is ±10%. Therefore, $\sigma_{\text{exp}} = 0.05$ was assigned to the missing experimental uncertainties.

The overall (relative) standard deviations (σ) of the transformed ST-IDT measurement datasets are summarized in Table A1, together with some selected experimental details.

Table 8. Experimental errors reported in the investigated shock tube ignition delay time measurement papers.

Reference	Apparatus	Error type	Error value (2σ)
Davidson (1990) [85]	ST	no error is reported	–
Mathieu (2015) [38]	ST	relative	10%
Shu (2019) [80]	ST	relative	20%
Chen (2021) [86]	ST	relative	20%

4.2.3.2. Concentration measurements

As can be seen in Tables 2 and 3, the concentrations of some species (listed in Table 10) are measured in JSR and FR experiments as a function of another quantity such as temperature. The concentrations of these species may be measured by various means, of which optical spectroscopy (usually in the infrared (IR) range) and gas chromatography (GC) were most frequently applied in the investigated experiments. Besides those techniques, mass spectrometry was also used in some cases (Table 9).

Table 9. Reported experimental error types of the investigated species concentrations measurements in jet stirred reactors (JSR) and flow reactors (FR).

Reference	Measured species	Measurement method	Error type
JSR			
Dagaut (2019) [89]	NH_3, NO, NO_2, N_2O, H_2O:	FT-IR	relative
Stagni (2020) [34]	NH_3: NO, NO_2:	cw-CRDS chemiluminescence anal.	relative
Sabia (2020) [90]	NO: H_2, O_2, N_2:	NDIR gas sensor GC	relative (with absolute minimum limit for NO)
Manna (2020) [91]	NO: H_2, O_2, N_2:	NDIR gas sensor GC	relative (with absolute minimum limit for NO)
Zhang (2021) [36]	NH_3, NO, N_2O, H_2O:	FT-IR	relative
Osipova (2022) [92]	NH_3, H_2O, H_2, N_2, O_2:	MS	no error is reported
Ding (2021) [53]	NO, CO: N_2O: H_2, O_2:	FT-IR + NDIR gas sensor FT-IR NDIR gas sensor	relative
FR			
Dean (1982) [93]	NH_3, NO:	chemiluminescence anal.	no error is reported
Hulgaard (1993) [81]	NH_3: NO: N_2O:	spectrophotometry NDUV gas sensor NDIR gas sensor	relative with absolute minimum limits
Caton (1995) [83]	NH_3, NO, N_2O:	FT-IR	no error is reported
Wargadalam (2000) [82]	NH_3, NO:	FT-IR	relative
Song (2016) [30]	NH_3, N_2O: O_2:	NDIR gas sensor GC	relative
Stagni (2020) [34]	NH_3, H_2O, N_2, O_2: NO: H_2:	MS chemiluminescence anal. GC	relative
Abián (2021) [94]	NH_3, N_2O, H_2, O_2: NO_2: NO:	GC chemiluminescence anal. NDIR gas sensor + chemiluminescence anal.	relative with absolute minimum limits

FT-IR = Fourier Transform Infrared spectroscopy,
cw-CRDS = continuous-wave cavity ring-down spectroscopy (it is based on IR absorption),
chemiluminescence anal. = chemiluminescence NO_x analyzer,
NDIR = non-dispersive ultraviolet,
NDUV = non-dispersive infrared,
GC = gas chromatography,
MS = mass spectrometry.

Table 10. Minimum overall relative and absolute errors defined for each species for concentration measurements in jet stirred and flow reactors.

Species	$\sigma_{\text{min}}^{\text{rel}}$	$\sigma_{\text{min}}^{\text{abs}}$ / ppm
NH_3	0.05 (5%)	5
NO	0.025 (2.5%)	5
NO_2	0.05 (5%)	5
N_2O	0.05 (5%)	5
H_2O	0.05 (5%)	5
H_2	0.025 (2.5%)	5
N_2	0.025 (2.5%)	5
O_2	0.025 (2.5%)	5
CO	0.025 (2.5%)	5

In these measurements, if the experimental uncertainty is published, it is always a relative error (Table 9). Therefore, constant relative error was assumed for the measured data points, that is, polynomials and splines were fitted to the logarithm of the data. The authors often publish a minimum absolute limit for the experimental error. It means that the absolute value of the error cannot be smaller than that limit. If it is smaller, the data point has an absolute error, which is important for small concentration values. To avoid using unrealistically small standard deviations, a minimum relative ($\sigma_{\text{min}}^{\text{rel}}$) and absolute standard deviation ($\sigma_{\text{min}}^{\text{abs}}$) were defined for each species based on previous experience from the literature (Table 10). These values helped to estimate the overall standard deviation (σ) of the datasets realistically.

For each dataset, the relative statistical scatter of the dataset was estimated using the program *Minimal Spline Fit* as described in Section 4.2.2. If the experimental standard deviation was reported in the publication, then equation (11) was used to estimate the overall standard deviation (σ) of the dataset. In some cases, both the statistical scatter and the experimental error were very small for a data point, and the resulting overall σ was smaller than $\sigma_{\text{min}}^{\text{rel}}$. If this happened, $\sigma_{\text{min}}^{\text{rel}}$ was taken as σ to avoid using unrealistically small standard deviations.

If the experimental standard deviation was not reported for the measurement, $\sigma_{\text{min}}^{\text{rel}}$ replaced σ_{exp} in equation (11) as follows:

$$\sigma = \sqrt{\sigma_{\text{fit}}^2 + \left(\sigma_{\text{min}}^{\text{rel}}\right)^2}, \tag{18}$$

which is inherently not smaller than $\sigma_{\mathrm{min}}^{\mathrm{rel}}$, so it was always accepted.

In a few cases, it was not possible to fit an appropriate model function to the dataset, for instance, because the number of data points in the dataset was too small. In these cases, if the experimental error was provided, $\sigma_{\mathrm{min}}^{\mathrm{rel}}$ was assigned to σ_{fit} in equation (11) as follows:

$$\sigma = \sqrt{\left(\sigma_{\mathrm{min}}^{\mathrm{rel}}\right)^2 + \sigma_{\mathrm{exp}}^2}. \tag{19}$$

If it was not provided, $\sigma_{\mathrm{min}}^{\mathrm{rel}}$ was assigned to both as σ_{fit} and σ_{exp}, so:

$$\sigma = \sqrt{2}\sigma_{\mathrm{min}}^{\mathrm{rel}}. \tag{20}$$

Let us denote the resulting relative σ value obtained using either equation (11), (18), (19), or (20) by σ^{rel}. For each data point, the absolute standard deviation was computed as (concentration value · σ^{rel}). If this value was not smaller than $\sigma_{\mathrm{min}}^{\mathrm{abs}}$ of the respective species, then σ^{rel} was accepted and relative error was considered for that data point. If it was smaller than $\sigma_{\mathrm{min}}^{\mathrm{abs}}$, $\sigma_{\mathrm{min}}^{\mathrm{abs}}$ was assigned to that data point and absolute error was considered.

From the previous arguments, it follows that data points within one dataset may have different error types (absolute or relative) in the case of concentration measurements. The overall absolute standard deviation values (or value ranges) are listed for each concentration dataset in Table A2 for JSR measurements and Table A3 for FR measurements, together with some selected experimental details of the corresponding experiments. These values (or value ranges) were obtained as follows. For all data points, the absolute values of the standard deviations were computed. If these values were the same for each data point within a dataset, that single value was assigned to the dataset and is written in the appropriate table. If these values were not uniform for each point of a dataset, then their range (minimum value–maximum value) is shown in the appropriate table.

Note that when the measured concentration of a species was zero, it was omitted from the relative error estimation, and $\sigma_{\mathrm{min}}^{\mathrm{abs}}$ of the respective species was assigned to that data point as an absolute error.

Finally, another concern arises when estimating the standard deviation of the logarithmically transformed concentration data, which is also discussed in the work of Kawka et al. [84]. It is not a good strategy to assign a relative error to concentration values that are relatively small within a dataset, because on the logarithmic scale, these data points would artificially be overweighted in the fitting process and bias the error function. Sometimes, if these points were included in the dataset in the model fitting process, no appropriate model

function could be found, but when these points were excluded, the other points could be described well by a model function. Therefore, concentration values that were more than ten times smaller than the largest value were sometimes excluded from the fitting process. A σ_{fit} value – that was calculated based on the relative standard deviation estimated using all the other data points in the dataset – was assigned as a relative error to these points.

4.2.3.3. Laminar burning velocity measurements

The very recent work of Zhang et al. [178] analyzes the experimental errors of laminar burning velocities measured by various experimental techniques including those that are used in the papers investigated in this study. The results of Zhang et al. [178] helped to estimate the standard deviations of laminar burning velocity measurements. The experimental publications can be divided into three cases based on how the experimental uncertainties are published. Table 11 shows which investigated publications belong to each case. The details of the three cases are discussed below.

Table 11. Categorization of laminar burning velocity measurement papers based on how experimental uncertainties are published.

Cases	Publication
Case 1:	Constant relative experimental error for each dataset – BF measurements: Osipova (2021) [103] – OPSF measurements: Lee (2010a) [95], Lee (2010b) [96]
Case 2:	Pointwise errors a) Absolute pointwise errors: – OPSF measurements: Hayakawa (2015) [97], Ichikawa (2015) [12], Mei (2019) [33], D. Wang (2020) [100], Mei (2021) [42], N. Wang (2021) [102], Gotama (2022) [37], Mei (2020) [17], Zhou (2021) [107], Yin (2021) [108] – HFB measurements: Han (2019) [14], Han (2020) [16], S. Wang (2020) [15] b) Relative pointwise errors: – OPSF measurements: Lhuillier (2020) [101], Shrestha (2021) [41]
Case 3:	No experimental error is published – BF measurements: Takeishi (2015) [98] – OPSF measurements: Liu (2019) [99]

BF = bunsen flame method
OPSF = outwardly propagating spherical flame method
HFB = heat flux burner method

- Case 1:

A constant relative experimental error is published for all data points within a dataset. In these cases, constant relative error was assumed for the dataset, and therefore equation (17) was used to estimate the $RMSD_{fit}$ and σ_{fit}. Consequently, all points within a dataset had the same relative error, while the absolute error values lay within a range.

- Case 2:

Pointwise absolute or relative experimental errors are published, that is, a different experimental error value (absolute or relative) is assigned to each data point within a dataset. In these cases, it is difficult to decide which error model should be applied to the dataset. Zhang et al. [178] reported that the measurements performed with the HFB method typically have a constant absolute error; therefore, equation (12) was used to determine the $RMSD_{fit}$ and σ_{fit} in these cases. In contrast, datasets obtained by the OPSF or BF methods have a constant relative error [178], so equation (17) was used for these data. There were two exceptions to these rules. In the OPSF measurements of Lhuillier et al. [101] and Shrestha et al. [41], relative errors are published for each data point. In these cases, the constant absolute error assumption seemed more appropriate based on the investigation of the error values.

If the experimental errors are published pointwise, the overall standard deviation (σ) is not uniform for a dataset.

- Case 3:

In some publications, the experimental errors are not reported. Zhang et al. [178] determined the typical standard deviations of laminar burning velocity measurements, they are

  - 1 cm / s absolute standard deviation for HFB measurements,
  - 5% relative standard deviation for OPSF measurements, and
  - 6% relative standard deviation for BF measurements.

These σ_{exp} values were assigned to experimental data points of this case and the corresponding error types were used to estimate the $RMSD_{fit}$ and σ_{fit}.

As can be seen in Table 11, only BF and OPSF measurements belonged to this case. For these methods, the constant relative error model was utilized, and therefore different absolute error value was assigned to each point within a dataset.

Note that in a few cases, it was not possible to fit an appropriate model function to the dataset, for instance, because the number of data points in the dataset was too small. In these

cases, the measurement-specific typical error values (see in the description of Case 3) were assigned to the σ_{fit} of the data points of the dataset.

Similarly to concentration measurements (see Section 4.2.3.2), both the experimental (σ_{exp}) and the statistical (σ_{fit}) standard deviations were very small for some data points. If this happened, the overall standard deviation (σ) of the data point was also very small. This may lead to a very high error function value for that data point, which would result in an artificially very high overall error function value. To avoid this, global minimum overall standard deviations were introduced [178]: a minimum relative standard deviation of $\sigma_{min}^{rel} = 1\%$, and minimum absolute standard deviation of $\sigma_{min}^{abs} = 0.5$ cm / s. The goal was to keep both the absolute value and the minimum value of the standard deviation of each point above these limiting values. This was achieved as described below.

For data points with a relative error, it was checked whether the corresponding σ was smaller than σ_{min}^{rel}. If it was not, the absolute value of the standard deviation was calculated as (LBV value $\cdot$ σ). If this value was greater than σ_{min}^{abs}, the overall relative σ was accepted, but if not, σ_{min}^{abs} as assigned to the data point. If σ was smaller σ_{min}^{rel}, the same procedure was carried out but using σ_{min}^{rel} as the relative σ.

For data points with an absolute error, first, the corresponding (σ / LBV value) relative standard deviation was calculated. If it was not smaller than σ_{min}^{rel}, it was checked whether the absolute σ was smaller than σ_{min}^{abs}. If it was not, the absolute σ was accepted, but if it was, σ_{min}^{abs} was assigned to the data point. If the (σ / LBV value) was smaller than σ_{min}^{rel}, σ was not accepted, and the (LBV value $\cdot$ σ_{min}^{rel}) absolute standard deviation was calculated. If it was not smaller than σ_{min}^{abs}, it was accepted as the absolute standard deviation, but if it was, σ_{min}^{abs} was assigned to the data point.

In Table A4, the overall absolute standard deviation values (or value ranges) are listed for the investigated datasets. These values (and value ranges) were obtained the same way as in the case of concentration measurements (see Section 4.2.3.2).

4.3. Local sensitivity analysis

As can be seen in Table 4, detailed chemical kinetic mechanisms are usually composed of several hundred or thousand reaction steps, which means that they contain a huge set of parameters. To further develop an existing model and to construct reduced reaction mechanisms that can be used for, e. g., computational fluid dynamics (CFD) calculations, we need to know which parameters of the model are important under various conditions. An input model parameter (for example, the preexponential factor of an Arrhenius equation) is considered important under a given circumstance if its change strongly influences the output of the mathematical model (for example, a computed laminar burning velocity, ignition delay time, or concentration). In other words, a parameter is *important* or *influential*, if a small alteration of its value results in a large change in the result computed with the model. To explore the importance of the model parameters under given conditions, one can apply the methods of *sensitivity analysis* [48], which can be divided into two groups: local and global sensitivity analysis methods. In my work, *local sensitivity analysis* is applied; therefore, only that is discussed here.

In the case of local sensitivity analysis, it is investigated how much the model prediction changes due to a small change in the value of a parameter from its nominal value. Let us denote the i-th model result by Y_i, and the j-th input model parameter by p_j. The partial derivative

$$s_{ij} \equiv \frac{\partial Y_i}{\partial p_j} \tag{21}$$

is called the first-order *local sensitivity coefficient*. The greater the absolute value of s_{ij}, the more influential the j-th model parameter on the i-th model result.

The local sensitivity coefficient calculated according to equation (21) has a dimension which is the dimension of the model result divided by that of the parameter. Therefore, it shows how much the model output changes in its appropriate unit due to a unit change in the value of the parameter. Since both model parameters and model results may have various units, the $\{s_{ij}\}$ coefficients also have different units, which means that the s_{ij} values cannot be compared to each other. To make the different sensitivity coefficients comparable to each other, we introduce the unitless *normalized local sensitivity coefficient*, defined as follows:

$$sn_{ij} \equiv \frac{p_j}{Y_i}\frac{\partial Y_i}{\partial p_j} = \frac{\partial \ln \tilde{Y}_i}{\partial \ln \tilde{p}_j}, \tag{22}$$

where $\tilde{Y}_i$ and $\tilde{p}_j$ are the dimensionless *i*-th model result and *j*-th parameter, respectively. The values of the $\{sn_{ij}\}$ coefficients are independent of the units of the model results and parameters, and according to this definition, ($sn_{ij} \cdot 100\%$) gives the percentage that the *i*-th model output changes due to a 1% change in the value of the *j*-th parameter. Consequently, the normalized sensitivity coefficients are comparable to each other.

Local sensitivity coefficients can usually be determined only numerically, and many numerical methods exist to determine them. The simplest method to obtain local sensitivity coefficients is the *brute force method* which uses the *finite difference approximation* as follows:

$$s_{ij} \approx \frac{Y_i' - Y_i}{p_j' - p_j} = \frac{\Delta Y_i}{\Delta p_j}, \tag{23}$$

where p_j' is the value of the *j*-th parameter after its original value (p_j) was changed (perturbed) by Δp_j, and Y_i' is the *i*-th model result obtained with the perturbed value of p_j. If equation (23) is inserted in the definition of the normalized sensitivity coefficient (equation (22)), we get

$$sn_{ij} \approx \frac{p_j}{Y_i} \cdot \frac{\Delta Y_i}{\Delta p_j} = \frac{p_j}{Y_i} \cdot \frac{Y_i' - Y_i}{p_j' - p_j} = \frac{p_j}{\underbrace{p_j' - p_j}_{f_{\text{pert}}}} \cdot \frac{Y_i' - Y_i}{Y_i} = \frac{1}{f_{\text{pert}}} \cdot \frac{Y_i' - Y_i}{Y_i}, \tag{24}$$

where f_{pert} is called the perturbation factor which gives how much the *j*-th parameter was changed relative to its original value. In this work, a constant perturbation factor is applied to compute local sensitivity coefficients of the kinetic parameters of the model.

Although the calculation of the sensitivity coefficients using the brute force method is simple, it may provide inaccurate coefficients. One reason for this is that equation (23) is accurate if there is a linear relationship between the model result and the parameter, but in the context of reaction kinetic models, it is rarely the case. The linear approximation is approximately valid only if the perturbation of the parameter is small. However, if the perturbation is too small, Y_i' and Y_i may be very close to each other, and so the obtained sensitivity coefficient will have a large relative error because computers can only store numbers up to a limited number of decimal digits. Consequently, to obtain reliable and accurate sensitivity coefficients, the parameter perturbation should be neither too large nor too small. In the case of kinetic parameters, $f_{\text{pert}} = 0.05$ is applied in this work, which corresponds to a 5% increase in the rate parameters, which is usually sufficient.

Even though normalized sensitivity coefficients are dimensionless, their direct comparison is difficult in the case of a large number of data points because their scaling is different. Therefore, to facilitate the evaluation of the results of the sensitivity analysis, let us rescale normalized sensitivity coefficients and define the *scaled normalized local sensitivity coefficient* ($\widetilde{sn}_{ij}$) as follows:

$$\widetilde{sn}_{ij} = \frac{sn_{ij}}{\max_j\{|sn_{ij}|\}}, \tag{25}$$

which means that sn_{ij} coefficients are computed for a given data point (Y_i) for all parameters ($\{p_j\}$), and each sn_{ij} value is divided by the one sn_{ij} value whose absolute value is maximal for that data point. Therefore, the resulting $\widetilde{sn}_{ij}$ values will be scaled into the [−1,1] interval. This way, we can say, for example, that parameter *j* is important for data point *i* if

$$|\widetilde{sn}_{ij}| \geq 0.1 \tag{26}$$

for that data point. This criterion can be applied to each simulation result.

4.3.1. Sensitivity analysis of thermodynamic parameters

Sensitivity analysis of the thermodynamic parameters of a model is performed in a slightly different way than it was described for the kinetic parameters (Section 4.2.3.3). Kovács et al. [191] performed local sensitivity analysis on thermodynamic parameters (see Section 3.2.1.1) of reaction mechanisms. Similar studies have been done by Turányi et al. [192], Zádor et al. [193], and Langer et al. [194] previously. The method of Kovács et al. [191] is used in this study for the sensitivity analysis of thermodynamic parameters. As discussed in Section 3.2.1.1, the temperature dependence of the thermodynamic properties of the species is described by NASA polynomials (equations (2)–(4)). For the better readability of the text, these equations are repeated here for species *k*:

$$\frac{c_{p,k}^{\ominus}}{R}(T) = a_{1,k} + a_{2,k}T + a_{3,k}T^2 + a_{4,k}T^3 + a_{5,k}T^4, \tag{27}$$

$$\frac{H_k^{\ominus}}{RT}(T) = a_{1,k} + \frac{a_{2,k}}{2}T + \frac{a_{3,k}}{3}T^2 + \frac{a_{4,k}}{4}T^3 + \frac{a_{5,k}}{5}T^4 + \frac{a_{6,k}}{T}, \tag{28}$$

$$\frac{S_k^{\ominus}}{R}(T) = a_{1,k}\ln T + a_{2,k}T + \frac{a_{3,k}}{2}T^2 + \frac{a_{4,k}}{3}T^3 + \frac{a_{5,k}}{4}T^4 + a_{7,k}\,. \tag{29}$$

We are interested in how much the three thermodynamic parameters, $c_{p,k}^{\ominus}$, $H_k^{\ominus}$, and $S_k^{\ominus}$, influence the model outputs; therefore, the following perturbations are applied separately:

– To investigate the sensitivity of $c_{p,k}^{\ominus}$: only $a_{1,k}$ is perturbed by an absolute value of +0.01, which is equivalent to a constant +0.08314 J / (mol K) shift of the $c_{p,k}^{\ominus}$, independent of temperature. Note, that the perturbation of $a_{1,k}$ influences the values of $H_k^{\ominus}$ and $S_k^{\ominus}$ as well, and this perturbation depends on temperature.

– To investigate the sensitivity of $H_k^{\ominus}$: only $a_{6,k}$ is perturbed by an absolute value of +3 K, which results in a constant +0.01 change in $a_{6,k} / T$ at 300 K. This causes a +24.79 J / mol shift of $H_k^{\ominus}$, independent of temperature.

– To investigate the sensitivity of $S_k^{\ominus}$: only $a_{7,k}$ is perturbed by an absolute value of +0.01; thus, the $S_k^{\ominus}$ values are shifted by a constant +0.08314 J / (mol K), independent of temperature.

Since absolute perturbations are applied in the case of thermodynamic parameters, it is more meaningful to write equation (24) in a slightly different form because the perturbation factor is not characteristic in this case. Sensitivity coefficients are calculated for the thermodynamic quantities at T_0 = 300 K. For molar heat capacity and molar enthalpy parameters ($a_{1,k}$ and $a_{7,k}$) at 300 K, the following formula is used:

$$sn_{ij} = \frac{q_j}{R} \cdot \frac{1}{Y_i} \cdot s_{ij} = \frac{q_j}{R} \cdot \frac{1}{Y_i} \cdot \frac{Y_i' - Y_i}{d}, \tag{30}$$

where q_j is the original value of the thermodynamic quantity, ($c_{p,k}^{\ominus}$(300 K) and $S_k^{\ominus}$(300 K), respectively, calculated according to the corresponding original NASA polynomials), and d = +0.01 in both cases. Note, that T_0 = 300 K is chosen arbitrarily as the temperature of the investigations; any other temperature (within the range of validity of the NASA coefficients) could be chosen. In equation (*30*), the quantity d characterizes the perturbation, unlike in equation (24), in which f_{pert} plays this role. Then, the scaled normalized ($\widetilde{sn}_{ij}$) sensitivity coefficients are computed according to equation (25).

In the case of the enthalpy parameter ($a_{6,k}$) at 300 K, full normalization of the sensitivity coefficients cannot be utilized because various species may have enthalpies of different signs and orders of magnitude, which would result in biased results. Consequently, in this case, so-called *semi-normalized sensitivity coefficients* (ssn_{ij}) are computed as follows:

$$ssn_{ij} = \frac{1}{R} \cdot \frac{1}{Y_i} \cdot s_{ij} = \frac{1}{R} \cdot \frac{1}{Y_i} \cdot \frac{Y_i' - Y_i}{d}, \tag{31}$$

where d = +3 K. Hence, semi-normalized sensitivity coefficients have a unit of (J^{-1} mol). *Scaled semi-normalized sensitivity coefficients* ($\widetilde{ssn}_{ij}$) are computed in a similar way to equation (25):

$$\widetilde{ssn}_{ij} = \frac{ssn_{ij}}{\max_j\{|ssn_{ij}|\}}. \tag{32}$$

In this case, criterion (26) is adapted as follows:

$$|\widetilde{ssn}_{ij}| \geq 0.1. \tag{33}$$

5. Results and discussion

5.1. Performance comparison of the investigated mechanisms

Comparison of the performance of the investigated mechanisms is based on the following principle: *mechanisms are compared based on the same set of data points*. It was not possible, however, to use all data points for the comparison, because the simulation of some points failed with one or more mechanisms. Also, some data points cannot be reproduced within their 3σ uncertainty limits with any of the investigated mechanisms, that is, the E_{ij} value of the data point is greater than 9 for all mechanisms. In this case, these experimental data points may have very large systematic errors that were not considered. It is also possible that under these experimental conditions none of the mechanisms can describe the experimental results satisfactorily, which may be due to, e. g., a missing important reaction path. From this investigation, it does not turn out which one of the aforementioned explanations is the real reason, but these data points need to be excluded from the quantitative investigations to make the comparisons unbiased.

From the previous paragraph, it follows that the filtering of the data points is needed to be able to compare the mechanisms in an unbiased way. This is achieved by a 3-step filtering process as follows:

(1) Those points are excluded for which the simulation was not successful with ***at least one*** of the investigated mechanisms. This kind of filtering is needed to fulfill the principle of mechanism comparison. The number of failed data points is an important indicator of the robustness of mechanisms.

(2) Besides the data points excluded in (1), those points are also excluded for which the E_{ij} value is greater than 9 with ***each*** of the investigated mechanisms.

(3) Besides the data points excluded in (1) and (2), those points are also excluded for which the E_{ij} value is greater than 400 with ***at least one*** of the investigated mechanisms. Application of this criterion is necessary to get unbiased average error function values because only a couple of extremely high E_{ij} values can significantly increase the averaged E value of a mechanism, which would lead us to false impressions about the performance of the mechanism. In this case, however, the problem is most likely with the mechanism and not the experiment; therefore, the number of excluded points in this

step is also a good indicator of the performance of mechanisms (in addition to the averaged E value).

To facilitate the visual interpretation of the results of mechanism comparison, the following background colors are used for the different E value ranges in the tables containing the results:

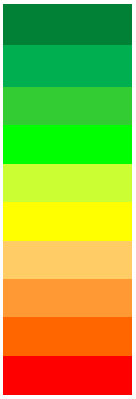

$0 \leq E < 4$
$4 \leq E < 9$
$9 \leq E < 16$
$16 \leq E < 25$
$25 \leq E < 36$
$36 \leq E < 49$
$49 \leq E < 64$
$64 \leq E < 81$
$81 \leq E < 100$
$100 \leq E$

5.1.1. NH_3/H_2 fuel mixtures

In this section, experiments with NH_3/H_2 fuel mixtures are used to compare the performances of the investigated mechanisms for each type of experiment, based on their averaged error function values (E). Then, their overall performances are also assessed.

5.1.1.1. Ignition delay time measurements in shock tubes

Table 12 summarizes the averaged error function values of the investigated mechanisms for ST-IDT experiments. Two sets of error functions are shown in the table. The first (left) set shows the error function values for all investigated mechanisms. In this case, it was found that the simulations of the same 29 data points failed with the Han-2020 and Okafor-2018 models (shown in red in the first part of the table), but no data point failed with the other mechanisms. These 29 data points are

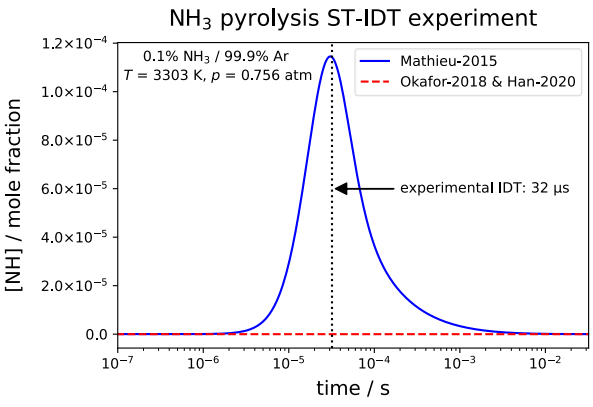

Figure 12. Computed NH concentration profiles during a shock tube NH_3 pyrolysis experiment of Davidson et al. [85] using the Mathieu-2015, Okafor-2018, and Han-2020 mechanisms. The ignition delay time is defined as the time elapsed between the arrival of the shock wave (time = 0 s in the figure) and the time when the NH concentration reaches its maximum value.

the measurements of Davidson et al. [85] which are the only experiments investigating the pyrolysis of NH_3; all other experiments study the oxidation of NH_3 or NH_3/H_2. In these measurements, the ignition delay time is defined as the time elapsed between the arrival of the shock wave and the time when the NH concentration reaches its maximum value. These are the only IDT measurements in which the IDT is defined based on the concentration profile of the NH radical.

In Figure 12, the computed NH concentration profiles are shown for the conditions of one of the experiments of Davidson et al. [85] with the two problematic mechanisms (Okafor-2018 and Han-2020) and the Mathieu-2015 mechanism. The concentration of NH is constant at zero using the two problematic models, while it goes through a maximum with

Table 12. Averaged error function values of the investigated mechanisms for ST-IDT measurements ($E_{\text{ST-IDT}}$) and the results of the data filtering process.

Mechanism	**All investigated mechanisms**			**Excluding Okafor-2018, Han-2020**		
	$E_{\text{ST-IDT}}$	**Failed**[a]	**Excl. in (3)**[b]	$E_{\text{ST-IDT}}$	**Failed**[a]	**Excl. in (3)**[b]
Tian-2009	9.09	0	0	17.81	0	0
Mathieu-2015	23.77	0	1	37.92	0	1
GDFKin-2016	28.28	0	0	26.60	0	0
Nakamura-2017	26.99	0	0	22.56	0	0
SanDiego-2018	48.44	0	9	58.21	0	9
Otomo-2018	9.52	0	0	9.16	0	0
Glarborg-2018	10.27	0	0	18.55	0	0
Okafor-2018	121.69	**29**	**54**	–	–	–
ELTE-2020	11.36	0	3	28.50	0	3
POLIMI-2020	10.38	0	0	13.52	0	0
NUIG-2020	15.45	0	0	22.32	0	0
Han-2020	11.69	**29**	1	–	–	–
Mei-2020	28.55	0	2	30.56	0	2
Konnov-2021	10.53	0	2	20.14	0	2
KAUST-2021	17.52	0	0	17.18	0	0
Shrestha-2021	11.21	0	0	17.72	0	0
Mei-2021	28.55	0	1	31.70	0	1
Zhou-2021	40.54	0	0	82.01	0	9
Gotama-2022	19.29	0	0	33.46	0	0
	Data filtration			**Data filtration**		
All points:	**229**			**229**		
Included points:	**140**	**(61.1%)**		**205**	**(98.3%)**	
Excluded in (1):	29	(12.7%)		0	(0.0%)	
Excluded in (2):	2	(0.9%)		2	(0.9%)	
Excluded in (3):	58	(25.3%)		22	(9.6%)	

[a]: Number of data points for which the simulations failed with the corresponding mechanism.
[b]: Number of data points for which $E_{ij} > 400$ was true for the corresponding mechanism in filtration step (3).

Mathieu-2015 as it is expected. This means that the Okafor-2018 and Han-2020 models cannot reproduce the formation of the NH radical in the absence of O_2. Probably, one or more reactions that are important for NH formation during NH_3 pyrolysis are missing from these two models but are present in the other models.

For this reason, the error function values are shown in Table 12 also without considering Okafor-2018 and Han-2020 in the comparison. This way, the NH_3 pyrolysis measurement of Davidson et al. [85] can be included in the comparison. Moreover, as shown in red in the first part of the table, most data points excluded in the third filtration step are due to the high E_{ij} values of the Okafor-2018 model. By excluding this model, most of these data points can also be included in the comparison; therefore, in the second comparison, 98.3% of the investigated data points are included, while only 61.1% in the first one.

None of the mechanisms can reproduce the data within their 3σ uncertainty limits ($E_{\text{ST-IDT}} \leq 9$) in either case. The best-performing model is Otomo-2018 with $E_{\text{ST-IDT}}$ values around 9 in both cases.

Averaged error function values for all investigated ST-IDT datasets (E_i) are summarized in Table A5 for each investigated mechanism.

5.1.1.2. Jet stirred reactor experiments

Table 13 shows the results of the performance comparison for the investigated outlet concentration measurements in JSRs. As has been described in Section 3.2.2, four of the investigated mechanisms do not contain species He; therefore, the JSR experiments of Stagni et al. [34](62 data points) cannot be reproduced by these models. For this reason, two kinds of comparison are made in Table 13: one from which experiments using He are excluded (first part of the table), and one in which all experiments are included but the four He-free models are excluded (second part of the table).

From the E_{JSR} values, it may seem that several mechanisms can reproduce the experimental data relatively well. Six models have an E_{JSR} value of less than 9 in the He-free case, and the E_{JSR} value of most models is smaller than 16 in both cases. However, the number of excluded points is large: approximately half of the investigated experimental data points had to be excluded from the comparison. This is mostly caused by the Nakamura-2017, Glarborg-2018, Gotama-2022, and ELTE-2020 models (these numbers are highlighted in red in the table). It is important to note that all failed data points belong to the measurements of Manna et al. [91] and Sabia et al. [90] (702 data points, altogether) which are the only

Table 13. Averaged error function values of the investigated mechanisms for JSR measurements (E_{JSR}) and the results of the data filtering process.

Mechanism	Excluding experiments using He			Including experiments using He		
	E_{JSR}	Failed[a]	Excl. in (3)[b]	E_{JSR}	Failed[a]	Excl. in (3)[b]
Tian-2009	11.57	0	66	–	–	–
Mathieu-2015	9.18	0	57	11.54	0	54
GDFKin-2016	12.80	50	76	–	–	–
Nakamura-2017	25.68	**200**	**149**	24.49	**200**	**136**
SanDiego-2018	10.05	0	77	9.56	0	79
Otomo-2018	8.60	0	65	10.87	0	57
Glarborg-2018	13.04	**114**	91	13.93	**114**	82
Okafor-2018	11.15	0	71	–	–	–
ELTE-2020	15.15	**100**	**122**	15.88	**100**	**109**
POLIMI-2020	8.61	0	70	11.47	0	54
NUIG-2020	15.34	17	94	16.32	17	73
Han-2020	11.18	4	79	14.96	4	65
Mei-2020	5.88	0	52	9.27	0	49
Konnov-2021	16.61	63	61	16.34	63	63
KAUST-2021	5.10	30	35	6.83	30	33
Shrestha-2021	17.05	9	**147**	16.37	9	85
Mei-2021	5.01	0	46	8.30	0	44
Zhou-2021	8.22	0	74	–	–	–
Gotama-2022	10.13	**109**	51	13.49	**109**	51
	Data filtration			**Data filtration**		
All points:	**1589**			**1651**		
Included points:	**786**	**(49.5%)**		**849**	**(51.4%)**	
Excluded in (1):	245	(15.4%)		245	(14.8%)	
Excluded in (2):	216	(13.6%)		225	(13.7%)	
Excluded in (3):	342	(21.5%)		331	(20.0%)	

[a]: Number of data points for which the simulations failed with the corresponding mechanism.
[b]: Number of data points for which $E_{ij} > 400$ was true for the corresponding mechanism in filtration step (3).

experiments that are simulated with the adiabatic reactor model, not the isothermal one (see Section 4). In the case of adiabatic simulations, the energy balance equation also has to be solved; therefore, these simulations converge less easily.

The large number of points excluded in the third filtration step can mostly be contributed to the Nakamura-2017, Shrestha-2021, and ELTE-2020 mechanisms in the He-free case, and to the Nakamura-2017 and ELTE-2020 models in the second case (these numbers are also highlighted in red in the table).

The KAUST-2021 and Mei-2021 models have an E_{JSR} value of less than 9 in both cases, and the fewest data points have an extremely high E_{JSR} value for these mechanisms.

Moreover, all simulations were successful for Mei-2021, so it can be considered also robust for this set of experimental data.

Averaged error function values for all investigated JSR datasets (E_i) are summarized in Table A6 (He-free experiments) and Table A9 (He-containing experiments) for each investigated mechanism.

5.1.1.3. Flow reactor experiments

Table 14 shows the averaged error function values of the mechanisms for the investigated flow reactor experiments (E_{FR}). Since the experiments of Dean et al. [93] and

Table 14. Averaged error function values of the investigated mechanisms for FR measurements (E_{FR}) and the results of the data filtering process.

Mechanism	Excluding experiments using He			Including experiments using He		
	E_{FR}	Failed[a]	Excl. in (3)[b]	E_{FR}	Failed[a]	Excl. in (3)[b]
Tian-2009	7.89	0	14	–	–	–
Mathieu-2015	6.51	0	14	5.99	0	19
GDFKin-2016	7.64	0	16	–	–	–
Nakamura-2017	7.53	0	21	7.32	0	38
SanDiego-2018	10.66	0	18	9.67	0	32
Otomo-2018	6.58	0	14	6.06	0	23
Glarborg-2018	4.71	0	20	4.39	0	29
Okafor-2018	10.91	0	19	–	–	–
ELTE-2020	4.46	0	19	4.18	0	33
POLIMI-2020	6.86	0	13	6.18	0	18
NUIG-2020	10.45	0	28	9.47	0	46
Han-2020	8.87	0	13	7.88	0	19
Mei-2020	9.09	0	16	8.16	0	16
Konnov-2021	8.24	0	28	22.02	0	57
KAUST-2021	2.91	0	9	2.69	0	11
Shrestha-2021	6.23	0	15	5.73	0	23
Mei-2021	8.96	0	17	8.07	0	23
Zhou-2021	8.43	0	14	–	–	–
Gotama-2022	8.27	0	17	7.61	0	23
	Data filtration			**Data filtration**		
All points:	**1003**			**1141**		
Included points:	**817**	**(81.5%)**		**903**	**(79.1%)**	
Excluded in (1):	0	(0.0%)		0	(0.0%)	
Excluded in (2):	123	(12.3%)		138	(12.1%)	
Excluded in (3):	63	(6.3%)		100	(8.8%)	

[a]: Number of data points for which the simulations failed with the corresponding mechanism.
[b]: Number of data points for which $E_{ij} > 400$ was true for the corresponding mechanism in filtration step (3).

Stagni et al. [34] use He as diluent gas (138 data points, altogether), He-free and He-containing cases were considered like in Section 5.1.1.2.

For this type of experiment, there were no failed simulations, and the total number of excluded data points is also relatively low in both cases. Moreover, the majority of mechanisms can reproduce the experimental data within their 3σ uncertainty limits ($E_{FR} \leq 9$); therefore, we can say that the investigated models can describe utilized FR experiments relatively well. The KAUST-2021 mechanism has the lowest E_{FR} values which are smaller than 4 (2σ uncertainty limits) in both cases, and it also has the lowest number of points with very high E_{ij} values in the third filtration step.

The averaged error function values for all investigated FR datasets (E_i) are summarized in Table A7 (He-free experiments) and Table A9 (He-containing experiments) for each investigated mechanism.

5.1.1.4. Laminar burning velocity measurements

Averaged error function values are summarized in Table 15 for the laminar burning velocity measurements (E_{LBV}). The experiments of Shrestha et al. [41] (7 data points, altogether) used He as diluent gas; therefore, He-free and He-containing cases were distinguished as in Sections 5.1.1.2 and 5.1.1.3.

Most simulations were successful with all mechanisms, and the number of data points excluded in step (2) of the filtration process is also small. As highlighted in red in the first part of Table 15, GDFKin-2016 caused the exclusion of most data points in the third step of data filtration. Since this mechanism does not contain species He, much fewer points are excluded in step (3) in the He-containing case. In this case, most of the exclusion of data points is caused by the ELTE-2020 model (also highlighted in red).

Several mechanisms can reproduce the experimental data within their 3σ uncertainty limits ($E_{LBV} \leq 9$) in both cases. Note that the majority of these models (Han-2020, Mei-2020, Shrestha-2021, Mei-2021, and Gotama-2022) were developed to describe primarily the LBVs of NH_3/H_2 or NH_3/syngas mixtures (see Table 5), so their good performance is not surprising for this type of experiments.

Averaged error function values for all investigated LBV datasets (E_i) are summarized in Table A8 (He-free experiments) and Table A9 (He-containing experiments) for each investigated mechanism.

Table 15. Averaged error function values of the investigated mechanisms for LBV measurements (E_{LBV}) and the results of the data filtering process.

Mechanism	Excluding experiments using He			Including experiments using He		
	E_{LBV}	Failed[a]	Excl. in (3)[b]	E_{LBV}	Failed[a]	Excl. in (3)[b]
Tian-2009	15.79	2	3	–	–	–
Mathieu-2015	25.86	11	1	30.19	11	2
GDFKin-2016	122.93	0	**139**	–	–	–
Nakamura-2017	12.82	0	0	14.94	0	2
SanDiego-2018	11.38	2	1	12.77	2	2
Otomo-2018	20.32	2	0	21.53	2	2
Glarborg-2018	51.40	0	16	72.67	0	15
Okafor-2018	23.38	0	7	–	–	–
ELTE-2020	65.77	0	**42**	91.23	0	**41**
POLIMI-2020	7.67	1	1	9.36	1	2
NUIG-2020	22.49	0	5	35.92	0	5
Han-2020	5.46	1	0	7.09	1	1
Mei-2020	5.75	1	0	6.67	1	1
Konnov-2021	9.31	1	1	12.36	1	2
KAUST-2021	7.92	2	0	9.62	2	2
Shrestha-2021	7.55	1	1	8.54	1	1
Mei-2021	6.58	3	0	7.43	3	2
Zhou-2021	13.78	2	5	–	–	–
Gotama-2022	5.35	1	0	8.16	1	0
	Data filtration			**Data filtration**		
All points:	**843**			**850**		
Included points:	**648**	**(76.9%)**		**772**	**(90.8%)**	
Excluded in (1):	12	(1.4%)		12	(1.4%)	
Excluded in (2):	15	(1.8%)		20	(2.4%)	
Excluded in (3):	168	(19.9%)		46	(5.4%)	

[a]: Number of data points for which the simulations failed with the corresponding mechanism.
[b]: Number of data points for which $E_{ij} > 400$ was true for the corresponding mechanism in filtration step (3).

5.1.1.5. Overall evaluation of mechanism performance

In Table 16, the averaged error function values of the 19 investigated mechanisms are summarized for each experiment type ($E_{\text{ST-IDT}}$, E_{JSR}, E_{FR}, E_{LBV}) for the He-free experiments. In the last column of the table, the unweighted averages of these type-specific error function values are shown (E_{average}), which are highlighted in bold. Unweighted final error function values are computed instead of XML-based weighting so as not to overweight LBV measurements (for which the number of XML files is much larger than that for other types of experiments) in the final error function values. This is important because the goal is to find the mechanisms that reproduce experimental data the most satisfactorily for *all* investigated types of experiments.

Based on the experience of Sections 5.1.1.1–5.1.1.4, the following mechanisms are excluded from further model comparison using experiments with NH_3/H_2 fuel mixtures because they are not among the models having the lowest E_{average} values (Table 16) and for the following reasons:

- Tian-2009, GDFKin-2016, Okafor-2018, Zhou-2021:

  These mechanisms do not include species He, so their exclusion enables us to include the He-containing experiments (207 data points) in the comparison. Moreover, the exclusion of Okafor-2018 allows more ST-IDT data points to be included in the comparison (see Section 5.1.1.1). As shown in Section 5.1.1.4, GDFKin-2016 caused the exclusion of most LBV data points in filtration step (3). By excluding this model, many of these points can be included.
- ELTE-2020:

  Several LBV and JSR data points had to be excluded in filtration step (3) due to this mechanism (see Sections 5.1.1.2 and 5.1.1.4). Also, the simulations of many JSR data points failed using this mechanism.
- Glarborg-2018:

  The simulations of many JSR data points failed with this mechanism (see Section 5.1.1.2).
- Nakamura-2017:

  It has the largest number of failed data points and data points with very high E_{ij} values in filtration step (3) in the case of JSR experiments (see Section 5.1.1.2).

Table 16. Averaged error function values for the He-free experiments in the case of NH_3/H_2 fuel mixtures considering all investigated mechanisms. The averaged error function values are shown for each experiment type, and the unweighted averages of these type-specific averaged error function values are in the last column of the table ($E_{average}$).

Mechanism	$E_{ST\text{-}IDT}$	E_{JSR}	E_{FR}	E_{LBV}	$E_{average}$
Included XMLs:	23	29	21	119	192
All points:	229	1589	1003	843	**3664**
Included points:	140	786	817	648	**2391**
Included (%):	61.1%	49.5%	81.5%	76.9%	**65.3%**
Excluded in (1):	29	245	0	12	286 (7.8%)
Excluded in (2):	2	216	123	15	356 (9.7%)
Excluded in (3):	58	342	63	168	631 (17.2%)
Tian-2009	9.09	11.57	7.89	15.79	**11.08**
Mathieu-2015	23.77	9.18	6.51	25.86	**16.33**
GDFKin-2016	28.28	12.80	7.64	122.93	**42.91**
Nakamura-2017	26.99	25.68	7.53	12.82	**18.25**
SanDiego-2018	48.44	10.05	10.66	11.38	**20.13**
Otomo-2018	9.52	8.60	6.58	20.32	**11.25**
Glarborg-2018	10.27	13.04	4.71	51.40	**19.85**
Okafor-2018	121.69	11.15	10.91	23.38	**41.78**
ELTE-2020	11.36	15.15	4.46	65.77	**24.19**
POLIMI-2020	10.38	8.61	6.86	7.67	**8.38**
NUIG-2020	15.45	15.34	10.45	22.49	**15.93**
Han-2020	11.69	11.18	8.87	5.46	**9.30**
Mei-2020	28.55	5.88	9.09	5.75	**12.32**
Konnov-2021	10.53	16.61	8.24	9.31	**11.17**
KAUST-2021	17.52	5.10	2.91	7.92	**8.36**
Shrestha-2021	11.21	17.05	6.23	7.55	**10.51**
Mei-2021	28.55	5.01	8.96	6.58	**12.28**
Zhou-2021	40.54	8.22	8.43	13.78	**17.74**
Gotama-2022	19.29	10.13	8.27	5.35	**10.76**

With the exclusion of these seven mechanisms, the number of data points excluded in filtration steps (1) and (3) can be decreased significantly. At the same time, decreasing the number of investigated mechanisms may result in more data points being excluded in filtration step (2). However, this is still a more preferable scenario because the filtration in steps (1) and (3) is based on individual mechanisms, while that in step (2) uses the E_{ij} values of *each* mechanism for a data point. Therefore, the comparison based on the averaged E values is less biased if the number of excluded data points in steps (1) and (3) is lower.

With the exclusion of Han-2020, the ST-IDT pyrolysis experiments of Davidson et al. [85] could also be included in the comparison (see Section 5.1.1.1), but the $E_{average}$ value of this mechanism is the lowest, so it is not excluded. As it was shown in Section 5.1.1.2, the

Table 17. Averaged error function values for only twelve selected mechanisms in the case of NH_3/H_2 fuel mixtures. The averaged error function values are shown for each experiment type, and the unweighted averages of these type-specific averaged error function values are in the last column of the table ($E_{average}$).

Mechanism	$E_{ST\text{-}IDT}$	E_{JSR}	E_{FR}	E_{LBV}	$E_{average}$
Included XMLs:	26	32	24	128	210
All points:	229	1651	1141	850	**3871**
Included points:	184	963	905	805	**2857**
Included (%):	80.3%	58.3%	79.3%	94.7%	**73.8%**
Excluded in (1):	29	109	0	12	150 (3.9%)
Excluded in (2):	3	319	141	27	490 (12.7%)
Excluded in (3):	13	260	95	6	374 (9.7%)
Mathieu-2015	43.09	14.94	5.92	30.96	**23.73**
SanDiego-2018	65.79	14.17	9.58	13.45	**25.75**
Otomo-2018	9.33	11.66	5.98	21.47	**12.11**
POLIMI-2020	14.17	12.41	6.12	10.55	**10.81**
NUIG-2020	18.07	16.74	9.40	39.86	**21.02**
Han-2020	35.64	16.48	7.83	7.61	**16.89**
Mei-2020	34.31	8.59	8.49	6.74	**14.53**
Konnov-2021	16.35	15.10	22.16	13.16	**16.69**
KAUST-2021	18.09	5.72	2.76	10.03	**9.15**
Shrestha-2021	19.89	18.11	5.66	9.48	**13.28**
Mei-2021	36.03	7.56	8.52	7.46	**14.89**
Gotama-2022	28.83	10.97	7.55	8.36	**13.93**

Shrestha-2021 model has a lot of points with very high E_{ij} values in the case of JSR experiments. However, due to its low $E_{average}$ value, it is also kept.

Averaged error function values are summarized in Table 17, considering only the non-excluded twelve mechanisms. If we compare the results of data filtration with those in Table 16, we see that the ratio of points included in the first and third filtration steps decreased, but it increased in the case of step (2), as was expected. The overall ratio of included data points increased from 65.3% to 73.8%, which is a significant improvement.

None of the twelve models can reproduce the experimental data within their 3σ uncertainty limits, on average ($E_{average} \leq 9$). KAUST-2021 has an $E_{average}$ value very close to 9 (9.15). The three best-performing mechanisms (in order) are KAUST-2021, POLIMI-2020, and Otomo-2018. KAUST-2021 and POLIMI-2020 were developed as comprehensive models for NH_3 oxidation and pyrolysis and were validated against various types of experimental data (see Table 5), so their overall good performance is not surprising. Otomo-2018 was created mainly to describe the LBVs and IDTs of NH_3/O_2 and $NH_3/H_2/O_2$ gas mixtures and was mostly validated against these kinds of experiments. Therefore, its relatively high overall error function value for LBV measurements is not expected. However, it has the best

performance for ST-IDT experiments among the investigated models, which agrees with its main target system.

5.1.2. NH_3/syngas fuel mixtures

Table 18 shows the computed averaged error function values for the experiments in which the gas mixtures contain CO. Because of the lower number of data points, all results are summarized in one table. The outlet concentration measurements in JSRs and FRs are treated together, and the averaged error function values are in the left part of the table for these types of experiments (E_{conc}). In the middle part of the table, the results for the LBV measurements are shown (E_{LBV}). In the rightmost part, the unweighted averages of these type-specific averaged error function values ($E_{average}$) are listed and highlighted in bold.

As can be seen in Table 18, the number of excluded data points is relatively low in filtration steps (2) and (3), especially in the case of LBV measurements, and all data points could be simulated with each mechanism. Three models have an $E_{average}$ value less than 9 (3σ uncertainty limits): Mei-2021, Mei-2020, and Shrestha-2021.

The Mei-2020 model was developed to describe primarily the LBVs of NH_3/syngas flames (see Table 5) and was validated against LBV measurements of NH_3, NH_3/H_2, and NH_3/syngas flames, and IDT measurements on NH_3/syngas. The main development and validation targets of Mei-2021 were the LBVs of NH_3 and NH_3/H_2 flames. It is an updated version of Mei-2020: the rate coefficients of six reactions were modified. Shrestha-2021 was developed primarily to model the LBVs of NH_3 and NH_3/H_2 flames, but it was validated against a large set of indirect experimental data containing various types of experiments. Therefore, the good performance of these three models is expected for the investigated LBV experiments, but they are also among the best-performing mechanisms for concentration measurements.

The averaged error function values for all experimental datasets are summarized in Table A10 for each mechanism (E_i).

Table 18. Averaged error function values for the experiments in which the gas mixtures contain CO. The averaged error function values are computed for the concentration measurements in JSRs snd FRs (E_{conc}), LBV measurements (E_{LBV}). In the rightmost part of the table, the unweighted averages of these type-specific averaged error function values are shown ($E_{average}$). The results of the data filtration are also shown in the lower part of the table.

Mechanism	JSR and FR experiments			LBV experiments			All experiment types		
	E_{conc}	Failed[a]	Excl. in (3)[b]	E_{LBV}	Failed[a]	Excl. in (3)[b]	$E_{average}$	Failed[a]	Excl. in (3)[b]
Tian-2009	9.13	0	5	42.44	0	5	**25.79**	0	10
Mathieu-2015	5.16	0	1	22.42	0	0	**13.79**	0	1
GDFKin-2016	4.48	0	2	66.49	0	1	**35.48**	0	3
SanDiego-2018	5.69	0	0	31.15	0	0	**18.42**	0	0
Glarborg-2018	4.11	0	2	74.06	0	5	**39.08**	0	7
Okafor-2018	9.15	0	6	73.87	0	13	**41.51**	0	19
NUIG-2020	8.81	0	3	16.88	0	0	**12.85**	0	3
Han-2020	13.00	0	7	11.24	0	0	**12.12**	0	7
Mei-2020	5.54	0	1	9.44	0	0	**7.49**	0	1
Konnov-2021	13.22	0	8	18.42	0	0	**15.82**	0	8
Shrestha-2021	6.66	0	1	9.49	0	0	**8.07**	0	1
Mei-2021	4.64	0	2	9.71	0	0	**7.17**	0	2
Zhou-2021	11.94	0	9	19.84	0	2	**15.89**	0	11
	Data filtration			**Data filtration**			**Data filtration**		
Included XMLs:	**9 (8 + 1)**			**80**			**89**		
All points:	**247**			**881**			**1128**		
Included points:	**189**	**(76.5%)**		**853**	**(96.8%)**		**1042**	**(92.4%)**	
Excluded in (1):	0	(0.0%)		0	(0.0%)		0	(0.0%)	
Excluded in (2):	42	(17.0%)		7	(0.8%)		49	(4.3%)	
Excluded in (3):	16	(6.5%)		21	(2.4%)		37	(3.3%)	

[a]: Number of data points for which the simulations failed with the corresponding mechanism.
[b]: Number of data points for which $E_{ij} > 400$ was true for the corresponding mechanism in filtration step (3).

5.2. Results of the sensitivity analysis

Local sensitivity analysis was carried out on the best-performing models identified in Section 5.1 according to the method described in Section 4.3. The sensitivities of both the kinetic parameters and the thermodynamic parameters were investigated. Parameter *j* is considered influential for data point *i* (in other words, data point *i* was *sensitive* to parameter *j*) if either criterion (26) (for kinetic, heat capacity, and entropy parameters) or criterion (33) (for enthalpy parameters) is true, that is, $\left|\widetilde{sn}_{ij}\right| \geq 0.1$ and $\left|\widetilde{ssn}_{ij}\right| \geq 0.1$, respectively. Using either of these conditions, the ratio of the number of experimental data points that were sensitive to parameter *j* and the total number of points was computed for each parameter; these values are called "frequency" in this section. This kind of investigation is important because we can identify the reactions and thermodynamic quantities whose parameters should be optimized using these combustion systems.

In the NH_3/syngas case (Section 5.2.2), the three best mechanisms, Mei-2021, Mei-2020, and Shrestha-2021, had E_{average} values less than nine, while the other models' E_{average} values were above twelve. Therefore, the three best models are chosen for sensitivity analysis. Since Mei-2020 and Mei-2021 are both among the investigated mechanisms, we will be able to see whether the six reactions whose rate parameters are updated in Mei-2021 relative to Mei-2020 are important under the conditions of these experiments.

In the NH_3/H_2 case, none of the twelve mechanisms in Table 17 reproduced the experimental data with $E_{\text{average}} < 9$. The best two models, KAUST-2021 (9.15) and POLIMI-2020 (10.81) are selected for further model analyses. These mechanisms do not have a wet CO submechanism, so they cannot used for the simulation of experiments with NH_3/syngas fuel mixtures. The third best mechanism was Otomo-2018 (12.11), but it does not have a wet CO oxidation scheme either. Therefore, Shrestha-2021 (13.28) is selected as the third model studied by sensitivity analysis instead of Otomo-2018. This way, we can compare the important model parameters between the NH_3/H_2 and NH_3/syngas cases for the Shrestha-2021 mechanism.

5.2.1. NH_3/H_2 fuel mixtures

As it was discussed above, the investigated models are KAUST-2021, POLIMI-2020, and Shrestha-2021. To decide which experimental data points should be used for the sensitivity analysis, a similar three-step filtering procedure was applied as in Section 5.1, which is described below for clarity:

(1) Those points are excluded for which the simulation was not successful with ***at least one*** of the investigated three mechanisms.

(2) Besides the data points excluded in (1), those points are also excluded that were excluded in filtration step (2) in Table 17 (altogether, 490 data points).

(3) Besides the data points excluded in (1) and (2), those points are also excluded for which the E_{ij} value is greater than 400 with ***at least one*** of the investigated three mechanisms.

Applying these criteria, the ratio of included data points increased from 73.8% (Table 17) to 80.6% (Table 19).

Table 19. Selected experimental data used for local sensitivity analysis in the case experiments with NH_3/H_2 fuel mixtures, and the performance of the selected models on this set of experimental data.

Mechanism	$E_{\text{ST-IDT}}$	E_{JSR}	E_{FR}	E_{LBV}	E_{average}
Included XMLs:	32	32	24	128	216
All points:	229	1651	1141	850	**3871**
Included points:	226	1105	968	820	**3119**
Included (%):	98.7%	66.9%	84.8%	96.5%	**80.6%**
Excluded in (1):	0	30	0	2	32 (0.8%)
Excluded in (2):	3	319	141	27	490 (12.7%)
Excluded in (3):	0	197	32	1	230 (5.9%)
POLIMI-2020	16.81	5.93	5.93	8.49	9.29
KAUST-2021	13.23	11.12	11.12	8.83	11.07
Shrestha-2021	16.19	17.36	17.36	8.83	14.94

5.2.1.1. Kinetic parameters

In the case of kinetic parameters, local sensitivity coefficients, s_{ij}, were computed for each preexponential factor (A, see equation (5)) and for each experimental data point using f_{pert} = 0.05 as the perturbation factor. Normalized (sn_{ij}) and scaled normalized ($\widetilde{sn}_{ij}$) sensitivity coefficients were computed according to equations (24) and (25), respectively.

Table 20 shows the results of the sensitivity analysis of chemical kinetic parameters for the three investigated mechanisms. The results are shown separately for ST-IDT (226 data points), concentration (2073 data points), and LBV measurements (820 data points).

In almost all cases, simulation results are most sensitive to a well-known H/O reaction, $O_2 + H = OH + O$, which is a major chain-branching step of H_2 oxidation. In laminar burning velocity experiments, this reaction is of particular importance ($\overline{|\widetilde{sn}_{ij}|}$ value is around 1.0 for each mechanism). The low-pressure limit of the termolecular, chain termination reaction of hydrogen oxidation, $H + O_2 + M = HO_2 + M$, also has large sensitivity in the case of concentration and laminar burning velocity measurements. However, its role is less emphasized in the Shrestha-2021 model than in the other two mechanisms. In the case of laminar burning velocity measurements, other H/O reactions also appear in the list but with a $\overline{|\widetilde{sn}_{ij}|}$ value less than 0.2: $H_2 + O = H + OH$ (chain-branching), $H_2 + OH = H + H_2O$ (chain propagation).

Other important reactions are contained in the NH_3 oxidation subset of the mechanisms (Figure 13). Most of these reactions include the species NH_3, NH_2, and/or NNH. As shown in Figure 13, reactive H/O radicals consume NH_3 primarily, and a H radical is abstracted by NH_3 in these reactions to form NH_2. In these experiments, the most sensitive reactions of this type are $NH_3 + H$, and less importantly, $NH_3 + OH$. However, in the case of LBV measurements, these reactions do not appear in Table 20 for any of the mechanisms.

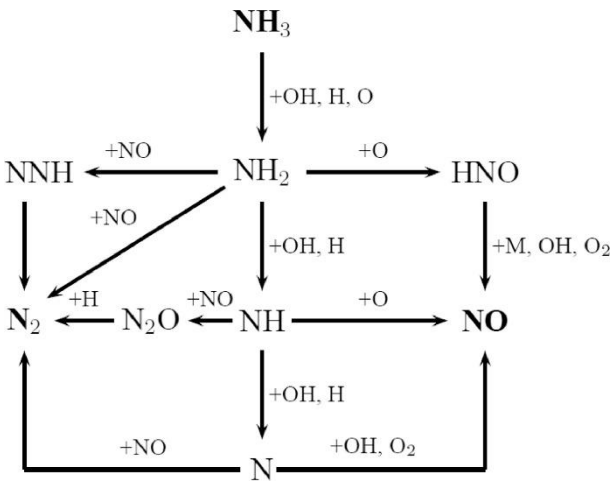

Figure 13. Reaction pathway diagram for NH_3 oxidation. During the thermal deNO_x process, the $NH_3 \rightarrow N_2$ oxidation path is dominant. The figure was adapted from the work of Glarborg et al. [44].

NH_2 may react further with NO in two possible channels: one forming NNH + OH, and the other resulting in

$N_2 + H_2O$. At least one of these channels appears in the list of most sensitive reactions for all types of experiments and each investigated mechanism. As highlighted in the work of Glarborg et al. [44], model predictions are usually very sensitive to the branching ratio of the two channels in NH_3 oxidation experiments.

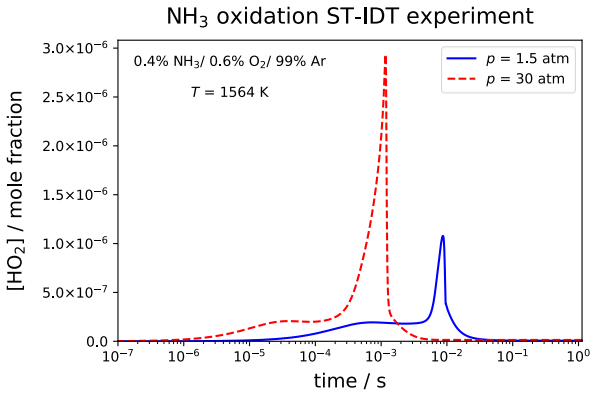

Figure 14. Computed HO_2 concentration profiles during a shock tube NH_3 oxidation experiment at two different pressures using the POLIMI-2020 mechanism. The peak HO_2 concentration is larger if the pressure is higher.

The recombination reaction of NH_2 and HO_2 radical species producing NH_3 and O_2 shows large sensitivity to the model outputs in the case of ST-IDT and concentration measurements for POLIMI-2020 and KAUST-2021. The concentration of the HO_2 radical reaches a higher level during combustion if large excess of O_2 is applied and/or the pressure is high (Figure 14) because under these circumstances, the reaction $H + O_2 + M = HO_2 + M$ is more dominant. In ST-IDT experiments, the latter, while in concentration measurements, the former may explain the importance of this reaction (see Table 2). Interestingly, the reaction does not appear in Table 20 for Shrestha-2021, although the model contains this reaction.

NH_2 may also react with radicals from the H/O radical pool, and these reactions compete with the reactions of NH_2 with NH_3 and amine radical species such as NH_2 or NH which may lead to the formation of N_2-amines, N_2H_2, and N_2H_3. Some of these reactions can also be found in Table 20, together with the reaction of NH_2 and molecular oxygen (O_2), forming nitroxide (H_2NO).

The reactions of the NH radical species (mainly formed by H-abstraction from NH_2) that are shown in Figure 13 do not seem to be very sensitive in these experiments in any of the mechanisms.

In the case of LBV simulations with Shrestha-2021, two reactions of the NNH radical species also appear at the top of the reaction list.

Table 20. Comparison of the sensitivity analysis results of chemical kinetic parameters (preexponential factors, *A*) for experiments with NH_3/H_2 fuel mixtures. The 10-10 most sensitive reactions are shown for the three investigated mechanisms for ST-IDT, concentration, and LBV measurements.

POLIMI-2020			KAUST-2021			Shrestha-2021		
Reaction	**Freq.[a]**	$\overline{\lvert\widetilde{sn}_{ij}\rvert}$[b]	**Reaction**	**Freq.[a]**	$\overline{\lvert\widetilde{sn}_{ij}\rvert}$[b]	**Reaction**	**Freq.[a]**	$\overline{\lvert\widetilde{sn}_{ij}\rvert}$[b]
ST-IDT: 226 investigated data points								
$O_2 + H = OH + O$	79.6%	0.541	$O_2 + H = OH + O$	68.6%	0.475	$O_2 + H = OH + O$	74.8%	0.534
$NH_3 + H = H_2 + NH_2$	58.8%	0.249	$NH_3 + H = NH_2 + H_2$	54.9%	0.221	$NH_3 + H = NH_2 + H_2$	69.0%	0.250
$NH_2 + NH = N_2H_2 + H$	55.3%	0.254	$NH_2 + NO = NNH + OH$	54.4%	0.201	$NH_2 + NH_2 = N_2H_2 + H_2$	64.6%	0.243
$NH_2 + HO_2 = NH_3 + O_2$	48.7%	0.239	$NH_2 + NO = N_2 + H_2O$ (DUP1)	54.4%	0.220	$NH_3 + NH_2 = N_2H_3 + H_2$	62.4%	0.278
$NH_2 + NO = NNH + OH$	47.3%	0.210	$NH_2 + HO_2 = NH_3 + O_2$	52.2%	0.258	$NH_2 + H + M = NH_3 + M$ (LP)	57.1%	0.296
$NH_2 + O_2 = H_2NO + O$	44.7%	0.211	$NH_3 + NH_2 = N_2H_3 + H_2$	52.2%	0.221	$N_2H_2 + M = NNH + H + M$	53.1%	0.250
$NH_2 + NH_2 = NH_3 + NH$	38.9%	0.198	$N_2H_2 + M = NNH + H + M$	47.8%	0.207	$NH_2 + NO = NNH + OH$	51.3%	0.279
$NH_3 + OH = H_2O + NH_2$	37.2%	0.183	$NH_3 + M = NH_2 + H + M$	47.8%	0.307	$N_2H_2 + H = NNH + H_2$	47.8%	0.186
$NH_2 + NO = N_2 + H_2O$	36.3%	0.187	$NH_2 + HO_2 = H_2NO + OH$	45.6%	0.272	$NH_2 + O_2 = H_2NO + O$	47.3%	0.194
$NH_3 = NH_2 + H$ (PLOG03)	35.4%	0.171	$NH_2 + NO = N_2 + H_2O$ (DUP2)	45.6%	0.161	$NH_3 + OH = NH_2 + H_2O$	44.7%	0.172
Concentration measurements in JSRs and FRs: 2073 investigated data points								
$NH_2 + HO_2 = NH_3 + O_2$	73.1%	0.483	$O_2 + H = OH + O$	75.5%	0.461	$O_2 + H = OH + O$	69.3%	0.386
$O_2 + H = OH + O$	71.0%	0.410	$NH_2 + HO_2 = NH_3 + O_2$	72.0%	0.405	$NH_2 + NO = NNH + OH$	47.5%	0.273
$NH_2 + O_2 = H_2NO + O$	56.8%	0.254	$NH_2 + NO = N_2 + H_2O$ (DUP1)	68.4%	0.426	$NH_2 + NO = N_2 + H_2O$	45.1%	0.282
$H + O_2 + M = HO_2 + M$ (LP)	52.9%	0.232	$H + O_2 + M = HO_2 + M$ (LP)	53.4%	0.205	$NH_3 + NH_2 = N_2H_3 + H_2$	34.6%	0.260
$NH_2 + NO = N_2 + H_2O$	50.9%	0.287	$NH_2 + NO = NNH + OH$	51.9%	0.196	$NH_3 + H = NH_2 + H_2$	32.4%	0.120
$NH_2 + NO = NNH + OH$	44.9%	0.183	$NH_2 + HO_2 = H_2NO + OH$	50.7%	0.304	$NH_2 + H + M = NH_3 + M$ (LP)	31.5%	0.186
$NH_2 + HO_2 = OH + H_2NO$	41.4%	0.255	$NH_2 + NO = N_2 + H_2O$ (DUP2)	50.4%	0.159	$NH_2 + O_2 = H_2NO + O$	27.9%	0.152
$H_2NO + O_2 = HNO + HO_2$	39.0%	0.138	$NH_3 + H = NH_2 + H_2$	45.9%	0.143	$H + O_2 + M = HO_2 + M$ (LP)	27.7%	0.128
$NH_3 + H = H_2 + NH_2$	37.5%	0.126	$NH_3 + NH_2 = N_2H_3 + H_2$	39.4%	0.263	$H_2NO + O_2 = HNO + HO_2$	24.6%	0.090
$NH_2 + NH_2 = NH_3 + NH$	26.2%	0.069	$NH_2 + O_2 = H_2NO + O$	37.8%	0.117	$NH_2 + HO_2 = H_2NO + OH$	23.0%	0.078
Laminar burning velocity measurements: 820 investigated data points								
$O_2 + H = O + OH$	100.0%	0.998	$O_2 + H = O + OH$	100.0%	0.998	$O_2 + H = OH + O$	99.9%	0.997
$NH_2 + NH = N_2H_2 + H$	95.9%	0.217	$NH_2 + NO = NNH + OH$	93.8%	0.236	$NNH = N_2 + H$	75.1%	0.180
$NH_2 + NO = NNH + OH$	76.5%	0.145	$H + O_2 + M = HO_2 + M$ (LP)	72.7%	0.148	$NNH + O_2 = N_2 + HO_2$	69.0%	0.161
$NH_2 + O = HNO + H$ (DUP1)	74.9%	0.124	$NH_2 + O = HNO + H$ (DUP1)	70.0%	0.110	$NH_2 + NO = NNH + OH$	64.4%	0.140
$H_2 + O = H + OH$	71.2%	0.142	$NH_2 + H = NH + H_2$	64.6%	0.107	$H_2 + OH = H + H_2O$	49.9%	0.122
$H + O_2 + M = HO_2 + M$ (LP)	69.5%	0.146	$NH_2 + NH = N_2H_2 + H$	57.6%	0.107	$N_2H_2 + H = NNH + H_2$	42.0%	0.076
$NH + H = N + H_2$	32.2%	0.086	$NH_2 + NO = N_2 + H_2O$ (DUP1)	54.6%	0.173	$N_2H_2 + M = NNH + H + M$	40.2%	0.080
$H_2 + OH = H + H_2O$	23.8%	0.090	$H_2 + O = OH + H$ (DUP2)	49.0%	0.110	$NH_2 + NH = N_2H_2 + H$	32.6%	0.079
$HNO + H = NO + H_2$	20.7%	0.066	$NH_2 + NO = N_2 + H_2O$ (DUP2)	31.5%	0.091	$H + O_2 + H_2O = HO_2 + H_2O$ (LP)	22.2%	0.060
$HNO = H + NO$ (PLOG02)	20.2%	0.053	$H_2 + OH = H + H_2O$	22.8%	0.091	$NO + H + M = HNO + M$ (LP)	22.1%	0.059

[a]: Number of data points for which the reaction has $\lvert\widetilde{sn}_{ij}\rvert \geq 0.1$ divided (normalized) by the total number of data points.

[b]: Average of the $\lvert\widetilde{sn}_{ij}\rvert$ values for all included data points for each reaction.

LP: low pressure limit reactions, PLOG: reactions parameterized by PLOG formalism, DUP: DUPLICATE reactions. See the text of Section 3.2.1.2 for further explanation.

5.2.1.2. Thermodynamic parameters

The authors of POLIMI-2020 obtained the thermodynamic parameters of H/O species, noble gases, and N_2 by fitting to the thermochemical data from version 1.122b (created in 2016) of the Active Thermochemical Tables (ATcT) Thermochemical Network (TN) [195-197]. The thermochemical data of most N-species were taken from the database of Goos, Burcat, and Ruscic [198], or the Glarborg-2018 model [44] in which the relevant thermodynamic data are also based on version 1.122b of the ATcT TN or directly taken from [198].

The thermodynamic data of Ar and OH* are from the database of Goos, Burcat, and Ruscic [198] in KAUST-2021, and those of all other H/O species, noble gases, and N_2 are from the high-temperature H_2/CO/C_1–C_4 combustion model of the Combustion Kinetics Laboratory at the University of South California (USC, 2007) [199]. The source of the data of N-species is primarily the GDFKin-2016 model [147]. Thermochemical data in GDFKin-2016 have various sources: the model of Dagaut et al. (1998) [200], that of Tan et al. (1994) [201], and the database of Burcat and McBride (1993) [202]. Most other N-species not included in GDFKin-2016 were also taken from [198], and the data for NH, NH_2, NNH, and N_2H_2 are from the recent theoretical calculations of the research group at KAUST [203]. In addition, the source of the thermodynamic data of HNO_2 and $HONO_2$ is the work of Rasmussen et al. (2008) [204], and the work of Mathieu et al. [205] for HON.

In Shrestha-2021, the thermochemical data of all H/O species, noble gases, and N_2 are from the database of Goos, Burcat, and Ruscic [198]. Similar to KAUST-2021, the source of most N-species is the GDFKin-2016 model [147]. Exceptions are the data of $HONO_2$ and HON which are from [204] and [205], respectively, like in KAUST-2021. However, the thermodynamic data of HNO_2 originate from the work of Bugler et al. [206].

Table 21 shows the overall results of the sensitivity analysis of thermodynamic parameters for the three investigated mechanisms for 0D experiments. In the table, overall results are shown because the results for the different types of experiments (ST-IDT, JSR, and FR) are very similar. Tables A11–A13 contain the results of the sensitivity analysis for the different types of 0D experiments separately.

The most sensitive species are very similar for each thermodynamic parameter, and also, for each mechanism, only minor differences can be observed. The H/O radicals that govern the combustion of hydrogen-containing fuels (H, O, OH, HO_2) are among the most sensitive species in POLIMI-2020 and KAUST-2021 for each thermodynamic property. The

same is true for Shrestha-2021, except for the O radical. In Shrestha-2021, the frequency value of the H radical is above 75% for each thermodynamic property.

NH_3 is present as a fuel in all experiments; therefore, it is not surprising that it is among the three most sensitive species in all cases. The amino radical (NH_2) is a key intermediate in ammonia oxidation, which is formed by H-abstraction from the NH_3 molecule (see Figure 13). Accordingly, the sensitivity of its thermodynamic data is similar to that of NH_3. In several experiments, the gas mixtures contain H_2 as a co-fuel (see Table 2), so H_2 is also among the most sensitive species in all cases. In all oxidation experiments, O_2 is the oxidizer, which explains its high sensitivity in all models. In POLIMI-2020 and KAUST-2021, it is among the three most sensitive species, but its sensitivity is significantly smaller in Shrestha-2021.

In Table 22, the results of the sensitivity analysis of thermodynamic properties are shown for LBV experiments. In these experiments, H_2 and H have very large sensitivities in all cases. As shown in Table 2, N_2 is the diluent gas in almost all LBV experiments. The results indicate that the simulation results are relatively sensitive to the isobar heat capacity and enthalpy of formation of N_2, but N_2 is not among the ten most sensitive species in the case of entropies for any of the mechanisms. As compared to the 0D experiments, the thermodynamic data of H_2O also shows relatively large sensitivity in the case of LBV experiments, although H_2O is not present in any of the initial gas mixtures (Table 2). This effect is most significant in the case of enthalpies of formation, and the overall sensitivities are smaller for the isobar heat capacity and entropy of H_2O. Interestingly, simulated LBV results are less sensitive to the thermodynamic data of NH_3 and NH_2 than the simulation results of 0D experiments.

Table 21. Comparison of the overall sensitivity analysis results of thermodynamic data for 0D experiments with NH_3/H_2 fuel mixtures (2299 investigated data points). The 10-10 most sensitive species of the three investigated mechanisms are shown for each thermodynamic property separately.

Zero-dimensional experiments (2299 investigated data points)								
POLIMI-2020			**KAUST-2021**			**Shrestha-2021**		
Species	**Freq.[a]**	$\overline{\lvert\widetilde{sn}_{ij}\rvert}$[b]	**Species**	**Freq.[a]**	$\overline{\lvert\widetilde{sn}_{ij}\rvert}$[b]	**Species**	**Freq.[a]**	$\overline{\lvert\widetilde{sn}_{ij}\rvert}$[b]
Standard isobar molar heat capacity at 300 K								
O_2	82.4%	0.523	NH_2	89.8%	0.681	NH_2	80.5%	0.631
NH_2	81.8%	0.543	NH_3	86.5%	0.679	H	79.3%	0.431
NH_3	80.1%	0.577	O_2	78.9%	0.472	NH_3	74.8%	0.556
HO_2	73.2%	0.470	H	66.2%	0.344	O_2	39.8%	0.200
H	66.9%	0.336	HO_2	65.9%	0.481	H_2	38.7%	0.215
H_2	40.6%	0.249	H_2	48.7%	0.280	HO_2	32.5%	0.154
O	39.7%	0.152	H_2NO	32.4%	0.138	OH	30.8%	0.168
H_2NO	38.2%	0.123	O	25.7%	0.113	N_2H_3	30.2%	0.153
OH	29.7%	0.136	N_2H_3	23.8%	0.109	H_2O	27.6%	0.122
HNOH	29.4%	0.101	HNOH	21.5%	0.099	H_2NO	26.5%	0.135
Standard enthalpy of formation at 300 K ($\widetilde{ssn}_{ij}$ values instead of $\widetilde{sn}_{ij}$ values)								
O_2	79.2%	0.540	NH_2	84.9%	0.625	H	79.3%	0.602
NH_2	77.3%	0.502	NH_3	81.9%	0.610	NH_2	77.4%	0.589
NH_3	74.7%	0.502	O_2	75.4%	0.518	NH_3	71.2%	0.498
H	67.9%	0.441	H	70.7%	0.453	O_2	40.7%	0.202
HO_2	65.1%	0.396	HO_2	61.0%	0.429	H_2	37.7%	0.222
O	41.1%	0.193	H_2	48.2%	0.262	OH	29.6%	0.159
H_2	40.2%	0.237	O	28.7%	0.145	HO_2	28.5%	0.125
H_2NO	31.9%	0.092	H_2NO	26.6%	0.109	N_2H_3	26.8%	0.117
OH	28.2%	0.131	N_2H_3	19.7%	0.080	O	26.8%	0.140
HNOH	23.5%	0.077	HNOH	16.3%	0.077	H_2O	25.9%	0.107
Standard molar entropy at 300 K								
O_2	81.2%	0.579	NH_2	87.6%	0.652	NH_2	78.9%	0.625
NH_2	79.2%	0.525	NH_3	84.3%	0.626	H	76.5%	0.404
NH_3	76.0%	0.519	O_2	80.2%	0.543	NH_3	72.4%	0.530
HO_2	71.8%	0.470	HO_2	65.1%	0.498	O_2	41.4%	0.225
H	62.9%	0.313	H	63.1%	0.330	H_2	34.7%	0.171
O	42.1%	0.175	H_2	43.8%	0.223	HO_2	33.0%	0.162
H_2NO	36.9%	0.112	H_2NO	33.0%	0.134	OH	30.1%	0.166
H_2	36.5%	0.201	O	29.3%	0.133	N_2H_3	29.5%	0.147
OH	28.8%	0.134	N_2H_3	22.1%	0.098	H_2NO	26.8%	0.135
HNOH	27.8%	0.099	HNOH	21.1%	0.095	H_2O	26.6%	0.115

[a]: Number of data points for which the thermodynamic property has $\lvert\widetilde{sn}_{ij}\rvert \geq 0.1$ or $\lvert\widetilde{ssn}_{ij}\rvert \geq 0.1$ divided (normalized) by the total number of data points.

[b]: Average of the $\lvert\widetilde{sn}_{ij}\rvert$ or $\lvert\widetilde{ssn}_{ij}\rvert$ values for all included data points for thermodynamic property.

Table 22. Comparison of the overall sensitivity analysis results of thermodynamic data for laminar burning velocity experiments with NH_3/H_2 fuel mixtures (820 investigated data points). The 10-10 most sensitive species of the three investigated mechanisms are shown for each thermodynamic property separately.

LBV experiments (820 investigated data points)								
POLIMI-2020			**KAUST-2021**			**Shrestha-2021**		
Species	**Freq.[a]**	$\overline{\lvert \widetilde{sn}_{ij} \rvert}$[b]	**Species**	**Freq.[a]**	$\overline{\lvert \widetilde{sn}_{ij} \rvert}$[b]	**Species**	**Freq.[a]**	$\overline{\lvert \widetilde{sn}_{ij} \rvert}$[b]
Standard isobar molar heat capacity at 300 K								
H_2	100.0%	0.996	H_2	100.0%	0.987	H_2	99.9%	0.967
H	99.9%	0.808	H	99.8%	0.893	H	99.8%	0.853
OH	93.8%	0.303	N_2	92.3%	0.292	N_2	93.3%	0.306
N_2	92.4%	0.292	NH_3	81.3%	0.286	H_2O	85.6%	0.334
H_2O	88.2%	0.332	NH_2	78.0%	0.238	NH_3	84.6%	0.368
NH_3	82.1%	0.292	OH	51.5%	0.196	NH_2	81.6%	0.333
NH_2	78.4%	0.233	O	47.3%	0.109	HO_2	76.6%	0.259
O_2	37.8%	0.120	H_2O	46.6%	0.127	OH	72.2%	0.191
O	7.0%	0.037	NH	33.8%	0.075	HNO	60.6%	0.158
HO_2	3.3%	0.031	O_2	22.9%	0.080	NO	52.9%	0.137
Standard enthalpy of formation at 300 K ($\widetilde{ssn}_{ij}$ values instead of $\widetilde{sn}_{ij}$ values)								
H_2O	100.0%	0.921	H_2O	100.0%	0.819	H_2O	99.9%	0.958
H_2	100.0%	0.744	H_2	100.0%	0.765	H_2	99.9%	0.721
O_2	100.0%	0.411	O_2	100.0%	0.393	O_2	99.9%	0.340
H	99.8%	0.837	H	99.8%	0.941	H	99.5%	0.829
N_2	93.9%	0.192	N_2	92.7%	0.206	N_2	95.4%	0.206
OH	84.0%	0.192	NH_3	82.1%	0.299	NH_3	82.4%	0.248
NH_3	82.9%	0.283	NH_2	71.6%	0.190	NH_2	70.5%	0.241
NH_2	72.1%	0.189	O	46.0%	0.102	HO_2	68.2%	0.136
O	5.1%	0.039	OH	38.4%	0.135	OH	54.0%	0.124
NH	0.1%	0.027	NH	18.5%	0.057	NO	41.2%	0.090
Standard molar entropy at 300 K								
H_2	100.0%	0.953	H_2	100.0%	0.880	H_2	99.9%	0.878
H	99.8%	0.955	H	99.8%	0.979	H	99.8%	0.942
H_2O	99.5%	0.603	H_2O	91.6%	0.272	H_2O	97.4%	0.577
OH	96.1%	0.386	NH_3	82.0%	0.330	NH_3	85.0%	0.411
NH_3	88.5%	0.355	NH_2	81.7%	0.288	NH_2	84.6%	0.399
NH_2	85.5%	0.300	O	66.2%	0.156	HO_2	83.7%	0.331
O_2	47.1%	0.166	OH	56.8%	0.231	OH	75.4%	0.235
O	17.1%	0.061	NH	47.2%	0.098	HNO	72.2%	0.197
NH	10.5%	0.050	O_2	25.6%	0.101	NO	66.3%	0.185
HO_2	6.7%	0.045	N_2H_3	11.8%	0.046	O	50.4%	0.117

[a]: Number of data points for which the thermodynamic property has $\lvert \widetilde{sn}_{ij} \rvert \geq 0.1$ or $\lvert \widetilde{ssn}_{ij} \rvert \geq 0.1$ divided (normalized) by the total number of data points.

[b]: Average of the $\lvert \widetilde{sn}_{ij} \rvert$ or $\lvert \widetilde{ssn}_{ij} \rvert$ values for all included data points for thermodynamic property.

5.2.2. NH_3/syngas fuel mixtures

In this type of experiment, the investigated models are Mei-2021, Mei-2020, and Shrestha-2021. The same filtering process is applied for the experimental data points as in the case of measurements with NH_3/H_2 fuel mixtures (Section 5.2.1). This way, ca. 95% of all investigated data points are included in the sensitivity analysis (Table 23). Sensitivity analyses of kinetic and thermodynamic parameters were performed using the same method as in the case of gas mixtures with NH_3/H_2 fuel mixtures.

Table 23. Selected experimental data used for local sensitivity analysis on experiments with NH_3/syngas fuel mixtures, and the performance of the selected models on this set of experimental data.

Mechanism	E_{conc}	E_{LBV}	$E_{average}$
Included XMLs:	9	80	89
All points:	247	881	**1128**
Included points:	202	874	**1076**
Included (%):	81.8%	99.2%	**95.4%**
Excluded in (1):	0	0	0 (0.0%)
Excluded in (2):	42	7	49 (4.3%)
Excluded in (3):	3	0	3 (0.3%)
Mei-2021	5.59	10.88	8.24
Mei-2020	7.37	10.52	8.94
Shrestha-2021	7.37	9.86	8.62

5.2.2.1. Kinetic parameters

Table 24 shows the results of the sensitivity analysis of kinetic parameters for the three investigated mechanisms, separately for concentration (202 data points) and LBV measurements (874 data points). Simulation results are generally most sensitive to H/O radical reactions H + O_2 = O + OH and H + O_2 + M = HO_2 + M. This accords with the results of Han et al. [14,16], Mei et al. [17], and Wang et al. [15]. Interestingly, results of LBV simulations do not show large sensitivity to the former reaction in the case of Shrestha-2021. Reaction CO + OH = CO_2 + H, which is the major CO oxidation pathway in the presence of H atoms [27], is the only sensitive C-containing reaction in all of the models. In addition to these reactions, reactions of the NH and NH_2 radical species appear among the most sensitive reactions, similarly to gas mixtures with NH_3/H_2 fuels. Although the Shrestha-2021 model contains reactions in which C-chemistry and N-chemistry are directly coupled, these reactions were found to be unimportant in the case of NH_3/CO oxidation. Hence, the two oxidation mechanisms, CO oxidation and NH_3 oxidation, are coupled through the H/O radical pool, but not through direct C/N reactions. These observations also agree with literature results [14-17] obtained for smaller sets of experimental data.

Table 24. Comparison of the overall results of the sensitivity analysis of chemical kinetic parameters (preexponential factors, *A*) for experiments with NH_3/syngas fuel mixtures. The 10-10 most sensitive reactions are shown for the three investigated mechanisms for concentration and LBV measurements.

Mei-2021			Mei-2020			Shrestha-2021		
Reaction	**Freq.[a]**	$\overline{\lvert\widetilde{sn}_{ij}\rvert}$[b]	**Reaction**	**Freq.[a]**	$\overline{\lvert\widetilde{sn}_{ij}\rvert}$[b]	**Reaction**	**Freq.[a]**	$\overline{\lvert\widetilde{sn}_{ij}\rvert}$[b]
Concentration measurements in JSRs and FRs: 202 investigated data points								
$H + O_2 + M = HO_2 + M$ (LP)	92.1%	0.588	$H + O_2 + M = HO_2 + M$ (LP)	92.6%	0.601	$H + O_2 + M = HO_2 + M$ (LP)	97.5%	0.674
$H + O_2 = O + OH$	76.7%	0.392	$H + O_2 = O + OH$	78.2%	0.419	$O_2 + H = OH + O$	83.2%	0.413
$NH_2 + NO = N_2 + H_2O$ (DUP1)	72.8%	0.427	$NH_2 + NO = N_2 + H_2O$ (DUP1)	71.3%	0.407	$NH_2 + NO = N_2 + H_2O$	55.4%	0.191
$NH + NO = N_2O + H$ (DUP1)	53.5%	0.353	$NH + NO = N_2O + H$	53.0%	0.304	$NH + NO = N_2O + H$	53.0%	0.356
$NO + O + M = NO_2 + M$ (LP)	49.0%	0.141	$NH_2 + NO = N_2 + H_2O$ (DUP2)	49.0%	0.141	$NH_2 + NO = NNH + OH$	50.5%	0.205
$NH_2 + NO = N_2 + H_2O$ (DUP2)	48.5%	0.151	$NH_2 + NO = NNH + OH$	46.5%	0.132	$NH + O = NO + H$	36.6%	0.092
$NH_2 + NO = NNH + OH$	48.0%	0.143	$CO + OH = CO_2 + H$	43.1%	0.261	$NH + OH = HNO + H$	34.7%	0.130
$CO + OH = CO_2 + H$	41.6%	0.281	$NO + O + M = NO_2 + M$ (LP)	41.6%	0.106	$CO + OH = CO_2 + H$ (DUP3)	33.7%	0.192
$NH + O = NO + H$	39.1%	0.100	$NH + O = NO + H$	38.6%	0.119	$CO + OH = CO_2 + H$ (DUP2)	32.2%	0.137
$NH + NO = N_2O + H$ (DUP2)	38.1%	0.093	$NH_2 + OH = NH + H_2O$	34.7%	0.113	$NH + NO = N_2 + OH$	28.2%	0.049
Laminar burning velocity measurements: 874 investigated data points								
$H + O_2 = O + OH$	100.0%	0.956	$H + O_2 = O + OH$	100.0%	0.957	$O_2 + H = OH + O$	99.9%	0.977
$H + O_2 + M = HO_2 + M$ (LP)	91.9%	0.218	$H + O_2 + M = HO_2 + M$ (LP)	91.2%	0.212	$NH_2 + NO = NNH + OH$	77.5%	0.139
$NH_2 + NO = NNH + OH$	89.4%	0.201	$NH_2 + NH = N_2H_2 + H$	85.6%	0.233	$NNH = N_2 + H$	74.0%	0.185
$NH_2 + NH = N_2H_2 + H$	81.8%	0.208	$NH_2 + NH = N_2H_3$	81.6%	0.189	$NNH + O_2 = N_2 + HO_2$	71.1%	0.167
$NH_2 + NH = N_2H_3$	78.0%	0.164	$NH_2 + NO = NNH + OH$	79.4%	0.162	$H + O_2 + H_2O = HO_2 + H_2O$ (LP)	57.2%	0.120
$CO + OH = CO_2 + H$	70.5%	0.312	$CO + OH = CO_2 + H$	70.5%	0.311	$CO + OH = CO_2 + H$ (DUP3)	51.0%	0.202
$O + H_2 = H + OH$	42.9%	0.105	$O + H_2 = H + OH$	38.0%	0.099	$H + OH + M = H_2O + M$	50.0%	0.099
$NH_2 + NO = N_2 + H_2O$ (DUP1)	40.4%	0.102	$NH_2 + OH = NH + H_2O$	36.0%	0.088	$NH_2 + NH = N_2H_2 + H$	45.5%	0.085
$NH_2 + OH = NH + H_2O$	32.6%	0.081	$NH_2 + NO = N_2 + H_2O$ (DUP1)	25.6%	0.076	$OH + H_2 = H + H_2O$	29.7%	0.092
$H_2 + OH = H_2O + H$	24.7%	0.082	$H_2 + OH = H_2O + H$	24.3%	0.081	$O + H_2 = H + OH$ (DUP2)	25.5%	0.082

[a]: Number of data points for which the reaction has $\lvert\widetilde{sn}_{ij}\rvert \geq 0.1$ divided (normalized) by the total number of data points.

[b]: Average of the $\lvert\widetilde{sn}_{ij}\rvert$ values for all included data points for each reaction.

LP: low pressure limit reactions, DUP: DUPLICATE reactions. See the text of Section 3.2.1.2 for further explanation.

As was mentioned previously, the rate parameters of six reactions were updated in Mei-2021 as compared to Mei-2020. Among these reactions, only two, H + O_2 = O + OH and NH + NO = N_2O + H, show large sensitivity to the simulation results, on average.

Table 25 summarizes sensitivity analysis results obtained with the Shrestha-2021 model for the NH_3/H_2 (see Section 5.2.1.1) and the NH_3/syngas cases. The experimental conditions are similar for the two types of systems. As can be seen in the table, the four most sensitive reactions are identical in the two cases, only their order varies slightly. The most important reaction is O_2 + H = OH + O, followed by three reactions from the NH_3 oxidation subset (see Figure 13). Besides these reactions, only H/O reactions and the CO oxidation reaction by OH have $\overline{|\widetilde{sn}_{ij}|}$ values above 0.1.

Table 25. Comparison of the sensitivity analysis results of chemical kinetic parameters (preexponential factors, *A*) of the Shrestha-2021 mechanism for NH_3/H_2 and NH_3/syngas LBV measurements. The 10-10 most sensitive reactions are shown for both cases.

Shrestha-2021 (NH_3/H_2)			**Shrestha-2021 (NH_3/CO)**		
LBV measurements: 820 investigated data points			**LBV measurements: 874 investigated data points**		
T = 298–476 K p = 0.50–10.00 atm Φ = 0.40–1.80			T = 298–443 K p = 1.00–10.00 atm Φ = 0.70–1.70		
Reaction	**Freq.[a]**	$\overline{\lvert\widetilde{sn}_{ij}\rvert}$[b]	**Reaction**	**Freq.[a]**	$\overline{\lvert\widetilde{sn}_{ij}\rvert}$[b]
O_2 + H = OH + O	99.9%	0.997	O_2 + H = OH + O	99.9%	0.977
NNH = N_2 + H	75.1%	0.180	NH_2 + NO = NNH + OH	77.5%	0.139
NNH + O_2 = N_2 + HO_2	69.0%	0.161	NNH = N_2 + H	74.0%	0.185
NH_2 + NO = NNH + OH	64.4%	0.140	NNH + O_2 = N_2 + HO_2	71.1%	0.167
OH + H_2 = H + H_2O	49.9%	0.122	H + O_2 + H_2O = HO_2 + H_2O (LP)	57.2%	0.120
N_2H_2 + H = NNH + H_2	42.0%	0.076	CO + OH = CO_2 + H (DUP3)	51.0%	0.202
N_2H_2 + M = NNH + H + M	40.2%	0.080	H + OH + M = H_2O + M	50.0%	0.099
NH_2 + NH = N_2H_2 + H	32.6%	0.079	NH_2 + NH = N_2H_2 + H	45.5%	0.085
H + O_2 + H_2O = HO_2 + H_2O (LP)	22.2%	0.060	OH + H_2 = H + H_2O	29.7%	0.092
NO + H + M = HNO + M (LP)	22.1%	0.059	O + H_2 = H + OH (DUP2)	25.5%	0.082

[a]: Number of data points for which the reaction has $|\widetilde{sn}_{ij}| \geq 0.1$ divided (normalized) by the total number of data points.

[b]: Average of the $|\widetilde{sn}_{ij}|$ values for all included data points for each reaction.

LP: low pressure limit reactions, DUP: DUPLICATE reactions. See the text of Section 3.2.1.2 for further explanation.

5.2.2.2. Thermodynamic parameters

The thermochemical data in Mei-2021 and Mei-2020 are identical. The data of almost all species are from the Glarborg-2018 model [44]. Exceptions are the parameters of HNO and NH_2 whose thermodynamic parameters were recalculated by the authors of Mei-2020 using quantum chemistry tools because they found discrepancies between data from different sources.

The sources of thermochemical data of H/O and N-species in Shrestha-2021 have been discussed in Section 5.2.1.1. Tables 26 and 27 show the results of the sensitivity analysis of thermochemical parameters for concentration and LBV measurements, respectively. As shown in the tables, the only sensitive C-containing species are CO and CO_2. The source of thermochemical data of these species is also the database of Goos, Burcat, and Ruscic [198].

In the case of experiments with NH_3/syngas fuel mixtures, simulation results are relatively sensitive to the thermochemical data of CO and CO_2 (CO_2 is the final product of the oxidation of CO) for all thermochemical parameters and each mechanism. Other than that, similar trends can be observed as in the case of NH_3/H_2 fuel mixtures with a few minor exceptions. One difference is that the HO_2 radical does not appear among the most sensitive species in these experiments. Also, simulation results are much less sensitive to the thermochemical properties of NH_3 and NH_2 in 0D experiments (concentration measurements: Table 26) than in the case of NH_3/H_2 fuel mixtures (Table 21). This can be explained by the fact that in JSR experiments (Ding et al. [53]), the fuel is an NH_3/H_2/CO mixture, and the molar ratio of NH_3 in the fuel is as small as 1/11. In addition, in FR experiments (Wargadalam et al. [82]), the fuel is an NH_3/CO gas mixture, in which the molar ratio of NH_3 is only 1/6, and the gas mixture is very oxidative ($\Phi = 0.01$).

Table 26. Comparison of the overall sensitivity analysis results of thermodynamic data for concentration measurements in JSRs and FRs using NH_3/syngas fuel mixtures (202 investigated data points). The 10-10 most sensitive species of the three investigated mechanisms are shown for each thermodynamic property separately.

Concentration measurements in JSRs and FRs: 202 investigated data points								
Mei-2021			**Mei-2020**			**Shrestha-2021**		
Species	**Freq.[a]**	$\overline{\lvert \widetilde{sn}_{ij} \rvert}$[b]	**Species**	**Freq.[a]**	$\overline{\lvert \widetilde{sn}_{ij} \rvert}$[b]	**Species**	**Freq.[a]**	$\overline{\lvert \widetilde{sn}_{ij} \rvert}$[b]
Standard isobar molar heat capacity at 300 K								
O_2	88.1%	0.517	H	88.6%	0.440	H	90.6%	0.372
H	83.7%	0.376	O_2	85.6%	0.491	O_2	87.1%	0.497
OH	73.3%	0.486	OH	72.8%	0.482	OH	87.1%	0.597
H_2O	69.8%	0.299	H_2O	68.8%	0.256	H_2O	86.1%	0.348
O	69.8%	0.257	CO_2	55.4%	0.349	CO	69.3%	0.368
CO_2	55.4%	0.360	NH_2	55.4%	0.367	CO_2	62.4%	0.418
CO	54.5%	0.292	CO	54.0%	0.285	O	44.6%	0.254
NO	41.1%	0.192	O	47.0%	0.151	H_2	32.7%	0.206
NH	40.6%	0.162	HNO	40.6%	0.184	NH_2	24.3%	0.175
H_2	34.2%	0.214	H_2	40.1%	0.232	H_2NO	17.3%	0.066
Standard enthalpy of formation at 300 K ($\widetilde{ssn}_{ij}$ values instead of $\widetilde{sn}_{ij}$ values)								
H	89.1%	0.514	H	93.1%	0.580	H	93.1%	0.521
O_2	86.1%	0.517	O_2	83.2%	0.490	OH	89.1%	0.585
O	75.7%	0.346	OH	75.2%	0.461	O_2	85.6%	0.494
OH	75.7%	0.474	O	64.9%	0.194	H_2O	84.7%	0.318
H_2O	68.3%	0.271	H_2O	63.4%	0.234	CO	68.3%	0.415
CO	54.5%	0.315	CO	54.0%	0.305	CO_2	61.4%	0.375
CO_2	54.0%	0.316	CO_2	53.0%	0.305	O	58.4%	0.317
NO	42.1%	0.179	NH_2	49.5%	0.322	H_2	32.2%	0.208
NH	41.6%	0.161	NH	40.1%	0.160	NH_2	24.3%	0.171
H_2	33.7%	0.219	H_2	39.6%	0.228	H_2NO	13.4%	0.056
Standard molar entropy at 300 K								
O_2	89.1%	0.576	O_2	88.1%	0.552	O_2	89.6%	0.555
H	82.7%	0.349	H	87.1%	0.412	H	88.6%	0.337
O	74.3%	0.298	OH	73.3%	0.488	OH	87.1%	0.600
OH	73.3%	0.491	H_2O	67.3%	0.248	H_2O	84.7%	0.333
H_2O	68.8%	0.283	O	60.4%	0.185	CO	68.8%	0.419
CO	56.4%	0.328	CO	55.0%	0.324	CO_2	61.9%	0.413
CO_2	56.4%	0.355	CO_2	55.0%	0.347	O	57.4%	0.284
NO	42.6%	0.208	NH_2	55.0%	0.348	H_2	29.7%	0.168
NH	41.1%	0.160	HNO	41.1%	0.182	NH_2	24.3%	0.172
H_2	31.7%	0.172	NH	40.1%	0.167	H_2NO	17.8%	0.067

[a]: Number of data points for which the thermodynamic property has $\lvert \widetilde{sn}_{ij} \rvert \geq 0.1$ or $\lvert \widetilde{ssn}_{ij} \rvert \geq 0.1$ divided (normalized) by the total number of data points.

[b]: Average of the $\lvert \widetilde{sn}_{ij} \rvert$ or $\lvert \widetilde{ssn}_{ij} \rvert$ values for all included data points for thermodynamic property.

Table 27. Comparison of the overall sensitivity analysis results of thermodynamic data for laminar burning velocity measurements with gas mixtures containing CO (874 investigated data points). The 10-10 most sensitive species of the three investigated mechanisms are shown for each thermodynamic property separately.

LBV experiments: 874 investigated data points								
Mei-2021			**Mei-2020**			**Shrestha-2021**		
Species	**Freq.[a]**	$\overline{\lvert \widetilde{sn}_{ij} \rvert}$[b]	**Species**	**Freq.[a]**	$\overline{\lvert \widetilde{sn}_{ij} \rvert}$[b]	**Species**	**Freq.[a]**	$\overline{\lvert \widetilde{sn}_{ij} \rvert}$[b]
Standard isobar molar heat capacity at 300 K								
N_2	97.7%	0.318	N_2	97.9%	0.329	N_2	97.6%	0.315
H	96.2%	0.810	H	95.3%	0.793	H	94.2%	0.771
H_2	92.9%	0.494	H_2	93.4%	0.512	H_2	93.8%	0.643
CO_2	91.0%	0.497	CO_2	91.3%	0.519	CO_2	91.2%	0.567
CO	90.4%	0.436	CO	90.7%	0.454	CO	89.5%	0.487
H_2O	89.8%	0.419	H_2O	87.9%	0.406	H_2O	84.1%	0.308
OH	76.0%	0.501	OH	80.2%	0.500	OH	81.4%	0.415
O_2	65.2%	0.238	HNO	78.3%	0.202	NH_3	71.6%	0.295
NH_2	61.6%	0.210	O_2	65.7%	0.259	NH_2	67.8%	0.260
NNH	61.0%	0.117	NH_2	64.9%	0.189	O_2	62.0%	0.219
Standard enthalpy of formation at 300 K ($\widetilde{ssn}_{ij}$ values instead of $\widetilde{sn}_{ij}$ values)								
O_2	100.0%	0.542	O_2	100.0%	0.574	O_2	96.1%	0.487
H	96.8%	0.853	H	96.2%	0.848	H	91.5%	0.791
H_2O	92.7%	0.469	H_2O	93.5%	0.500	H_2	91.2%	0.528
NH_3	92.0%	0.370	NH_3	93.2%	0.395	H_2O	88.1%	0.555
H_2	91.9%	0.418	H_2	92.4%	0.435	CO	85.8%	0.456
CO	89.2%	0.420	CO	89.1%	0.441	CO_2	85.6%	0.461
CO_2	89.2%	0.424	CO_2	89.1%	0.446	N_2	81.1%	0.161
N_2	82.4%	0.158	N_2	83.1%	0.166	NH_3	77.8%	0.192
OH	66.2%	0.435	OH	70.8%	0.436	OH	71.6%	0.355
NH_2	53.5%	0.144	HNO	65.8%	0.126	NH_2	58.8%	0.183
Standard molar entropy at 300 K								
H	95.8%	0.795	H	95.0%	0.781	H	92.4%	0.752
CO_2	93.4%	0.522	CO_2	93.5%	0.542	CO_2	92.4%	0.581
CO	92.4%	0.482	CO	92.4%	0.498	CO	91.9%	0.530
H_2	88.3%	0.388	H_2	89.1%	0.402	H_2	90.2%	0.509
H_2O	82.4%	0.325	H_2O	82.7%	0.321	H_2O	82.3%	0.303
OH	77.5%	0.519	OH	81.6%	0.517	OH	82.2%	0.436
O_2	67.8%	0.269	HNO	79.4%	0.231	NH_3	68.6%	0.287
NNH	63.3%	0.131	O_2	68.4%	0.293	NH_2	66.9%	0.278
NH_2	61.3%	0.220	NH_2	65.2%	0.196	O_2	65.3%	0.249
NO	61.0%	0.137	O	64.3%	0.140	HO_2	55.7%	0.201

[a]: Number of data points for which the thermodynamic property has $\lvert \widetilde{sn}_{ij} \rvert \geq 0.1$ or $\lvert \widetilde{ssn}_{ij} \rvert \geq 0.1$ divided (normalized) by the total number of data points.

[b]: Average of the $\lvert \widetilde{sn}_{ij} \rvert$ or $\lvert \widetilde{ssn}_{ij} \rvert$ values for all included data points for thermodynamic property.

6. Conclusions and outlook

In this work, a large set of indirect experimental data on the combustion of NH_3/H_2 and NH_3/syngas fuel mixtures was collected and digitized into XML-format data files which can be used as inputs for numerical simulations using the *Optima++* framework [79]. The data included ST-IDT, JSR, FR, and LBV experiments. Standard deviations of the collected datasets were estimated using the computer program Minimal Spline Fit [180,181], and an overall standard deviation was assigned to each data point using the estimated and the reported experimental errors.

19 detailed combustion mechanisms were utilized from the literature which can be used for the modeling of the target systems of this work. The performance of these models was assessed quantitatively, using an error function, against the investigated indirect experiments. This error function allows the quantitative comparison of several mechanisms on large experimental datasets. It was found that the overall performances of the investigated mechanisms vary largely, and the performance of each mechanism is not the same for different types of experiments.

Local sensitivity analysis was also carried out on the kinetic and thermodynamic parameters of the best-performing mechanisms It was found that simulation results are generally very sensitive to the H/O reactions $O_2 + H = OH + O$ and $H + O_2 + M = HO_2 + M$. Reaction from the NH_3 oxidation subset are also important in NH_3/H_2 and NH_3/syngas oxidation. Sensitivity analysis of NH_3/syngas gas mixtures showed the importance of the CO oxidation reaction $CO + OH = CO_2 + H$, but no direct C/N coupling reaction was found to be important in the investigated systems. These observations are in agreement with literature results. When comparing results for NH_3/H_2 and NH_3/syngas fuel mixtures with the Shrestha-2021 mechanism, the most sensitive reactions were identical in the two cases.

Sensitivity analysis of thermochemical parameters showed that model outputs are generally most sensitive to the thermodynamic data of H/O radical species (H, O, OH, HO_2), NH_3, NH_2, H_2, O_2, and H_2O. These are supplemented with CO and CO_2 in the case of NH_3/syngas fuel mixtures.

The most important model parameters identified by sensitivity analysis may be the primary targets of model optimization. Therefore, the results presented in this study may facilitate further mechanism development work on NH_3/H_2 and NH_3/syngas combustion systems in the future.

7. Acknowledgments

First of all, I would like to thank my supervisor, Tamás Turányi for his support during my work at the Chemical Kinetics Laboratory of ELTE. He gave me this interesting project one year ago and always carefully reviewed my reports including this treatise.

István Gyula Zsély provided me with valuable pieces of advice throughout the project that ensured the flow of the work.

This thesis could have never been completed without the software development work of Máté Papp who always implemented my requests into the *Optima++* framework readily.

I am also grateful to Márton Kovács whose work guided me in the sensitivity analysis of the thermodynamic parameters in kinetic models.

I also have to express my gratitude to Tibor Nagy for developing the *Minimal Spline Fit* computer program that I used in the estimation of the standard deviation of experimental datasets.

My work was supported by NKFIH grant OTKA K132109 of the Hungarian National Research, Development and Innovation Office.

Appendix

Table A1. Investigated shock tube ignition delay time measurements: experimental details and standard deviations for each XML data file.

Reference	XML ID	*T* / K	*p* / atm	Φ	Fuel	Ox.[a]	Dopant	Diluent	Meas.[b]	Dp.[c]	St. dev.[d]
Chen (2021) [86]	x10100003	1499–1939	1.11–1.23	1.00	NH_3/H_2	O_2	–	Ar	IDT	8	0.126
Chen (2021) [86]	x10100004	1394–1956	9.25–11.36	1.00	NH_3/H_2	O_2	–	Ar	IDT	12	0.242
Chen (2021) [86]	x10100005	1199–1825	1.17–1.21	1.00	NH_3/H_2	O_2	–	Ar	IDT	7	0.146
Chen (2021) [86]	x10100006	1206–1939	9.32–12.60	1.00	NH_3/H_2	O_2	–	Ar	IDT	9	0.196
Chen (2021) [86]	x10100007	1022–1600	1.09–1.26	1.00	NH_3/H_2	O_2	–	Ar	IDT	5	0.153
Chen (2021) [86]	x10100008	1052–1296	9.23–9.96	1.00	NH_3/H_2	O_2	–	Ar	IDT	7	0.237
Mathieu (2015) [38]	x10199009	1564–1894	27.70–29.70	0.50	NH_3	O_2	–	Ar	IDT	8	0.091
Mathieu (2015) [38]	x10199010	1927–2479	1.29–1.58	0.50	NH_3	O_2	–	Ar	IDT	11	0.067
Mathieu (2015) [38]	x10199011	1626–2015	10.40–11.40	0.50	NH_3	O_2	–	Ar	IDT	9	0.093
Mathieu (2015) [38]	x10199012	1586–1926	27.70–29.60	1.00	NH_3	O_2	–	Ar	IDT	9	0.079
Mathieu (2015) [38]	x10199013	1987–2489	1.29–1.51	1.00	NH_3	O_2	–	Ar	IDT	10	0.063
Mathieu (2015) [38]	x10199014	1663–2079	10.60–11.20	1.00	NH_3	O_2	–	Ar	IDT	9	0.062
Mathieu (2015) [38]	x10199015	1566–1866	28.00–29.70	1.00	NH_3	O_2	–	Ar	IDT	7	0.121
Mathieu (2015) [38]	x10199016	1827–2454	1.25–1.52	1.00	NH_3	O_2	–	Ar	IDT	9	0.060
Mathieu (2015) [38]	x10199017	1618–2085	10.10–10.90	1.00	NH_3	O_2	–	Ar	IDT	7	0.083
Mathieu (2015) [38]	x10199018	1584–1906	27.50–30.40	2.00	NH_3	O_2	–	Ar	IDT	7	0.112
Mathieu (2015) [38]	x10199019	1992–2404	1.35–1.49	2.00	NH_3	O_2	–	Ar	IDT	10	0.058
Mathieu (2015) [38]	x10199020	1651–2038	10.10–11.30	2.00	NH_3	O_2	–	Ar	IDT	8	0.076
Davidson (1990) [85]	x10199021	2268–3303	0.76–1.01	–	NH_3	–	–	Ar	IDT	5	0.082
Davidson (1990) [85]	x10199022	2297–3263	0.76–1.00	–	NH_3	–	–	Ar	IDT	8	0.095

Reference	XML ID	*T* / K	*p* / atm	Φ	Fuel	Ox.[a]	Dopant	Diluent	Meas.[b]	Dp.[c]	St. dev.[d]
Davidson (1990) [85]	x10199023	2281–3085	0.80–1.01	–	NH_3	–	–	Ar	IDT	4	0.127
Davidson (1990) [85]	x10199024	2274–3194	0.78–1.01	–	NH_3	–	–	Ar	IDT	4	0.183
Davidson (1990) [85]	x10199025	2224–3156	0.79–1.02	–	NH_3	–	–	Ar	IDT	4	0.146
Davidson (1990) [85]	x10199026	2336–3162	0.45	–	NH_3	–	–	Ar	IDT	4	0.130
Shu (2019) [80]	x10199029	1213–1492	19.05–19.74	0.50	NH_3	O_2	–	N_2	IDT	5	0.155
Shu (2019) [80]	x10199030	1181–1524	37.50–41.65	0.50	NH_3	O_2	–	N_2	IDT	5	0.152
Shu (2019) [80]	x10199031	1264–1525	19.25–20.33	1.00	NH_3	O_2	–	N_2	IDT	5	0.108
Shu (2019) [80]	x10199032	1280–1581	37.01–41.65	1.00	NH_3	O_2	–	N_2	IDT	5	0.125
Shu (2019) [80]	x10199033	1183–1543	15.89–19.74	1.99	NH_3	O_2	–	N_2	IDT	5	0.175
Shu (2019) [80]	x10199034	1195–1554	37.11–41.35	1.99	NH_3	O_2	–	N_2	IDT	5	0.132
Chen (2021) [86]	x10199035	1613–1899	1.01–1.31	1.00	NH_3	O_2	–	Ar	IDT	11	0.118
Chen (2021) [86]	x10199036	1441–1787	9.80–10.53	1.00	NH_3	O_2	–	Ar	IDT	7	0.205

[a]: Oxidizer.
[b:] Measured quantity.
[c]: Number of data points in the experimental XML file (dataset).
[d]: Overall relative standard deviations of the data points in the experimental XML file (dataset).

Table A2. Investigated concentration profile measurements in jet stirred reactors: experimental details for each XML data file and standard deviations for each dataset.

Reference	XML ID	*T* / K	*p* / atm	Φ	Fuel	Ox.[a]	Dopant	Diluent	Meas.[b]	Dp.[c]	St. dev. [d] / ppm
Zhang (2021) [36]	x00100000	900–1277	1.00	0.15	NH_3/H_2	O_2	–	N_2	H_2O	10	5–280
									NH_3	10	5–137
									NO	10	5
									N_2O	10	5
Zhang (2021) [36]	x00100001	900–1220	1.00	0.16	NH_3/H_2	O_2	–	N_2	H_2O	9	5–165
									NH_3	9	5–69
									NO	9	5
									N_2O	9	5
Zhang (2021) [36]	x00100002	800–1170	1.00	0.18	NH_3/H_2	O_2	–	N_2	H_2O	10	5–122
									NH_3	10	5–134
									NO	10	5
									N_2O	10	5
Zhang (2021) [36]	x00100003	800–1060	1.00	0.20	NH_3/H_2	O_2	–	N_2	H_2O	9	5–223
									NH_3	9	5–33
									NO	9	5
									N_2O	9	5
Zhang (2021) [36]	x00100004	900–1281	1.00	0.62	NH_3/H_2	O_2	–	N_2	H_2O	10	5–162
									NH_3	10	5–93
									NO	10	5
									N_2O	10	5
Zhang (2021) [36]	x00100005	900–1220	1.00	0.66	NH_3/H_2	O_2	–	N_2	H_2O	8	5–322
									NH_3	8	5–66
									NO	8	5
									N_2O	8	5

Reference	XML ID	*T* / K	*p* / atm	Φ	Fuel	Ox.[a]	Dopant	Diluent	Meas.[b]	Dp.[c]	St. dev. [d] / ppm
Zhang (2021) [36]	x00100006	800–1120	1.00	0.71	NH_3/H_2	O_2	–	N_2	H_2O	9	5–233
									NH_3	9	5–52
									NO	9	5
									N_2O	9	5
Zhang (2021) [36]	x00100007	800–1060	1.00	0.79	NH_3/H_2	O_2	–	N_2	H_2O	9	5–154
									NH_3	9	5–28
									NO	9	5
									N_2O	9	5
Osipova (2022) [92]	x00100008	800–1300	1.00	1.00	NH_3/H_2	O_2	–	Ar	H_2	18	8–39
									NH_3	18	6–136
									H_2O	18	5–622
									N_2	18	5–41
									O_2	18	5–73
Osipova (2022) [92]	x00100009	800–1300	1.00	0.60	NH_3/H_2	O_2	–	Ar	H_2	18	5–27
									NH_3	18	5–110
									H_2O	18	5–251
									N_2	18	5–69
									O_2	18	29–85
Osipova (2022) [92]	x00100010	800–1300	1.00	1.50	NH_3/H_2	O_2	–	Ar	H_2	18	19–32
									NH_3	18	22–112
									N_2	18	5–30
									O_2	18	5–48
									H_2O	17	5–204
Stagni (2020) [34]	x00199000	500–1200	1.05	0.02	NH_3	O_2	–	He	NH_3	12	14–26
									NO	7	5

Reference	XML ID	*T* / K	*p* / atm	Φ	Fuel	Ox.[a]	Dopant	Diluent	Meas.[b]	Dp.[c]	St. dev. [d] / ppm
									NO_2	7	5
Stagni (2020) [34]	x00199001	500–1200	1.05	0.01	NH_3	O_2	–	He	NH_3	8	6–25
									NO	8	5
									NO_2	8	5
Stagni (2020) [34]	x00199002	500–1200	1.05	–	NH_3	–	–	He	NH_3	12	25–26
Dagaut (2019) [89]	x00199003	1101–1452	1.00	0.06	NH_3	O_2	–	N_2	NH_3	15	5–62
									H_2O	15	5–114
									NO_2	15	5
									NO	15	5–17
									N_2O	15	5
Dagaut (2019) [89]	x00199004	1253–1450	1.00	0.30	NH_3	O_2	–	N_2	NH_3	9	12–270
									H_2O	9	5–90
									NO	9	5
Dagaut (2019) [89]	x00199005	1250–1452	1.00	0.60	NH_3	O_2	–	N_2	NH_3	9	17–249
									H_2O	9	5–79
									NO	9	5
Dagaut (2019) [89]	x00199006	1304–1450	1.00	1.20	NH_3	O_2	–	N_2	NH_3	7	40–147
									H_2O	7	5–80
									NO	7	5
Manna (2020) [91]	x00199007	953–1293	1.20	1.00	NH_3	O_2	–	Ar	H_2	12	69–524
									O_2	12	43–1562
									N_2	12	5–14367
									NO	12	5–5
Manna (2020) [91]	x00199008	953–1313	1.20	1.00	NH_3	O_2	H_2O	Ar	H_2	13	84–557
									O_2	13	43–1630

Reference	XML ID	*T* / K	*p* / atm	Φ	Fuel	Ox.[a]	Dopant	Diluent	Meas.[b]	Dp.[c]	St. dev. [d] / ppm
									N_2	13	5–11287
									NO	13	5–6
Manna (2020) [91]	x00199009	993–1271	1.20	–	NH_3	–	–	Ar	H_2	11	153–13451
									N_2	11	5–4135
Manna (2020)[91]	x00199010	993–1264	1.20	–	NH_3	–	H_2O	Ar	H_2	11	66–3831
									N_2	11	5–971
Sabia (2020) [90]	x00199011	966–1288	1.20	0.80	NH_3	O_2	–	N_2	H_2	30	9–146
									O_2	30	466–1664
									NO	30	5
Sabia (2020) [90]	x00199012	965–1293	1.20	1.00	NH_3	O_2	–	N_2	H_2	26	15–220
									O_2	26	351–13537
									NO	26	5
Sabia (2020) [90]	x00199013	1012–1293	1.20	1.20	NH_3	O_2	–	N_2	H_2	34	39–780
									O_2	34	119–2998
									NO	34	5
Sabia (2020) [90]	x00199014	1100	1.20	0.60–1.40	NH_3	O_2	–	N_2	H_2	26	43–68
									O_2	26	1163–1882
									NO	26	5
Sabia (2020) [90]	x00199015	1225	1.20	0.60–1.40	NH_3	O_2	–	N_2	H_2	26	22–61
									O_2	26	1537–3124
									NO	26	5
Sabia (2020) [90]	x00199016	1270	1.20	0.60–1.40	NH_3	O_2	–	N_2	H_2	18	12–1291
									O_2	18	335–3471
									NO	18	5
Sabia (2020) [90]	x00199017	923–1283	1.20	1.00	NH_3	O_2	H_2O	N_2	H_2	26	5–297

Reference	XML ID	*T* / K	*p* / atm	Φ	Fuel	Ox.[a]	Dopant	Diluent	Meas.[b]	Dp.[c]	St. dev. [d] / ppm
									O_2	26	95–3709
									NO	26	5
Zhang (2021) [36]	x00199018	900–1277	1.00	0.15	NH_3	O_2	–	N_2	H_2O	10	5–149
									NH_3	10	27–106
									NO	10	5
									N_2O	10	5
Zhang (2021) [36]	x00199019	900–1277	1.00	0.60	NH_3	O_2	–	N_2	H_2O	10	5–173
									NH_3	10	11–105
									NO	10	5
									N_2O	10	5
Osipova (2022) [92]	x00199020	900–1300	1.00	1.00	NH_3	O_2	–	Ar	NH_3	24	30–179
									O_2	24	12–54
									H_2O	22	5–174
									N_2	22	5–144
Ding (2021) [53]	x00101000	1300	1.00	0.57	$NH_3/H_2/CO$	O_2	–	CO_2/N_2	O_2	3	102–122
									CO	3	5–31
									H_2	3	5
									N_2O	3	5
									NO	3	5
Ding (2021) [53]	x00101001	1300	1.00	1.15	$NH_3/H_2/CO$	O_2	–	CO_2/N_2	O_2	3	5–20
									CO	3	15–63
									H_2	3	5–10
									N_2O	3	5
									NO	3	5
Ding (2021) [53]	x00101002	900–1300	1.00	0.57	$NH_3/H_2/CO$	O_2	–	N_2	O_2	6	230–409

Reference	XML ID	*T* / K	*p* / atm	Φ	Fuel	Ox.[a]	Dopant	Diluent	Meas.[b]	Dp.[c]	St. dev. [d] / ppm
									CO	6	5–104
									H_2	6	5–38
									N_2O	6	5
									NO	6	5–27
Ding (2021) [53]	x00101003	900–1350	1.00	0.57	$NH_3/H_2/CO$	O_2	–	CO_2/N_2	O_2	7	315–624
									CO	7	67–624
									H_2	7	5–58
									N_2O	7	5
									NO	7	5–8
Ding (2021) [53]	x00101004	900–1300	1.00	1.15	$NH_3/H_2/CO$	O_2	–	N_2	O_2	6	5–56
									CO	6	154–1520
									H_2	6	22–329
									NO	6	5–15
									N_2O	5	5
Ding (2021) [53]	x00101005	900–1350	1.00	1.15	$NH_3/H_2/CO$	O_2	–	CO_2/N_2	O_2	7	102–1465
									CO	7	520–1233
									H_2	7	5–76
									N_2O	7	5
									NO	7	5–13
Ding (2021) [53]	x00101006	1300	1.00	0.40–1.37	$NH_3/H_2/CO$	O_2	–	N_2	O_2	7	5–1333
									CO	7	11–213
									H_2	7	5–30
									N_2O	7	5
									NO	7	5–21
Ding (2021) [53]	x00101007	1300	1.00	0.38–1.51	$NH_3/H_2/CO$	O_2	–	CO_2/N_2	O_2	7	8–1605

Reference	XML ID	*T* / K	*p* / atm	Φ	Fuel	Ox.[a]	Dopant	Diluent	Meas.[b]	Dp.[c]	St. dev. [d] / ppm
									CO	7	54–393
									H_2	7	5
									N_2O	7	5
									NO	7	9–18

[a]: Oxidizer.
[a:] Measured species.
[b]: Number of data points in the dataset.
[c]: Overall absolute standard deviations of the data points in the dataset.

Table A3. Investigated concentration profile measurements in flow reactors: experimental details for each XML data file and standard deviations for each dataset.

Reference	XML ID	*T* / K	*p* / atm	Φ	Fuel	Ox.[a]	Dopant	Diluent	Meas.[b]	Dp.[c]	St. dev. [d] / ppm
Wargadalam (2000) [82]	x30100001	873–1273	1.00	0.00	NH_3/H_2	O_2	–	N_2	NH_3	9	5–26
									NO	9	5–12
Hulgaard (1993) [81]	x30199001	938–1373	1.04	0.02	NH_3	O_2	H_2O	–	NO	11	5
									N_2O	10	5
Hulgaard (1993) [81]	x30199003	974–1369	1.04	0.02	NH_3	O_2	–	N_2	N_2O	10	5
									NH_3	7	5–142
									NO	12	5
Wargadalam (2000) [82]	x30199006	873–1274	1.00	0.00	NH_3	O_2	–	N_2	NH_3	9	5–12
									NO	9	5
Song (2016) [30]	x30199007	453–925	29.61	0.62	NH_3	O_2	–	N_2	O_2	7	28–29
									NH_3	7	37–39
Song (2016) [30]	x30199009	451–902	98.69	0.62	NH_3	O_2	–	N_2	O_2	6	25–27
									NH_3	6	34–36
Song (2016) [30]	x30199011	453–900	29.61	0.01	NH_3	O_2	–	N_2	O_2	6	5
									NH_3	6	24–109
Song (2016) [30]	x30199013	453–925	29.61	0.01	NH_3	O_2	–	N_2	O_2	5	5
									NH_3	5	28–42
Song (2016) [30]	x30199015	692–902	98.69	0.01	NH_3	O_2	–	N_2	N_2O	4	5–10
									NH_3	9	5–39
Song (2016) [30]	x30199017	692–902	98.69	0.01	NH_3	O_2	–	N_2	N_2O	9	5–9
Caton (1995) [83]	x30199018	798–1200	1.01	0.00	NH_3	O_2	–	N_2	NO	15	5–6
									N_2O	15	5
									NH_3	15	5–50
Dean (1982) [93]	x30199019	1279	1.18	0.02	NH_3	O_2	–	He	NH_3	4	17–49

Reference	XML ID	*T* / K	*p* / atm	Φ	Fuel	Ox.[a]	Dopant	Diluent	Meas.[b]	Dp.[c]	St. dev. [d] / ppm
									NO	4	5
Dean (1982) [93]	x30199020	1279	1.18	0.02	NH_3	O_2	H_2O	–	NH_3	8	42–87
									NO	8	5
Stagni (2020) [34]	x30199021	1073–1973	1.25	0.38	NH_3	O_2	–	He	NH_3	19	5–55
									O_2	19	76–134
									NO	19	5–5
									N_2	19	5–27
									H_2O	19	5–113
									H_2	19	5
Abián (2021) [94]	x30199022	1175–1425	1.00	–	NH_3	–	–	N_2	NH_3	8	53–56
									H_2	8	5–13
Abián (2021) [94]	x30199023	875–1475	1.00	2.44	NH_3	O_2	–	N_2	NH_3	16	27–49
									O_2	16	5–11
									H_2	16	5
									NO	16	5
									NO_2	16	5
									N_2O	16	5
Abián (2021) [94]	x30199024	875–1425	1.00	1.34	NH_3	O_2	–	N_2	NH_3	14	24–52
									O_2	14	11–30
									H_2	14	5–5
									NO	14	5
									NO_2	14	5
									N_2O	14	5
Abián (2021) [94]	x30199025	875–1425	1.00	0.94	NH_3	O_2	–	N_2	NH_3	13	5–49
									O_2	13	5–35

Reference	XML ID	*T* / K	*p* / atm	Φ	Fuel	Ox.[a]	Dopant	Diluent	Meas.[b]	Dp.[c]	St. dev. [d] / ppm
									H_2	13	5
									NO	13	5
									NO_2	13	5
									N_2O	13	5
Abián (2021) [94]	x30199026	875–1425	1.00	0.87	NH_3	O_2	–	N_2	NH_3	14	5–46
									O_2	14	5–66
									H_2	14	5
									NO	14	5
									NO_2	14	5
									N_2O	14	5
Abián (2021) [94]	x30199027	875–1425	1.00	0.47	NH_3	O_2	–	N_2	NH_3	15	5–50
									O_2	15	70–129
									H_2	15	5
									NO	15	5–44
									NO_2	15	5
									N_2O	15	5
Abián (2021) [94]	x30199028	875–1425	1.00	0.19	NH_3	O_2	–	N_2	NH_3	13	5–44
									O_2	13	99–124
									H_2	13	5
									NO	13	5–28
									NO_2	13	5
									N_2O	13	5
Abián (2021) [94]	x30199029	1025–1425	1.00	0.09	NH_3	O_2	–	N_2	NH_3	15	5–54
									O_2	15	192–220
									H_2	15	5

Reference	XML ID	*T* / K	*p* / atm	Φ	Fuel	Ox.[a]	Dopant	Diluent	Meas.[b]	Dp.[c]	St. dev. [d] / ppm
									NO	15	5–23
									NO_2	15	5
									N_2O	15	5
Abián (2021) [94]	x30199030	875–1425	1.00	0.05	NH_3	O_2	–	N_2	NH_3	15	5–52
									O_2	15	418–438
									H_2	15	5
									NO	15	5
									NO_2	15	5
									N_2O	15	5
Abián (2021) [94]	x30199031	875–1450	1.00	0.88	NH_3	O_2	H_2O	–	NH_3	16	5–48
									O_2	16	5–42
									H_2	16	5–7
									NO	16	5
									NO_2	16	5
									N_2O	16	5
Wargadalam (2000) [82]	x30101006	873–1273	1.00	0.01	NH_3/CO	O_2	–	N_2	NH_3	9	5–18
									NO	9	5–8

[a]: Oxidizer.
[a:] Measured species.
[b]: Number of data points in the dataset.
[c]: Overall absolute standard deviations of the data points in the dataset.

Table A4. Investigated laminar burning velocity measurements: experimental details and standard deviations by datasets.

Reference [a]	XML ID	*T* / K	*p* / atm	Φ	Fuel	Ox.[a]	Dopant	Diluent	Meas. [b]	Dp. [c]	Method [d]	St. dev. [e] / cm s^{-1}
Lee (2010a) [95]	x20100004	298	1.00	0.60	NH_3/H_2	O_2	–	N_2	LBV	5	OPSF	1.98–5.74
Lee (2010a) [95]	x20100005	298	1.00	1.00	NH_3/H_2	O_2	–	N_2	LBV	5	OPSF	6.53–15.60
Lee (2010a) [95]	x20100006	298	1.00	1.67	NH_3/H_2	O_2	–	N_2	LBV	5	OPSF	4.12–21.63
Lee (2010b) [96]	x20100007	298	1.00	0.60	NH_3/H_2	O_2	–	N_2	LBV	2	OPSF	0.50–1.06
Lee (2010b) [96]	x20100008	298	1.00	0.80	NH_3/H_2	O_2	–	N_2	LBV	2	OPSF	1.00–2.04
Lee (2010b) [96]	x20100009	298	1.00	1.00	NH_3/H_2	O_2	–	N_2	LBV	3	OPSF	0.91–3.03
Lee (2010b) [96]	x20100010	298	1.00	1.25	NH_3/H_2	O_2	–	N_2	LBV	2	OPSF	1.36–2.74
Lee (2010b) [96]	x20100011	298	1.00	1.67	NH_3/H_2	O_2	–	N_2	LBV	1	OPSF	1.46
Ichikawa (2015) [12]	x20100012	298	0.99	1.00	NH_3/H_2	O_2	–	N_2	LBV	9	OPSF	0.50–19.39
Ichikawa (2015) [12]	x20100013	298	0.99	1.00	NH_3/H_2	O_2	–	N_2	LBV	7	OPSF	0.34–0.77
Ichikawa (2015) [12]	x20100014	298	0.99	1.00	NH_3/H_2	O_2	–	N_2	LBV	6	OPSF	0.50–0.56
Han (2019) [14]	x20100018	298	1.00	1.00	NH_3/H_2	O_2	–	N_2	LBV	19	HFB	0.50
Han (2019) [14]	x20100019	298	1.00	0.75–1.40	NH_3/H_2	O_2	–	N_2	LBV	14	HFB	0.50
Han (2019) [14]	x20100020	298	1.00	0.70–1.60	NH_3/H_2	O_2	–	N_2	LBV	19	HFB	0.50
Han (2019) [14]	x20100021	298	1.00	0.70–1.60	NH_3/H_2	O_2	–	N_2	LBV	19	HFB	0.50
Han (2019) [14]	x20100022	298	1.00	0.70–1.60	NH_3/H_2	O_2	–	N_2	LBV	19	HFB	0.50
S. Wang (2020) [15]	x20100023	298	0.99	0.60–1.60	NH_3/H_2	O_2	–	N_2	LBV	15	HFB	0.61–0.76
S. Wang (2020) [15]	x20100024	298	2.96	0.60–1.60	NH_3/H_2	O_2	–	N_2	LBV	15	HFB	0.60–0.87
S. Wang (2020) [15]	x20100025	298	0.99	0.70–1.50	NH_3/H_2	O_2	–	N_2	LBV	12	HFB	0.50–0.89
S. Wang (2020) [15]	x20100026	298	2.96	0.70–1.60	NH_3/H_2	O_2	–	N_2	LBV	13	HFB	0.50
S. Wang (2020) [15]	x20100027	298	4.93	0.70–1.50	NH_3/H_2	O_2	–	N_2	LBV	12	HFB	0.50
Lhuillier (2020) [101]	x20100028	298	0.99	0.80–1.20	NH_3/H_2	O_2	–	N_2	LBV	5	OPSF	0.74–0.80
Lhuillier (2020) [101]	x20100029	323	0.99	0.80–1.30	NH_3/H_2	O_2	–	N_2	LBV	6	OPSF	0.70–0.80

Reference [a]	XML ID	T / K	p / atm	Φ	Fuel	Ox.[a]	Dopant	Diluent	Meas. [b]	Dp. [c]	Method [d]	St. dev. [e] / cm s^{-1}
Lhuillier (2020) [101]	x20100030	373	0.99	0.80–1.40	NH_3/H_2	O_2	–	N_2	LBV	7	OPSF	0.85–1.38
Lhuillier (2020) [101]	x20100031	423	0.99	0.80–1.40	NH_3/H_2	O_2	–	N_2	LBV	7	OPSF	0.91–1.39
Lhuillier (2020) [101]	x20100032	473	0.99	0.80–1.40	NH_3/H_2	O_2	–	N_2	LBV	7	OPSF	0.71–1.31
Lhuillier (2020) [101]	x20100033	298	0.99	0.80–1.30	NH_3/H_2	O_2	–	N_2	LBV	6	OPSF	0.83–0.99
Lhuillier (2020) [101]	x20100034	323	0.99	0.80–1.30	NH_3/H_2	O_2	–	N_2	LBV	6	OPSF	0.53–0.75
Lhuillier (2020) [101]	x20100035	373	0.99	0.80–1.40	NH_3/H_2	O_2	–	N_2	LBV	7	OPSF	0.97–1.13
Lhuillier (2020) [101]	x20100036	423	0.99	0.80–1.40	NH_3/H_2	O_2	–	N_2	LBV	7	OPSF	1.38–1.87
Lhuillier (2020) [101]	x20100037	473	0.99	0.80–1.40	NH_3/H_2	O_2	–	N_2	LBV	7	OPSF	0.76–2.30
Lhuillier (2020) [101]	x20100038	298	0.99	0.80–1.40	NH_3/H_2	O_2	–	N_2	LBV	7	OPSF	0.66–0.84
Lhuillier (2020) [101]	x20100039	323	0.99	0.80–1.40	NH_3/H_2	O_2	–	N_2	LBV	7	OPSF	0.86–1.05
Lhuillier (2020) [101]	x20100040	373	0.99	0.80–1.40	NH_3/H_2	O_2	–	N_2	LBV	7	OPSF	1.22–1.44
Lhuillier (2020) [101]	x20100041	423	0.99	0.80–1.40	NH_3/H_2	O_2	–	N_2	LBV	7	OPSF	1.37–1.66
Lhuillier (2020) [101]	x20100042	473	0.99	0.80–1.40	NH_3/H_2	O_2	–	N_2	LBV	7	OPSF	1.18–2.22
Lhuillier (2020) [101]	x20100043	298	0.99	0.80–1.40	NH_3/H_2	O_2	–	N_2	LBV	7	OPSF	1.57–1.71
Lhuillier (2020) [101]	x20100044	323	0.99	0.80–1.40	NH_3/H_2	O_2	–	N_2	LBV	7	OPSF	1.15–1.47
Lhuillier (2020) [101]	x20100045	373	0.99	0.80–1.40	NH_3/H_2	O_2	–	N_2	LBV	7	OPSF	1.44–1.74
Lhuillier (2020) [101]	x20100046	423	0.99	0.80–1.40	NH_3/H_2	O_2	–	N_2	LBV	7	OPSF	1.65–2.54
Lhuillier (2020) [101]	x20100047	473	0.99	0.80–1.40	NH_3/H_2	O_2	–	N_2	LBV	7	OPSF	2.32–2.71
Lhuillier (2020) [101]	x20100048	298	0.99	0.80–1.40	NH_3/H_2	O_2	–	N_2	LBV	7	OPSF	1.55–2.09
Lhuillier (2020) [101]	x20100049	323	0.99	0.80–1.40	NH_3/H_2	O_2	–	N_2	LBV	7	OPSF	1.67–2.28
Lhuillier (2020) [101]	x20100050	373	0.99	0.80–1.40	NH_3/H_2	O_2	–	N_2	LBV	7	OPSF	1.45–2.51
Lhuillier (2020) [101]	x20100051	423	0.99	0.80–1.40	NH_3/H_2	O_2	–	N_2	LBV	7	OPSF	2.33–3.24
Lhuillier (2020) [101]	x20100052	473	0.99	0.80–1.40	NH_3/H_2	O_2	–	N_2	LBV	7	OPSF	2.57–3.64
Lhuillier (2020) [101]	x20100053	298	0.99	0.80–1.40	NH_3/H_2	O_2	–	N_2	LBV	7	OPSF	2.03–2.63

Reference [a]	XML ID	T / K	p / atm	Φ	Fuel	Ox.[a]	Dopant	Diluent	Meas. [b]	Dp. [c]	Method [d]	St. dev. [e] / cm s^{-1}
Lhuillier (2020) [101]	x20100054	323	0.99	0.80–1.40	NH_3/H_2	O_2	–	N_2	LBV	7	OPSF	1.64–2.02
Lhuillier (2020) [101]	x20100055	373	0.99	0.80–1.40	NH_3/H_2	O_2	–	N_2	LBV	7	OPSF	3.30–3.59
Lhuillier (2020) [101]	x20100056	423	0.99	0.80–1.40	NH_3/H_2	O_2	–	N_2	LBV	7	OPSF	3.05–3.42
Lhuillier (2020) [101]	x20100057	473	0.99	0.80–1.40	NH_3/H_2	O_2	–	N_2	LBV	7	OPSF	3.43–4.80
Lhuillier (2020) [101]	x20100058	298	0.99	0.80–1.40	NH_3/H_2	O_2	–	N_2	LBV	7	OPSF	2.94–3.66
Lhuillier (2020) [101]	x20100059	323	0.99	0.80–1.40	NH_3/H_2	O_2	–	N_2	LBV	7	OPSF	3.25–4.35
Lhuillier (2020) [101]	x20100060	373	0.99	0.80–1.40	NH_3/H_2	O_2	–	N_2	LBV	7	OPSF	3.65–5.51
Lhuillier (2020) [101]	x20100061	423	0.99	0.80–1.40	NH_3/H_2	O_2	–	N_2	LBV	7	OPSF	5.25–6.02
Lhuillier (2020) [101]	x20100062	473	0.99	0.80–1.30	NH_3/H_2	O_2	–	N_2	LBV	6	OPSF	5.74–6.95
Shrestha (2021) [41]	x20100063	472	2.92	1.10	NH_3/H_2	O_2	–	N_2	LBV	1	OPSF	0.50
Shrestha (2021) [41]	x20100064	473–476	2.89–2.94	0.80–1.40	NH_3/H_2	O_2	–	N_2	LBV	7	OPSF	0.88–1.13
Shrestha (2021) [41]	x20100065	470	2.88	1.10	NH_3/H_2	O_2	–	N_2	LBV	1	OPSF	0.50
Shrestha (2021) [41]	x20100066	470	2.90	1.10	NH_3/H_2	O_2	–	N_2	LBV	1	OPSF	0.50
Shrestha (2021) [41]	x20100067	468–474	4.84–4.87	1.10	NH_3/H_2	O_2	–	N_2	LBV	4	OPSF	0.50–1.04
Shrestha (2021) [41]	x20100068	468–475	6.86–6.88	1.10	NH_3/H_2	O_2	–	N_2	LBV	4	OPSF	0.50–1.53
Shrestha (2021) [41]	x20100069	476	9.43	1.10	NH_3/H_2	O_2	–	N_2	LBV	1	OPSF	3.32
Gotama (2022) [37]	x20100070	298	0.99	0.80–1.80	NH_3/H_2	O_2	–	N_2	LBV	8	OPSF	0.17–0.58
Gotama (2022) [37]	x20100071	298	4.93	1.00–1.80	NH_3/H_2	O_2	–	N_2	LBV	6	OPSF	0.50–0.74
Mei (2021) [42]	x20100072	298	1.00	0.70–1.40	NH_3/H_2	O_2	–	N_2	LBV	8	OPSF	0.56–0.79
Mei (2021) [42]	x20100073	298	2.00	0.80–1.40	NH_3/H_2	O_2	–	N_2	LBV	7	OPSF	0.92–1.42
Mei (2021) [42]	x20100074	298	5.00	1.10–1.40	NH_3/H_2	O_2	–	N_2	LBV	4	OPSF	0.38–0.49
Mei (2021) [42]	x20100075	298	10.00	1.10–1.40	NH_3/H_2	O_2	–	N_2	LBV	4	OPSF	0.43–0.71
Mei (2021) [42]	x20100076	298	1.00	1.00	NH_3/H_2	O_2	–	N_2	LBV	8	OPSF	0.50–5.53
Mei (2021) [42]	x20100077	298	2.00	1.00	NH_3/H_2	O_2	–	N_2	LBV	6	OPSF	0.41–1.32

Reference [a]	XML ID	T / K	p / atm	Φ	Fuel	Ox.[a]	Dopant	Diluent	Meas. [b]	Dp. [c]	Method [d]	St. dev. [e] / cm s^{-1}
Mei (2021) [42]	x20100078	298	5.00	1.00	NH_3/H_2	O_2	–	N_2	LBV	3	OPSF	0.50–0.98
Wang (2021) [102]	x20100079	360	0.99	0.50–1.50	NH_3/H_2	O_2	–	N_2	LBV	11	OPSF	0.50–1.92
Wang (2021) [102]	x20100080	360	0.99–4.93	1.00	NH_3/H_2	O_2	–	N_2	LBV	3	OPSF	0.50–1.53
Wang (2021) [102]	x20100081	360	0.99–4.93	1.00	NH_3/H_2	O_2	–	N_2	LBV	3	OPSF	0.50–2.85
Osipova (2021) [103]	x20100082	368	1.00	0.70–1.50	NH_3/H_2	O_2	–	N_2	LBV	9	BF	2.58–4.51
Hayakawa (2015) [97]	x20199002	298	0.99	0.80–1.20	NH_3	O_2	–	N_2	LBV	5	OPSF	0.50
Hayakawa (2015) [97]	x20199003	298	2.96	0.90–1.20	NH_3	O_2	–	N_2	LBV	4	OPSF	0.50
Hayakawa (2015) [97]	x20199004	298	4.93	0.90–1.20	NH_3	O_2	–	N_2	LBV	4	OPSF	0.50
Han (2019) [14]	x20199005	298	1.00	0.85–1.25	NH_3	O_2	–	N_2	LBV	9	HFB	1.41
Liu (2019) [99]	x20199006	298	0.50	0.50–1.30	NH_3	O_2	–	–	LBV	4	OPSF	5.57–8.85
Liu (2019) [99]	x20199007	298	0.70	0.50–1.30	NH_3	O_2	–	–	LBV	3	OPSF	5.27–7.42
Liu (2019) [99]	x20199008	298	1.00	0.40–2.00	NH_3	O_2	–	–	LBV	10	OPSF	1.97–17.76
Liu (2019) [99]	x20199009	298	1.40	0.75–1.75	NH_3	O_2	–	–	LBV	4	OPSF	4.91–11.34
Liu (2019) [99]	x20199010	298	1.60	0.50–1.75	NH_3	O_2	–	–	LBV	5	OPSF	3.80–9.44
Mei (2019) [33]	x20199011	298	1.00	0.90–1.30	NH_3	O_2	–	N_2	LBV	5	OPSF	0.50
Mei (2019) [33]	x20199012	298	1.00	0.60–1.50	NH_3	O_2	–	N_2	LBV	10	OPSF	0.50–0.83
Mei (2019) [33]	x20199013	298	2.00	0.60–1.50	NH_3	O_2	–	N_2	LBV	10	OPSF	0.40–0.52
Mei (2019) [33]	x20199014	298	5.00	0.60–1.50	NH_3	O_2	–	N_2	LBV	10	OPSF	0.36–0.50
Mei (2019) [33]	x20199015	298	1.00	0.70	NH_3	O_2	–	N_2	LBV	5	OPSF	0.50–2.16
Mei (2019) [33]	x20199016	298	1.00	1.00	NH_3	O_2	–	N_2	LBV	6	OPSF	0.50–1.55
Mei (2019) [33]	x20199017	298	1.00	1.50	NH_3	O_2	–	N_2	LBV	5	OPSF	0.43–0.62
D. Wang (2020) [100]	x20199018	303	0.99	0.60–1.40	NH_3	O_2	–	N_2	LBV	9	OPSF	2.18–3.34
D. Wang (2020) [100]	x20199019	303	0.99	0.60–1.40	NH_3	O_2	–	N_2	LBV	9	OPSF	2.20–3.36
D. Wang (2020) [100]	x20199020	303	0.99	0.60–1.40	NH_3	O_2	–	–	LBV	9	OPSF	2.15–3.52

Reference [a]	XML ID	T / K	p / atm	Φ	Fuel	Ox.[a]	Dopant	Diluent	Meas. [b]	Dp. [c]	Method [d]	St. dev. [e] / cm s^{-1}
D. Wang (2020) [100]	x20199021	303–393	0.99	0.70	NH_3	O_2	–	N_2	LBV	4	OPSF	1.40–2.69
D. Wang (2020) [100]	x20199022	303–393	0.99	0.70	NH_3	O_2	–	N_2	LBV	4	OPSF	2.64–4.74
D. Wang (2020) [100]	x20199023	303–393	0.99	0.70	NH_3	O_2	–	–	LBV	4	OPSF	3.24–4.39
D. Wang (2020) [100]	x20199024	303–393	0.99	1.40	NH_3	O_2	–	N_2	LBV	4	OPSF	1.73–1.99
D. Wang (2020) [100]	x20199025	303–393	0.99	1.40	NH_3	O_2	–	N_2	LBV	4	OPSF	1.78–2.42
D. Wang (2020) [100]	x20199026	303–393	0.99	1.40	NH_3	O_2	–	–	LBV	4	OPSF	2.00–3.00
Lhuillier (2020) [101]	x20199027	298	0.99	0.90–1.10	NH_3	O_2	–	N_2	LBV	3	OPSF	0.57–0.64
Lhuillier (2020) [101]	x20199028	323	0.99	0.90–1.20	NH_3	O_2	–	N_2	LBV	4	OPSF	0.50–0.63
Lhuillier (2020) [101]	x20199029	373	0.99	0.90–1.30	NH_3	O_2	–	N_2	LBV	5	OPSF	0.50–0.70
Lhuillier (2020) [101]	x20199030	423	0.99	0.80–1.30	NH_3	O_2	–	N_2	LBV	6	OPSF	0.75–0.91
Lhuillier (2020) [101]	x20199031	473	0.99	0.80–1.40	NH_3	O_2	–	N_2	LBV	7	OPSF	0.97–1.14
Shrestha (2021) [41]	x20199032	472–475	2.92–2.98	0.80–1.40	NH_3	O_2	–	N_2	LBV	7	OPSF	0.85–0.93
Shrestha (2021) [41]	x20199033	298	0.99	0.90–1.10	NH_3	O_2	–	N_2	LBV	3	OPSF	0.50
Shrestha (2021) [41]	x20199034	298	0.99	0.90–1.20	NH_3	O_2	–	N_2	LBV	4	OPSF	0.50
Shrestha (2021) [41]	x20199035	298	0.99	0.80–1.30	NH_3	O_2	–	N_2	LBV	6	OPSF	0.59–2.15
Shrestha (2021) [41]	x20199036	298	0.99	0.80–1.30	NH_3	O_2	–	N_2	LBV	6	OPSF	0.50–1.19
Shrestha (2021) [41]	x20199037	298	0.99	0.80–1.30	NH_3	O_2	–	N_2	LBV	6	OPSF	0.50–0.95
Shrestha (2021) [41]	x20199038	323	0.99	0.90–1.20	NH_3	O_2	–	N_2	LBV	4	OPSF	0.50–0.60
Shrestha (2021) [41]	x20199039	323	0.99	0.90–1.20	NH_3	O_2	–	N_2	LBV	4	OPSF	0.50–0.61
Shrestha (2021) [41]	x20199040	323	0.99	0.80–1.30	NH_3	O_2	–	N_2	LBV	6	OPSF	0.75–1.24
Shrestha (2021) [41]	x20199041	323	0.99	0.80–1.30	NH_3	O_2	–	N_2	LBV	6	OPSF	0.70–1.40
Shrestha (2021) [41]	x20199042	323	0.99	0.80–1.30	NH_3	O_2	–	N_2	LBV	6	OPSF	0.72–1.39
Shrestha (2021) [41]	x20199043	373	0.99	1.00–1.30	NH_3	O_2	–	N_2	LBV	4	OPSF	0.50–2.48
Shrestha (2021) [41]	x20199044	373	0.99	0.80–1.30	NH_3	O_2	–	N_2	LBV	6	OPSF	0.69–3.56

Reference [a]	XML ID	T / K	p / atm	Φ	Fuel	Ox.[a]	Dopant	Diluent	Meas. [b]	Dp. [c]	Method [d]	St. dev. [e] / cm s^{-1}
Shrestha (2021) [41]	x20199045	373	0.99	0.80–1.30	NH_3	O_2	–	N_2	LBV	6	OPSF	0.90–1.67
Shrestha (2021) [41]	x20199046	373	0.99	0.80–1.30	NH_3	O_2	–	N_2	LBV	6	OPSF	0.63–1.43
Shrestha (2021) [41]	x20199047	373	0.99	0.80–1.30	NH_3	O_2	–	N_2	LBV	6	OPSF	0.93–1.52
Shrestha (2021) [41]	x20199048	298	0.99	0.90–1.10	NH_3	O_2	–	He	LBV	3	OPSF	0.64–1.51
Shrestha (2021) [41]	x20199049	298	0.99	0.90–1.20	NH_3	O_2	–	He	LBV	4	OPSF	0.83–0.98
Takeishi (2015) [98]	x20199050	298	1.00	0.90–1.40	NH_3	O_2	–	N_2	LBV	8	BF	0.73–1.42
Takeishi (2015) [98]	x20199051	298	1.00	0.80–1.40	NH_3	O_2	–	N_2	LBV	9	BF	1.06–1.71
Takeishi (2015) [98]	x20199052	298	1.00	0.80–1.40	NH_3	O_2	–	N_2	LBV	11	BF	1.47–2.31
N. Wang (2021) [102]	x20199053	360	0.99	0.70–1.40	NH_3	O_2	–	N_2	LBV	8	OPSF	0.50
N. Wang (2021) [102]	x20199054	360	0.99–4.93	1.00	NH_3	O_2	–	N_2	LBV	3	OPSF	0.50
Han (2019) [14]	x20101000	298	1.00	1.00	NH_3/CO	O_2	–	N_2	LBV	44	HFB	0.50
Han (2019) [14]	x20101001	298	1.00	0.80–1.45	NH_3/CO	O_2	–	N_2	LBV	14	HFB	0.50
Han (2019) [14]	x20101002	298	1.00	0.70–1.60	NH_3/CO	O_2	–	N_2	LBV	19	HFB	0.50
Han (2019) [14]	x20101003	298	1.00	0.70–1.60	NH_3/CO	O_2	–	N_2	LBV	19	HFB	0.50
Han (2019) [14]	x20101004	298	1.00	0.70–1.70	NH_3/CO	O_2	–	N_2	LBV	21	HFB	0.50–0.52
Han (2020) [16]	x20101005	298	1.00	1.00	NH_3/H_2/CO	O_2	–	N_2	LBV	42	HFB	0.52–0.58
Han (2020) [16]	x20101006	298	1.00	0.85–1.40	NH_3/H_2/CO	O_2	–	N_2	LBV	12	HFB	0.50
Han (2020) [16]	x20101007	298	1.00	0.70–1.60	NH_3/H_2/CO	O_2	–	N_2	LBV	19	HFB	0.50
Han (2020) [16]	x20101008	298	1.00	0.70–1.60	NH_3/H_2/CO	O_2	–	N_2	LBV	19	HFB	0.50
Han (2020) [16]	x20101009	298	1.00	1.00	NH_3/H_2/CO	O_2	–	N_2	LBV	29	HFB	0.50–0.51
Han (2020) [16]	x20101010	298	1.00	0.80–1.40	NH_3/H_2/CO	O_2	–	N_2	LBV	13	HFB	0.50
Han (2020) [16]	x20101011	298	1.00	0.70–1.60	NH_3/H_2/CO	O_2	–	N_2	LBV	19	HFB	0.50
Han (2020) [16]	x20101012	298	1.00	0.70–1.60	NH_3/H_2/CO	O_2	–	N_2	LBV	19	HFB	0.50
Mei (2020) [17]	x20101013	298	1.00	1.00	NH_3/H_2/CO	O_2	–	N_2	LBV	6	OPSF	0.50–4.85

Reference [a]	XML ID	T / K	p / atm	Φ	Fuel	Ox.[a]	Dopant	Diluent	Meas. [b]	Dp. [c]	Method [d]	St. dev. [e] / cm s^{-1}
Mei (2020) [17]	x20101014	298	1.00	1.00	$NH_3/H_2/CO$	O_2	–	N_2	LBV	5	OPSF	0.50–4.28
Mei (2020) [17]	x20101015	298	1.00	1.00	$NH_3/H_2/CO$	O_2	–	N_2	LBV	5	OPSF	0.72–8.33
Mei (2020) [17]	x20101016	298	1.00	0.70–1.50	$NH_3/H_2/CO$	O_2	–	N_2	LBV	9	OPSF	0.47–0.60
Mei (2020) [17]	x20101017	298	2.00	0.70–1.50	$NH_3/H_2/CO$	O_2	–	N_2	LBV	9	OPSF	0.38–0.50
Mei (2020) [17]	x20101018	298	5.00	0.90–1.50	$NH_3/H_2/CO$	O_2	–	N_2	LBV	7	OPSF	0.36–0.50
Mei (2020) [17]	x20101019	298	10.00	1.10–1.40	$NH_3/H_2/CO$	O_2	–	N_2	LBV	4	OPSF	0.37–0.50
Mei (2020) [17]	x20101020	298	1.00	0.70–1.50	$NH_3/H_2/CO$	O_2	–	N_2	LBV	9	OPSF	0.60–0.97
Mei (2020) [17]	x20101021	298	2.00	0.70–1.50	$NH_3/H_2/CO$	O_2	–	N_2	LBV	9	OPSF	0.48–0.81
Mei (2020) [17]	x20101022	298	5.00	1.10–1.50	$NH_3/H_2/CO$	O_2	–	N_2	LBV	5	OPSF	0.48–0.68
Mei (2020) [17]	x20101023	298	10.00	1.10–1.40	$NH_3/H_2/CO$	O_2	–	N_2	LBV	4	OPSF	0.50–0.76
Mei (2020) [17]	x20101024	298	1.00	0.70–1.50	$NH_3/H_2/CO$	O_2	–	N_2	LBV	9	OPSF	0.74–1.35
Mei (2020) [17]	x20101025	298	2.00	0.70–1.50	$NH_3/H_2/CO$	O_2	–	N_2	LBV	9	OPSF	0.64–1.22
Mei (2020) [17]	x20101026	298	5.00	1.10–1.50	$NH_3/H_2/CO$	O_2	–	N_2	LBV	5	OPSF	0.40–0.52
Mei (2020) [17]	x20101027	298	10.00	1.10–1.50	$NH_3/H_2/CO$	O_2	–	N_2	LBV	5	OPSF	0.47–0.61
S. Wang (2020) [15]	x20101028	298	1.00	1.00	$NH_3/H_2/CO$	O_2	–	N_2	LBV	17	HFB	0.50–0.72
S. Wang (2020) [15]	x20101029	298	3.00	1.00	$NH_3/H_2/CO$	O_2	–	N_2	LBV	14	HFB	0.50–0.90
S. Wang (2020) [15]	x20101030	298	5.00	1.00	$NH_3/H_2/CO$	O_2	–	N_2	LBV	13	HFB	0.50
S. Wang (2020) [15]	x20101031	298	1.00	1.00	NH_3/CO	O_2	–	N_2	LBV	21	HFB	0.50–0.53
S. Wang (2020) [15]	x20101032	298	3.00	1.00	NH_3/CO	O_2	–	N_2	LBV	21	HFB	0.50–0.89
S. Wang (2020) [15]	x20101033	298	5.00	1.00	NH_3/CO	O_2	–	N_2	LBV	18	HFB	0.50
S. Wang (2020) [15]	x20101034	298	1.00	0.80–1.60	$NH_3/H_2/CO$	O_2	–	N_2	LBV	11	HFB	0.50–0.65
S. Wang (2020) [15]	x20101035	298	3.00	0.70–1.60	$NH_3/H_2/CO$	O_2	–	N_2	LBV	12	HFB	0.50–0.55
S. Wang (2020) [15]	x20101036	298	5.00	0.70–1.60	$NH_3/H_2/CO$	O_2	–	N_2	LBV	10	HFB	0.50
S. Wang (2020) [15]	x20101037	298	1.00	0.70–1.60	$NH_3/H_2/CO$	O_2	–	N_2	LBV	12	HFB	0.50–0.51

Reference [a]	XML ID	T / K	p / atm	Φ	Fuel	Ox.[a]	Dopant	Diluent	Meas. [b]	Dp. [c]	Method [d]	St. dev. [e] / cm s^{-1}
S. Wang (2020) [15]	x20101038	298	3.00	0.70–1.60	$NH_3/H_2/CO$	O_2	–	N_2	LBV	11	HFB	0.50
S. Wang (2020) [15]	x20101039	298	5.00	0.80–1.60	$NH_3/H_2/CO$	O_2	–	N_2	LBV	9	HFB	0.51–0.63
S. Wang (2020) [15]	x20101040	298	1.00	0.80–1.60	NH_3/CO	O_2	–	N_2	LBV	11	HFB	0.50–0.64
S. Wang (2020) [15]	x20101041	298	3.00	0.70–1.60	NH_3/CO	O_2	–	N_2	LBV	12	HFB	0.50
S. Wang (2020) [15]	x20101042	298	5.00	0.70–1.40	NH_3/CO	O_2	–	N_2	LBV	10	HFB	0.50
S. Wang (2020) [15]	x20101043	298	1.00	0.80–1.60	NH_3/CO	O_2	–	N_2	LBV	11	HFB	0.50
S. Wang (2020) [15]	x20101044	298	3.00	0.80–1.40	NH_3/CO	O_2	–	N_2	LBV	9	HFB	0.50
S. Wang (2020) [15]	x20101045	298	5.00	0.80–1.30	NH_3/CO	O_2	–	N_2	LBV	8	HFB	0.50
Zhou (2021) [107]	x20101046	297–298	1.00	0.70–1.41	$NH_3/H_2/CO$	O_2	–	N_2	LBV	8	OPSF	0.47–1.04
Zhou (2021) [107]	x20101047	322–323	1.00	0.71–1.41	$NH_3/H_2/CO$	O_2	–	N_2	LBV	8	OPSF	0.49–1.33
Zhou (2021) [107]	x20101048	372–373	1.00	0.70–1.42	$NH_3/H_2/CO$	O_2	–	N_2	LBV	8	OPSF	0.56–1.34
Zhou (2021) [107]	x20101049	422–423	1.00	0.71–1.41	$NH_3/H_2/CO$	O_2	–	N_2	LBV	8	OPSF	0.87–1.34
Zhou (2021) [107]	x20101050	298	1.00	0.71–1.41	$NH_3/H_2/CO$	O_2	–	N_2	LBV	8	OPSF	0.62–1.48
Zhou (2021) [107]	x20101051	323	1.00	0.70–1.42	$NH_3/H_2/CO$	O_2	–	N_2	LBV	8	OPSF	0.47–1.37
Zhou (2021) [107]	x20101052	372–373	1.00	0.71–1.41	$NH_3/H_2/CO$	O_2	–	N_2	LBV	8	OPSF	0.72–1.26
Zhou (2021) [107]	x20101053	422–423	1.00	0.70–1.40	$NH_3/H_2/CO$	O_2	–	N_2	LBV	8	OPSF	1.05–1.87
Zhou (2021) [107]	x20101054	297–298	1.00	0.81–1.42	$NH_3/H_2/CO$	O_2	–	N_2	LBV	7	OPSF	0.73–1.40
Zhou (2021) [107]	x20101055	323	1.00	0.81–1.41	$NH_3/H_2/CO$	O_2	–	N_2	LBV	7	OPSF	1.31–2.09
Zhou (2021) [107]	x20101056	372–373	1.00	0.81–1.41	$NH_3/H_2/CO$	O_2	–	N_2	LBV	7	OPSF	1.09–1.91
Zhou (2021) [107]	x20101057	422–423	1.00	0.91–1.41	$NH_3/H_2/CO$	O_2	–	N_2	LBV	6	OPSF	1.34–2.20
Zhou (2021) [107]	x20101058	298	1.00	0.98–1.02	$NH_3/H_2/CO$	O_2	–	CO_2/N_2	LBV	11	OPSF	0.50–1.76
Zhou (2021) [107]	x20101059	298	1.00	0.80–1.30	$NH_3/H_2/CO$	O_2	–	CO_2/N_2	LBV	6	OPSF	0.50–0.61
Zhou (2021) [107]	x20101060	323	1.00	0.80–1.31	$NH_3/H_2/CO$	O_2	–	CO_2/N_2	LBV	6	OPSF	0.50–0.78
Zhou (2021) [107]	x20101061	372–373	1.00	0.80–1.31	$NH_3/H_2/CO$	O_2	–	CO_2/N_2	LBV	6	OPSF	0.80–1.09

Reference [a]	XML ID	T / K	p / atm	Φ	Fuel	Ox.[a]	Dopant	Diluent	Meas. [b]	Dp. [c]	Method [d]	St. dev. [e] / cm s^{-1}
Zhou (2021) [107]	x20101062	422–423	1.00	0.81–1.32	$NH_3/H_2/CO$	O_2	–	CO_2/N_2	LBV	6	OPSF	0.73–0.98
Zhou (2021) [107]	x20101063	297–298	1.00	0.81–1.31	$NH_3/H_2/CO$	O_2	–	CO_2/N_2	LBV	6	OPSF	0.39–0.81
Zhou (2021) [107]	x20101064	323	1.00	0.80–1.31	$NH_3/H_2/CO$	O_2	–	CO_2/N_2	LBV	6	OPSF	0.54–0.89
Zhou (2021) [107]	x20101065	372–373	1.00	0.80–1.31	$NH_3/H_2/CO$	O_2	–	CO_2/N_2	LBV	6	OPSF	0.76–1.05
Zhou (2021) [107]	x20101066	422–423	1.00	0.81–1.32	$NH_3/H_2/CO$	O_2	–	CO_2/N_2	LBV	6	OPSF	0.50–1.00
Zhou (2021) [107]	x20101067	298	1.00	0.79–1.32	$NH_3/H_2/CO$	O_2	–	CO_2/N_2	LBV	6	OPSF	0.44–1.15
Zhou (2021) [107]	x20101068	322–323	1.00	0.71–1.41	$NH_3/H_2/CO$	O_2	–	CO_2/N_2	LBV	8	OPSF	0.59–1.01
Zhou (2021) [107]	x20101069	372–373	1.00	0.70–1.42	$NH_3/H_2/CO$	O_2	–	CO_2/N_2	LBV	8	OPSF	0.68–1.05
Zhou (2021) [107]	x20101070	422–423	1.00	0.70–1.40	$NH_3/H_2/CO$	O_2	–	CO_2/N_2	LBV	8	OPSF	0.74–1.01
Yin (2021) [108]	x20101071	298	1.00	0.70–1.60	$NH_3/H_2/CO$	O_2	–	N_2	LBV	10	OPSF	0.91–1.50
Yin (2021) [108]	x20101072	373	1.00	0.70–1.60	$NH_3/H_2/CO$	O_2	–	N_2	LBV	10	OPSF	0.59–1.52
Yin (2021) [108]	x20101073	443	1.00	0.70–1.60	$NH_3/H_2/CO$	O_2	–	N_2	LBV	10	OPSF	0.99–2.24
Yin (2021) [108]	x20101074	298	2.00	0.70–1.60	$NH_3/H_2/CO$	O_2	–	N_2	LBV	10	OPSF	0.39–0.86
Yin (2021) [108]	x20101075	298	3.00	0.70–1.60	$NH_3/H_2/CO$	O_2	–	N_2	LBV	10	OPSF	0.31–0.62
Yin (2021) [108]	x20101076	298	1.00	1.00–1.20	$NH_3/H_2/CO$	O_2	–	N_2	LBV	3	OPSF	0.50
Yin (2021) [108]	x20101077	298	1.00	0.70–1.50	$NH_3/H_2/CO$	O_2	–	N_2	LBV	9	OPSF	0.32–0.87
Yin (2021) [108]	x20101078	298	1.00	0.70–1.60	$NH_3/H_2/CO$	O_2	–	N_2	LBV	10	OPSF	0.58–1.43
Yin (2021) [108]	x20101079	298	1.00	0.70–1.60	$NH_3/H_2/CO$	O_2	–	N_2	LBV	10	OPSF	0.54–1.22

[a]: Oxidizer.
[b:] Measured quantity.
[c]: Number of data points in the experimental XML file (dataset).
[d]: Measurement method (BF = Bunsen flame, OPSF = outwardly propagating spherical flame, HFB = heat flux burner)
[e]: Overall absolute standard deviations of the data points in the experimental XML file (dataset).

Table A5. Averaged error function values for each investigated mechanism for the utilized shock tube ignition delay time measurement datasets (E_i) in the case of NH_3/H_2 fuel mixtures. In the table, "excl." means that no data point was included in the comparison from the corresponding dataset.

XML ID	Profile	All points	Included points	Excluded points	Tian-2009	Mathieu-2015	GDFKin-2016	Nakamura-2017	SanDiego-2018	Otomo-2018	Glarborg-2018	Okafor-2018	ELTE-2020	POLIMI-2020	NUIG-2020	Han-2020	Mei-2020	Konnov-2021	KAUST-2021	Shrestha-2021	Mei-2021	Zhou-2021	Gotama-2022
x10100003	IDT	8	8	0	9.7	1.1	57.3	3.7	0.8	0.5	0.3	2.1	0.3	7.4	1.2	3.5	19.0	2.4	10.6	2.8	17.7	4.3	4.2
x10100004	IDT	12	12	0	6.4	4.0	26.3	6.2	6.1	1.2	4.7	0.6	5.5	3.8	2.1	2.4	3.3	3.7	3.3	2.4	3.1	3.9	3.0
x10100005	IDT	7	7	0	2.6	4.3	28.6	2.1	2.4	7.8	1.5	3.0	3.5	2.4	1.7	15.8	4.3	1.0	1.7	1.1	3.8	10.5	14.0
x10100006	IDT	9	7	2	14.4	15.3	27.3	12.7	17.5	2.7	11.9	5.6	17.6	9.1	5.7	12.1	5.7	6.7	5.9	9.2	6.2	10.9	15.1
x10100007	IDT	5	5	0	2.5	2.9	6.7	3.5	3.0	5.0	1.4	4.3	2.8	2.2	0.7	7.1	4.9	1.5	2.0	6.4	5.6	18.2	7.2
x10100008	IDT	7	7	0	8.2	13.8	47.6	14.6	11.0	2.1	5.9	1.3	15.9	18.5	9.9	19.5	9.2	7.1	3.8	15.2	14.2	16.1	18.1
x10199009	IDT	8	8	0	4.5	14.6	21.9	18.4	62.9	7.4	8.0	71.7	8.3	2.1	3.0	5.0	12.4	11.6	12.4	3.4	11.5	39.3	16.5
x10199010	IDT	11	5	6	25.2	26.9	42.3	34.5	116.9	0.9	1.0	303.4	2.3	10.1	44.3	3.6	63.5	51.7	45.4	34.9	77.9	1.5	28.7
x10199011	IDT	9	9	0	2.2	30.2	9.9	15.1	96.6	8.4	2.4	136.5	1.8	2.5	4.0	1.3	19.4	7.0	12.3	5.4	19.5	14.1	2.5
x10199012	IDT	9	9	0	8.0	37.7	55.0	13.2	96.8	27.7	14.9	171.2	13.6	4.9	6.9	6.7	22.1	3.4	57.0	17.8	19.0	96.5	84.7
x10199013	IDT	10	0	10	excl	excl	excl	excl	excl	excl	excl	excl	excl	excl	excl	excl	excl	excl	excl	excl	excl	excl	excl
x10199014	IDT	9	4	5	4.3	81.6	69.5	36.9	243.1	25.2	2.9	378.4	3.0	2.2	5.0	2.0	25.9	2.0	30.7	6.3	21.8	89.9	35.3
x10199015	IDT	7	7	0	5.8	2.3	50.9	14.9	13.8	4.4	10.3	34.4	12.9	1.7	1.3	2.6	6.1	5.2	19.3	7.7	5.6	27.3	11.7
x10199016	IDT	9	3	6	15.6	60.5	62.8	36.9	190.1	9.4	40.0	369.6	40.9	10.2	16.1	0.3	80.6	6.6	54.6	34.3	82.4	11.4	5.1
x10199017	IDT	7	7	0	7.6	14.0	60.0	28.4	66.9	3.7	6.6	152.8	6.1	7.6	6.9	2.9	31.6	6.5	31.8	19.1	29.3	18.9	1.6
x10199018	IDT	7	3	4	30.8	101.5	12.7	8.1	77.0	3.8	9.5	171.4	5.9	55.2	79.2	31.4	240.6	47.6	46.8	33.3	235.4	193.4	114.4
x10199019	IDT	10	0	10	excl	excl	excl	excl	excl	excl	excl	excl	excl	excl	excl	excl	excl	excl	excl	excl	excl	excl	excl
x10199020	IDT	8	0	8	excl	excl	excl	excl	excl	excl	excl	excl	excl	excl	excl	excl	excl	excl	excl	excl	excl	excl	excl
x10199021	IDT	5	0	5	excl	excl	excl	excl	excl	excl	excl	excl	excl	excl	excl	excl	excl	excl	excl	excl	excl	excl	excl
x10199022	IDT	8	0	8	excl	excl	excl	excl	excl	excl	excl	excl	excl	excl	excl	excl	excl	excl	excl	excl	excl	excl	excl
x10199023	IDT	4	0	4	excl	excl	excl	excl	excl	excl	excl	excl	excl	excl	excl	excl	excl	excl	excl	excl	excl	excl	excl
x10199024	IDT	4	0	4	excl	excl	excl	excl	excl	excl	excl	excl	excl	excl	excl	excl	excl	excl	excl	excl	excl	excl	excl

XML ID	Profile	All points	Included points	Excluded points	Tian-2009	Mathieu-2015	GDFKin-2016	Nakamura-2017	SanDiego-2018	Otomo-2018	Glarborg-2018	Okafor-2018	ELTE-2020	POLIMI-2020	NUIG-2020	Han-2020	Mei-2020	Konnov-2021	KAUST-2021	Shrestha-2021	Mei-2021	Zhou-2021	Gotama-2022
x10199025	IDT	4	0	4	excl	excl	excl	excl	excl	excl	excl	excl	excl	excl	excl	excl	excl	excl	excl	excl	excl	excl	excl
x10199026	IDT	4	0	4	excl	excl	excl	excl	excl	excl	excl	excl	excl	excl	excl	excl	excl	excl	excl	excl	excl	excl	excl
x10199029	IDT	5	4	1	3.1	3.2	6.8	49.6	1.4	2.7	1.6	99.3	1.8	8.8	2.3	19.2	10.8	13.6	4.0	2.8	10.6	47.9	8.9
x10199030	IDT	5	4	1	3.2	2.9	14.6	84.1	6.3	3.9	3.8	105.3	3.3	3.0	3.6	12.0	4.9	28.7	11.8	2.8	4.8	35.9	5.5
x10199031	IDT	5	2	3	16.0	42.6	0.0	39.1	23.2	35.8	30.1	192.2	31.4	29.5	49.9	33.5	17.0	2.2	0.3	20.3	16.5	98.3	14.1
x10199032	IDT	5	4	1	7.4	22.1	2.1	55.7	12.7	17.6	15.1	165.0	16.9	14.6	30.8	23.2	9.3	8.4	4.1	13.8	9.0	67.8	11.6
x10199033	IDT	5	4	1	21.0	34.6	7.0	26.0	15.3	24.5	27.7	179.9	28.4	24.4	39.4	36.0	20.1	2.5	6.0	9.1	19.7	66.4	24.1
x10199034	IDT	5	3	2	6.3	23.6	3.1	93.3	9.4	13.4	15.3	199.7	16.8	8.1	35.5	18.3	5.0	11.4	8.9	4.4	4.8	52.5	9.6
x10199035	IDT	11	11	0	2.2	6.2	20.2	7.5	39.6	10.0	19.7	44.5	20.7	5.6	5.0	5.7	32.7	3.1	20.1	2.8	30.7	4.1	4.5
x10199036	IDT	7	7	0	2.3	0.8	17.9	16.6	1.7	0.8	1.8	6.6	1.8	4.7	1.0	4.8	8.3	8.1	10.1	2.6	7.7	3.5	3.3

Table A6. Averaged error function values for each investigated mechanism for the utilized He-free concentration measurement datasets (E_i) in jet stirred reactors in the case of NH_3/H_2 fuel mixtures. In the table, "excl" means that no data point was included in the comparison from the corresponding dataset.

XML ID	Profile	All points	Included points	Excluded points	Tian-2009	Mathieu-2015	GDFKin-2016	Nakamura-2017	SanDiego-2018	Otomo-2018	Glarborg-2018	Okafor-2018	ELTE-2020	POLIMI-2020	NUIG-2020	Han-2020	Mei-2020	Konnov-2021	KAUST-2021	Shrestha-2021	Mei-2021	Zhou-2021	Gotama-2022
x00100000	H_2O	10	5	5	13.0	1.6	27.6	33.4	30.3	5.0	28.7	8.8	27.1	5.0	28.4	18.4	1.6	17.8	1.1	31.6	1.2	10.9	15.8
x00100000	NH_3	10	6	4	0.4	12.3	2.4	78.3	5.4	0.2	2.5	0.8	2.3	0.5	0.5	1.7	7.3	0.4	1.6	4.8	9.4	1.3	1.6
x00100000	NO	10	9	1	5.2	0.5	7.6	4.1	0.6	3.3	4.5	0.4	3.6	1.0	27.3	0.5	0.0	51.5	0.3	2.2	0.1	2.0	4.7
x00100000	N_2O	10	7	3	6.9	1.5	0.0	15.2	12.3	1.7	4.5	21.0	1.9	5.4	17.2	0.0	0.0	16.7	0.0	15.4	0.0	0.1	3.1
x00100001	H_2O	9	3	6	13.7	5.8	15.0	13.7	10.0	9.7	16.6	2.4	15.4	1.4	16.5	12.5	1.9	11.5	2.2	15.2	0.4	0.8	13.7
x00100001	NH_3	9	6	3	8.7	6.5	6.1	97.1	2.0	2.6	12.5	4.5	13.4	4.0	1.3	11.1	7.4	1.3	3.0	41.3	6.1	8.0	9.2
x00100001	NO	9	9	0	5.0	1.6	2.2	1.0	1.2	2.8	1.4	0.3	1.2	0.8	13.3	0.4	0.6	24.6	0.4	1.3	0.3	0.7	1.1
x00100001	N_2O	9	7	2	7.0	4.7	0.1	10.0	1.9	4.4	6.7	4.1	3.1	8.4	9.6	0.1	0.1	1.4	0.1	14.3	0.1	0.6	3.7
x00100002	H_2O	10	6	4	35.9	25.8	26.7	32.3	15.6	28.7	37.6	0.5	35.4	9.2	25.8	38.6	1.6	18.0	10.0	34.5	12.0	7.5	11.1
x00100002	NH_3	10	10	0	53.7	19.4	26.5	36.7	6.9	33.6	62.3	0.4	51.0	6.1	35.4	2.3	0.5	23.3	5.5	48.4	7.8	3.2	29.4
x00100002	NO	10	10	0	5.4	0.9	0.2	0.1	1.6	3.0	0.2	0.8	0.2	1.0	5.7	1.4	1.1	11.8	0.1	1.0	0.4	0.3	0.4
x00100002	N_2O	10	9	1	3.6	5.7	0.3	5.2	0.9	5.9	6.5	0.0	2.2	57.5	5.4	7.2	1.3	1.8	0.2	18.7	0.3	19.8	26.0
x00100003	H_2O	9	5	4	8.0	6.4	5.8	6.9	4.8	7.2	7.8	0.1	7.3	4.1	7.4	8.7	2.4	6.6	3.6	6.9	6.3	4.3	2.5
x00100003	NH_3	9	6	3	18.1	9.4	4.3	15.0	3.4	8.3	12.0	5.2	17.9	4.2	4.0	7.2	5.2	3.5	3.4	23.2	4.2	5.4	6.5
x00100003	NO	9	9	0	7.2	0.3	0.8	0.5	0.3	4.9	0.7	0.4	0.7	0.2	3.3	0.8	0.3	5.6	0.4	0.5	0.8	0.6	0.3
x00100003	N_2O	9	9	0	2.2	4.8	0.7	4.3	1.0	4.8	5.2	0.6	1.6	43.2	4.6	2.3	2.0	2.4	0.6	11.8	1.6	12.8	14.9
x00100004	H_2O	10	5	5	23.7	3.0	68.9	58.1	30.0	4.7	70.3	4.1	72.4	15.5	62.8	117.9	11.7	22.8	4.5	77.1	8.7	84.9	65.5
x00100004	NH_3	10	6	4	8.5	31.4	11.8	14.9	5.3	7.5	12.5	6.9	12.7	7.3	10.9	0.7	4.8	10.4	2.4	7.6	2.9	3.8	7.5
x00100004	NO	10	10	0	3.8	0.4	4.3	1.0	0.1	1.3	2.9	1.1	4.0	0.2	24.5	0.2	0.3	24.7	0.1	0.3	0.1	0.1	0.1
x00100004	N_2O	10	10	0	7.4	26.4	0.6	10.1	27.8	7.1	16.7	2.9	4.0	31.0	30.8	1.9	2.3	7.5	0.3	7.0	2.1	7.3	7.1
x00100005	H_2O	8	5	3	3.6	5.8	7.3	11.1	5.1	1.3	13.7	3.4	17.1	0.7	1.8	91.0	3.3	2.5	0.5	10.1	1.9	7.4	53.8
x00100005	NH_3	8	5	3	0.9	1.0	1.6	14.2	1.0	1.0	10.3	4.5	15.0	1.6	1.0	7.9	3.5	1.0	1.7	2.8	2.1	4.2	6.5

XML ID	Profile	All points	Included points	Excluded points	Tian-2009	Mathieu-2015	GDFKin-2016	Nakamura-2017	SanDiego-2018	Otomo-2018	Glarborg-2018	Okafor-2018	ELTE-2020	POLIMI-2020	NUIG-2020	Han-2020	Mei-2020	Konnov-2021	KAUST-2021	Shrestha-2021	Mei-2021	Zhou-2021	Gotama-2022
x00100005	NO	8	8	0	1.0	1.2	0.5	0.2	0.6	0.1	0.4	0.1	0.7	0.4	5.8	1.1	1.5	8.2	0.3	0.6	0.3	0.1	0.2
x00100005	N_2O	8	8	0	2.6	14.2	0.3	5.0	8.1	3.9	7.6	1.0	0.8	19.7	13.2	2.3	1.9	1.6	0.1	3.2	1.2	13.9	11.1
x00100006	H_2O	9	5	4	0.9	1.5	0.5	0.6	0.8	5.3	3.5	26.1	5.0	0.3	0.2	56.7	8.0	0.1	3.4	2.5	1.1	0.5	14.7
x00100006	NH_3	9	6	3	5.2	6.3	9.1	4.6	9.5	8.5	11.8	25.2	19.9	8.4	5.7	29.0	18.2	3.6	13.0	4.2	10.6	12.7	20.7
x00100006	NO	9	9	0	0.9	0.2	0.2	0.3	0.1	0.3	0.5	0.1	0.6	0.1	1.5	0.2	0.2	3.0	0.1	0.2	0.3	0.4	0.1
x00100006	N_2O	9	9	0	1.2	4.5	0.4	2.8	2.9	2.7	3.6	0.5	0.2	8.9	5.2	0.6	0.6	0.4	0.0	1.7	0.5	10.1	6.3
x00100007	H_2O	9	2	7	15.8	22.7	34.4	1.8	14.1	22.8	1.6	197.0	1.6	1.5	1.6	63.1	25.3	1.6	23.2	1.6	1.6	1.6	1.5
x00100007	NH_3	9	4	5	8.8	13.7	24.3	5.2	17.0	11.6	71.1	51.1	78.2	5.7	5.3	53.6	30.6	27.1	23.0	30.0	5.8	74.3	31.3
x00100007	NO	9	9	0	0.7	0.4	0.3	0.0	0.2	0.5	0.1	0.6	0.1	0.0	1.0	0.3	0.3	2.9	0.1	0.2	0.2	0.4	0.0
x00100007	N_2O	9	9	0	0.4	0.9	0.4	1.1	0.5	1.1	1.9	0.6	0.0	5.7	4.3	1.6	0.2	0.2	0.0	1.1	0.3	7.7	3.1
x00100008	H_2	18	10	8	2.5	27.1	16.9	14.4	49.6	0.4	0.2	2.5	0.8	0.2	0.3	21.0	3.5	0.2	0.5	21.1	3.8	7.5	27.2
x00100008	NH_3	18	10	8	0.2	0.0	0.2	1.5	0.3	0.6	2.3	2.2	10.8	0.0	0.1	2.0	1.3	0.0	0.5	6.2	0.7	0.5	1.7
x00100008	H_2O	18	6	12	6.9	12.7	7.1	6.9	11.0	3.7	11.6	3.6	19.7	5.4	4.9	36.9	3.2	6.6	3.3	21.6	5.0	4.1	55.4
x00100008	N_2	18	7	11	11.6	15.6	3.5	42.1	3.1	5.6	24.4	8.1	62.8	4.5	6.9	9.4	3.3	11.4	1.9	98.2	2.2	5.8	10.3
x00100008	O_2	18	10	8	1.0	0.6	0.4	0.1	0.6	3.3	2.2	7.1	15.9	0.6	1.1	13.6	3.9	0.6	2.1	12.4	2.2	4.6	14.0
x00100009	H_2	18	12	6	4.8	48.5	11.1	5.4	87.8	2.4	2.5	3.8	5.6	3.1	2.5	28.1	5.7	2.0	2.4	62.5	6.8	16.4	30.5
x00100009	NH_3	18	13	5	0.7	1.5	0.7	10.4	1.0	0.6	3.2	1.9	11.1	0.7	0.7	2.1	3.9	0.6	0.8	3.1	2.6	1.1	2.0
x00100009	H_2O	18	10	8	0.8	2.1	1.0	12.5	0.6	3.2	10.0	17.8	18.4	1.2	0.8	47.3	8.9	0.8	0.8	12.0	2.9	2.5	37.7
x00100009	N_2	18	15	3	16.5	26.4	6.8	80.6	4.4	9.3	38.0	51.5	67.9	7.1	7.5	34.2	10.5	9.1	2.0	77.2	3.2	2.3	28.4
x00100009	O_2	18	14	4	2.9	10.7	2.9	20.5	11.7	19.6	18.8	31.5	32.5	2.2	0.8	31.8	33.7	1.5	5.6	32.9	19.9	2.4	5.6
x00100010	H_2	18	18	0	6.6	18.9	14.7	79.3	29.0	1.8	38.9	14.4	51.0	14.4	36.1	27.7	28.0	5.3	0.6	87.1	20.7	10.9	36.6
x00100010	NH_3	18	17	1	10.1	8.3	5.6	10.6	3.8	14.1	23.3	16.0	54.4	1.4	11.5	21.8	32.1	0.5	3.6	119.4	27.3	9.5	14.7
x00100010	N_2	18	14	4	7.2	5.7	14.2	31.7	2.4	17.7	48.2	33.8	92.1	11.9	19.4	17.6	24.0	14.8	1.8	119.6	13.3	2.1	7.4
x00100010	O_2	18	11	7	0.9	3.3	0.8	0.3	3.1	3.1	9.9	6.1	34.5	0.2	0.3	13.3	2.6	0.9	0.8	45.4	1.2	1.6	14.1
x00100010	H_2O	17	12	5	0.7	7.5	3.4	1.9	3.2	2.5	9.3	5.7	20.6	1.8	2.4	26.3	2.1	2.6	0.5	50.8	1.0	1.2	32.7

XML ID	Profile	All points	Included points	Excluded points	Tian-2009	Mathieu-2015	GDFKin-2016	Nakamura-2017	SanDiego-2018	Otomo-2018	Glarborg-2018	Okafor-2018	ELTE-2020	POLIMI-2020	NUIG-2020	Han-2020	Mei-2020	Konnov-2021	KAUST-2021	Shrestha-2021	Mei-2021	Zhou-2021	Gotama-2022
x00199000	NH_3	12	0	12	excl	excl	excl	excl	excl	excl	excl	excl	excl	excl	excl	excl	excl	excl	excl	excl	excl	excl	excl
x00199000	NO	7	0	7	excl	excl	excl	excl	excl	excl	excl	excl	excl	excl	excl	excl	excl	excl	excl	excl	excl	excl	excl
x00199000	NO_2	7	0	7	excl	excl	excl	excl	excl	excl	excl	excl	excl	excl	excl	excl	excl	excl	excl	excl	excl	excl	excl
x00199001	NH_3	8	0	8	excl	excl	excl	excl	excl	excl	excl	excl	excl	excl	excl	excl	excl	excl	excl	excl	excl	excl	excl
x00199001	NO	8	0	8	excl	excl	excl	excl	excl	excl	excl	excl	excl	excl	excl	excl	excl	excl	excl	excl	excl	excl	excl
x00199001	NO_2	8	0	8	excl	excl	excl	excl	excl	excl	excl	excl	excl	excl	excl	excl	excl	excl	excl	excl	excl	excl	excl
x00199002	NH_3	12	0	12	excl	excl	excl	excl	excl	excl	excl	excl	excl	excl	excl	excl	excl	excl	excl	excl	excl	excl	excl
x00199003	NH_3	15	8	7	33.7	6.6	37.2	26.0	56.4	37.1	41.1	28.4	37.4	31.9	44.4	22.0	7.8	44.3	15.0	30.6	14.6	29.5	34.6
x00199003	H_2O	15	7	8	0.6	1.4	0.6	1.0	0.6	0.6	0.6	0.6	0.6	0.6	0.6	0.7	2.5	1.0	0.9	0.6	3.1	0.6	0.6
x00199003	NO_2	15	15	0	0.1	0.0	0.0	0.1	0.0	0.0	0.0	0.2	0.0	0.0	0.0	0.0	0.0	0.0	0.0	0.0	0.0	0.0	0.0
x00199003	NO	15	11	4	17.3	11.1	7.1	5.6	2.7	19.1	10.6	10.3	9.1	4.6	38.5	4.8	7.7	54.9	4.9	2.7	5.2	9.7	6.5
x00199003	N_2O	15	12	3	4.4	3.6	6.1	10.5	22.3	8.8	11.4	9.4	3.5	90.2	28.8	8.8	1.0	24.8	0.1	27.6	0.2	17.6	14.8
x00199004	NH_3	9	8	1	97.9	12.9	116.2	36.9	78.8	83.5	129.7	59.0	123.9	67.7	146.8	23.9	6.2	134.9	34.0	81.4	5.5	30.8	42.2
x00199004	H_2O	9	6	3	4.3	1.1	4.4	3.2	4.1	4.3	4.4	4.2	4.4	4.1	4.5	2.9	1.4	4.4	3.3	4.0	1.3	3.6	4.1
x00199004	NO	9	1	8	33.8	0.8	45.7	14.9	5.2	4.5	31.4	0.0	36.8	2.2	190.6	0.1	0.1	227.2	0.6	7.6	0.2	0.0	0.0
x00199005	NH_3	9	5	4	102.9	2.0	108.5	29.4	50.7	86.6	120.9	56.1	126.8	60.9	136.6	22.6	6.1	124.4	33.8	77.1	5.9	38.7	50.2
x00199005	H_2O	9	4	5	2.9	0.3	2.8	1.7	2.5	2.8	2.9	2.7	2.9	2.5	2.9	1.9	0.9	2.9	2.1	2.6	0.9	2.3	2.6
x00199005	NO	9	5	4	35.4	1.2	26.6	4.3	1.1	9.8	16.0	3.3	28.6	0.9	124.2	1.0	0.8	160.6	0.3	0.3	0.2	3.1	1.0
x00199006	NH_3	7	7	0	22.8	4.4	105.4	12.3	16.0	9.6	31.5	30.9	44.7	12.0	53.6	4.0	2.9	18.0	2.5	23.3	2.6	20.6	8.5
x00199006	H_2O	7	1	6	6.7	1.0	10.0	3.0	0.5	2.8	7.0	3.2	8.5	3.6	7.3	2.2	1.9	5.7	1.3	6.6	1.6	1.6	0.9
x00199006	NO	7	7	0	0.1	1.1	0.3	0.4	1.9	0.6	0.7	2.2	0.6	0.6	0.1	1.1	1.1	0.2	0.5	1.0	0.6	1.8	1.4
x00199007	H_2	12	0	12	excl	excl	excl	excl	excl	excl	excl	excl	excl	excl	excl	excl	excl	excl	excl	excl	excl	excl	excl
x00199007	O_2	12	4	8	1.4	1.4	1.4	97.5	1.9	1.4	1.4	1.4	1.4	1.4	1.5	1.4	1.4	1.4	1.4	1.4	1.4	1.4	1.4
x00199007	N_2	12	0	12	excl	excl	excl	excl	excl	excl	excl	excl	excl	excl	excl	excl	excl	excl	excl	excl	excl	excl	excl
x00199007	NO	12	5	7	10.8	8.1	7.0	0.1	13.8	9.1	8.0	14.2	7.9	11.4	1.2	12.5	11.4	9.8	9.8	4.9	11.4	12.8	11.5

XML ID	Profile	All points	Included points	Excluded points	Tian-2009	Mathieu-2015	GDFKin-2016	Nakamura-2017	SanDiego-2018	Otomo-2018	Glarborg-2018	Okafor-2018	ELTE-2020	POLIMI-2020	NUIG-2020	Han-2020	Mei-2020	Konnov-2021	KAUST-2021	Shrestha-2021	Mei-2021	Zhou-2021	Gotama-2022
x00199008	H_2	13	0	13	excl	excl	excl	excl	excl	excl	excl	excl	excl	excl	excl	excl	excl	excl	excl	excl	excl	excl	excl
x00199008	O_2	13	3	10	3.2	3.2	3.2	129.1	3.6	3.2	3.3	3.2	3.3	3.2	3.5	3.2	3.2	3.3	3.3	3.4	3.2	3.2	3.2
x00199008	N_2	13	0	13	excl	excl	excl	excl	excl	excl	excl	excl	excl	excl	excl	excl	excl	excl	excl	excl	excl	excl	excl
x00199008	NO	13	6	7	5.5	2.9	1.7	1.6	8.8	4.1	3.7	9.4	3.7	6.5	0.0	7.5	6.6	4.9	4.9	0.9	6.6	7.8	6.4
x00199009	H_2	11	0	11	excl	excl	excl	excl	excl	excl	excl	excl	excl	excl	excl	excl	excl	excl	excl	excl	excl	excl	excl
x00199009	N_2	11	4	7	0.0	0.0	0.0	0.0	0.0	0.0	0.0	0.0	0.0	0.0	0.0	0.0	0.1	0.0	0.1	0.0	0.1	0.0	0.0
x00199010	H_2	11	0	11	excl	excl	excl	excl	excl	excl	excl	excl	excl	excl	excl	excl	excl	excl	excl	excl	excl	excl	excl
x00199010	N_2	11	3	8	0.0	0.0	0.0	0.0	0.0	0.0	0.0	0.0	0.0	0.0	0.0	0.0	0.0	0.0	0.0	0.0	0.0	0.0	0.0
x00199011	H_2	30	0	30	excl	excl	excl	excl	excl	excl	excl	excl	excl	excl	excl	excl	excl	excl	excl	excl	excl	excl	excl
x00199011	O_2	30	13	17	1.2	1.2	1.2	63.5	0.7	1.2	1.1	1.2	1.1	1.2	1.0	1.2	1.2	1.1	1.2	1.1	1.2	1.2	1.2
x00199011	NO	30	7	23	32.7	29.1	26.4	5.2	36.2	29.9	27.3	36.9	27.1	33.3	13.4	34.9	33.5	30.4	30.7	24.6	33.5	35.3	33.8
x00199012	H_2	26	0	26	excl	excl	excl	excl	excl	excl	excl	excl	excl	excl	excl	excl	excl	excl	excl	excl	excl	excl	excl
x00199012	O_2	26	15	11	0.0	0.0	0.0	4.1	0.0	0.0	0.0	0.0	0.0	0.0	0.0	0.0	0.0	0.0	0.0	0.0	0.0	0.0	0.0
x00199012	NO	26	12	14	19.8	15.8	14.8	3.6	24.5	17.3	16.0	25.6	15.8	21.0	6.0	22.6	21.0	18.2	18.2	11.7	21.0	23.2	21.0
x00199013	H_2	34	0	34	excl	excl	excl	excl	excl	excl	excl	excl	excl	excl	excl	excl	excl	excl	excl	excl	excl	excl	excl
x00199013	O_2	34	15	19	2.0	1.9	1.2	137.6	1.0	1.9	1.8	2.1	1.8	2.0	1.5	2.0	2.0	1.5	1.9	0.4	2.0	2.1	2.0
x00199013	NO	34	27	7	22.5	25.3	21.9	7.8	13.7	12.7	8.8	19.8	8.9	10.6	8.9	12.2	11.1	17.1	9.9	26.0	11.0	14.1	9.9
x00199014	H_2	26	0	26	excl	excl	excl	excl	excl	excl	excl	excl	excl	excl	excl	excl	excl	excl	excl	excl	excl	excl	excl
x00199014	O_2	26	2	24	3.2	3.1	2.9	332.6	0.4	3.1	2.9	3.3	2.9	3.2	2.4	3.2	3.2	2.6	3.0	1.5	3.2	3.3	3.2
x00199014	NO	26	26	0	48.0	34.0	23.9	1.7	62.1	40.7	38.9	64.9	38.4	52.3	10.6	57.1	53.2	45.4	45.0	15.6	53.2	58.5	52.6
x00199015	H_2	26	0	26	excl	excl	excl	excl	excl	excl	excl	excl	excl	excl	excl	excl	excl	excl	excl	excl	excl	excl	excl
x00199015	O_2	26	0	26	excl	excl	excl	excl	excl	excl	excl	excl	excl	excl	excl	excl	excl	excl	excl	excl	excl	excl	excl
x00199015	NO	26	12	14	9.4	29.2	37.1	25.1	0.1	7.4	13.9	3.7	15.6	0.0	16.3	0.1	0.0	9.2	1.7	70.9	0.0	0.6	0.3
x00199016	H_2	18	0	18	excl	excl	excl	excl	excl	excl	excl	excl	excl	excl	excl	excl	excl	excl	excl	excl	excl	excl	excl
x00199016	O_2	18	0	18	excl	excl	excl	excl	excl	excl	excl	excl	excl	excl	excl	excl	excl	excl	excl	excl	excl	excl	excl

XML ID	Profile	All points	Included points	Excluded points	Tian-2009	Mathieu-2015	GDFKin-2016	Nakamura-2017	SanDiego-2018	Otomo-2018	Glarborg-2018	Okafor-2018	ELTE-2020	POLIMI-2020	NUIG-2020	Han-2020	Mei-2020	Konnov-2021	KAUST-2021	Shrestha-2021	Mei-2021	Zhou-2021	Gotama-2022
x00199016	NO	18	6	12	35.0	46.7	7.4	6.2	0.6	13.9	0.6	6.6	0.7	0.1	12.5	0.2	0.6	28.2	6.8	24.6	0.5	2.6	0.3
x00199017	H_2	26	0	26	excl	excl	excl	excl	excl	excl	excl	excl	excl	excl	excl	excl	excl	excl	excl	excl	excl	excl	excl
x00199017	O_2	26	16	10	0.4	0.4	0.4	80.7	1.2	0.4	0.4	0.4	0.4	0.4	0.4	0.4	0.4	0.4	0.4	0.8	0.4	0.4	0.4
x00199017	NO	26	15	11	25.8	20.2	15.0	1.9	31.7	22.9	21.8	33.1	21.6	27.6	8.5	29.5	27.8	24.2	24.1	11.7	27.7	30.3	27.6
x00199018	H_2O	10	2	8	0.0	0.0	0.0	0.0	0.0	0.0	0.0	0.0	0.0	0.0	0.0	0.0	0.0	0.0	0.0	0.0	0.0	0.0	0.0
x00199018	NH_3	10	4	6	0.5	0.5	0.5	38.9	2.3	0.5	0.5	0.5	0.5	0.5	0.7	0.5	0.5	0.5	0.5	0.6	0.5	0.5	0.5
x00199018	NO	10	9	1	1.4	0.1	4.1	3.2	0.5	0.6	1.8	0.1	1.4	0.4	15.1	0.1	0.0	34.1	0.0	1.4	0.0	0.0	1.3
x00199018	N_2O	10	8	2	2.9	0.1	0.2	18.9	25.1	0.4	3.6	17.9	1.7	1.6	20.6	0.1	0.1	25.1	0.1	16.1	0.1	0.0	0.0
x00199019	H_2O	10	4	6	0.0	0.0	0.0	9.7	0.0	0.0	0.0	0.0	0.0	0.0	0.0	0.0	0.0	0.0	0.0	0.0	0.0	0.0	0.0
x00199019	NH_3	10	6	4	0.1	0.1	22.5	44.6	11.3	0.1	0.5	0.1	0.8	0.1	0.4	0.1	0.1	0.2	0.2	0.7	0.1	0.1	0.1
x00199019	NO	10	10	0	1.9	0.1	3.8	0.7	0.0	0.5	2.2	0.6	2.9	0.1	20.5	0.3	0.2	16.8	0.0	0.1	0.1	0.5	0.1
x00199019	N_2O	10	10	0	12.6	23.3	2.8	16.7	49.1	12.6	25.7	6.7	8.6	36.9	51.5	2.2	2.0	13.4	1.0	9.0	2.0	3.6	1.1
x00199020	NH_3	24	13	11	0.1	0.1	26.5	8.0	1.7	0.1	5.4	0.1	29.3	0.2	1.7	0.1	0.0	0.1	0.0	0.8	0.0	0.1	0.1
x00199020	O_2	24	11	13	0.1	0.3	41.4	6.1	3.6	0.3	0.9	0.3	18.8	0.1	0.3	0.2	0.2	0.2	0.1	0.2	0.2	0.3	0.3
x00199020	H_2O	22	8	14	0.0	0.0	0.0	44.6	0.0	0.0	0.0	0.0	0.0	0.0	0.0	0.0	0.1	0.0	0.1	1.3	0.1	0.0	0.0
x00199020	N_2	22	8	14	0.0	0.0	0.0	11.6	0.0	0.0	0.0	0.0	0.0	0.0	0.0	0.0	0.0	0.0	0.0	0.2	0.0	0.0	0.0

Table A7. Averaged error function values for each investigated mechanism for the utilized He-free concentration measurement datasets (E_i) in flow reactors in the case of NH_3/H_2 fuel mixtures. In the table, "excl" means that no data point was included in the comparison from the corresponding dataset.

XML ID	Profile	All points	Included points	Excluded points	Tian-2009	Mathieu-2015	GDFKin-2016	Nakamura-2017	SanDiego-2018	Otomo-2018	Glarborg-2018	Okafor-2018	ELTE-2020	POLIMI-2020	NUIG-2020	Han-2020	Mei-2020	Konnov-2021	KAUST-2021	Shrestha-2021	Mei-2021	Zhou-2021	Gotama-2022
x30100001	NH_3	9	8	1	11.0	12.0	1.4	5.9	0.9	4.7	5.8	0.6	4.8	0.9	17.3	0.9	0.0	2.4	1.0	9.8	0.0	0.2	1.2
x30100001	NO	9	5	4	17.4	1.1	3.2	0.5	14.8	9.9	4.4	16.4	2.6	0.7	8.6	7.8	1.6	3.8	0.9	1.8	1.5	1.5	4.2
x30199001	NO	11	5	6	8.3	8.3	8.2	7.9	8.3	8.3	8.3	8.3	8.3	7.9	8.3	8.0	8.0	2.6	7.5	8.3	8.0	8.2	8.2
x30199001	N_2O	10	10	0	0.3	1.0	5.8	6.5	10.2	1.3	2.5	0.4	0.5	61.9	5.4	5.7	0.3	8.8	0.2	0.5	0.6	0.7	1.0
x30199003	N_2O	10	10	0	0.2	0.5	4.6	7.0	0.6	0.6	0.5	0.6	0.5	32.2	3.3	4.4	0.1	9.0	0.1	0.6	0.2	4.0	0.5
x30199003	NH_3	7	5	2	1.1	1.1	1.1	0.8	1.2	1.2	1.2	1.1	1.2	1.1	1.2	1.0	1.1	23.4	1.0	1.2	1.1	1.1	1.1
x30199003	NO	12	6	6	10.9	10.9	10.8	9.5	10.9	10.9	10.9	10.9	10.9	9.7	10.9	9.9	10.2	2.4	9.0	10.9	10.2	10.5	10.5
x30199006	NH_3	9	6	3	0.0	0.0	3.0	13.1	0.1	0.1	0.1	0.1	0.1	0.0	0.1	0.0	0.0	26.8	0.0	0.1	0.0	0.0	0.0
x30199006	NO	9	9	0	1.4	2.3	1.7	0.6	0.7	0.9	0.8	6.7	0.8	1.1	7.9	2.2	7.9	59.7	1.5	1.7	7.0	0.2	1.8
x30199007	O_2	7	7	0	0.2	0.2	0.2	0.7	0.2	0.2	0.2	0.2	0.2	0.2	0.2	0.2	0.2	0.2	0.2	0.2	0.2	0.2	0.2
x30199007	NH_3	7	7	0	0.2	0.2	0.2	0.8	0.2	0.2	0.2	0.2	0.2	0.2	0.2	0.2	0.2	0.2	0.2	0.2	0.2	0.2	0.2
x30199009	O_2	6	6	0	2.6	2.5	2.5	21.8	2.3	2.5	2.4	2.6	2.4	2.5	2.0	2.6	2.6	1.8	2.5	2.6	2.6	2.6	2.6
x30199009	NH_3	6	6	0	0.2	0.2	0.2	42.7	0.1	0.2	0.2	0.2	0.2	0.2	0.1	0.2	0.2	0.0	0.2	0.2	0.2	0.2	0.2
x30199011	O_2	6	0	6	excl	excl	excl	excl	excl	excl	excl	excl	excl	excl	excl	excl	excl	excl	excl	excl	excl	excl	excl
x30199011	NH_3	6	4	2	0.0	0.1	0.0	0.3	0.0	0.0	0.4	0.0	0.4	0.0	16.8	0.0	0.0	0.2	0.0	0.0	0.0	0.0	0.0
x30199013	O_2	5	0	5	excl	excl	excl	excl	excl	excl	excl	excl	excl	excl	excl	excl	excl	excl	excl	excl	excl	excl	excl
x30199013	NH_3	5	2	3	0.0	0.2	0.0	1.1	0.0	0.0	0.1	0.0	0.1	0.0	4.4	0.0	0.0	0.5	0.0	0.0	0.0	0.0	0.0
x30199015	N_2O	4	1	3	201.3	143.0	202.4	110.3	243.3	149.0	5.6	243.2	5.7	11.9	3.1	243.1	237.1	138.9	43.6	135.9	237.1	243.2	242.7
x30199015	NH_3	9	3	6	0.1	0.1	0.1	0.1	0.1	0.1	0.6	0.1	0.7	0.1	1.7	0.1	0.1	0.1	0.1	0.1	0.1	0.1	0.1
x30199017	N_2O	9	6	3	2.9	1.4	3.1	0.6	4.3	1.6	32.3	4.3	32.2	19.0	79.3	4.3	4.1	1.2	0.7	1.5	4.1	4.3	4.3
x30199018	NO	15	15	0	1.6	2.1	4.0	1.0	36.9	1.6	1.8	49.5	2.4	6.5	57.5	35.2	30.6	2.9	2.5	1.1	27.9	22.4	11.4
x30199018	N_2O	15	15	0	8.7	13.0	6.5	17.7	11.5	2.6	24.1	44.2	20.3	67.0	84.6	8.4	7.3	3.8	15.5	12.4	7.1	6.3	6.7

XML ID	Profile	All points	Included points	Excluded points	Tian-2009	Mathieu-2015	GDFKin-2016	Nakamura-2017	SanDiego-2018	Otomo-2018	Glarborg-2018	Okafor-2018	ELTE-2020	POLIMI-2020	NUIG-2020	Han-2020	Mei-2020	Konnov-2021	KAUST-2021	Shrestha-2021	Mei-2021	Zhou-2021	Gotama-2022
x30199018	NH_3	15	6	9	0.2	0.5	0.2	8.7	0.5	0.5	0.5	0.5	0.5	0.4	0.5	0.5	0.5	1.1	0.4	0.5	0.5	0.5	0.5
x30199021	NH_3	19	0	19	excl	excl	excl	excl	excl	excl	excl	excl	excl	excl	excl	excl	excl	excl	excl	excl	excl	excl	excl
x30199021	O_2	19	0	19	excl	excl	excl	excl	excl	excl	excl	excl	excl	excl	excl	excl	excl	excl	excl	excl	excl	excl	excl
x30199021	NO	19	0	19	excl	excl	excl	excl	excl	excl	excl	excl	excl	excl	excl	excl	excl	excl	excl	excl	excl	excl	excl
x30199021	N_2	19	0	19	excl	excl	excl	excl	excl	excl	excl	excl	excl	excl	excl	excl	excl	excl	excl	excl	excl	excl	excl
x30199021	H_2O	19	0	19	excl	excl	excl	excl	excl	excl	excl	excl	excl	excl	excl	excl	excl	excl	excl	excl	excl	excl	excl
x30199021	H_2	19	0	19	excl	excl	excl	excl	excl	excl	excl	excl	excl	excl	excl	excl	excl	excl	excl	excl	excl	excl	excl
x30199022	NH_3	8	8	0	1.1	1.1	1.1	1.0	1.1	1.1	1.1	1.1	1.1	1.1	1.1	1.1	1.0	1.1	1.0	1.1	1.0	1.1	1.1
x30199022	H_2	8	3	5	3.7	3.7	3.7	3.7	3.7	3.7	3.7	3.7	3.7	3.7	3.7	3.7	3.7	3.7	3.7	3.7	3.7	3.7	3.7
x30199023	NH_3	16	7	9	23.4	23.5	23.4	5.5	23.6	23.5	23.5	23.6	23.5	23.2	23.4	23.1	4.2	23.2	14.0	21.4	4.3	23.4	23.1
x30199023	O_2	16	1	15	0.0	0.0	0.0	0.0	0.0	0.0	0.0	0.0	0.0	0.0	0.0	0.0	0.0	0.0	0.0	0.0	0.0	0.0	0.0
x30199023	H_2	16	14	2	2.4	2.4	2.4	9.5	2.4	2.4	2.4	2.4	2.4	2.3	2.4	2.3	23.5	2.4	1.6	2.2	24.5	2.4	2.3
x30199023	NO	16	16	0	0.0	0.0	0.0	0.1	0.0	0.0	0.0	0.0	0.0	0.0	0.0	0.0	0.0	0.0	0.0	0.0	0.0	0.0	0.0
x30199023	NO_2	16	16	0	0.0	0.0	0.0	0.0	0.0	0.0	0.0	0.0	0.0	0.0	0.0	0.0	0.0	0.0	0.0	0.0	0.0	0.0	0.0
x30199023	N_2O	16	16	0	0.0	0.0	0.0	0.0	0.0	0.0	0.0	0.0	0.0	0.0	0.0	0.0	0.0	0.0	0.0	0.0	0.0	0.0	0.0
x30199024	NH_3	14	11	3	5.7	5.7	5.7	3.2	5.7	5.7	5.7	5.7	5.7	5.7	5.7	5.5	2.1	5.7	3.8	5.7	2.1	5.7	5.6
x30199024	O_2	14	1	13	0.0	0.0	0.0	0.0	0.0	0.0	0.0	0.0	0.0	0.0	0.0	0.0	0.0	0.0	0.0	0.0	0.0	0.0	0.0
x30199024	H_2	14	12	2	0.0	0.0	0.0	3.5	0.0	0.0	0.0	0.0	0.0	0.0	0.0	0.0	16.3	0.0	2.6	0.0	16.5	0.0	0.0
x30199024	NO	14	14	0	0.3	0.3	0.3	0.2	0.3	0.3	0.3	0.3	0.3	0.3	0.3	0.3	0.2	0.3	0.1	0.3	0.1	0.3	0.3
x30199024	NO_2	14	14	0	0.0	0.0	0.0	0.0	0.0	0.0	0.0	0.0	0.0	0.0	0.0	0.0	0.0	0.0	0.0	0.0	0.0	0.0	0.0
x30199024	N_2O	14	14	0	0.0	0.0	0.0	0.2	0.0	0.0	0.0	0.0	0.0	0.0	0.0	0.0	0.0	0.0	0.0	0.0	0.0	0.0	0.0
x30199025	NH_3	13	5	8	1.3	1.3	1.3	1.3	1.3	1.3	1.3	1.3	1.3	1.3	1.3	1.3	1.3	1.3	1.3	1.3	1.3	1.3	1.3
x30199025	O_2	13	6	7	1.9	1.9	1.9	1.9	1.9	1.9	1.9	1.9	1.9	1.9	1.9	1.9	1.9	1.9	1.9	1.9	1.9	1.9	1.9
x30199025	H_2	13	11	2	0.0	0.0	0.0	21.1	0.0	0.0	0.0	0.0	0.0	0.0	0.0	0.0	40.4	0.0	7.1	0.0	39.0	0.0	0.0
x30199025	NO	13	13	0	2.3	2.3	2.3	0.4	2.3	2.3	2.3	2.3	2.3	2.1	2.3	1.9	0.5	2.0	0.7	2.2	0.2	2.2	2.1

XML ID	Profile	All points	Included points	Excluded points	Tian-2009	Mathieu-2015	GDFKin-2016	Nakamura-2017	SanDiego-2018	Otomo-2018	Glarborg-2018	Okafor-2018	ELTE-2020	POLIMI-2020	NUIG-2020	Han-2020	Mei-2020	Konnov-2021	KAUST-2021	Shrestha-2021	Mei-2021	Zhou-2021	Gotama-2022
x30199025	NO_2	13	13	0	0.0	0.0	0.0	0.0	0.0	0.0	0.0	0.0	0.0	0.0	0.0	0.0	0.0	0.0	0.0	0.0	0.0	0.0	0.0
x30199025	N_2O	13	13	0	0.0	0.0	0.0	1.2	0.0	0.0	0.0	0.0	0.0	0.0	0.0	0.0	0.4	0.0	0.3	0.0	0.4	0.0	0.0
x30199026	NH_3	14	7	7	2.0	2.0	2.0	2.0	2.0	2.0	2.0	2.0	2.0	2.0	2.0	2.0	2.0	2.0	2.0	2.0	2.0	2.0	2.0
x30199026	O_2	14	10	4	5.7	5.7	5.7	2.9	5.7	5.7	5.7	5.7	5.7	5.7	5.7	5.6	2.2	5.7	4.1	5.7	2.2	5.7	5.7
x30199026	H_2	14	12	2	0.0	0.0	0.0	19.5	0.0	0.0	0.0	0.0	0.0	0.0	0.0	0.0	34.5	0.0	6.1	0.0	33.4	0.0	0.0
x30199026	NO	14	14	0	2.4	2.4	2.3	1.9	2.4	2.4	2.4	2.4	2.4	2.2	2.4	2.0	0.2	2.0	0.7	2.3	0.2	2.3	2.2
x30199026	NO_2	14	14	0	0.0	0.0	0.0	0.0	0.0	0.0	0.0	0.0	0.0	0.0	0.0	0.0	0.0	0.0	0.0	0.0	0.0	0.0	0.0
x30199026	N_2O	14	14	0	0.0	0.0	0.0	0.4	0.0	0.0	0.0	0.0	0.0	0.0	0.0	0.0	0.5	0.0	0.3	0.0	0.5	0.0	0.0
x30199027	NH_3	15	11	4	3.0	3.0	3.0	2.4	3.0	3.0	3.0	3.0	3.0	3.0	3.0	2.9	1.4	3.0	2.1	3.0	1.4	3.0	3.0
x30199027	O_2	15	15	0	11.5	11.6	8.3	1.1	11.6	11.6	11.6	11.6	11.6	5.5	11.6	6.4	0.7	6.6	2.0	11.3	0.9	11.4	11.1
x30199027	H_2	15	12	3	0.0	0.0	6.9	1.5	0.0	0.0	0.0	0.0	0.0	0.1	0.0	0.5	7.0	0.2	1.7	5.3	6.6	0.1	2.9
x30199027	NO	15	15	0	28.7	31.7	21.8	0.9	62.6	41.4	39.0	60.6	38.5	4.8	36.7	3.9	0.6	4.2	0.9	31.9	0.7	13.1	10.0
x30199027	NO_2	15	15	0	0.0	0.0	0.0	0.0	0.0	0.0	0.0	0.0	0.0	0.0	0.0	0.0	0.0	0.0	0.0	0.0	0.0	0.0	0.0
x30199027	N_2O	15	15	0	0.0	0.0	1.4	0.8	0.0	0.0	0.0	0.0	0.0	4.4	0.0	1.6	1.9	0.7	1.0	0.0	1.5	0.0	0.0
x30199028	NH_3	13	9	4	3.6	3.6	3.5	1.1	3.6	3.6	3.6	3.6	3.6	3.3	3.6	3.2	1.2	2.9	1.7	3.6	1.3	3.5	3.4
x30199028	O_2	13	13	0	5.1	5.1	2.3	3.2	8.1	5.2	5.1	8.1	5.1	1.6	5.2	1.0	1.1	2.2	1.2	5.1	1.1	4.8	4.8
x30199028	H_2	13	13	0	0.0	0.1	0.1	11.1	0.0	0.1	0.0	0.0	0.0	1.8	0.0	13.1	15.3	30.7	12.9	0.0	13.1	0.2	0.4
x30199028	NO	13	12	1	20.8	25.2	7.3	4.4	71.5	37.9	32.8	60.4	32.4	2.9	30.4	1.1	1.7	6.8	2.8	38.0	2.4	8.2	8.0
x30199028	NO_2	13	13	0	0.0	0.0	0.0	0.0	0.0	0.0	0.0	0.0	0.0	0.0	0.0	0.0	0.0	0.0	0.0	0.0	0.0	0.0	0.0
x30199028	N_2O	13	13	0	1.4	18.5	6.8	13.5	0.0	4.6	1.3	0.0	0.5	28.9	2.2	5.5	6.3	7.2	3.9	0.9	5.4	3.1	1.6
x30199029	NH_3	15	10	5	0.7	0.7	0.7	0.3	0.7	0.7	0.7	0.7	0.7	0.6	0.7	0.6	0.5	0.2	0.5	0.7	0.5	0.7	0.7
x30199029	O_2	15	15	0	5.9	8.2	4.7	3.4	11.6	8.4	6.5	9.1	6.5	4.5	6.2	4.7	4.7	3.0	4.7	9.2	4.7	6.6	8.8
x30199029	H_2	15	15	0	1.2	1.8	0.1	2.5	0.0	1.4	0.0	0.0	0.0	4.0	0.0	2.7	5.7	0.9	2.1	0.1	4.2	0.6	2.5
x30199029	NO	15	13	2	6.8	5.7	9.0	8.3	58.5	15.1	11.0	31.2	10.8	4.7	9.2	3.6	2.5	14.0	4.0	26.3	3.3	4.0	7.4
x30199029	NO_2	15	15	0	0.0	0.0	0.0	0.0	0.0	0.0	0.0	0.0	0.0	0.0	0.0	0.0	0.0	0.0	0.0	0.0	0.0	0.0	0.0

XML ID	Profile	All points	Included points	Excluded points	Tian-2009	Mathieu-2015	GDFKin-2016	Nakamura-2017	SanDiego-2018	Otomo-2018	Glarborg-2018	Okafor-2018	ELTE-2020	POLIMI-2020	NUIG-2020	Han-2020	Mei-2020	Konnov-2021	KAUST-2021	Shrestha-2021	Mei-2021	Zhou-2021	Gotama-2022
x30199029	N_2O	15	14	1	11.4	27.4	14.9	21.6	5.3	15.1	9.5	9.8	3.7	40.6	15.3	8.6	6.2	14.6	3.7	8.1	4.6	13.9	8.0
x30199030	NH_3	15	11	4	0.6	0.8	0.5	0.1	0.6	0.6	0.6	0.6	0.6	0.5	0.6	0.4	0.4	0.5	0.4	0.6	0.4	0.5	0.5
x30199030	O_2	15	15	0	1.7	1.3	2.4	3.0	1.5	1.6	1.7	1.4	1.7	1.9	2.3	2.0	1.6	3.5	1.6	1.3	1.5	1.6	1.3
x30199030	H_2	15	15	0	0.4	0.2	0.7	3.3	9.6	0.1	0.6	1.2	1.0	0.6	0.0	1.0	2.9	0.5	0.9	1.2	2.1	0.5	1.4
x30199030	NO	15	8	7	1.3	1.3	1.2	0.7	1.3	1.3	1.3	1.3	1.3	1.0	1.3	1.0	1.1	0.8	0.8	1.3	1.1	1.2	1.2
x30199030	NO_2	15	15	0	0.1	0.0	0.0	0.0	0.0	0.1	0.0	0.2	0.0	0.0	0.1	0.0	0.0	0.1	0.0	0.0	0.0	0.0	0.0
x30199030	N_2O	15	13	2	4.8	2.8	15.0	16.8	8.0	8.7	4.4	3.5	1.8	49.7	13.6	7.0	2.3	12.8	1.2	1.5	1.2	6.9	0.8
x30199031	NH_3	16	10	6	12.4	12.4	12.4	5.3	12.4	12.4	12.4	12.4	12.4	12.2	12.4	12.1	3.2	12.3	7.2	12.4	3.2	12.3	12.2
x30199031	O_2	16	11	5	15.5	15.5	15.5	4.7	15.5	15.5	15.5	15.5	15.5	15.2	15.5	15.0	4.9	15.2	7.5	15.4	4.0	15.4	15.3
x30199031	H_2	16	12	4	0.0	0.0	0.0	7.1	0.0	0.0	0.0	0.0	0.0	0.0	0.0	0.0	27.5	0.0	4.5	0.0	26.5	0.0	0.0
x30199031	NO	16	16	0	2.3	2.3	2.2	7.0	2.4	2.4	2.4	2.4	2.4	1.2	2.4	2.0	1.3	1.7	0.3	2.2	2.7	2.3	2.2
x30199031	NO_2	16	16	0	0.0	0.0	0.0	0.0	0.0	0.0	0.0	0.0	0.0	0.0	0.0	0.0	0.0	0.0	0.0	0.0	0.0	0.0	0.0
x30199031	N_2O	16	16	0	0.0	0.0	0.0	1.3	0.0	0.0	0.0	0.0	0.0	0.2	0.0	0.0	0.7	0.0	1.3	0.0	0.8	0.0	0.0

Table A8. Averaged error function values for each investigated mechanism for the utilized He-free LBV measurement datasets (E_i) in the case of NH_3/H_2 fuel mixtures. In the table, "excl" means that no data point was included in the comparison from the corresponding dataset.

XML ID	Profile	All points	Included points	Excluded points	Tian-2009	Mathieu-2015	GDFKin-2016	Nakamura-2017	SanDiego-2018	Otomo-2018	Glarborg-2018	Okafor-2018	ELTE-2020	POLIMI-2020	NUIG-2020	Han-2020	Mei-2020	Konnov-2021	KAUST-2021	Shrestha-2021	Mei-2021	Zhou-2021	Gotama-2022
x20100004	LBV	5	5	0	21.0	7.8	18.4	6.6	8.6	12.5	4.3	29.6	5.2	4.7	5.8	8.4	9.7	34.1	17.7	11.6	6.8	8.2	21.9
x20100005	LBV	5	5	0	2.3	0.8	1.4	0.8	1.0	0.9	1.1	1.6	0.9	1.0	0.8	0.7	0.6	1.5	0.9	0.4	0.7	9.4	0.9
x20100006	LBV	5	5	0	0.4	2.6	0.6	3.4	2.6	0.4	4.1	1.4	5.3	2.7	1.2	4.7	0.8	0.9	0.8	2.4	1.0	12.2	1.2
x20100007	LBV	2	2	0	34.9	53.4	2.4	2.0	61.6	24.2	3.3	79.9	8.4	4.6	0.7	21.4	21.6	24.6	8.0	26.2	16.4	11.0	5.6
x20100008	LBV	2	2	0	15.8	22.4	5.7	0.4	14.9	15.6	8.2	31.9	13.2	1.4	0.7	3.6	5.7	7.3	2.4	9.5	5.2	2.3	0.8
x20100009	LBV	3	3	0	25.8	55.2	9.2	8.7	24.9	38.3	3.0	34.7	5.2	13.6	1.0	16.3	17.9	11.5	17.6	18.4	20.1	11.1	10.8
x20100010	LBV	2	2	0	5.8	2.1	11.2	1.8	0.2	17.7	12.7	15.5	19.2	0.8	0.2	1.1	2.6	0.2	0.8	1.3	3.1	3.7	1.5
x20100011	LBV	1	1	0	0.0	12.1	25.1	6.2	18.3	7.2	22.3	4.6	35.9	6.7	2.3	1.7	0.1	7.9	4.1	7.0	0.1	13.9	0.3
x20100012	LBV	9	9	0	6.9	25.4	67.4	1.8	7.7	12.5	17.0	9.8	23.3	3.4	7.6	3.9	5.8	3.0	5.9	5.2	6.9	4.5	2.4
x20100013	LBV	7	0	7	excl	excl	excl	excl	excl	excl	excl	excl	excl	excl	excl	excl	excl	excl	excl	excl	excl	excl	excl
x20100014	LBV	6	0	6	excl	excl	excl	excl	excl	excl	excl	excl	excl	excl	excl	excl	excl	excl	excl	excl	excl	excl	excl
x20100018	LBV	19	19	0	55.0	45.4	264.0	4.7	28.9	67.6	178.7	73.0	236.3	0.7	36.1	8.1	6.7	6.2	2.6	5.9	6.4	16.9	4.1
x20100019	LBV	14	7	7	3.1	42.8	250.9	1.0	7.4	10.9	110.6	7.4	147.5	0.4	48.1	0.5	4.1	1.0	1.9	6.1	5.7	1.8	2.1
x20100020	LBV	19	10	9	14.3	50.8	237.0	6.5	22.8	26.4	153.9	23.6	212.1	6.5	37.3	2.5	5.5	6.3	5.4	11.9	5.7	5.0	1.3
x20100021	LBV	19	8	11	54.7	61.2	120.5	5.7	41.4	71.1	167.4	98.8	233.1	0.5	12.6	11.6	7.3	7.6	2.0	17.5	6.7	13.6	1.8
x20100022	LBV	19	11	8	65.3	36.0	158.6	20.1	67.7	77.2	192.8	107.9	285.5	15.6	12.2	10.3	5.7	21.3	8.2	15.7	5.2	38.4	3.5
x20100023	LBV	15	4	11	136.2	20.5	37.6	24.9	41.0	61.5	62.5	297.1	88.8	26.0	22.7	12.5	13.0	138.3	18.2	27.6	7.9	124.4	9.4
x20100024	LBV	15	14	1	93.0	31.1	28.2	57.8	64.0	49.3	69.1	166.8	87.2	25.2	25.3	33.0	12.4	60.2	24.1	49.2	9.9	113.9	42.3
x20100025	LBV	12	10	2	120.7	49.7	85.3	7.8	78.4	148.1	144.2	178.6	211.0	5.8	3.2	30.1	20.8	30.2	10.9	25.0	21.0	22.6	14.6
x20100026	LBV	13	13	0	11.1	20.1	139.8	53.7	32.9	13.7	154.4	17.1	200.7	22.2	39.6	4.2	1.5	16.0	8.0	11.9	1.0	33.3	0.7
x20100027	LBV	12	12	0	18.3	12.0	104.2	58.8	31.3	1.7	132.5	8.7	160.2	24.9	51.9	6.8	2.3	19.3	10.5	4.8	1.9	26.4	1.0
x20100028	LBV	5	5	0	0.6	15.3	106.5	0.3	2.3	5.2	28.2	2.5	40.5	0.6	13.1	0.7	2.5	0.1	1.6	1.9	3.5	2.1	0.6

XML ID	Profile	All points	Included points	Excluded points	Tian-2009	Mathieu-2015	GDFKin-2016	Nakamura-2017	SanDiego-2018	Otomo-2018	Glarborg-2018	Okafor-2018	ELTE-2020	POLIMI-2020	NUIG-2020	Han-2020	Mei-2020	Konnov-2021	KAUST-2021	Shrestha-2021	Mei-2021	Zhou-2021	Gotama-2022
x20100029	LBV	6	5	1	0.5	20.4	169.1	0.4	1.5	6.7	43.2	3.0	63.5	0.8	15.8	0.6	1.9	0.2	1.4	1.1	2.9	1.4	0.5
x20100030	LBV	7	7	0	0.8	14.8	177.9	0.5	0.5	4.8	46.7	2.5	65.8	0.3	20.3	0.9	0.9	1.3	0.3	0.4	1.3	1.6	2.2
x20100031	LBV	7	7	0	0.5	25.4	216.3	0.4	2.1	9.7	48.7	5.1	70.9	0.8	18.3	1.0	2.0	0.5	2.0	1.6	3.1	1.8	1.5
x20100032	LBV	7	2	5	0.1	26.8	195.4	0.1	3.1	2.4	63.2	1.8	77.7	0.4	42.1	0.1	2.1	0.8	2.2	2.5	3.4	0.1	4.2
x20100033	LBV	6	6	0	2.3	17.7	79.6	1.4	3.9	7.5	23.4	4.4	35.5	2.2	7.5	1.8	3.6	1.1	3.0	3.3	4.5	2.2	0.8
x20100034	LBV	6	6	0	3.1	47.7	225.1	1.6	7.7	24.4	62.1	13.8	96.0	3.4	18.0	4.4	9.1	0.9	6.3	6.7	11.8	4.3	2.5
x20100035	LBV	7	7	0	0.3	13.8	142.6	0.5	0.8	6.6	42.7	3.4	61.5	0.4	15.6	0.9	1.3	0.7	0.6	0.9	1.9	1.1	1.9
x20100036	LBV	7	7	0	1.5	18.2	93.6	1.1	3.4	9.3	23.8	5.5	36.2	1.7	6.5	1.5	3.0	0.5	3.1	3.0	3.9	1.2	0.9
x20100037	LBV	7	3	4	0.9	30.4	173.6	0.6	4.5	8.0	61.3	4.0	79.6	1.5	27.5	0.3	2.5	0.2	3.6	3.2	4.0	0.0	1.8
x20100038	LBV	7	7	0	4.7	19.0	94.7	1.8	3.0	23.1	40.1	16.6	61.9	1.4	10.3	6.0	9.1	1.6	3.2	4.8	10.0	4.9	6.4
x20100039	LBV	7	7	0	7.9	26.3	74.1	1.9	8.1	24.5	26.7	16.9	45.0	4.1	2.6	5.7	8.7	2.7	6.2	7.6	10.6	2.4	3.6
x20100040	LBV	7	7	0	1.5	11.1	86.7	0.5	1.7	11.2	37.2	6.4	55.5	0.7	8.1	0.7	1.7	0.4	1.1	1.2	2.3	0.5	1.1
x20100041	LBV	7	7	0	3.8	20.0	92.2	0.9	3.8	19.1	35.7	11.7	54.9	1.6	6.1	1.8	3.7	0.5	3.1	3.6	4.7	0.5	1.6
x20100042	LBV	7	7	0	5.1	32.5	168.0	1.2	5.8	31.8	62.9	18.3	95.6	2.2	9.9	1.8	4.4	0.3	4.8	4.7	6.1	1.0	1.8
x20100043	LBV	7	6	1	5.4	6.2	13.3	0.8	2.5	12.4	9.5	10.2	15.5	1.1	1.3	3.0	4.3	1.3	1.8	2.6	4.7	1.2	2.8
x20100044	LBV	7	7	0	22.9	28.4	25.7	3.3	17.3	41.0	14.9	33.5	27.9	7.0	0.9	11.8	14.5	7.9	9.8	12.2	15.0	2.0	8.9
x20100045	LBV	7	7	0	10.3	15.1	42.4	0.2	6.7	25.9	27.8	19.9	44.4	1.2	1.0	3.2	4.8	1.4	2.5	4.0	5.7	0.3	2.0
x20100046	LBV	7	7	0	17.4	24.6	37.9	2.1	13.5	34.4	20.6	27.7	35.5	4.4	0.2	6.4	8.7	4.6	6.7	9.1	9.8	0.4	4.1
x20100047	LBV	7	7	0	11.5	18.2	38.4	0.9	8.3	25.8	21.7	20.4	35.1	2.2	0.4	3.0	4.7	2.0	3.8	5.5	5.6	0.6	1.6
x20100048	LBV	7	7	0	16.6	6.1	3.6	1.8	5.7	27.0	8.6	26.3	13.9	2.9	2.6	6.9	8.9	4.4	4.2	3.6	9.4	2.1	7.1
x20100049	LBV	7	7	0	23.0	11.0	5.2	0.8	12.5	31.2	8.6	33.2	15.7	2.4	1.8	8.3	8.6	6.9	4.7	5.5	9.1	0.3	6.8
x20100050	LBV	7	7	0	27.1	10.3	13.7	0.2	11.5	41.4	22.0	42.6	36.1	1.4	0.6	6.3	7.6	5.1	3.3	3.9	8.3	2.8	5.3
x20100051	LBV	7	7	0	34.9	20.6	7.0	3.5	22.0	43.4	9.0	48.4	16.6	5.6	4.5	12.0	12.4	12.8	9.2	11.3	12.8	1.1	9.2
x20100052	LBV	7	7	0	24.5	11.4	12.7	0.5	11.4	34.8	18.2	36.5	29.4	1.6	0.8	4.4	5.4	5.2	3.6	4.5	6.1	3.7	3.5
x20100053	LBV	7	7	0	27.3	5.4	3.7	2.4	12.6	23.5	6.6	38.4	10.7	2.1	5.9	7.2	7.2	11.5	5.5	4.5	6.9	2.9	7.5

XML ID	Profile	All points	Included points	Excluded points	Tian-2009	Mathieu-2015	GDFKin-2016	Nakamura-2017	SanDiego-2018	Otomo-2018	Glarborg-2018	Okafor-2018	ELTE-2020	POLIMI-2020	NUIG-2020	Han-2020	Mei-2020	Konnov-2021	KAUST-2021	Shrestha-2021	Mei-2021	Zhou-2021	Gotama-2022
x20100054	LBV	7	7	0	48.2	7.3	4.7	2.7	19.0	41.9	14.3	69.6	23.5	1.8	7.9	10.0	10.5	18.2	7.1	5.7	9.9	6.7	10.6
x20100055	LBV	7	7	0	17.5	1.4	0.8	0.4	5.1	16.0	6.4	26.4	10.3	0.4	1.8	2.2	3.0	5.2	1.7	0.9	3.1	4.0	2.9
x20100056	LBV	7	7	0	22.9	2.0	4.5	2.2	6.9	20.3	18.5	36.0	27.3	0.9	2.1	1.9	2.1	6.6	1.7	2.3	2.3	13.9	2.0
x20100057	LBV	7	7	0	33.6	3.4	0.8	0.6	9.0	29.7	9.3	48.1	15.4	1.4	4.0	3.3	5.4	9.6	3.9	1.7	5.7	8.4	4.6
x20100058	LBV	7	7	0	27.1	3.9	9.3	3.0	10.4	14.3	2.7	36.1	3.7	2.0	8.3	3.8	5.4	16.3	7.2	3.5	4.6	3.7	6.5
x20100059	LBV	7	7	0	24.4	2.1	6.8	1.4	7.6	12.4	1.6	32.9	2.6	1.0	6.1	2.2	4.3	13.3	5.4	1.8	3.7	3.5	5.0
x20100060	LBV	7	7	0	22.6	1.6	4.7	1.4	6.3	10.3	3.3	31.3	5.1	0.8	4.9	1.2	2.8	11.8	4.0	1.6	2.2	7.9	3.0
x20100061	LBV	7	7	0	13.3	0.6	1.5	1.0	2.4	5.4	3.9	19.0	6.0	0.7	1.8	0.3	0.8	5.5	1.4	1.0	0.7	9.7	0.8
x20100062	LBV	7	7	0	17.9	1.1	2.2	1.3	3.4	7.9	4.4	25.0	7.0	1.1	2.9	0.8	1.5	8.1	2.3	1.5	1.3	12.8	1.3
x20100063	LBV	1	0	1	excl	excl	excl	excl	excl	excl	excl	excl	excl	excl	excl	excl	excl	excl	excl	excl	excl	excl	excl
x20100064	LBV	7	7	0	8.8	15.3	260.1	6.6	1.4	5.3	93.2	3.2	112.0	2.3	49.2	3.4	1.9	7.6	0.8	1.5	2.1	3.9	7.0
x20100065	LBV	1	0	1	excl	excl	excl	excl	excl	excl	excl	excl	excl	excl	excl	excl	excl	excl	excl	excl	excl	excl	excl
x20100066	LBV	1	0	1	excl	excl	excl	excl	excl	excl	excl	excl	excl	excl	excl	excl	excl	excl	excl	excl	excl	excl	excl
x20100067	LBV	4	2	2	17.4	4.6	156.4	14.2	5.7	0.0	83.1	5.3	97.1	4.7	36.7	2.3	1.1	10.0	1.2	2.0	0.6	5.6	1.1
x20100068	LBV	4	3	1	41.5	2.5	158.1	21.3	8.8	2.4	99.1	18.6	110.8	6.7	47.1	2.1	1.1	14.9	2.6	10.9	0.4	1.8	0.9
x20100069	LBV	1	1	0	5.5	0.2	9.6	3.2	1.9	1.5	8.3	3.6	8.8	1.6	4.8	0.9	0.8	2.5	1.2	2.9	0.7	0.5	0.7
x20100070	LBV	8	4	4	160.1	42.8	88.9	13.0	69.3	234.2	167.0	269.2	227.0	2.5	4.6	26.7	18.1	22.3	7.6	23.0	22.5	35.7	14.5
x20100071	LBV	6	6	0	32.6	25.5	77.2	46.8	60.8	5.0	82.8	15.0	105.2	33.7	38.6	8.2	4.5	30.4	17.7	10.8	4.4	19.1	1.8
x20100072	LBV	8	6	2	26.6	28.0	52.0	74.3	13.3	8.9	181.3	94.2	220.6	60.1	21.4	13.8	14.2	17.1	23.5	39.9	16.5	150.4	13.4
x20100073	LBV	7	7	0	5.6	21.9	43.3	49.9	22.0	0.7	78.0	7.4	89.8	33.0	26.7	15.6	12.8	17.7	20.5	9.9	12.7	62.6	9.2
x20100074	LBV	4	1	3	21.2	45.3	145.3	204.5	57.9	6.6	279.4	5.0	285.2	113.9	121.4	37.6	54.7	59.9	54.5	5.3	52.6	203.1	11.3
x20100075	LBV	4	1	3	26.3	14.6	36.9	66.3	30.7	11.6	79.4	21.6	81.9	33.6	47.9	13.1	16.5	26.1	16.9	10.3	15.1	42.8	3.2
x20100076	LBV	8	7	1	3.9	7.5	22.0	12.3	2.8	5.7	34.6	7.7	39.6	13.3	9.5	7.9	5.4	1.9	2.8	6.9	6.9	34.5	3.6
x20100077	LBV	6	6	0	7.4	15.0	141.1	67.4	1.8	3.9	158.6	18.0	173.1	47.5	57.2	12.3	15.7	11.4	11.8	4.4	18.9	105.4	7.5
x20100078	LBV	3	3	0	9.9	1.1	91.9	20.3	5.7	1.6	74.4	4.9	77.8	6.2	48.7	2.1	1.5	10.9	2.9	1.9	1.2	5.1	2.8

XML ID	Profile	All points	Included points	Excluded points	Tian-2009	Mathieu-2015	GDFKin-2016	Nakamura-2017	SanDiego-2018	Otomo-2018	Glarborg-2018	Okafor-2018	ELTE-2020	POLIMI-2020	NUIG-2020	Han-2020	Mei-2020	Konnov-2021	KAUST-2021	Shrestha-2021	Mei-2021	Zhou-2021	Gotama-2022
x20100079	LBV	11	8	3	7.0	15.6	86.1	8.0	9.9	3.1	52.3	4.4	68.3	7.4	24.1	4.7	4.4	7.6	5.5	7.6	4.0	6.6	6.1
x20100080	LBV	3	2	1	28.3	4.6	167.7	25.4	14.1	10.1	105.4	18.0	109.9	12.2	76.0	7.4	5.2	21.7	7.2	11.9	3.7	4.5	10.0
x20100081	LBV	3	3	0	13.1	1.6	107.6	17.0	6.5	3.1	75.5	7.3	79.4	6.9	50.3	2.8	1.6	12.3	2.6	3.5	1.2	4.0	4.7
x20100082	LBV	9	9	0	4.3	9.2	29.3	1.4	5.3	6.0	16.8	5.8	21.8	1.6	3.8	2.3	2.6	2.9	1.8	4.4	2.5	7.3	1.7
x20199002	LBV	5	2	3	6.5	26.9	346.4	4.6	3.0	4.2	96.8	1.6	132.0	4.4	46.6	3.5	3.3	5.4	4.2	3.8	4.0	3.8	3.9
x20199003	LBV	4	4	0	10.0	6.8	146.1	8.4	1.6	1.7	55.8	1.9	65.1	3.1	38.0	1.1	0.7	5.3	1.3	1.3	1.0	1.1	2.6
x20199004	LBV	4	4	0	13.4	2.5	79.6	9.6	1.9	1.6	44.3	3.6	48.9	2.5	29.6	0.6	0.2	5.0	0.9	2.5	0.2	1.2	1.3
x20199005	LBV	9	8	1	2.1	1.2	49.1	1.8	0.6	0.2	15.6	0.3	20.3	1.5	8.9	0.9	0.5	1.8	0.8	0.8	0.4	0.4	1.5
x20199006	LBV	4	4	0	7.1	1.6	36.3	0.3	2.4	1.7	11.2	3.5	9.4	2.6	15.6	6.6	1.9	2.0	0.7	16.3	1.2	19.3	10.1
x20199007	LBV	3	3	0	4.7	3.7	38.0	0.7	0.8	2.2	9.5	1.6	7.5	1.6	14.1	3.9	0.4	0.5	0.5	14.2	0.2	16.0	7.6
x20199008	LBV	10	9	1	4.1	0.7	15.9	0.7	2.4	1.2	4.2	1.9	4.0	1.9	4.2	2.4	2.0	1.7	1.1	5.5	1.8	4.8	3.4
x20199009	LBV	4	4	0	1.2	3.2	12.5	3.4	0.4	3.4	2.0	2.1	1.5	1.1	3.1	1.8	0.6	1.1	1.8	4.5	0.5	3.9	1.6
x20199010	LBV	5	5	0	1.7	3.2	18.8	2.6	0.2	2.6	3.9	1.5	2.7	0.8	5.9	1.7	0.2	0.5	1.2	6.2	0.3	4.7	2.6
x20199011	LBV	5	4	1	2.3	29.4	300.9	1.3	1.1	6.2	68.8	2.7	100.1	1.3	26.7	0.4	1.5	0.8	1.0	0.4	2.5	3.3	0.3
x20199012	LBV	10	6	4	11.7	73.4	371.4	8.7	0.9	32.2	70.5	12.8	90.5	2.9	29.1	4.2	0.5	2.1	7.4	4.7	0.3	11.2	4.1
x20199013	LBV	10	0	10	excl	excl	excl	excl	excl	excl	excl	excl	excl	excl	excl	excl	excl	excl	excl	excl	excl	excl	excl
x20199014	LBV	10	3	7	50.8	24.4	317.9	16.4	10.7	24.2	197.6	16.8	179.0	13.8	205.0	28.2	1.5	38.4	0.6	26.1	0.1	22.7	62.5
x20199015	LBV	5	3	2	6.1	8.9	95.4	1.9	1.0	3.7	54.9	3.7	53.2	4.9	59.9	11.4	1.4	9.3	0.8	4.9	0.4	16.0	25.7
x20199016	LBV	6	6	0	11.2	40.3	267.6	2.3	0.8	3.7	97.9	2.2	108.1	1.5	69.9	4.7	2.0	8.2	3.0	10.2	1.1	17.8	12.0
x20199017	LBV	5	0	5	excl	excl	excl	excl	excl	excl	excl	excl	excl	excl	excl	excl	excl	excl	excl	excl	excl	excl	excl
x20199018	LBV	9	9	0	1.1	54.1	59.1	19.3	8.3	23.5	10.9	6.4	8.7	12.8	14.9	3.3	7.0	5.0	21.5	2.4	11.2	4.0	4.4
x20199019	LBV	9	9	0	0.9	100.1	85.7	45.7	15.8	49.6	8.2	10.7	4.6	26.0	17.1	4.6	14.9	13.4	47.0	10.0	23.9	9.3	4.1
x20199020	LBV	9	9	0	3.5	91.5	101.4	46.5	15.4	57.0	13.6	12.6	8.8	29.1	27.3	6.9	11.7	15.3	46.7	28.5	17.9	23.9	9.6
x20199021	LBV	4	4	0	2.3	126.5	202.4	29.1	7.5	8.1	75.9	1.6	58.1	3.6	104.1	3.0	12.8	1.4	28.5	14.7	26.7	29.1	20.8
x20199022	LBV	4	4	0	0.2	107.7	87.8	44.1	11.2	19.6	16.9	2.9	8.3	9.0	34.5	0.6	18.4	9.0	39.3	12.9	32.5	14.0	2.9

XML ID	Profile	All points	Included points	Excluded points	Tian-2009	Mathieu-2015	GDFKin-2016	Nakamura-2017	SanDiego-2018	Otomo-2018	Glarborg-2018	Okafor-2018	ELTE-2020	POLIMI-2020	NUIG-2020	Han-2020	Mei-2020	Konnov-2021	KAUST-2021	Shrestha-2021	Mei-2021	Zhou-2021	Gotama-2022
x20199023	LBV	4	4	0	0.1	120.7	82.5	60.7	13.6	29.9	8.8	3.2	2.3	12.2	25.0	1.1	21.8	16.3	50.3	23.6	37.5	18.9	1.8
x20199024	LBV	4	4	0	5.2	47.7	203.8	32.6	2.4	55.6	3.2	15.3	6.6	13.6	2.7	2.3	1.1	5.1	21.8	8.9	1.6	4.4	0.6
x20199025	LBV	4	4	0	12.7	41.5	252.8	29.9	0.5	53.1	4.5	6.6	7.3	11.2	1.3	0.2	0.1	2.5	19.8	33.7	0.3	26.3	1.0
x20199026	LBV	4	4	0	7.8	67.2	222.4	51.6	6.0	82.4	1.1	15.4	1.3	27.6	9.3	2.2	4.1	11.1	41.6	35.7	5.3	27.5	1.4
x20199027	LBV	3	2	1	1.7	22.1	247.1	0.8	0.6	3.3	64.7	0.3	89.8	0.6	30.7	0.3	0.8	1.1	0.8	0.5	1.7	0.8	0.8
x20199028	LBV	4	3	1	2.1	34.0	344.4	0.8	1.1	7.4	82.0	2.0	118.0	0.7	31.7	0.1	1.4	1.1	1.2	0.5	2.8	1.4	0.3
x20199029	LBV	5	2	3	4.4	26.2	347.1	1.5	1.1	1.7	81.7	1.2	108.8	2.2	48.7	0.1	0.9	1.9	1.8	0.8	1.8	1.5	3.5
x20199030	LBV	6	3	3	2.0	28.7	300.7	0.6	1.0	2.1	71.7	1.6	92.2	0.6	49.0	0.7	0.8	2.1	0.8	0.7	1.7	1.4	5.6
x20199031	LBV	7	5	2	5.6	15.8	325.1	1.4	0.8	1.3	77.2	1.0	99.0	2.0	46.2	1.4	0.5	4.5	1.0	0.5	0.6	1.1	6.3
x20199032	LBV	7	7	0	13.7	10.3	255.8	6.4	1.6	2.4	79.3	2.9	91.8	2.5	49.5	2.5	0.6	7.9	0.6	1.4	0.5	2.9	5.5
x20199033	LBV	3	2	1	2.7	27.0	335.4	1.3	0.5	3.7	90.2	0.2	123.6	0.8	43.4	0.4	0.8	2.3	0.8	0.6	1.7	0.7	1.5
x20199034	LBV	4	1	3	0.1	75.5	333.6	3.7	12.7	34.7	44.8	22.2	82.2	3.4	3.7	7.8	9.4	2.7	8.0	7.9	12.0	13.3	5.8
x20199035	LBV	6	3	3	0.3	17.8	120.3	1.1	1.9	8.1	16.6	5.2	27.5	0.5	4.4	1.9	1.4	0.6	1.6	1.3	1.8	3.0	1.7
x20199036	LBV	6	1	5	0.0	18.2	97.7	2.9	2.7	10.0	7.4	7.8	14.4	1.5	0.1	3.2	1.9	1.3	2.8	1.8	2.2	4.3	2.1
x20199037	LBV	6	1	5	2.5	25.0	244.5	3.0	1.3	14.6	23.8	7.4	39.0	0.7	1.6	1.5	0.2	0.4	2.4	0.2	0.6	1.3	0.5
x20199038	LBV	4	1	3	0.7	27.7	292.6	0.1	1.2	3.5	76.2	0.3	97.5	0.2	44.1	0.1	1.4	1.3	1.6	0.7	2.8	0.9	0.9
x20199039	LBV	4	1	3	1.8	44.1	364.7	0.2	3.1	16.5	62.3	8.4	101.7	0.1	11.5	1.0	1.5	0.0	2.0	1.1	2.5	2.8	0.3
x20199040	LBV	6	4	2	3.4	10.4	184.6	1.6	0.5	3.9	48.0	2.1	61.9	1.2	29.0	2.8	0.8	3.5	0.6	0.9	0.5	2.6	6.5
x20199041	LBV	6	2	4	0.5	15.6	123.7	1.4	1.1	8.2	14.2	4.4	23.7	0.6	1.5	1.1	0.5	0.3	1.5	0.5	0.9	1.4	0.6
x20199042	LBV	6	2	4	5.8	13.1	232.3	0.3	0.0	5.8	36.2	1.1	52.5	0.1	8.3	0.2	0.6	0.5	0.5	0.9	0.2	1.1	0.6
x20199043	LBV	4	2	2	0.3	12.9	96.0	0.1	1.0	4.6	15.8	3.0	27.2	0.1	2.9	0.6	1.1	0.0	0.4	0.4	1.5	1.7	0.3
x20199044	LBV	6	5	1	2.5	11.8	202.0	1.5	0.2	1.9	60.7	0.9	73.5	0.9	44.4	2.4	0.3	3.9	0.2	0.3	0.2	1.3	8.2
x20199045	LBV	6	4	2	1.2	25.8	246.2	2.0	1.6	10.0	54.3	4.5	71.3	1.6	32.4	2.6	0.7	2.4	2.5	0.7	1.4	2.4	6.5
x20199046	LBV	6	2	4	3.1	24.1	278.2	0.7	0.4	9.0	55.0	1.4	75.9	0.6	18.9	0.1	0.0	0.5	2.0	0.2	0.2	1.4	0.7
x20199047	LBV	6	2	4	0.8	34.5	232.7	7.4	3.6	21.2	20.5	10.9	34.1	4.1	2.0	3.2	1.5	1.9	7.3	1.2	2.2	2.0	2.0

XML ID	Profile	All points	Included points	Excluded points	Tian-2009	Mathieu-2015	GDFKin-2016	Nakamura-2017	SanDiego-2018	Otomo-2018	Glarborg-2018	Okafor-2018	ELTE-2020	POLIMI-2020	NUIG-2020	Han-2020	Mei-2020	Konnov-2021	KAUST-2021	Shrestha-2021	Mei-2021	Zhou-2021	Gotama-2022
x20199048	LBV	3	0	3	excl	excl	excl	excl	excl	excl	excl	excl	excl	excl	excl	excl	excl	excl	excl	excl	excl	excl	excl
x20199049	LBV	4	0	4	excl	excl	excl	excl	excl	excl	excl	excl	excl	excl	excl	excl	excl	excl	excl	excl	excl	excl	excl
x20199050	LBV	8	8	0	7.9	65.0	75.8	12.4	16.4	23.5	14.5	12.6	20.5	14.7	4.2	7.9	12.6	6.0	19.5	9.5	16.0	4.9	4.0
x20199051	LBV	9	9	0	15.9	109.6	31.8	32.7	36.4	49.8	0.9	34.1	2.3	32.4	1.0	22.2	29.3	18.1	41.9	23.7	35.4	16.5	13.7
x20199052	LBV	11	11	0	6.2	71.6	31.1	21.7	19.8	32.3	1.7	18.1	2.5	20.2	1.6	10.9	15.1	9.4	27.1	7.9	19.2	4.6	6.3
x20199053	LBV	8	0	8	excl	excl	excl	excl	excl	excl	excl	excl	excl	excl	excl	excl	excl	excl	excl	excl	excl	excl	excl
x20199054	LBV	3	2	1	40.5	0.4	315.8	29.7	15.3	11.4	151.6	22.9	158.5	13.6	113.6	8.5	5.5	28.2	8.0	14.9	3.3	2.0	13.1

Table A9. Averaged error function values for each investigated mechanism for the utilized He-containing experimental datasets (E_i) in the case of NH_3/H_2 fuel mixtures. In the table, "excl" means that no data point was included in the comparison from the corresponding dataset.

XML ID	Profile	All points	Included points	Excluded points	Mathieu-2015	Nakamura-2017	SanDiego-2018	Otomo-2018	Glarborg-2018	ELTE-2020	POLIMI-2020	NUIG-2020	Han-2020	Mei-2020	Konnov-2021	KAUST-2021	Shrestha-2021	Mei-2021	Gotama-2022
x00199000	NH_3	12	9	3	0.1	25.2	12.9	0.1	1.2	1.2	0.0	8.8	0.0	0.0	0.1	0.0	2.2	0.0	0.0
x00199000	NO	7	7	0	0.3	0.6	0.1	0.3	0.2	0.2	0.0	1.5	0.0	0.0	10.0	0.0	0.3	0.0	0.1
x00199000	NO_2	7	7	0	0.0	0.0	0.0	0.0	0.0	0.0	0.0	0.0	0.0	0.0	0.0	0.0	0.0	0.0	0.0
x00199001	NH_3	8	3	5	3.2	51.6	29.5	1.4	15.9	15.6	0.0	127.0	0.0	0.0	1.3	0.0	12.6	0.0	0.0
x00199001	NO	8	8	0	0.4	0.2	0.1	0.3	0.2	0.1	0.0	2.1	0.2	0.3	5.3	0.1	0.1	0.3	0.3
x00199001	NO_2	8	8	0	0.2	0.1	0.0	0.1	0.0	0.0	0.1	0.3	0.0	0.0	0.0	0.0	0.1	0.0	0.0
x00199002	NH_3	12	12	0	0.0	0.0	0.0	0.0	0.0	0.0	0.0	0.0	0.0	0.0	0.0	0.0	0.0	0.0	0.0
x30199019	NH_3	4	1	3	4.6	2.5	4.6	4.6	4.6	4.6	3.1	4.6	1.5	3.4	164.6	2.4	4.6	3.4	4.0
x30199019	NO	4	0	4	excl	excl	excl	excl	excl	excl	excl	excl	excl	excl	excl	excl	excl	excl	excl
x30199020	NH_3	8	1	7	0.8	1.9	0.8	0.7	0.6	0.6	0.4	0.6	0.2	0.6	97.7	0.3	0.8	0.6	0.7
x30199020	NO	8	1	7	1.7	25.1	1.7	1.0	0.5	0.2	0.0	0.3	0.2	0.5	271.8	0.3	1.5	0.4	0.9
x30199021	NH_3	19	15	4	0.7	0.6	0.7	0.7	0.7	0.7	0.6	0.7	0.6	0.3	0.7	0.4	0.7	0.3	0.6
x30199021	O_2	19	18	1	2.2	1.7	7.2	1.2	1.1	1.2	0.8	1.7	0.9	1.2	2.8	0.4	0.8	1.5	0.9
x30199021	NO	19	8	11	0.1	0.0	0.1	0.1	0.1	0.1	0.1	0.1	0.0	0.0	0.1	0.0	0.1	0.0	0.0
x30199021	N_2	19	13	6	0.6	5.8	3.2	5.4	3.3	4.8	1.1	11.0	2.5	2.0	31.4	2.9	0.3	5.7	1.4
x30199021	H_2O	19	12	7	2.0	1.9	2.0	2.0	2.0	2.0	1.9	2.0	1.8	1.5	2.0	1.5	2.0	1.5	1.8
x30199021	H_2	19	17	2	1.0	0.4	0.9	0.9	0.9	0.9	0.8	0.9	0.8	0.0	0.9	0.0	1.5	0.0	19.6
x20199048	LBV	3	1	2	346.8	136.7	126.6	158.5	1.6	3.5	116.9	1.7	62.5	97.1	102.4	160.1	58.7	120.8	32.0
x20199049	LBV	4	0	4	excl	excl	excl	excl	excl	excl	excl	excl	excl	excl	excl	excl	excl	excl	excl

Table A10. Averaged error function values for each investigated mechanism for all of the utilized experimental datasets (E_i) in the case of NH_3/syngas fuel mixtures. In the table, "excl" means that no data point was included in the comparison from the corresponding dataset.

XML ID	Profile	All points	Included points	Excluded points	Tian-2009	Mathieu-2015	GDFKin-2016	SanDiego-2018	Glarborg-2018	Okafor-2018	NUIG-2020	Han-2020	Mei-2020	Konnov-2021	Shrestha-2021	Mei-2021	Zhou-2021
x00101000	O_2	3	3	0	1.6	2.6	2.2	2.5	2.2	1.8	1.6	2.4	2.6	1.2	3.2	2.1	2.0
x00101000	CO	3	2	1	50.8	18.0	27.5	19.3	19.2	36.1	46.9	31.5	22.0	16.6	30.6	29.0	41.4
x00101000	H_2	3	3	0	8.4	8.4	7.9	7.8	8.5	7.6	7.7	8.3	8.3	7.9	8.2	8.0	4.8
x00101000	N_2O	3	3	0	0.5	0.7	0.9	0.9	1.6	1.4	2.1	21.6	1.1	1.1	0.1	0.9	1.5
x00101000	NO	3	0	3	excl	excl	excl	excl	excl	excl	excl	excl	excl	excl	excl	excl	excl
x00101001	O_2	3	0	3	excl	excl	excl	excl	excl	excl	excl	excl	excl	excl	excl	excl	excl
x00101001	CO	3	0	3	excl	excl	excl	excl	excl	excl	excl	excl	excl	excl	excl	excl	excl
x00101001	H_2	3	0	3	excl	excl	excl	excl	excl	excl	excl	excl	excl	excl	excl	excl	excl
x00101001	N_2O	3	3	0	0.4	0.5	0.3	0.4	0.4	1.0	0.6	4.7	0.4	0.8	0.8	0.4	0.7
x00101001	NO	3	1	2	2.8	4.2	0.8	14.7	4.4	0.4	5.6	4.5	2.0	3.6	8.8	0.2	10.4
x00101002	O_2	6	6	0	5.3	5.9	7.7	8.1	5.9	15.9	6.3	25.6	12.0	5.0	5.9	8.1	9.0
x00101002	CO	6	3	3	7.9	24.5	3.8	3.5	2.3	13.5	15.2	82.9	27.4	9.1	12.1	25.5	22.3
x00101002	H_2	6	3	3	8.5	10.0	9.1	7.6	9.1	12.2	8.9	11.7	8.8	8.7	10.1	8.5	3.2
x00101002	N_2O	6	5	1	0.6	0.5	1.1	1.2	4.3	0.6	3.8	28.9	0.6	19.9	2.5	0.1	75.2
x00101002	NO	6	5	1	12.4	7.9	3.4	11.4	4.1	11.1	14.5	18.2	12.6	21.5	16.1	5.5	7.9
x00101003	O_2	7	7	0	3.5	3.5	4.7	3.1	2.8	4.9	2.8	19.4	8.4	2.2	2.7	4.9	5.1
x00101003	CO	7	7	0	13.9	7.6	9.4	4.5	4.9	8.3	3.7	26.9	18.8	3.8	4.1	8.2	9.4
x00101003	H_2	7	4	3	3.1	4.5	3.8	3.1	3.4	4.0	3.5	7.1	3.6	3.1	3.1	3.4	4.2
x00101003	N_2O	7	7	0	0.8	1.1	4.2	2.7	4.4	4.5	4.9	38.9	6.6	12.9	2.4	3.7	4.8
x00101003	NO	7	6	1	100.2	8.2	1.6	12.7	3.4	62.7	36.5	18.9	11.8	135.0	10.7	8.5	92.3
x00101004	O_2	6	0	6	excl	excl	excl	excl	excl	excl	excl	excl	excl	excl	excl	excl	excl
x00101004	CO	6	6	0	1.3	1.5	2.2	1.4	1.1	3.5	1.1	1.6	1.5	1.2	1.0	1.2	1.4
x00101004	H_2	6	3	3	1.6	1.7	10.6	2.7	6.7	59.1	6.6	42.7	6.7	6.5	3.5	11.5	15.3

XML_ID	Profile	All points	Included points	Excluded points	Tian-2009	Mathieu-2015	GDFKin-2016	SanDiego-2018	Glarborg-2018	Okafor-2018	NUIG-2020	Han-2020	Mei-2020	Konnov-2021	Shrestha-2021	Mei-2021	Zhou-2021
x00101004	NO	6	6	0	4.9	12.0	4.7	22.5	12.5	21.3	11.1	17.7	7.5	1.5	13.2	4.1	3.8
x00101004	N_2O	5	5	0	0.6	0.7	2.3	1.0	0.9	3.1	2.3	4.1	1.9	6.3	1.4	1.6	1.9
x00101005	O_2	7	7	0	2.3	4.6	6.0	4.4	3.0	6.4	2.7	9.4	6.5	2.5	2.4	2.9	2.3
x00101005	CO	7	7	0	0.1	1.0	1.5	1.1	0.4	1.6	0.5	2.0	1.6	0.3	0.1	0.4	0.4
x00101005	H_2	7	0	7	excl	excl	excl	excl	excl	excl	excl	excl	excl	excl	excl	excl	excl
x00101005	N_2O	7	7	0	1.0	2.4	4.7	3.6	3.1	5.5	5.5	9.9	4.9	0.5	3.7	4.4	1.2
x00101005	NO	7	7	0	13.9	4.3	1.8	7.3	1.2	18.6	6.0	7.1	2.5	27.6	2.0	2.1	28.9
x00101006	O_2	7	6	1	2.8	3.1	2.7	3.1	3.0	2.6	2.7	2.8	2.9	2.6	3.1	2.6	2.5
x00101006	CO	7	7	0	3.7	4.4	3.5	3.6	3.6	3.5	4.6	4.9	4.5	3.5	3.9	4.7	4.6
x00101006	H_2	7	3	4	7.6	8.1	7.6	7.8	8.6	6.8	7.1	7.6	8.1	7.8	7.4	7.7	5.1
x00101006	N_2O	7	7	0	1.0	1.2	1.1	1.3	1.1	0.9	1.0	5.3	1.1	1.0	1.4	1.1	3.9
x00101006	NO	7	5	2	9.5	13.3	2.2	11.4	1.3	3.7	11.6	10.7	12.4	22.4	39.7	0.4	1.5
x00101007	O_2	7	6	1	1.8	1.9	2.3	2.6	1.9	2.9	2.8	2.4	2.0	2.4	1.5	2.3	3.0
x00101007	CO	7	6	1	4.4	2.7	2.0	2.5	2.8	1.9	1.8	1.9	2.3	2.8	3.8	2.1	2.0
x00101007	H_2	7	4	3	8.8	8.2	7.8	7.6	8.3	7.9	7.7	8.2	8.0	8.0	8.6	7.8	4.6
x00101007	N_2O	7	7	0	0.1	0.6	1.5	0.3	2.0	0.4	2.5	17.0	1.1	0.2	0.3	0.6	0.3
x00101007	NO	7	7	0	15.4	7.5	0.7	9.2	1.0	21.7	7.9	7.4	4.4	39.2	7.8	1.3	36.2
x30101006	NH_3	9	7	2	0.0	0.2	0.7	0.0	0.0	0.0	7.7	0.0	0.0	9.6	3.1	0.0	0.0
x30101006	NO	9	8	1	33.0	9.2	10.6	7.1	7.5	4.1	37.7	7.1	0.8	62.9	13.5	6.2	32.6
x20101000	LBV	44	44	0	21.6	40.4	99.0	37.6	78.2	38.8	18.8	10.7	11.5	14.3	6.6	10.1	11.0
x20101001	LBV	14	14	0	4.2	39.6	250.3	8.4	97.4	8.2	27.5	0.7	2.7	2.9	4.4	3.8	1.5
x20101002	LBV	19	19	0	24.9	47.3	137.5	31.1	116.7	46.9	7.3	5.8	4.0	1.7	4.6	5.0	0.2
x20101003	LBV	19	19	0	87.4	6.4	10.0	54.4	94.4	143.2	8.9	14.8	7.0	17.5	10.8	8.9	17.1
x20101004	LBV	21	19	2	50.8	8.7	26.5	63.7	38.1	36.6	42.9	4.9	11.2	90.6	19.1	10.1	34.2
x20101005	LBV	42	42	0	19.2	22.9	113.3	21.3	112.2	33.5	19.8	1.1	1.7	7.1	12.5	1.7	32.2

XML_ID	Profile	All points	Included points	Excluded points	Tian-2009	Mathieu-2015	GDFKin-2016	SanDiego-2018	Glarborg-2018	Okafor-2018	NUIG-2020	Han-2020	Mei-2020	Konnov-2021	Shrestha-2021	Mei-2021	Zhou-2021
x20101006	LBV	12	12	0	2.4	33.0	277.0	5.3	113.5	5.6	33.8	0.2	1.1	3.9	2.2	1.9	0.3
x20101007	LBV	19	19	0	19.1	35.0	154.5	22.0	137.6	38.7	12.9	3.0	2.8	2.6	1.4	4.0	3.1
x20101008	LBV	19	19	0	90.2	4.7	13.1	45.3	115.0	143.7	7.0	14.4	9.8	15.0	16.1	12.3	30.3
x20101009	LBV	29	27	2	30.9	31.9	215.8	16.9	218.5	56.5	34.8	4.6	5.2	3.9	18.1	7.6	68.5
x20101010	LBV	13	13	0	3.2	23.2	321.5	6.3	148.1	4.0	46.7	1.1	1.0	7.9	3.3	1.2	2.2
x20101011	LBV	19	19	0	17.7	17.6	219.3	23.0	237.7	41.8	26.6	1.1	0.1	9.9	8.4	0.5	24.3
x20101012	LBV	19	14	5	81.7	26.1	14.8	8.3	281.7	147.3	2.3	11.7	16.0	8.2	82.1	20.4	219.4
x20101013	LBV	6	6	0	0.7	9.2	54.8	1.5	21.1	1.9	8.9	0.2	0.5	0.5	0.7	0.8	1.2
x20101014	LBV	5	4	1	5.7	3.9	22.4	3.2	24.6	8.5	6.0	0.6	0.8	3.2	0.6	0.5	7.1
x20101015	LBV	5	5	0	10.0	16.8	20.9	6.1	12.9	12.4	3.1	1.8	3.2	2.9	2.7	3.7	5.1
x20101016	LBV	9	9	0	41.4	11.1	55.3	31.1	101.4	88.2	3.5	4.6	2.6	1.9	5.0	4.0	12.4
x20101017	LBV	9	9	0	26.5	21.1	83.3	29.7	127.2	67.7	15.9	4.7	3.1	4.6	8.2	4.3	14.8
x20101018	LBV	7	7	0	4.9	19.1	77.8	10.6	100.4	11.7	29.9	2.8	0.8	8.0	8.8	0.5	7.7
x20101019	LBV	4	4	0	18.7	2.8	51.2	10.2	74.8	12.8	36.8	3.3	3.6	15.2	3.9	3.1	7.8
x20101020	LBV	9	9	0	34.3	1.6	24.6	14.7	68.0	78.0	1.5	2.1	2.2	3.6	3.8	3.1	15.4
x20101021	LBV	9	9	0	19.7	8.3	30.5	18.6	61.3	54.4	5.9	4.0	1.1	4.9	7.1	1.4	13.4
x20101022	LBV	5	5	0	10.5	6.0	53.9	18.0	73.8	3.5	27.3	5.0	1.9	15.0	1.7	1.4	22.2
x20101023	LBV	4	4	0	32.0	6.2	39.9	26.8	74.0	24.6	38.7	7.7	4.5	21.7	7.8	3.8	17.8
x20101024	LBV	9	9	0	35.8	3.2	13.7	13.2	49.8	79.6	1.8	1.7	1.9	9.6	5.2	2.0	24.2
x20101025	LBV	9	9	0	16.3	8.4	19.0	17.9	44.1	49.2	4.7	4.1	1.0	9.8	5.7	0.5	22.4
x20101026	LBV	5	5	0	28.4	37.8	106.9	77.5	184.4	9.7	62.0	19.0	5.8	42.8	3.7	4.4	96.2
x20101027	LBV	5	5	0	49.1	20.8	38.7	59.9	96.7	39.0	49.1	11.8	5.3	34.5	11.3	4.6	33.9
x20101028	LBV	17	17	0	66.2	38.6	148.8	41.4	139.1	89.8	22.6	4.6	5.9	33.1	11.1	6.6	59.3
x20101029	LBV	14	14	0	23.3	28.3	83.3	24.3	62.1	44.8	22.9	11.0	4.9	10.5	18.4	5.5	5.5
x20101030	LBV	13	13	0	8.1	14.9	59.5	9.1	60.2	17.9	24.0	5.8	2.2	4.4	10.0	2.9	5.3

XML_ID	Profile	All points	Included points	Excluded points	Tian-2009	Mathieu-2015	GDFKin-2016	SanDiego-2018	Glarborg-2018	Okafor-2018	NUIG-2020	Han-2020	Mei-2020	Konnov-2021	Shrestha-2021	Mei-2021	Zhou-2021
x20101031	LBV	21	21	0	28.9	50.8	101.1	49.1	67.6	47.1	22.8	16.0	15.9	21.3	6.7	14.7	6.8
x20101032	LBV	21	21	0	4.5	19.1	60.4	16.7	45.1	15.3	19.8	8.4	4.9	7.3	4.8	5.2	3.9
x20101033	LBV	18	18	0	4.2	18.5	40.3	17.4	34.2	15.9	19.2	11.3	3.2	6.5	6.8	3.9	2.4
x20101034	LBV	11	11	0	163.6	4.4	7.9	39.0	140.3	242.3	12.5	10.9	15.2	34.8	24.2	17.4	83.6
x20101035	LBV	12	10	2	68.7	16.5	13.3	56.8	74.0	143.8	14.2	24.1	8.4	31.0	34.9	8.6	34.7
x20101036	LBV	10	10	0	34.9	15.2	7.8	36.3	51.6	76.5	6.7	19.7	5.1	15.8	40.3	5.3	17.1
x20101037	LBV	12	12	0	40.1	34.0	158.4	32.4	180.1	76.7	8.8	6.7	5.7	3.9	5.2	6.4	9.4
x20101038	LBV	11	11	0	5.2	15.1	103.2	11.0	96.9	10.5	24.6	1.4	0.7	5.6	7.6	1.0	3.9
x20101039	LBV	9	9	0	4.3	3.3	58.0	5.2	59.2	0.6	22.3	0.4	1.1	4.9	1.1	1.4	1.7
x20101040	LBV	11	11	0	116.0	21.4	3.3	81.9	46.0	169.0	25.1	32.5	19.8	36.8	2.2	22.0	8.7
x20101041	LBV	12	12	0	9.7	5.6	38.1	23.0	96.3	33.9	9.9	4.6	3.9	5.4	4.7	3.4	25.5
x20101042	LBV	10	10	0	5.4	9.7	21.8	18.0	59.2	23.4	6.4	5.9	2.7	2.5	9.0	2.4	10.8
x20101043	LBV	11	11	0	38.8	63.7	121.1	41.9	103.0	64.5	3.0	11.6	9.5	1.6	5.2	11.3	1.6
x20101044	LBV	9	9	0	1.7	21.7	100.9	4.8	83.8	7.6	22.5	0.7	0.6	3.5	6.2	0.7	1.0
x20101045	LBV	8	8	0	1.9	11.4	73.6	1.7	68.1	1.3	29.0	0.6	0.3	6.0	1.7	0.2	1.1
x20101046	LBV	8	8	0	67.3	22.9	23.8	45.0	58.2	110.2	1.8	14.9	10.1	5.5	0.2	12.5	7.0
x20101047	LBV	8	8	0	85.8	35.2	14.0	74.6	47.6	135.3	4.6	21.1	11.1	12.5	2.4	12.8	5.6
x20101048	LBV	8	8	0	96.9	49.1	11.8	86.2	41.0	153.9	5.4	25.3	14.0	16.5	6.5	16.2	2.6
x20101049	LBV	8	7	1	110.4	60.8	16.7	99.7	50.7	170.6	6.8	27.1	15.8	18.6	6.8	19.0	5.9
x20101050	LBV	8	8	0	55.3	8.7	3.1	31.1	27.3	99.7	2.3	9.5	6.2	11.2	1.1	6.3	5.1
x20101051	LBV	8	5	3	87.8	27.1	3.0	67.3	28.3	192.2	9.4	24.3	17.5	32.8	6.5	17.5	4.1
x20101052	LBV	8	6	2	150.8	47.5	5.4	84.3	29.1	272.3	18.2	43.4	40.4	46.8	14.0	43.5	0.6
x20101053	LBV	8	6	2	137.5	53.2	0.6	101.7	11.7	235.0	23.8	39.5	32.4	55.6	24.8	33.1	2.3
x20101054	LBV	7	7	0	83.0	7.2	2.3	29.5	22.4	151.3	7.0	13.0	13.6	25.3	3.0	13.7	9.1
x20101055	LBV	7	7	0	75.0	16.4	4.2	35.3	5.2	131.5	14.6	20.2	21.4	32.8	8.6	20.8	1.5

XML_ID	Profile	All points	Included points	Excluded points	Tian-2009	Mathieu-2015	GDFKin-2016	SanDiego-2018	Glarborg-2018	Okafor-2018	NUIG-2020	Han-2020	Mei-2020	Konnov-2021	Shrestha-2021	Mei-2021	Zhou-2021
x20101056	LBV	7	6	1	162.0	42.4	16.9	79.5	12.2	276.9	39.2	47.3	54.5	77.2	31.3	54.0	4.3
x20101057	LBV	6	4	2	191.1	36.8	5.5	71.8	5.1	273.9	35.9	42.4	49.1	64.7	19.8	52.2	1.1
x20101058	LBV	11	11	0	5.7	18.1	139.4	5.2	57.9	12.1	22.7	2.3	1.7	2.5	1.0	2.1	2.3
x20101059	LBV	6	6	0	6.5	19.9	105.4	3.4	76.3	17.6	19.7	6.7	11.1	2.8	0.7	12.2	6.4
x20101060	LBV	6	6	0	11.2	33.1	78.0	8.3	56.2	27.2	11.6	9.3	15.4	1.4	3.0	16.6	9.1
x20101061	LBV	6	6	0	15.3	45.8	31.0	15.0	19.3	31.3	1.7	10.3	15.2	2.1	7.6	16.5	9.0
x20101062	LBV	6	6	0	28.4	92.7	76.2	27.5	48.9	59.2	6.7	16.9	24.5	3.8	13.8	27.3	13.8
x20101063	LBV	6	6	0	45.6	7.7	9.7	22.9	37.6	95.0	3.3	23.2	17.9	5.8	1.3	17.2	7.0
x20101064	LBV	6	6	0	53.0	9.3	4.9	24.3	26.2	107.3	2.3	26.5	21.4	6.7	0.4	20.4	5.1
x20101065	LBV	6	6	0	40.1	8.3	5.8	24.3	24.5	76.5	1.7	15.5	8.3	5.0	1.1	7.6	1.5
x20101066	LBV	6	3	3	110.9	41.5	22.1	79.6	75.0	257.8	12.7	57.2	51.2	25.1	4.7	51.7	29.4
x20101067	LBV	6	6	0	10.8	1.8	21.9	11.1	9.9	28.5	5.5	1.3	1.4	33.9	3.3	0.6	14.1
x20101068	LBV	8	8	0	17.4	6.9	32.7	16.0	2.0	42.7	11.2	7.2	6.9	42.8	3.3	4.7	7.4
x20101069	LBV	8	8	0	16.2	5.8	32.2	15.9	7.1	44.9	10.8	6.7	5.9	48.6	8.6	4.5	18.4
x20101070	LBV	8	8	0	22.7	10.2	41.1	22.0	17.9	60.9	15.6	13.5	10.1	70.5	20.7	10.2	46.0
x20101071	LBV	10	10	0	8.6	2.4	19.4	7.7	37.0	24.1	3.2	0.9	0.5	3.8	5.7	0.5	10.3
x20101072	LBV	10	10	0	25.2	5.8	80.4	22.3	128.5	79.1	9.2	1.9	0.4	10.3	14.9	0.7	42.0
x20101073	LBV	10	10	0	30.6	6.8	53.7	22.8	77.6	72.6	5.5	3.5	1.1	10.6	8.7	1.0	24.8
x20101074	LBV	10	10	0	14.1	12.9	71.8	27.2	107.1	43.8	17.7	4.4	0.7	13.6	6.2	0.6	29.7
x20101075	LBV	10	9	1	23.6	32.5	93.5	45.2	138.2	58.1	33.7	17.2	5.4	25.2	24.7	4.0	42.0
x20101076	LBV	3	3	0	0.5	28.9	325.1	0.8	103.9	3.1	36.4	0.0	1.0	2.1	0.3	2.5	0.2
x20101077	LBV	9	9	0	17.2	65.4	158.4	25.5	111.8	39.6	22.7	2.8	5.3	3.3	8.8	6.4	0.9
x20101078	LBV	10	10	0	103.3	10.5	32.6	33.9	34.5	149.7	21.7	5.7	7.3	75.9	17.5	4.9	49.6
x20101079	LBV	10	9	1	73.0	14.5	29.9	32.7	18.4	8.9	4.7	14.7	33.7	79.7	12.1	18.9	140.6

Table A11. Comparison of the overall sensitivity analysis results of thermodynamic data for the investigated shock tube ignition delay time measurements in the case of NH_3/H_2 fuel mixtures (226 investigated data points). The 10-10 most sensitive species of the three investigated mechanisms are shown for each thermodynamic property separately.

POLIMI-2020			KAUST-2021			Shrestha-2021		
Species	**Freq.[a]**	$\overline{\lvert \widetilde{sn}_{ij} \rvert}$[b]	**Species**	**Freq.[a]**	$\overline{\lvert \widetilde{sn}_{ij} \rvert}$[b]	**Species**	**Freq.[a]**	$\overline{\lvert \widetilde{sn}_{ij} \rvert}$[b]
Standard isobar molar heat capacity at 300 K								
NH_2	88.1%	0.562	NH_2	86.7%	0.594	NH_3	92.5%	0.716
NH_3	88.1%	0.608	NH_3	85.0%	0.573	H	92.0%	0.514
H_2	68.6%	0.455	HO_2	68.6%	0.420	NH_2	89.8%	0.649
H	66.8%	0.386	H	67.3%	0.431	H_2	58.4%	0.375
HO_2	60.2%	0.346	H_2	64.6%	0.467	HO_2	46.0%	0.238
O_2	54.9%	0.311	O_2	62.4%	0.362	OH	42.9%	0.189
OH	40.7%	0.192	N_2H_3	43.8%	0.143	O	38.9%	0.143
NH	40.3%	0.218	NH	28.8%	0.141	N_2H_3	38.5%	0.125
O	38.1%	0.146	H_2NO	23.5%	0.117	HNO	31.4%	0.115
H_2NO	28.3%	0.140	HNOH	15.9%	0.083	NH	31.0%	0.136
Standard enthalpy of formation at 300 K ($\widetilde{ssn}_{ij}$ values instead of $\widetilde{sn}_{ij}$ values)								
NH_2	88.1%	0.617	NH_2	82.3%	0.575	H	90.3%	0.772
NH_3	81.0%	0.518	NH_3	79.2%	0.516	NH_2	86.7%	0.652
H	66.4%	0.549	H	74.3%	0.560	NH_3	85.8%	0.644
H_2	60.6%	0.422	O_2	64.6%	0.408	H_2	50.0%	0.317
O_2	52.7%	0.280	HO_2	58.8%	0.369	O	37.6%	0.136
HO_2	44.7%	0.251	H_2	57.1%	0.354	HO_2	36.3%	0.147
O	37.2%	0.168	N_2H_3	34.1%	0.087	OH	31.0%	0.121
NH	35.0%	0.174	NH	16.8%	0.083	N_2H_3	28.8%	0.090
OH	34.5%	0.169	H_2O	9.7%	0.063	NH	15.9%	0.076
H_2NO	13.7%	0.050	H_2NO	4.9%	0.035	NO	15.5%	0.051
Standard molar entropy at 300 K								
NH_2	85.8%	0.633	NH_2	84.1%	0.623	NH_3	88.5%	0.699
NH_3	76.5%	0.547	NH_3	81.4%	0.548	NH_2	86.3%	0.670
H	56.6%	0.393	HO_2	69.0%	0.484	H	84.5%	0.517
H_2	54.9%	0.372	O_2	66.8%	0.414	H_2	50.0%	0.279
HO_2	53.5%	0.330	H	64.2%	0.446	HO_2	39.8%	0.228
O_2	52.2%	0.338	H_2	50.4%	0.343	N_2H_3	35.4%	0.123
NH	40.3%	0.193	N_2H_3	38.1%	0.110	OH	35.4%	0.158
O	35.8%	0.175	NH	23.0%	0.113	O	33.2%	0.138
OH	34.5%	0.181	H_2NO	13.7%	0.073	NO	25.7%	0.094
HNOH	19.0%	0.083	HNOH	9.7%	0.052	HNO	24.3%	0.073

[a]: Number of data points for which the thermodynamic property has $\lvert \widetilde{sn}_{ij} \rvert \geq 0.1$ or $\lvert \widetilde{ssn}_{ij} \rvert \geq 0.1$ divided (normalized) by the total number of data points.
[b]: Average of the $\lvert \widetilde{sn}_{ij} \rvert$ or $\lvert \widetilde{ssn}_{ij} \rvert$ values for all included data points for each thermodynamic property.

Table A12. Comparison of the overall sensitivity analysis results of thermodynamic data for the investigated concentration measurements in jet stirred reactors in the case of NH_3/H_2 fuel mixtures (1105 investigated data points). The 10-10 most sensitive species of the three investigated mechanisms are shown for each thermodynamic property separately.

POLIMI-2020			KAUST-2021			Shrestha-2021		
Species	**Freq.[a]**	$\overline{\lvert \widetilde{sn}_{ij} \rvert}$[b]	**Species**	**Freq.[a]**	$\overline{\lvert \widetilde{sn}_{ij} \rvert}$[b]	**Species**	**Freq.[a]**	$\overline{\lvert \widetilde{sn}_{ij} \rvert}$[b]
Standard isobar molar heat capacity at 300 K								
NH_2	87.6%	0.585	NH_2	91.3%	0.668	NH_2	82.7%	0.663
O_2	87.0%	0.601	NH_3	83.8%	0.629	H	80.6%	0.397
NH_3	86.5%	0.641	H	74.3%	0.420	NH_3	69.6%	0.461
HO_2	79.5%	0.573	O_2	70.0%	0.391	H_2	55.9%	0.308
H	63.9%	0.341	H_2	60.3%	0.341	N_2H_3	50.0%	0.277
H_2	53.2%	0.340	HO_2	45.7%	0.346	O_2	40.5%	0.192
H_2NO	36.8%	0.110	N_2H_3	37.9%	0.183	H_2NO	38.8%	0.219
O	28.6%	0.116	H_2NO	34.8%	0.130	OH	37.3%	0.205
N_2H_4	27.4%	0.085	O	27.9%	0.114	H_2O	36.0%	0.135
HNOH	20.5%	0.068	N_2H_4	16.2%	0.057	N_2H_4	33.2%	0.134
Standard enthalpy of formation at 300 K ($\widetilde{ssn}_{ij}$ values instead of $\widetilde{sn}_{ij}$ values)								
O_2	85.1%	0.647	NH_2	87.6%	0.610	H	83.6%	0.576
NH_2	83.2%	0.531	NH_3	81.1%	0.558	NH_2	80.9%	0.647
NH_3	83.0%	0.573	H	77.6%	0.546	NH_3	68.1%	0.433
HO_2	73.1%	0.504	O_2	66.6%	0.430	H_2	56.3%	0.343
H	67.3%	0.438	H_2	59.9%	0.334	N_2H_3	45.9%	0.212
H_2	53.8%	0.325	HO_2	44.0%	0.316	O_2	44.4%	0.195
O	31.3%	0.148	O	32.9%	0.150	OH	38.3%	0.203
H_2NO	31.1%	0.085	N_2H_3	32.4%	0.136	H_2O	35.7%	0.131
N_2H_4	16.3%	0.050	H_2NO	29.0%	0.104	H_2NO	35.5%	0.189
HNOH	14.5%	0.053	OH	15.5%	0.105	O	29.1%	0.156
Standard molar entropy at 300 K								
O_2	87.8%	0.675	NH_2	89.6%	0.647	NH_2	82.5%	0.670
NH_2	85.9%	0.559	NH_3	82.3%	0.582	H	79.5%	0.376
NH_3	84.8%	0.587	O_2	72.8%	0.443	NH_3	68.0%	0.443
HO_2	79.5%	0.581	H	70.5%	0.396	H_2	51.3%	0.250
H	62.4%	0.330	H_2	55.4%	0.273	N_2H_3	49.3%	0.265
H_2	50.5%	0.278	HO_2	45.5%	0.348	O_2	44.4%	0.216
H_2NO	37.2%	0.103	H_2NO	36.2%	0.129	H_2NO	39.5%	0.223
O	32.4%	0.132	N_2H_3	36.1%	0.168	OH	37.8%	0.209
N_2H_4	21.6%	0.073	O	33.0%	0.136	H_2O	35.3%	0.132
HNOH	18.1%	0.067	OH	16.2%	0.110	HO_2	31.7%	0.127

[a]: Number of data points for which the thermodynamic property has $\lvert \widetilde{sn}_{ij} \rvert \geq 0.1$ or $\lvert \widetilde{ssn}_{ij} \rvert \geq 0.1$ divided (normalized) by the total number of data points.
[b]: Average of the $\lvert \widetilde{sn}_{ij} \rvert$ or $\lvert \widetilde{ssn}_{ij} \rvert$ values for all included data points for each thermodynamic property.

Table A13. Comparison of the overall sensitivity analysis results of thermodynamic data for the investigated concentration measurements in flow reactors in the case of NH_3/H_2 fuel mixtures (968 investigated data points). The 10-10 most sensitive species of the three investigated mechanisms are shown for each thermodynamic property separately.

POLIMI-2020			KAUST-2021			Shrestha-2021		
Species	**Freq.[a]**	$\overline{\lvert \widetilde{sn}_{ij} \rvert}$[b]	**Species**	**Freq.[a]**	$\overline{\lvert \widetilde{sn}_{ij} \rvert}$[b]	**Species**	**Freq.[a]**	$\overline{\lvert \widetilde{sn}_{ij} \rvert}$[b]
Standard isobar molar heat capacity at 300 K								
O_2	83.7%	0.483	O_2	92.9%	0.589	NH_3	76.5%	0.627
NH_2	73.9%	0.491	NH_3	89.9%	0.762	NH_2	75.8%	0.591
NH_3	71.0%	0.497	NH_2	88.8%	0.716	H	74.8%	0.451
H	70.2%	0.318	HO_2	88.1%	0.650	O_2	43.8%	0.235
HO_2	69.1%	0.382	H	56.8%	0.238	HO_2	33.5%	0.177
O	52.6%	0.194	H_2	31.8%	0.167	OH	20.6%	0.120
OH	44.6%	0.166	H_2NO	31.8%	0.152	H_2O	20.2%	0.114
H_2NO	42.0%	0.134	HNOH	31.7%	0.141	O	19.6%	0.088
HNOH	40.7%	0.137	O	26.7%	0.126	N_2O	18.0%	0.139
N_2H_2	22.3%	0.137	OH	20.9%	0.109	H_2	14.6%	0.072
Standard enthalpy of formation at 300 K ($\widetilde{ssn}_{ij}$ values instead of $\widetilde{sn}_{ij}$ values)								
O_2	78.7%	0.478	O_2	87.9%	0.644	H	71.9%	0.593
H	68.9%	0.420	NH_3	83.5%	0.690	NH_3	71.3%	0.538
NH_2	68.1%	0.443	NH_2	82.3%	0.655	NH_2	71.2%	0.509
NH_3	63.8%	0.418	HO_2	80.9%	0.571	O_2	42.5%	0.244
HO_2	60.7%	0.307	H	61.9%	0.321	HO_2	28.5%	0.145
O	53.2%	0.249	H_2	32.6%	0.159	O	21.6%	0.124
OH	42.7%	0.158	O	30.2%	0.167	OH	19.4%	0.118
H_2NO	37.2%	0.110	H_2NO	28.9%	0.132	H_2O	18.6%	0.097
HNOH	36.5%	0.112	HNOH	27.4%	0.118	N_2O	17.0%	0.131
N_2H_2	21.8%	0.135	OH	20.4%	0.103	H_2	13.6%	0.063
Standard molar entropy at 300 K								
O_2	80.6%	0.526	O_2	91.8%	0.688	NH_3	73.7%	0.589
NH_2	69.9%	0.461	NH_3	87.3%	0.695	NH_2	73.0%	0.563
HO_2	67.4%	0.376	HO_2	86.6%	0.672	H	71.3%	0.409
NH_3	65.9%	0.434	NH_2	86.1%	0.663	O_2	44.4%	0.274
H	65.0%	0.275	H	54.3%	0.229	HO_2	33.0%	0.186
O	54.5%	0.225	H_2NO	33.8%	0.154	O	21.5%	0.104
OH	43.6%	0.162	HNOH	31.7%	0.140	OH	20.1%	0.120
H_2NO	41.6%	0.133	O	29.9%	0.150	H_2O	19.9%	0.107
HNOH	40.8%	0.140	H_2	28.9%	0.137	N_2O	17.6%	0.137
N_2H_2	22.8%	0.139	OH	21.0%	0.108	NO	13.9%	0.068

[a]: Number of data points for which the thermodynamic property has $\lvert \widetilde{sn}_{ij} \rvert \geq 0.1$ or $\lvert \widetilde{ssn}_{ij} \rvert \geq 0.1$ divided (normalized) by the total number of data points.
[b]: Average of the $\lvert \widetilde{sn}_{ij} \rvert$ or $\lvert \widetilde{ssn}_{ij} \rvert$ values for all included data points for each thermodynamic property.

References

[1] O. Elishav, B. Mosevitzky Lis, E. M. Miller, D. J. Arent, A. Valera-Medina, A. Grinberg Dana, G. E. Shter, G. S. Grader, Progress and Prospective of Nitrogen-Based Alternative Fuels, *Chem. Rev.* 120 (2020) 5352−5436. (URL: https://doi.org/10.1021/acs.chemrev.9b00538)

[2] A. Valera-Medina, H. Xiao, M. Owen-Jones, W. I. F. David, P. J. Bowen, Ammonia for power, *Prog. Energy Combust. Sci.* 69 (2018) 63–102. (URL: https://doi.org/10.1016/j.pecs.2018.07.001)

[3] C. Zamfirescu, I. Dincer, Ammonia as a green fuel and hydrogen source for vehicular applications, *Fuel Process. Technol.* 90 (2009) 729–737. (URL: https://doi.org/10.1016/j.fuproc.2009.02.004)

[4] C. Zamfirescu, I. Dincer, Using ammonia as a sustainable fuel, *J. Power Sources* 185 (2008) 459–465. (URL: https://doi.org/10.1016/j.jpowsour.2008.02.097)

[5] E. Morgan, J. Manwell, J. Mcgowan, Wind-powered ammonia fuel production for remote islands: A case study, *Renewable Energy* 72 (2014) 51–61. (URL: https://doi.org/10.1016/j.renene.2014.06.034)

[6] H. Kobayashi, A. Hayakawa, A. Somarathne, Kunkuma, K.D., C. Okafor, Ekenechukwu, Science and technology of ammonia combustion, *Proc. Combust. Inst.* 37 (2019) 109−133. (URL: https://doi.org/10.1016/j.proci.2018.09.029)

[7] National Institute of Standard and Technology (NIST), NIST Chemistry WebBook, SRD 69, Thermophysical Properties of Fluid Systems (2022), available at https://webbook.nist.gov/chemistry/fluid/ (accessed 2022/02/02)

[8] K. Takizawa, A. Takahashi, K. Tokuhashi, S. Kondo, A. Sekiya, Burning velocity measurements of nitrogen-containing compounds, *J. Hazard. Mater.* 155 (2008) 144–152. (URL: https://doi.org/10.1016/j.jhazmat.2007.11.089)

[9] F. J. Verkamp, M. C. Hardin, J. R. Williams, Ammonia combustion properties and performance in gas-turbine burners, *Proc. Combust. Inst.* 11 (1967) 985–992. (URL: https://doi.org/10.1016/S0082-0784(67)80225-X)

[10] P. Kumar, T. R. Meyer, Experimental and modeling study of chemical-kinetics mechanisms for H_2–NH_3–air mixtures in laminar premixed jet flames, *Fuel* 108 (2013) 166–176. (URL: https://doi.org/10.1016/j.fuel.2012.06.103)

[11] J. Li, H. Huang, N. Kobayashi, Z. He, Y. Nagai, Study on using hydrogen and ammonia as fuels: Combustion characteristics and NO_x formation, *Int. J. Energ. Res.* 38 (2014) 1214–1223. (URL: https://doi.org/10.1002/er.3141)

[12] A. Ichikawa, A. Hayakawa, Y. Kitagawa, K. D. Kunkuma Amila Somarathne, T. Kudo, H. Kobayashi, Laminar burning velocity and Markstein length of ammonia/hydrogen/air premixed flames at elevated pressures, *Int. J. Hydrog. Energy* 40 (2015) 9570–9578. (URL: https://doi.org/10.1016/j.ijhydene.2015.04.024)

[13] A. Valera-Medina, S. Morris, J. Runyon, D. G. Pugh, R. Marsh, P. Beasley, T. Hughes, Ammonia, Methane and Hydrogen for Gas Turbines, *Energy Procedia* 75 (2015) 118–123. (URL: https://doi.org/10.1016/j.egypro.2015.07.205)

[14] X. Han, Z. Wang, M. Costa, Z. Sun, Y. He, K. Cen, Experimental and kinetic modeling study of laminar burning velocities of NH_3/air, NH_3/H_2/air, NH_3/CO/air and

NH_3/CH_4/air premixed flames, *Combust. Flame* 206 (2019) 214–226. (URL: https://doi.org/10.1016/j.combustflame.2019.05.003)

[15] S. Wang, Z. Wang, A. M. Elbaz, X. Han, Y. He, M. Costa, A. A. Konnov, W. L. Roberts, Experimental study and kinetic analysis of the laminar burning velocity of NH_3/syngas/air, NH_3/CO/air and NH_3/H_2/air premixed flames at elevated pressures, *Combust. Flame* 221 (2020) 270–287. (URL: https://doi.org/10.1016/j.combustflame.2020.08.004)

[16] X. Han, Z. Wang, Y. He, Y. Zhu, K. Cen, Experimental and kinetic modeling study of laminar burning velocities of NH_3/syngas/air premixed flames, *Combust. Flame* 213 (2020) 1–13. (URL: https://doi.org/10.1016/j.combustflame.2019.11.032)

[17] B. Mei, S. Ma, Y. Zhang, X. Zhang, W. Li, Y. Li, Exploration on laminar flame propagation of ammonia and syngas mixtures up to 10 atm, *Combust. Flame* 220 (2020) 368–377. (URL: https://doi.org/10.1016/j.combustflame.2020.07.011)

[18] S. M. Grannell, D. N. Assanis, S. V. Bohac, D. E. Gillespie, The Fuel Mix Limits and Efficiency of a Stoichiometric, Ammonia, and Gasoline Dual Fueled Spark Ignition Engine, *Journal of Engineering for Gas Turbines and Power* 130 (2008) 042802 (042808 pages). (URL: https://doi.org/10.1115/1.2898837)

[19] A. J. Reiter, S.-C. Kong, Combustion and emissions characteristics of compression-ignition engine using dual ammonia-diesel fuel, *Fuel* 90 (2011) 87–97. (URL: https://doi.org/10.1016/j.fuel.2010.07.055)

[20] A. J. Reiter, S.-C. Kong, Demonstration of Compression-Ignition Engine Combustion Using Ammonia in Reducing Greenhouse Gas Emissions, *Energy Fuels* 22 (2008) 2963–2971. (URL: https://doi.org/10.1021/ef800140f)

[21] C. W. Gross, S.-C. Kong, Performance characteristics of a compression-ignition engine using direct-injection ammonia–DME mixtures, *Fuel* 103 (2013) 1069–1079. (URL: https://doi.org/10.1016/j.fuel.2012.08.026)

[22] K. P. Shrestha, B. R. Giri, A. M. Elbaz, G. Issayev, W. L. Roberts, L. Seidel, F. Mauss, A. Farooq, A detailed chemical insights into the kinetics of diethyl ether enhancing ammonia combustion and the importance of NO*x* recycling mechanism, *Fuel Communications* 10 (2022) 100051. (URL: https://doi.org/10.1016/j.jfueco.2022.100051)

[23] B. M. Jenkins, L. L. Baxter, T. R. Miles, T. R. Miles, Combustion properties of biomass, *Fuel Process. Technol.* 54 (1998) 17–46. (URL: https://doi.org/10.1016/S0378-3820(97)00059-3)

[24] J. Werther, M. Saenger, E.-U. Hartge, T. Ogada, Z. Siagi, Combustion of agricultural residues, *Prog. Energy Combust. Sci.* 26 (2000) 1–27. (URL: https://doi.org/10.1016/S0360-1285(99)00005-2)

[25] R. Zanzi, K. Sjöström, E. Björnbom, Rapid high-temperature pyrolysis of biomass in a free-fall reactor, *Fuel* 75 (1996) 545–550. (URL: https://doi.org/10.1016/0016-2361(95)00304-5)

[26] K. J. Whitty, H. R. Zhang, E. G. Eddings, Emissions from Syngas Combustion, *Combust. Sci. Technol.* 180 (2008) 1117–1136. (URL: https://doi.org/10.1080/00102200801963326)

[27] C. K. Westbrook, F. L. Dryer, Chemical kinetic modeling of hydrocarbon combustion, *Prog. Energy Combust. Sci.* 10 (1984) 1–57. (URL: https://doi.org/10.1016/0360-1285(84)90118-7)

[28] O. Kurata, N. Iki, T. Matsunuma, T. Inoue, T. Tsujimura, H. Furutani, H. Kobayashi, A. Hayakawa, Performances and emission characteristics of NH_3–air and NH_3–CH_4–air combustion gas-turbine power generations, *Proc. Combust. Inst.* 36 (2017) 3351–3359. (URL: https://doi.org/10.1016/j.proci.2016.07.088)

[29] C. Duynslaegher, F. Contino, J. Vandooren, H. Jeanmart, Modeling of ammonia combustion at low pressure, *Combust. Flame* 159 (2012) 2799–2805. (URL: http://dx.doi.org/10.1016/j.combustflame.2012.06.003)

[30] Y. Song, H. Hashemi, J. M. Christensen, C. Zou, P. Marshall, P. Glarborg, Ammonia oxidation at high pressure and intermediate temperatures, *Fuel* 181 (2016) 358–365. (URL: https://doi.org/10.1016/j.fuel.2016.04.100)

[31] H. Nakamura, S. Hasegawa, T. Tezuka, Kinetic modeling of ammonia/air weak flames in a micro flow reactor with a controlled temperature profile, *Combust. Flame* 185 (2017) 16–27. (URL: https://doi.org/10.1016/j.combustflame.2017.06.021)

[32] J. Otomo, M. Koshi, T. Mitsumori, H. Iwasaki, K. Yamada, Chemical kinetic modeling of ammonia oxidation with improved reaction mechanism for ammonia/air and ammonia/hydrogen/air combustion, *Int. J. Hydrog. Energy* 43 (2018) 3004–3014. (URL: https://doi.org/10.1016/j.ijhydene.2017.12.066)

[33] B. Mei, X. Zhang, S. Ma, M. Cui, H. Guo, Z. Cao, Y. Li, Experimental and kinetic modeling investigation on the laminar flame propagation of ammonia under oxygen enrichment and elevated pressure conditions, *Combust. Flame* 210 (2019) 236–246. (URL: https://doi.org/10.1016/j.combustflame.2019.08.033)

[34] A. Stagni, C. Cavallotti, S. Arunthanayothin, Y. Song, O. Herbinet, F. Battin-Leclerc, T. Faravelli, An experimental, theoretical and kinetic-modeling study of the gas-phase oxidation of ammonia, *React. Chem. Eng.* 5 (2020) 696–711. (URL: https://doi.org/10.1039/c9re00429g)

[35] X. Han, M. Lubrano Lavadera, A. A. Konnov, An experimental and kinetic modeling study on the laminar burning velocity of NH_3 + N_2O + air flames, *Combust. Flame* 228 (2021) 13–28. (URL: https://doi.org/10.1016/j.combustflame.2021.01.027)

[36] X. Zhang, S. P. Moosakutty, R. P. Rajan, M. Younes, S. M. Sarathy, Combustion chemistry of ammonia/hydrogen mixtures: Jet-stirred reactor measurements and comprehensive kinetic modeling, *Combust. Flame* 234 (2021) 111653. (URL: https://doi.org/10.1016/j.combustflame.2021.111653)

[37] G. J. Gotama, A. Hayakawa, E. C. Okafor, R. Kanoshima, M. Hayashi, T. Kudo, H. Kobayashi, Measurement of the laminar burning velocity and kinetics study of the importance of the hydrogen recovery mechanism of ammonia/hydrogen/air premixed flames, *Combust. Flame* 236 (2022) 111753. (URL: https://doi.org/10.1016/j.combustflame.2021.111753)

[38] O. Mathieu, E. L. Petersen, Experimental and modeling study on the high-temperature oxidation of Ammonia and related NO_x chemistry, *Combust. Flame* 162 (2015) 554–570. (URL: https://doi.org/10.1016/j.combustflame.2014.08.022)

[39] K. P. Shrestha, L. Seidel, T. Zeuch, F. Mauss, Detailed Kinetic Mechanism for the Oxidation of Ammonia Including the Formation and Reduction of Nitrogen Oxides,

Energy Fuels 32 (2018) 10202−10217. (URL: https://doi.org/10.1021/acs.energyfuels.8b01056)

[40] E. C. Okafor, Y. Naito, S. Colson, A. Ichikawa, T. Kudo, A. Hayakawa, H. Kobayashi, Measurement and modelling of the laminar burning velocity of methane-ammonia-air flames at high pressures using a reduced reaction mechanism, *Combust. Flame* 204 (2019) 162–175. (URL: https://doi.org/10.1016/j.combustflame.2019.03.008)

[41] K. P. Shrestha, C. Lhuillier, A. A. Barbosa, P. Brequigny, F. Contino, C. Mounaïm-Rousselle, L. Seidel, F. Mauss, An experimental and modeling study of ammonia with enriched oxygen content and ammonia/hydrogen laminar flame speed at elevated pressure and temperature, *Proc. Combust. Inst.* 38 (2021) 2163–2174. (URL: https://doi.org/10.1016/j.proci.2020.06.197)

[42] B. Mei, J. Zhang, X. Shi, Z. Xi, Y. Li, Enhancement of ammonia combustion with partial fuel cracking strategy: Laminar flame propagation and kinetic modeling investigation of $NH_3/H_2/N_2$/air mixtures up to 10 atm, *Combust. Flame* 231 (2021) 111472. (URL: https://doi.org/10.1016/j.combustflame.2021.111472)

[43] J. A. Miller, C. T. Bowman, Mechanism and modeling of nitrogen chemistry in combustion, *Prog. Energy Combust. Sci.* 15 (1989) 287–338. (URL: https://doi.org/10.1016/0360-1285(89)90017-8)

[44] P. Glarborg, J. A. Miller, B. Ruscic, S. J. Klippenstein, Modeling nitrogen chemistry in combustion, *Prog. Energy Combust. Sci.* 67 (2018) 31–68. (URL: https://doi.org/10.1016/j.pecs.2018.01.002)

[45] J. Miller, M. Branch, R. Kee, A chemical kinetic model for the selective reduction of nitric oxide by ammonia, *Combust. Flame* 43 (1981) 81–98. (URL: https://doi.org/10.1016/0010-2180(81)90008-0)

[46] T. Turányi, Chemical Kinetics Laboratory, ELTE, 2016. http://garfield.chem.elte.hu/ (accessed 19 May 2021)

[47] C. Olm, I. G. Zsély, R. Pálvölgyi, T. Varga, T. Nagy, H. J. Curran, T. Turányi, Comparison of the performance of several recent hydrogen combustion mechanisms, *Combust. Flame* 161 (2014) 2219–2234. (URL: https://doi.org/10.1016/j.combustflame.2014.03.006)

[48] T. Turányi, A. S. Tomlin, Analysis of Kinetic Reaction Mechanisms, Ed., *Springer–Verlag*, Berlin, Heidelberg, 2014. (ISBN: 978-3-662-44561-7)

[49] Y. Zhang, Z. Huang, L. Wei, J. Zhang, C. K. Law, Experimental and modeling study on ignition delays of lean mixtures of methane, hydrogen, oxygen, and argon at elevated pressures, *Combust. Flame* 159 (2012) 918–931. (URL: https://doi.org/10.1002/kin.20218)

[50] S. M. Burke, U. Burke, R. Mc Donagh, O. Mathieu, I. Osorio, C. Keesee, A. Morones, E. L. Petersen, W. Wang, T. A. DeVerter, M. A. Oehlschlaeger, B. Rhodes, R. K. Hanson, D. F. Davidson, B. W. Weber, C.-J. Sung, J. Santner, Y. Ju, F. M. Haas, F. L. Dryer, E. N. Volkov, E. J. K. Nilsson, A. A. Konnov, M. Alrefae, F. Khaled, A. Farooq, P. Dirrenberger, P.-A. Glaude, F. Battin-Leclerc, H. J. Curran, An experimental and modeling study of propene oxidation. Part 2: Ignition delay time and flame speed measurements, *Combust. Flame* 162 (2015) 296–314. (URL: https://doi.org/10.1016/j.combustflame.2014.07.032)

[51] F. Battin-Leclerc, J. M. Simmie, E. Blurock (Eds.), Cleaner Combustion – Developing Detailed Chemical Kinetic Models, Ed. 1, *Springer–Verlag*, London, UK, 2013. (ISBN: 978-1-4471-5306-1)

[52] X. He, B. Shu, D. Nascimento, K. Moshammer, M. Costa, R. X. Fernandes, Auto-ignition kinetics of ammonia and ammonia/hydrogen mixtures at intermediate temperatures and high pressures, *Combust. Flame* 206 (2019) 189–200. (URL: https://doi.org/10.1016/j.combustflame.2019.04.050)

[53] C. Ding, P. Li, K. Wang, G. Shi, F. Wang, Z. Liu, Experimental and Kinetic Study on the Oxidation of Syngas-Ammonia under Both N_2 and CO_2 Atmospheres in a Jet-Stirred Reactor, *Energy Fuels* 35 (2021) 11445–11456. (URL: https://doi.org/10.1021/acs.energyfuels.1c00647)

[54] F. Sen, B. Shu, T. Kasper, J. Herzler, O. Welz, M. Fikri, B. Atakan, C. Schulz, Shock-tube and plug-flow reactor study of the oxidation of fuel-rich CH_4/O_2 mixtures enhanced with additives, *Combust. Flame* 169 (2016) 307–320. (URL: https://doi.org/10.1016/j.combustflame.2016.03.030)

[55] T. Kick, J. Herbst, T. Kathrotia, J. Marquetand, M. Braun-Unkhoff, C. Naumann, U. Riedel, An experimental and modeling study of burning velocities of possible future synthetic jet fuels, *Energy* 43 (2012) 111–123. (URL: https://doi.org/10.1016/j.energy.2012.01.035)

[56] S. Hu, J. Gao, C. Gong, Y. Zhou, X. S. Bai, Z. S. Li, M. Alden, Assessment of uncertainties of laminar flame speed of premixed flames as determined using a Bunsen burner at varying pressures, *Applied Energy* 227 (2018) 149–158. (URL: https://doi.org/10.1016/j.apenergy.2017.09.083)

[57] R. Mével, F. Lafosse, N. Chaumeix, G. Dupré, C.-E. Paillard, Spherical expanding flames in H_2–N_2O–Ar mixtures: flame speed measurements and kinetic modeling, *Int. J. Hydrog. Energy* 34 (2009) 9007–9018. (URL: https://doi.org/10.1016/j.ijhydene.2009.08.054)

[58] S. P. M. Bane, R. Mével, S. A. Coronel, J. E. Shepherd, Flame burning speeds and combustion characteristics of undiluted and nitrogen-diluted hydrogen–nitrous oxide mixtures, *Int. J. Hydrog. Energy* 36 (2011) 10107–10116. (URL: https://doi.org/10.1016/j.ijhydene.2011.04.232)

[59] Lund University, Division of Combustion Physics, Combustion Chemistry Group, Counterflow burner rig, 2015. https://www.forbrf.lth.se/english/research/combustion-chemistry/facilities/counterflow-burner-rig/ (accessed 2021/04/01.)

[60] F. N. Egolfopoulos, P. Cho, C. K. Law, Laminar flame speeds of methane-air mixtures under reduced and elevated pressures, *Combust. Flame* 76 (1989) 375–391. (URL: https://doi.org/10.1016/0010-2180(89)90119-3)

[61] P. S. Veloo, Y. L. Wang, F. N. Egolfopoulos, C. K. Westbrook, A comparative experimental and computational study of methanol, ethanol, and *n*-butanol flames, *Combust. Flame* 157 (2010) 1989–2004. (URL: https://doi.org/10.1016/j.combustflame.2010.04.001)

[62] C. M. Vagelopoulos, F. N. Egolfopoulos, Direct experimental determination of laminar flame speeds, *Symposium (International) on Combustion* 27 (1998) 513–519. (URL: https://doi.org/10.1016/S0082-0784(98)80441-4)

[63] C. K. Wu, C. K. Law, On the determination of laminar flame speeds from stretched flames, *Proc. Combust. Inst.* 20 (1985) 1941–1949. (URL: https://doi.org/10.1016/S0082-0784(85)80693-7)

[64] G. T. Kim, N. I. Kim, Laminar burning velocity predictions by meso-scale flames in an annular diverging tube, *Fuel* 90 (2011) 2217–2223. (URL: https://doi.org/10.1016/j.fuel.2011.02.039)

[65] Z. Liu, N. I. Kim, An assembled annular stepwise diverging tube for the measurement of laminar burning velocity and quenching distance, *Combust. Flame* 161 (2014) 1499–1506. (URL: https://doi.org/10.1016/j.combustflame.2013.11.020)

[66] Z. Liu, M. J. Lee, N. I. Kim, Direct prediction of laminar burning velocity using an adapted annular stepwise diverging tube, *Proc. Combust. Inst.* 34 (2013) 755–762. (URL: https://doi.org/10.1016/j.proci.2012.06.080)

[67] L. P. H. De Goey, A. Van Maaren, R. M. Quax, Stabilization of Adiabatic Premixed Laminar Flames on a Flat Flame Burner, *Combust. Sci. Technol.* 92 (1993) 201–207. (URL: https://doi.org/10.1080/00102209308907668)

[68] K. Bosschaart, L. P. H. De Goey, Detailed analysis of the heat flux method for measuring burning velocities, *Combust. Flame* 132 (2003) 170−180. (URL: https://doi.org/10.1016/S0010-2180(02)00433-9)

[69] M. Akram, S. Minaev, S. Kumar, Investigations on the Formation of Planar Flames in Mesoscale Divergent Channels and Prediction of Burning Velocity at High Temperatures, *Combust. Sci. Technol.* 185 (2013) 645–660. (URL: https://doi.org/10.1080/00102202.2012.739224)

[70] R. J. Varghese, H. Kolekar, V. Hariharan, S. Kumar, Effect of CO content on laminar burning velocities of syngas-air premixed flames at elevated temperatures, *Fuel* 214 (2018) 144–153. (URL: https://doi.org/10.1016/j.fuel.2017.10.131)

[71] A. A. Konnov, A. Mohammad, V. R. Kishore, N. I. Kim, C. Prathap, S. Kumar, A comprehensive review of measurements and data analysis of laminar burning velocities for various fuel+air mixtures, *Prog. Energy Combust. Sci.* 68 (2018) 197–267. (URL: https://doi.org/10.1016/j.pecs.2018.05.003)

[72] F. N. Egolfopoulos, N. Hansen, Y. Ju, K. Kohse-Höinghaus, C. K. Law, F. Qi, Advances and challenges in laminar flame experiments and implications for combustion chemistry, *Prog. Energy Combust. Sci.* 43 (2014) 36–67. (URL: https://doi.org/10.1016/j.pecs.2014.04.004)

[73] J. P. Botha, D. B. Spalding, The laminar flame speed of propane/air mixtures with heat extraction from the flame, *Proc. R. Soc. London, Ser. A* 225 (1954) 71–96. (URL: https://doi.org/10.1098/rspa.1954.0188)

[74] M. Frenklach, PrlMe (for Process Informatics Model), http://primekinetics.org:8080/#/ (accessed 20 May 2021)

[75] ELKH-ELTE Complex Chemical Systems Research Group, ReSpecTh information system, 2014. https://respecth.hu/ (accessed 19 May 2021)

[76] ELKH-ELTE Research Group on Complex Chemical Systems, 2013. http://kkrk.chem.elte.hu/kkrk/ (accessed 20/05/2021)

[77] Laboratory of Molecular Structure and Dynamics, 2012. http://kkrk.chem.elte.hu/lmsd/ (accessed 20/05/2021)

[78] T. Varga, C. Olm, M. Papp, Á. Busai, I. G. Zsély, ReSpecTh Kinetics Data Format Specification v2.3, Eötvös Loránd University (ELTE), Institute of Chemistry, Chemical Kinetics Laboratory, 2020. http://respecth.chem.elte.hu/respecth/reac/ReSpecTh_Kinetics_Data_Format_Specification_v2.3.pdf (accessed 7 April 2020)

[79] M. Papp, T. Varga, Á. Busai, I. G. Zsély, T. Nagy, T. Turányi, Computer programs for the analysis, optimization and reduction of reaction mechanisms – Optima++, http://respecth.chem.elte.hu/respecth/reac/compProgs.php (accessed 25/05/2021)

[80] B. Shu, S. K. Vallabhuni, X. He, G. Issayev, K. Moshammer, A. Farooq, R. X. Fernandes, A shock tube and modeling study on the autoignition properties of ammonia at intermediate temperatures, *Proc. Combust. Inst.* 37 (2019) 205–211. (URL: https://doi.org/10.1016/j.proci.2018.07.074)

[81] T. Hulgaard, K. Dam-Johansen, Homogeneous nitrous oxide formation and destruction under combustion conditions, *AIChE J.* 39 (1993) 1342–1354. (URL: https://doi.org/10.1002/aic.690390811)

[82] V. J. Wargadalam, G. Löffler, F. Winter, H. Hofbauer, Homogeneous formation of NO and N_2O from the oxidation of HCN and NH_3 at 600–1000 °C, *Combust. Flame* 120 (2000) 465–478. (URL: https://doi.org/10.1016/S0010-2180(99)00107-8)

[83] J. A. Caton, J. K. Narney, H. C. Cariappa, W. R. Laster, The selective non-catalytic reduction of nitric oxide using ammonia at up to 15% oxygen, *Can. J. Chem. Eng.* 73 (1995) 345–350. (URL: https://doi.org/10.1002/cjce.5450730311)

[84] L. Kawka, G. Juhász, M. Papp, T. Nagy, I. G. Zsély, T. Turányi, Comparison of detailed reaction mechanisms for homogeneous ammonia combustion, *Z. Phys. Chem.* 234 (2020) 1329–1357. (URL: https://doi.org/10.1515/zpch-2020-1649)

[85] D. F. Davidson, K. Kohse-Höinghaus, A. Y. Chang, R. K. Hanson, A pyrolysis mechanism for ammonia, *Int. J. Chem. Kinet.* 22 (1990) 513–535. (URL: https://doi.org/10.1002/kin.550220508)

[86] J. Chen, X. Jiang, X. Qin, Z. Huang, Effect of hydrogen blending on the high temperature auto-ignition of ammonia at elevated pressure, *Fuel* 287 (2021) 119563. (URL: https://doi.org/10.1016/j.fuel.2020.119563)

[87] M. Pochet, V. Dias, B. Moreau, F. Foucher, H. Jeanmart, F. Contino, Experimental and numerical study, under LTC conditions, of ammonia ignition delay with and without hydrogen addition, *Proc. Combust. Inst.* 37 (2019) 621–629. (URL: https://doi.org/10.1016/j.proci.2018.05.138)

[88] L. Dai, S. Gersen, P. Glarborg, H. Levinsky, A. Mokhov, Experimental and numerical analysis of the autoignition behavior of NH_3 and NH_3/H_2 mixtures at high pressure, *Combust. Flame* 215 (2020) 134–144. (URL: https://doi.org/10.1016/j.combustflame.2020.01.023)

[89] P. Dagaut, On the Oxidation of Ammonia and Mutual Sensitization of the Oxidation of No and Ammonia: Experimental and Kinetic Modeling, *Combust. Sci. Technol.* 0 (2019) 1–13. (URL: https://doi.org/10.1080/00102202.2019.1678380)

[90] P. Sabia, M. V. Manna, A. Cavaliere, R. Ragucci, M. De Joannon, Ammonia oxidation features in a Jet Stirred Flow Reactor. The role of NH_2 chemistry., *Fuel* 276 (2020) 118054. (URL: https://doi.org/10.1016/j.fuel.2020.118054)

[91] M. V. Manna, P. Sabia, R. Ragucci, M. De Joannon, Oxidation and pyrolysis of ammonia mixtures in model reactors, *Fuel* 264 (2020) 116768. (URL: https://doi.org/10.1016/j.fuel.2019.116768)

[92] K. N. Osipova, X. Zhang, S. M. Sarathy, O. P. Korobeinichev, A. G. Shmakov, Ammonia and ammonia/hydrogen blends oxidation in a jet-stirred reactor: Experimental and numerical study, *Fuel* 310 (2022) 122202. (URL: https://doi.org/10.1016/j.fuel.2021.122202)

[93] A. M. Dean, J. E. Hardy, R. K. Lyon, Kinetics and mechanism of NH_3 oxidation, *Symposium (International) on Combustion* 19 (1982) 97–105. (URL: https://doi.org/10.1016/S0082-0784(82)80182-3)

[94] M. Abián, M. Benés, A. D. Goñi, B. Muñoz, M. U. Alzueta, Study of the oxidation of ammonia in a flow reactor. Experiments and kinetic modeling simulation, *Fuel* 300 (2021) 120979. (URL: https://doi.org/10.1016/j.fuel.2021.120979)

[95] J. H. Lee, S. I. Lee, O. C. Kwon, Effects of ammonia substitution on hydrogen/air flame propagation and emissions, *Int. J. Hydrog. Energy* 35 (2010) 11332–11341. (URL: https://doi.org/10.1016/j.ijhydene.2010.07.104)

[96] J. H. Lee, J. H. Kim, J. H. Park, O. C. Kwon, Studies on properties of laminar premixed hydrogen-added ammonia/air flames for hydrogen production, *Int. J. Hydrog. Energy* 35 (2010) 1054–1064. (URL: https://doi.org/10.1016/j.ijhydene.2009.11.071)

[97] A. Hayakawa, T. Goto, R. Mimoto, Y. Arakawa, T. Kudo, H. Kobayashi, Laminar burning velocity and Markstein length of ammonia/air premixed flames at various pressures, *Fuel* 159 (2015) 98–106. (URL: https://doi.org/10.1016/j.fuel.2015.06.070)

[98] H. Takeishi, J. Hayashi, S. Kono, W. Arita, K. Iino, F. Akamatsu, Characteristics of ammonia/N_2/O_2 laminar flame in oxygen-enriched air condition, *Transactions of the JSME (in Japanese)* 81 (2015) 414-–423. (URL: https://doi.org/10.1299/transjsme.14-00423)

[99] Q. Liu, X. Chen, J. Huang, Y. Shen, Y. Zhang, Z. Liu, The characteristics of flame propagation in ammonia/oxygen mixtures, *J. Hazard. Mater.* 363 (2019) 187–196. (URL: https://doi.org/10.1016/j.jhazmat.2018.09.073)

[100] D. Wang, C. Ji, Z. Wang, S. Wang, T. Zhang, J. Yang, Measurement of oxy-ammonia laminar burning velocity at normal and elevated temperatures, *Fuel* 279 (2020) 118425. (URL: https://doi.org/10.1016/j.fuel.2020.118425)

[101] C. Lhuillier, P. Brequigny, N. Lamoureux, F. Contino, C. Mounaïm-Rousselle, Experimental investigation on laminar burning velocities of ammonia/hydrogen/air mixtures at elevated temperatures, *Fuel* 263 (2020) 116653. (URL: https://doi.org/10.1016/j.fuel.2019.116653)

[102] N. Wang, S. Huang, Z. Zhang, T. Li, P. Yi, D. Wu, G. Chen, Laminar burning characteristics of ammonia/hydrogen/air mixtures with laser ignition, *Int. J. Hydrog. Energy* 46 (2021) 31879–31893. (URL: https://doi.org/10.1016/j.ijhydene.2021.07.063)

[103] K. N. Osipova, O. P. Korobeinichev, A. G. Shmakov, Chemical structure and laminar burning velocity of atmospheric pressure premixed ammonia/hydrogen flames, *Int. J. Hydrog. Energy* 46 (2021) 39942–39954. (URL: https://doi.org/10.1016/j.ijhydene.2021.09.188)

[104] J. Bian, J. Vandooren, P. J. Van Tiggelen, Experimental study of the formation of nitrous and nitric oxides in H_2−O_2−Ar flames seeded with NO and/or NH_3, *Symposium (International) on Combustion* 23 (1991) 379–386. (URL: https://doi.org/10.1016/S0082-0784(06)80282-1)

[105] J. Vandooren, Comparison of the Experimental Structure of an Ammonia Seeded Rich-Hydrogen-Oxygen-Argon Flame with the Calculated Ones Along Several Reaction Mechanisms, *Combust. Sci. Technol.* 84 (1992) 335-344. (URL: https://doi.org/10.1080/00102209208951861)

[106] C. Duynslaegher, H. Jeanmart, J. Vandooren, Flame structure studies of premixed ammonia/hydrogen/oxygen/argon flames: Experimental and numerical investigation, *Proc. Combust. Inst.* 32 (2009) 1277-1284. (URL: https://doi.org/10.1016/j.proci.2008.06.036)

[107] S. Zhou, W. Yang, H. Tan, Q. An, J. Wang, H. Dai, X. Wang, X. Wang, S. Deng, Experimental and kinetic modeling study on NH_3/syngas/air and NH_3/bio-syngas/air premixed laminar flames at elevated temperature, *Combust. Flame* 233 (2021) 111594. (URL: https://doi.org/10.1016/j.combustflame.2021.111594)

[108] G. Yin, C. Wang, M. Zhou, Y. Zhou, E. Hu, Z. Huang, Experimental and kinetic study on laminar flame speeds of ammonia/syngas/air at a high temperature and elevated pressure, *Front. Energ.* (2021) (URL: https://doi.org/10.1007/s11708-021-0791-7)

[109] N. Fujii, H. Miyama, M. Koshi, T. Asaba, Kinetics of ammonia oxidation in shock waves, *Proc. Combust. Inst.* 18 (1981) 873–883. (URL: https://doi.org/10.1016/S0082-0784(81)80091-4)

[110] J. E. Dove, W. S. Nip, A shock-tube study of ammonia pyrolysis, *Can. J. Chem.* 57 (1979) 689–701. (URL: https://doi.org/10.1139/v79-112)

[111] L. J. Drummond, High temperature oxidation of ammonia, *Combust. Sci. Technol.* 5 (1972) 175–182. (URL: https://doi.org/10.1080/00102207208952518)

[112] D. C. Bull, A shock tube study of the oxidation of ammonia, *Combust. Flame* 12 (1968) 603–610. (URL: https://doi.org/10.1016/0010-2180(68)90079-5)

[113] J. N. Bradley, R. N. Butlin, D. Lewis, Oxidation of ammonia in shock waves, *Trans. Faraday Soc.* 64 (1968) 71–78. (URL: http://dx.doi.org/10.1039/TF9686400071)

[114] H. Miyama, Kinetic Studies of Ammonia Oxidation in Shock Waves. IV. Comparison of Induction Periods for the Ignition of NH_3-O_2-N_2 with Those for NH_3-O_2-Ar Mixtures, *Bull. Chem. Soc. Jpn.* 41 (1968) 1761–1765. (URL: https://doi.org/10.1246/bcsj.41.1761)

[115] H. Miyama, Ignition of Ammonia–Oxygen Mixtures by Shock Waves, *J. Chem. Phys.* 48 (1968) 1421–1422. (URL: https://doi.org/10.1063/1.1668832)

[116] H. Miyama, R. Endoh, Ignition of ammonia-air mixtures by reflected shock waves, *Combust. Flame* 11 (1967) 359–360. (URL: https://doi.org/10.1016/0010-2180(67)90027-2)

[117] H. Miyama, R. Endoh, Vibrational Relaxation of Nitrogen in Shock-Heated NH_3–O_2–N_2 Mixtures, *J. Chem. Phys.* 46 (1967) 2011–2012. (URL: https://doi.org/10.1063/1.1840982)

[118] T. Takeyama, H. Miyama, A shock-tube study of the ammonia-oxygen reaction, *Symposium (International) on Combustion* 11 (1967) 845–852. (URL: https://doi.org/10.1016/S0082-0784(67)80210-8)

[119] T. Takeyama, H. Miyama, Kinetic Studies of Ammonia Oxidation in Shock Waves. I. The Reaction Mechanism for the Induction Period, *Bull. Chem. Soc. Jpn.* 38 (1965) 1670–1674. (URL: https://doi.org/10.1246/bcsj.38.1670)

[120] T. Takeyama, H. Miyama, Reaction Mechanism of Ammonia Oxidation in Shock Waves, *J. Chem. Phys.* 42 (1965) 3737–3738. (URL: https://doi.org/10.1063/1.1695800)

[121] O. Mathieu, M. M. Kopp, E. L. Petersen, Shock-tube study of the ignition of multi-component syngas mixtures with and without ammonia impurities, *Proc. Combust. Inst.* 34 (2013) 3211–3218. (URL: https://doi.org/10.1016/j.proci.2012.05.008)

[122] H. Nakamura, S. Hasegawa, Combustion and ignition characteristics of ammonia/air mixtures in a micro flow reactor with a controlled temperature profile, *Proc. Combust. Inst.* 36 (2017) 4217–4226. (URL: https://doi.org/10.1016/j.proci.2016.06.153)

[123] T. Jabbour, D. F. Clodic, Burning Velocity and Refrigerant Flammability Classification, *ASHRAE Tran.* 110 (2004) 522–533.

[124] U. J. Pfahl, M. C. Ross, J. E. Shepherd, K. O. Pasamehmetoglu, C. Unal, Flammability limits, ignition energy, and flame speeds in H_2–CH_4–NH_3–N_2O–O_2–N_2 mixtures, *Combust. Flame* 123 (2000) 140–158. (URL: https://doi.org/10.1016/S0010-2180(00)00152-8)

[125] P. D. Ronney, Effect of Chemistry and Transport Properties on Near-Limit Flames at Microgravity, *Combust. Sci. Technol.* 59 (1988) 123–141. (URL: https://doi.org/10.1080/00102208808947092)

[126] V. F. Zakaznov, L. A. Kursheva, Z. I. Fedina, Determination of normal flame velocity and critical diameter of flame extinction in ammonia-air mixture, *Combust. Explos. Shock Waves* 14 (1978) 710–713. (URL: https://doi.org/10.1007/BF00786097)

[127] S. G. Davis, J. L. Pagliaro, T. F. Debold, M. Van Wingerden, K. Van Wingerden, Flammability and explosion characteristics of mildly flammable refrigerants, *Journal of Loss Prevention in the Process Industries* 49 (2017) 662–674. (URL: https://doi.org/10.1016/j.jlp.2017.05.019)

[128] A. G. Shmakov, O. P. Korobeinichev, I. V. Rybitskaya, A. A. Chernov, D. A. Knyazkov, T. A. Bolshova, A. A. Konnov, Formation and consumption of NO in H_2+O_2+N_2 flames doped with NO or NH_3 at atmospheric pressure, *Combust. Flame* 157 (2010) 556–565. (URL: https://doi.org/10.1016/j.combustflame.2009.10.008)

[129] C. Brackmann, V. A. Alekseev, B. Zhou, E. Nordström, P.-E. Bengtsson, Z. Li, M. Aldén, A. A. Konnov, Structure of premixed ammonia + air flames at atmospheric pressure: Laser diagnostics and kinetic modeling, *Combust. Flame* 163 (2016) 370–381. (URL: https://doi.org/10.1016/j.combustflame.2015.10.012)

[130] J. Bian, J. Vandooren, P. J. Van Tiggelen, Experimental study of the structure of an ammonia-oxygen flame, *Symposium (International) on Combustion* 21 (1988) 953–963. (URL: https://doi.org/10.1016/S0082-0784(88)80327-8)

[131] C. J. Dasch, R. J. Blint, A Mechanistic and Experimental Study of Ammonia Flames, *Combust. Sci. Technol.* 41 (1984) 223–244. (URL: https://doi.org/10.1080/00102208408923833)

[132] R. J. Blint, C. J. Dasch, Formation of NO and N_2 from NH_3 in Flames, The Chemistry of Combustion Processes1983, pp. 87–101.

[133] R. J. Kee, F. M. Rupley, J. A. Miller, M. E. Coltrin, J. F. Grcar, E. Meeks, H. K. Moffat, A. E. Lutz, G. Dixon-Lewis, M. D. Smooke, J. Warnatz, G. H. Evans, R. S. Larson, R. E. Mitchell, L. R. Petzold, W. C. Reynolds, M. Caracotsios, W. E. Stewart, P. Glarborg, C. Wang, C. L. McLellan, O. Adigun, W. G. H. C. P. Chou, S. F. Miller, P. Ho, P. D. Young, D. J. Young, CHEMKIN Release 4.0.2: Theory Manual, *Reaction Design*, San Diego, CA, 2005.

[134] R. J. Kee, F. M. Rupley, J. A. Miller, M. E. Coltrin, J. F. Grcar, E. Meeks, H. K. M. A. E. Lutz, G. Dixon-Lewis, M. D. Smooke, J. Warnatz, G. H. Evans, R. S. Larson, R. E. Mitchell, L. R. Petzold, W. C. Reynolds, M. Caracotsios, W. E. Stewart, P. Glarborg, C. Wang, C. L. McLellan, O. Adigun, W. G. Houf, C. P. Chou, S. F. Miller, P. Ho, P. D. Young, D. J. Young, CHEMKIN Release 4.0.2: Input Manual, *Reaction Design*, San Diego, CA, 2005.

[135] ANSYS, Chemkin Theory Manual 17.0 (15151), *Reaction Design*, San Diego, CA, 2015. (URL: https://personal.ems.psu.edu/~radovic/ChemKin_Theory_PaSR.pdf, accessed 2022/02/03)

[136] S. Gordon, B. J. McBride, Computer program for calculation of complex chemical equilibrium compositions, rocket performance, incident and reflected shocks and Chapman-Jouguet detonations (NASA-SP-273), *NASA Lewis Research Center*, Cleveland, Ohio, 1971. (URL: https://www1.grc.nasa.gov/research-and-engineering/ceaweb/publications/, accessed 2022/03/22)

[137] S. Gordon, B. J. McBride, Computer program for calculation of complex chemical equilibrium compositions and applications. Part 1: Analysis (NASA-RP-1311), *NASA Lewis Research Center*, Cleveland, Ohio, 1994. (URL: https://ntrs.nasa.gov/citations/19950013764, accessed 2022/02/03)

[138] E. Keszei, Chemical Thermodynamics – An Introduction, Ed. 1, *Springer–Verlag*, Berlin, Heidelberg, 2012. (ISBN: 978-3-642-19863-2)

[139] F. A. Lindemann, S. Arrhenius, I. Langmuir, N. R. Dhar, J. Perrin, W. C. Mcc. Lewis, Discussion on "the radiation theory of chemical action", *Trans. Faraday Soc.* 17 (1922) 598–606. (URL: https://doi.org/10.1039/TF9221700598)

[140] J. Troe, Theory of Thermal Unimolecular Reactions in the Fall-off Range. I. Strong Collision Rate Constants, *Ber. Bunsenges. Phys. Chem.* 87 (1983) 161–169. (URL: https://doi.org/10.1002/bbpc.19830870217)

[141] R. G. Gilbert, K. Luther, J. Troe, Theory of Thermal Unimolecular Reactions in the Fall-off Range. II. Weak Collision Rate Constants, *Ber. Bunsenges. Phys. Chem.* 87 (1983) 169–177. (URL: https://doi.org/10.1002/bbpc.19830870218)

[142] P. H. Stewart, C. W. Larson, D. M. Golden, Pressure and temperature dependence of reactions proceeding via a bound complex. 2. Application to $2\,CH_3 \rightarrow C_2H_5 + H$, *Combust. Flame* 75 (1989) 25–31. (URL: https://doi.org/10.1016/0010-2180(89)90084-9)

[143] J. Zádor, C. A. Taatjes, R. X. Fernandes, Kinetics of elementary reactions in low-temperature autoignition chemistry, *Prog. Energy Combust. Sci.* 37 (2011) 371–421. (URL: https://doi.org/10.1016/j.pecs.2010.06.006)

[144] T. J. Rivlin, Chebyshev Polynomials: From Approximation Theory to Algebra and Number Theory, Ed. 2, *Wiley-Interscience*, New York, USA, 1990. (ISBN: 9780471628965)

[145] P. K. Venkatesh, A. Y. Chang, A. M. Dean, M. H. Cohen, R. W. Carr, Parameterization of pressure- and temperature-dependent kinetics in multiple well reactions, *AIChE J.* 43 (1997) 1331–1340. (URL: https://doi.org/10.1002/aic.690430522)

[146] Z. Tian, Y. Li, L. Zhang, P. Glarborg, F. Qi, An experimental and kinetic modeling study of premixed $NH_3/CH_4/O_2$/Ar flames at low pressure, *Combust. Flame* 156 (2009) 1413–1426. (URL: https://doi.org/10.1016/j.combustflame.2009.03.005)

[147] N. Lamoureux, H. E. Merhubi, L. Pillier, S. De Persis, P. Desgroux, Modeling of NO formation in low pressure premixed flames, *Combust. Flame* 163 (2016) 557−575. (URL: https://doi.org/10.1016/j.combustflame.2015.11.007)

[148] Mechanical and Aerospace Engineering (Combustion Research), University of California at San Diego, Chemical-Kinetic Mechanisms for Combustion Applications, San Diego Mechanism web page, 2012. http://web.eng.ucsd.edu/mae/groups/combustion/mechanism.html (accessed 2021/04/04.)

[149] E. C. Okafor, Y. Naito, S. Colson, A. Ichikawa, T. Kudo, A. Hayakawa, H. Kobayashi, Experimental and numerical study of the laminar burning velocity of CH_4–NH_3–air premixed flames, *Combust. Flame* 187 (2018) 185–198. (URL: https://doi.org/10.1016/j.combustflame.2017.09.002)

[150] M. Kovács, M. Papp, I. G. Zsély, T. Turányi, Determination of rate parameters of key N/H/O elementary reactions based on $H_2/O_2/NO_x$ combustion experiments, *Fuel* 264 (2020) 116720. (URL: https://doi.org/10.1016/j.fuel.2019.116720)

[151] The CRECK Modeling Group (Politecnico di Milano), NH_3 mechanism (Version 2003, March 2020), 2020. http://creckmodeling.chem.polimi.it/menu-kinetics/menu-kinetics-special-mechanisms/menu-kinetics-nh3-mechanism (accessed 2022/01/01)

[152] Q.-D. Wang, Y. Sun, H. J. Curran, Comparative Chemical Kinetic Analysis and Skeletal Mechanism Generation for Syngas Combustion with NOx Chemistry, *Energy Fuels* 34 (2020) 949−964. (URL: https://doi.org/10.1021/acs.energyfuels.9b03440)

[153] M. L. Lavadera, A. A. Konnov, Laminar burning velocities of methane + formic acid + air flames: Experimental and modeling study, *Combust. Flame* 225 (2021) 65–73. (URL: https://doi.org/10.1016/j.combustflame.2020.10.050)

[154] A. Kéromnès, W. K. Metcalfe, K. A. Heufer, N. Donohoe, A. K. Das, C.-J. Sung, J. Herzler, C. Naumann, P. Griebel, O. Mathieu, M. C. Krejci, E. L. Petersen, W. J. Pitz, H. J. Curran, An experimental and detailed chemical kinetic modeling study of hydrogen and syngas mixture oxidation at elevated pressures, *Combust. Flame* 160 (2013) 995–1011. (URL: https://doi.org/10.1016/j.combustflame.2013.01.001)

[155] T. Varga, C. Olm, T. Nagy, I. G. Zsély, É. Valkó, R. Pálvölgyi, H. J. Curran, T. Turányi, Development of a Joint Hydrogen and Syngas Combustion Mechanism Based on an Optimization Approach, *Int. J. Chem. Kinet.* 48 (2016) 407–422. (URL: https://doi.org/10.1002/kin.21006)

[156] T. Mendiara, P. Glarborg, Ammonia chemistry in oxy-fuel combustion of methane, *Combust. Flame* 156 (2009) 1937–1949. (URL: https://doi.org/10.1016/j.combustflame.2009.07.006)

[157] R. Mével, S. Javoy, F. Lafosse, N. Chaumeix, G. Dupré, C.-E. Paillard, Hydrogen–nitrous oxide delay times: Shock tube experimental study and kinetic modelling, *Proc. Combust. Inst.* 32 (2009) 359–366. (URL: https://doi.org/10.1016/j.proci.2008.06.171)

[158] S. J. Klippenstein, L. B. Harding, P. Glarborg, J. A. Miller, The role of NNH in NO formation and control, *Combust. Flame* 158 (2011) 774–789. (URL: https://doi.org/10.1016/j.combustflame.2010.12.013)

[159] M. Abian, M. U. Alzueta, P. Glarborg, Formation of NO from N_2/O_2 Mixtures in a Flow Reactor: Toward an Accurate Prediction of Thermal NO, *Int. J. Chem. Kinet.* 47 (2015) 518–532. (URL: https://doi.org/10.1002/kin.20929)

[160] Y. Zhang, O. Mathieu, E. L. Petersen, G. Bourque, H. J. Curran, Assessing the predictions of a NO_x kinetic mechanism on recent hydrogen and syngas experimental data, *Combust. Flame* 182 (2017) 122–141. (URL: https://doi.org/10.1016/j.combustflame.2017.03.019)

[161] S. J. Klippenstein, M. Pfeifle, A. W. Jasper, P. Glarborg, Theory and modeling of relevance to prompt-NO formation at high pressure, *Combust. Flame* 195 (2018) 3–17. (URL: https://doi.org/10.1016/j.combustflame.2018.04.029)

[162] B. Mei, S. Ma, X. Zhang, Y. Li, Characterizing ammonia and nitric oxide interaction with outwardly propagating spherical flame method, *Proc. Combust. Inst.* 38 (2021) 2477–2485. (URL: https://doi.org/10.1016/j.proci.2020.07.133)

[163] R. J. Kee, F. M. Rupley, J. A. Miller, Chemkin-II: A Fortran chemical kinetics package for the analysis of gas-phase chemical kinetics (SAND-89-8009), *Sandia National Lab. (SNL-CA), Livermore, CA (US)*, United States, 1989. (URL: https://doi.org/10.2172/5681118, accessed 2022/03/02)

[164] Institut für Technische Verbrennung, RWTH Aachen University, FlameMaster: A C++ Computer Program for 0D Combustion and 1D Laminar Flame Calculations, 2018. https://www.itv.rwth-aachen.de/en/downloads/flamemaster/ (accessed 24/05/2021)

[165] The CRECK Modeling Group (Politecnico di Milano), OpenSMOKE++: a general framework developed for numerical simulations of reacting systems with detailed kinetic mechanisms, including thousands of chemical species and reactions, 2021. https://www.opensmokepp.polimi.it/ (accessed 26/05/2021)

[166] A. Cuoci, A. Frassoldati, T. Faravelli, E. Ranzi, OpenSMOKE++: An object-oriented framework for the numerical modeling of reactive systems with detailed kinetic mechanisms, *Comput. Phys. Commun.* 192 (2015) 237–264. (URL: https://doi.org/10.1016/j.cpc.2015.02.014)

[167] A. Cuoci, A. Frassoldati, T. Faravelli, E. Ranzi, Numerical Modeling of Laminar Flames with Detailed Kinetics Based on the Operator-Splitting Method, *Energy Fuels* 27 (2013) 7730−7753. (URL: https://doi.org/10.1021/ef4016334)

[168] A. Stagni, A. Cuoci, A. Frassoldati, T. Faravelli, E. Ranzi, Lumping and Reduction of Detailed Kinetic Schemes: an Effective Coupling, *Ind. Eng. Chem. Res.* 53 (2014) 9004−9016. (URL: https://doi.org/10.1021/ie403272f)

[169] D. G. Goodwin, R. L. Speth, H. K. Moffat, B. W. Weber, Cantera: An object-oriented software toolkit for chemical kinetics, thermodynamics, and transport processes, Version: 2.5.1, 2021. https://www.cantera.org (accessed 2022/02/03) (DOI: 10.5281/zenodo.4527812)

[170] Lawrence Livermore National Laboratory (LLNL), Zero-Order Reaction Kinetics (ZERO-RK), https://ipo.llnl.gov/technologies/software/zero-order-reaction-kinetics-zero-rk (accessed 20 May 2022)

[171] R. J. Kee, F. M. Rupley, J. A. Miller, M. E. Coltrin, J. F. Grcar, E. Meeks, H. K. Moffat, A. E. Lutz, G. Dixon-Lewis, M. D. Smooke, J. W. G. H. Evans, R. S. Larson, R. E. Mitchell, L. R. Petzold, W. C. Reynolds, M. Caracotsios, W. E. Stewart, P. Glarborg, C. Wang, O. Adigun, CHEMKIN Collection, Release 3.6, *Reaction Design*, San Diego, CA, 2000.

[172] C. Olm, I. G. Zsély, T. Varga, H. J. Curran, T. Turányi, Comparison of the performance of several recent syngas combustion mechanisms, *Combust. Flame* 162 (2015) 1793–1812. (URL: https://doi.org/10.1016/j.combustflame.2014.12.001)

[173] V. Samu, T. Varga, K. Brezinsky, T. Turányi, Investigation of ethane pyrolysis and oxidation at high pressures using global optimization based on shock tube data, *Proc. Combust. Inst.* 36 (2017) 691–698. (URL: https://doi.org/10.1016/j.proci.2016.05.039)

[174] T. Varga, T. Nagy, C. Olm, I. G. Zsély, R. Pálvölgyi, É. Valkó, G. Vincze, M. Cserháti, H. J. Curran, T. Turányi, Optimization of a hydrogen combustion mechanism using both direct and indirect measurements, *Proc. Combust. Inst.* 35 (2015) 589–596. (URL: https://doi.org/10.1016/j.proci.2014.06.071)

[175] T. Varga, I. G. Zsély, T. Turányi, T. Bentz, M. Olzmann, Kinetic Analysis of Ethyl Iodide Pyrolysis Based on Shock Tube Measurements, *Int. J. Chem. Kinet.* 46 (2014) 295−304. (URL: https://doi.org/10.1002/kin.20829)

[176] C. Olm, T. Varga, É. Valkó, H. J. Curran, T. Turányi, Uncertainty quantification of a newly optimized methanol and formaldehyde combustion mechanism, *Combust. Flame* 186 (2017) 45–64. (URL: http://dx.doi.org/10.1016/j.combustflame.2017.07.029)

[177] C. Olm, T. Varga, É. Valkó, S. Hartl, C. Hasse, T. Turányi, Development of an Ethanol Combustion Mechanism Based on a Hierarchical Optimization Approach, *Int. J. Chem. Kinet.* 48 (2016) 423–441. (URL: https://doi.org/10.1002/kin.20998)

[178] P. Zhang, I. G. Zsély, M. Papp, T. Nagy, T. Turányi, Comparison of methane combustion mechanisms using laminar burning velocity measurements, *Combust. Flame* 238 (2022) 111867. (URL: https://doi.org/10.1016/j.combustflame.2021.111867)

[179] P. Zhang, I. G. Zsély, V. Samu, T. Nagy, T. Turányi, Comparison of Methane Combustion Mechanisms Using Shock Tube and Rapid Compression Machine Ignition Delay Time Measurements, *Energy Fuels* 35 (2021) 12329–12351. (URL: https://doi.org/10.1021/acs.energyfuels.0c04277)

[180] T. Nagy, Minimal Spline Fit Introducing Root-Mean-Square Fitting of Data Series with Akima Splines, Version: January 5 (2020), 2020. http://respecth.chem.elte.hu/respecth/reac/compProgs.php (accessed 2022/02/03)

[181] T. Nagy, T. Turányi, Minimal Spline Fit: a model-free method for determining statistical noise of experimental data series, *Proceedings of the European Combustion*

Meeting, Paper 337, Naples, Italy, 2021, 14-15 April. (URL: http://garfield.chem.elte.hu/Turanyi/pdf/153_Nagy_ECM21-336.pdf, accessed 2022/02/03)

[182] H. Akima, A New Method of Interpolation and Smooth Curve Fitting Based on Local Procedures, *J. ACM* 17 (1970) 589−602. (URL: https://doi.org/10.1145/321607.321609)

[183] H. Akaike, A new look at the statistical model identification, *IEEE Trans. Automat. Contr.* 19 (1974) 716−723. (URL: http://doi.org/10.1109/TAC.1974.1100705)

[184] E. J. Bedrick, C.-L. Tsai, Model Selection for Multivariate Regression in Small Samples, *Biometrics* 50 (1994) 226–231. (URL: https://doi.org/10.2307/2533213)

[185] C. M. Hurvich, C.-L. Tsai, Regression and time series model selection in small samples, *Biometrika* 76 (1989) 297–307. (URL: https://doi.org/10.1093/biomet/76.2.297)

[186] J. E. Cavanaugh, Unifying the derivations for the Akaike and corrected Akaike information criteria, *Stat. Probab. Lett.* 33 (1997) 201–208. (URL: https://doi.org/10.1016/S0167-7152(96)00128-9)

[187] M. Kopp, M. Brower, O. Mathieu, E. Petersen, F. Güthe, CO_2* chemiluminescence study at low and elevated pressures., *Appl. Phys. B* 107 (2012) 529–538. (URL: https://doi.org/10.1007/s00340-012-5051-4)

[188] O. Mathieu, A. Levacque, E. L. Petersen, Effects of N_2O addition on the ignition of H_2–O_2 mixtures: Experimental and detailed kinetic modeling study, *Int. J. Hydrog. Energy* 37 (2012) 15393–15405. (URL: https://doi.org/10.1016/j.ijhydene.2012.07.071)

[189] O. Mathieu, A. Levacque, E. L. Petersen, Effects of NO_2 addition on hydrogen ignition behind reflected shock waves, *Proc. Combust. Inst.* 34 (2013) 633–640. (URL: https://doi.org/10.1016/j.proci.2012.05.067)

[190] C. R. Mulvihill, O. Mathieu, E. L. Petersen, The unimportance of the reaction $H_2 + N_2O \leftrightarrows H_2O + N_2$: A shock-tube study using H_2O time histories and ignition delay times, *Combust. Flame* 196 (2018) 478–486. (URL: https://doi.org/10.1016/j.combustflame.2018.07.003)

[191] M. Kovács, M. Papp, I. G. Zsély, T. Turányi, Main sources of uncertainty in recent methanol/NO_x combustion models, *Int. J. Chem. Kinet.* 53 (2021) 884–900. (URL: https://doi.org/10.1002/kin.21490)

[192] T. Turányi, L. Zalotai, S. Dóbé, T. Bérces, Effect of the uncertainty of kinetic and thermodynamic data on methane flame simulation results, *Phys. Chem. Chem. Phys.* 4 (2002) 2568–2578. (URL: https://doi.org/10.1039/b109154a)

[193] J. Zádor, I. G. Zsély, T. Turányi, M. Ratto, S. Tarantola, A. Saltelli, Local and Global Uncertainty Analyses of a Methane Flame Model, *J. Phys. Chem. A* 109 (2005) 9795–9807. (URL: https://doi.org/10.1021/jp053270i)

[194] R. Langer, J. Lotz, L. Cai, F. Vom Lehn, K. Leppkes, U. Naumann, H. Pitsch, Adjoint sensitivity analysis of kinetic, thermochemical, and transport data of nitrogen and ammonia chemistry, *Proc. Combust. Inst.* 38 (2021) 777–785. (URL: https://doi.org/10.1016/j.proci.2020.07.020)

[195] B. Ruscic, D. H. Bross, Active Thermochemical Tables (ATcT) values based on ver. 1.122b of the Thermochemical Network (2016), available at https://atct.anl.gov/ (accessed 2021/11/13)

[196] B. Ruscic, R. E. Pinzon, G. v. Laszewski, D. Kodeboyina, A. Burcat, D. Leahy, D. Montoy, A. F. Wagner, Active Thermochemical Tables: thermochemistry for the 21st century, *J. Phys. Conf. Ser.* 16 (2005) 561–570. (URL: https://doi.org/10.1088/1742-6596/16/1/078)

[197] B. Ruscic, R. E. Pinzon, M. L. Morton, G. Von Laszevski, S. J. Bittner, S. G. Nijsure, K. A. Amin, M. Minkoff, A. F. Wagner, Introduction to Active Thermochemical Tables: Several "Key" Enthalpies of Formation Revisited, *J. Phys. Chem. A* 108 (2004) 9979–9997. (URL: https://doi.org/10.1021/jp047912y)

[198] E. Goos, A. Burcat, B. Ruscic, Extended Third Millennium Ideal Gas and Condensed Phase Thermochemical Database for Combustion and Air Pollution with Updates from Active Thermochemical Tables (2018) *Technion – Israel Institute of Technology*, available at https://burcat.technion.ac.il/ (accessed 2202/03/02)

[199] H. Wang, X. You, A. V. Joshi, S. G. Davis, A. Laskin, F. Egolfopoulos, C. K. Law, USC Mech Version II. High-Temperature Combustion Reaction Model of H_2/CO/C_1-C_4 Compounds (May 2007), available at http://ignis.usc.edu/USC_Mech_II.htm (accessed 2022/03/02)

[200] P. Dagaut, F. Lecomte, S. Chevailler, M. Cathonnet, Experimental and Detailed Kinetic Modeling of Nitric Oxide Reduction by a Natural Gas Blend in Simulated Reburning Conditions, *Combust. Sci. Technol.* 139 (1998) 329–363. (URL: https://doi.org/10.1080/00102209808952093)

[201] Y. Tan, P. Dagaut, M. Cathonnet, J. Claude Boettner, J. Sylvain Bachman, P. Carlier, Natural gas and blends oxidation and ignition: Experiments and modeling, *Symposium (International) on Combustion* 25 (1994) 1563–1569. (URL: https://doi.org/10.1016/S0082-0784(06)80801-5)

[202] A. Burcat, B. McBride, Ideal Gas Thermodynamic Data for Compounds Used in Combustion and Air Pollution (TAE 675), *Technion-Israel Institute of Technology, Haifa, Israel*, 1993.

[203] Y. Li, S. M. Sarathy, Probing hydrogen–nitrogen chemistry: A theoretical study of important reactions in N_xH_y, HCN and HNCO oxidation, *Int. J. Hydrog. Energy* 45 (2020) 23624–23637. (URL: https://doi.org/10.1016/j.ijhydene.2020.06.083)

[204] C. L. Rasmussen, J. Hansen, P. Marshall, P. Glarborg, Experimental measurements and kinetic modeling of CO/H_2/O_2/NO_x conversion at high pressure, *Int. J. Chem. Kinet.* 40 (2008) 454–480. (URL: https://doi.org/10.1002/kin.20327)

[205] O. Mathieu, B. Giri, A. R. Agard, T. N. Adams, J. D. Mertens, E. L. Petersen, Nitromethane ignition behind reflected shock waves: Experimental and numerical study, *Fuel* 182 (2016) 597–612. (URL: https://doi.org/10.1016/j.fuel.2016.05.060)

[206] J. Bugler, K. P. Somers, J. M. Simmie, F. Güthe, H. J. Curran, Modeling Nitrogen Species as Pollutants: Thermochemical Influences, *J. Phys. Chem. A* 120 (2016) 7192–7197. (URL: https://doi.org/10.1021/acs.jpca.6b05723)